MOLECULAR PROCESSES OF ADAPTIVE RESPONSE IN HUMAN PERIPHERAL MONONUCLEAR CELLS IN RESPONSE TO IONIZING RADIATION

By
NEHA R. PARASWANI

LIFE01201304003

BHABHA ATOMIC RESEARCH CENTRE, MUMBAI

A thesis submitted to the

Board of Studies in Life Sciences

In partial fulfillment of requirements

for the Degree of

DOCTOR OF PHILOSOPHY

of

HOMI BHABHA NATIONAL INSTITUTE

December, 2019

Homi Bhabha National Institute

Report of Ph.D. Viva-Voce
Board of Studies in Life Sciences

A. General Details:

1. **Name of the Constituent Institution:** Bhabha Atomic Research Centre, Mumbai

2. **Name of the Student:** Ms. Neha R. Paraswani

2. **Enrolment Number:** LIFE01201304003

3. **Date of Enrolment in HBNI:** 01/01/2013

4. **Date of Submission of Thesis:** 31/12/2019

5. **Title of the Thesis:** Molecular processes of adaptive response in human peripheral blood mononuclear cells in response to ionizing radiation.

7. **Number of Doctoral Committee Meetings held with respective dates:**

Review Period	Date	Review Period	Date
1. Jan 2013 to Dec 2014	14-01-2015	2. Dec 2015 to Dec 2015	07-03-2016
3. Dec 2015 to Dec 2016	07-04-2017	4. Jan 2017 to April 2018	21-05-2018
5. Pre-synopsis	15-11-2019	6.	

8. **Name and Affiliation of the Thesis Examiner 1:** Prof Vibha Tandon
Special Centre for Molecular Medicine, Jawaharlal Nehru University, New Delhi – 110067

   Recommendations of the Examiner 1 (Thesis Evaluation) (i) accepted, (ii) accepted after revisions, or (iii) rejected:

   ACCEPTED

9. **Name and Affiliation of the Thesis Examiner 2:** Prof. Carmel Mothersill
McMaster University. General Sciences Building, 1280 Main Street West Hamilton, Ontario, Canada

   Recommendations of the Examiner 2 (Thesis Evaluation) (i) accepted, (ii) accepted after revisions, or (iii) rejected:

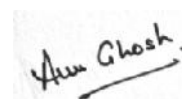   ACCEPTED

B. Record of the Viva-Voce Examination

1. **Date of Viva Voce Examination: 25-05-2020**

2. Name and affiliation of External Examiner: Prof Vibha Tandon
   Special Centre for Molecular Medicine, Jawaharlal Nehru University, New Delhi – 110067

3. **Whether there were other experts / faculty/students present ? Please enclose a soft copy of attendance sheet indicating participation in person/over video as per proforma given below at (5)**   Attendance sheet attached separately

4. **Recommendations for the award of the Ph.D. degree: Recommended / Not Recommended**
   (If Recommended, give summary of main findings and overall quality of thesis)
   (If Not Recommended, give reasons for not recommending and guidelines to be communicated by Convener of the Doctoral committee to the student for further work)

The viva voce of Ms Neha R. Paraswani (LIFE01201304003) was conducted by Prof. Vibha Tandon, Special Centre for Molecular Medicine. Jawaharlal Nehru University. New Delhi-110 067 in an open forum on 25th May, 2020 remotely through 'Google Meet', which she defended duly and successfully. Ms Neha presented her thesis work in a lucid form and provided significant data on molecular processes of radioadaptive response in human PBMCs from healthy individuals. The objectives of the thesis are highly relevant for addressing the differences in radio- sensitivities among individuals and also for prediction of health effects due to low doses of radiation, especially in occupational workers of nuclear industry and individuals living in high background radiation areas of the world. Both the reviewers raised only minor queries during thesis evaluation, which were answered by Ms Neha. She also responded effectively to the questions raised by the examiner, committee and other participants who joined the online meet.

In view of the above, the Doctoral Committee and the External Examiner Prof Vibha Tandon have great pleasure in recommending the thesis submitted by Ms Neha R. Paraswani for the award of Ph.D. degree of Homi Bhabha National Institute.

5. **Attendance at Viva Voce (Doctoral Committee, External Examiner, others):**

Sr No	Composition	Name	Attended in person or through video; if in person, signature
1.	**Chairman**	Dr. Santosh Kumar, BARC, Mumbai	Through Google Meet
2.	**Convener** (Guide)	Dr. Anu Ghosh, BARC, Mumbai	Through Google Meet
3.	**Co-Guide/External Guide** (if any)	-	-
4.	**External Examiner**	Dr. Vibha Tandon, JNU, Delhi	Through Google Meet
5.	**Member**	Dr. Anand Ballal, BARC, Mumbai	Through Google Meet
6.	**Member**	Dr. Sahayog Jamdar, BARC Mumbai	Through Google Meet
7.	**Member**	Dr. Sorab Dalal, ACTREC, Mumbai	Through Google Meet
Others As per the list appended separately			

02.06,2020
(Convener, Viva Voce Board)

STATEMENT BY AUTHOR

This dissertation has been submitted in partial fulfillment of requirements for an advanced degree at Homi Bhabha National Institute (HBNI) and is deposited in the Library to be made available to borrowers under rules of the HBNI.

Brief quotations from this dissertation are allowable without special permission, provided that accurate acknowledgement of source is made. Requests for permission for extended quotation from or reproduction of this manuscript in whole or in part may be granted by the Competent Authority of HBNI when in his or her judgment the proposed use of the material is in the interests of scholarship. In all other instances, however, permission must be obtained from the author.

10.10.2020

Neha R. Paraswani

DECLARATION

I, hereby declare that the investigation presented in the thesis has been carried out by me. The work is original and has not been submitted earlier as a whole or in part for a degree / diploma at this or any other Institution / University.

10.10.2020

Neha R. Paraswani

List of Publications arising from the thesis

Journal

1. Early antioxidant responses via the concerted activation of NF-κB and Nrf2 characterize the gamma-radiation-induced adaptive response in quiescent human peripheral blood mononuclear cells.

   Paraswani N, Thoh M, Bhilwade HN, Ghosh A. Mutat Res Genet Toxicol Environ Mutagen, 2018, 831:50-61.

Conferences

1. P 015 - Cellular redox status mediates adaptive response to ionizing radiation in human peripheral blood mononuclear cells.

   Paraswani N, Thoh M, Ghosh A

   Free Radical Biology and Medicine 108 (2017): S22.

   OCC World Congress and Annual SFRR-E Conference 2017 Metabolic Stress and Redox Regulation. Berlin, Germany; 21-23 June 2017.

2. Adaptive response to low dose ionizing radiation in human peripheral blood mononuclear cells is associated with up-regulation of redox genes.

   Paraswani N and Ghosh A

   XL All India Cell Biology Conference & International Symposium on Functional Genomics and Epigenomics Jiwaji University, Gwalior. November 17-19 2016.

3. Possible role of oxidative stress in the radioadaptive response of G_0 human PBMCs to ionizing radiation.

   Paraswani N, Thoh M, Bhilwade HN, Ghosh A

   SFRR-India 14th annual meeting of the Society for Free Radical Research-India and international conference on translational research in ionizing radiation, free radicals, antioxidants and functional food. Kalyani, West Bengal, India; 7-9 Jan 2016.

   10.10.2020

   Neha R. Paraswani

DEDICATED

TO

MY LOVING FAMILY

ACKNOWLEDGEMENTS

CONTENTS

CHAPTER 2

CHAPTER 4

PROTEOMIC ANALYSIS DURING RADIATION INDUCED-ADAPTIVE

List of figures

List of tables

List of annexures

SUMMARY

The biological effects of low dose radiation are often considered contentious and their long-term impact remains uncertain. Numerous studies have shown that when a biological system is exposed to a small 'priming' stress, it induces specific biological mechanisms that makes it better able to cope with (adapt to) subsequent exposures to high 'challenge' doses. However, the mechanisms involved in radiation induced-adaptive response (RI-AR) are highly complex and remain unclear. The broad objective of the present work was therefore, to use non-dividing G_0 human PBMCs from the same set of five healthy individuals and a defined protocol to elicit adaptive response so as to be able to derive definite conclusions. For this, the PBMCs were challenged with a high dose of 2 Gy subsequent to the exposure to a priming dose of 100 mGy given 4 h earlier. We showed that RI-AR in human PBMCs involves lower DNA damage as measured with comet assay and better efficiency of DSBs repair as measured with γH2AX. This was accompanied with a small increase in cell survival in primed cells. The primed cells further exhibited better antioxidant defence involving upregulation of catalase, superoxide dismutase, thioredoxin reductase, and glutathione peroxidase enzymes that compensated for a small increase in ROS. An early binding of transcription factors NF-κB and Nrf2 and an early activation of pro-survival pERK was seen in primed cells as compared to non-primed cells. Since proteins are considered as the effector molecules of cellular function, we also used a proteomics approach to understand RI-AR. Using a combination of gel based 2D-DIGE and gel-free shotgun proteomics, we identified several proteins unique to primed cells. Both 2D-DIGE and label-free proteomics identified similar pathways, though an overlap between the two methods at the level of protein IDs were very limited. Primed cells showed specific enrichment of biological processes

like transcription, chromatin remodeling, ubiquitination and, KEGG pathways like HIF-1 signaling pathway and FOXO signaling pathway. Besides this, several proteins like CAT, HIF1A, FOXO1, NFATC1, NOS2, KLF2 and CHUK involved in redox mediated processes and key cell signaling proteins like AKT1, AKT2, AKT3, TLR4, HSP90B1, PLK1, CREB3L4 which are known to be activated in response to oxidative stress, were detected in primed cells relative to non-primed cells. Our data thus, indicated a pivotal role of DNA damage response and antioxidant mechanisms in RI-AR of human PBMCs. Our findings further echo the growing opinion in the scientific community that we should be aware of the fallacy of extrapolating the radiation risk at low doses from responses at high doses. A better understanding of molecular mechanisms of RI-AR will perhaps allow us to characterize persistent fingerprints of adaptive response.

KEY CONCLUSIONS AND FUTURE DIRECTIONS

Radiation induced-adaptive response is a biological phenomenon in which resistance to a high challenge dose is induced by a small preceding radiation dose. RI-AR has been observed in various cell lines *in vitro* and *in vivo* using various end points. The molecular mechanisms governing this response have yet not been completely elucidated. There have been suggestions that RI-AR involves similar processes like that to other common environmental stressors like metal toxicity, heat shock, pesticides etc. However, different studies have used diverse protocols on independent models; which makes understanding entire sequence of events difficult. The present study, thus attempts to understand the molecular processes involved in RI-AR in a singular cellular model (human PBMCs) using the same sample set and a defined regime for inducing adaptive response.

With the help of two different methods to assess DNA damage and repair - alkaline comet assay and γH2AX assay, we first demonstrated that PBMCs primed with a low dose of radiation show lesser initial damage and better repair of DSBs than non-primed cells. This indicated that RI-AR in human PBMCs is associated with higher efficiency of repair of DSBs. Decreased DNA damage lead to better survival and higher mitochondrial membrane potential in primed cells. Further, primed cells showed low levels of ROS that corresponded with early activation of antioxidant enzymes like CAT, SOD, TXNRD1 and GPX. We further showed increased binding of transcription factors Nrf2 and NFκB in the primed cells that occurred early after irradiation. Pre-exposure to low dose radiation also showed early activation of pERK pro-survival signaling molecule. We thus, hypothesize that RI-AR in human PBMCs is mediated through reduced oxidative stress and increased antioxidant activity in primed cells.

Additionally, we used an integrated approach of gel based 2D-DIGE and gel-free LC-MS based label-free analysis to identify proteomic responses during radioadaptation. Number of proteins identified using label-free analysis in each treatment group were almost 14 times more than the number of proteins identified using 2D-DIGE. Both the proteomics methods showed good assay reproducibility and minimum variation between the experimental replicates. 2D-DIGE analysis identified 28 differentially expressed protein spots out of which 2 were up-regulated (WDR1 and ACTG/B) and 26 were down-regulated (e.g. VINC, VIME, FIBG, ACTG, TBB) in primed cells when compared with non-primed cells. A poor overlap was seen between proteins identified by 2D-DIGE and label-free analysis with only five proteins common between the two methods: P18206 (VINC), P63261 (ACTB/G), P60709 (ACTG/B), P11142 (HSP7C) and P02787 (TRFE). Label-free quantitative proteomic analysis identified 2422 proteins in the primed cells. DAVID analysis identified significant enrichment of 34 biological processes (Benjamini-Hochberg p-value $\leq$ 0.1) in the three treatment groups. Enrichment of proteins involved in transcriptional regulation, ubiquitination and chromatin remodeling processes were unique to primed cells. Functional pathway analysis using KEGG identified enrichment of 18 pathways in the three treatment groups (Benjamini-Hochberg p-value $\leq$ 0.1) that may play a critical role in cellular response to radiation. Several key proteins involved in cellular redox homeostasis (CAT, HIF1A, FOXO1, NFATC1, NOS2, KLF2 and CHUK) were detected only in primed cells. Important cell signaling proteins like AKT1, AKT2, AKT3, TLR4, HSP90B1, PLK1, CREB3L4 which are known to be activated in response to oxidative stress were also unique to the primed cells. These findings again supported our hypothesis that increased

activity of antioxidant enzymes lead to rapid scavenging of ROS and consequently less cellular damage in the primed cells.

The present work identified a large list of unique proteins in primed PBMCs. In the follow-up approach, candidate redox sensitive transcription factors and other antioxidant proteins will be verified using functional assays and targeted proteomics. This will help develop biomarkers of radio-adaptation in human cells. Furthermore, we used only a small fixed period of time between the adapting and challenging dose (4 h) and studied protein expression only at one time point after irradiation (1 h). Characterization of radiation-sensitive proteins at later time points will be interesting and should help better understanding of the long-term implications of radiation-induced adaptive response. This will have huge implications for radiation occupational workers and space astronauts on manned missions.

We are aware of various limitations of our current knowledge of RI-AR. The physiological, genetic and epigenetic factors which may contribute to interindividual variation and affect development of RI-AR have not been tested. Various studies have used contrasting PD and CD in varied cellular systems, indicating different systems might respond to different dose regimes for RI-AR induction. Thus, the hypothesized mechanisms need to be rigorously tested in other cellular systems and animal models to validate their universality. Additionally, development of RI-AR in individuals with dysfunctional repair and immune system is not known and should be tested. New research in the field of low dose radiation is highly pertinent in the modern world. The contribution of non-targeted effects like radioadaptive response, especially in this low dose range, will have important implications for defining an appropriate dose-response model for radiation protection.

Homi Bhabha National Institute

SYNOPSIS OF Ph. D. THESIS

1. **Name of the Student: Neha R. Paraswani**

2. **Name of the Constituent Institution: Bhabha Atomic Research Centre**

3. **Enrolment No.: LIFE01201304003**

4. **Title of the Thesis: Molecular processes of adaptive response in human peripheral mononuclear cells in response to ionizing radiation**

5. **Board of Studies: Life Sciences**

SYNOPSIS

Humans are continually exposed to low doses of natural and anthropogenic ionizing radiation. Accumulating evidence suggests that exposure of mammalian cells to low doses of ionizing radiation may induce several unique processes like hyper-radiosensitivity, bystander effects, genomic instability or adaptive responses [1]. These responses result in a distinctive dose-response curve at low doses significantly different from the linear quadratic model observed at high doses of radiation. Radiation-induced adaptive response (RI-AR) is a phenomenon induced by relatively low 'priming dose' (PD) that protects cells and whole organisms against damage due to subsequent high 'challenge dose' (CD) of radiation. RI-AR was first recognized in 1984 by Olivieri *et al* in human lymphocytes exposed to low concentrations of radioactive thymidine [2]. Subsequently, several authors reported evidence of RI-AR in various cell lines, with different pre-irradiation doses and variable challenging

doses [3-5]. However, the precise mechanism(s) of RI-AR and its exact role in cellular homeostasis remains unknown. Relevant research in this field has become increasingly important due to the expansion of nuclear power plants worldwide, and increased use of radioisotopes for medical diagnosis and radiotherapy as well as for various industrial applications.

Several mechanisms for the induction of RI-AR in human cells have been proposed. This includes DNA repair, cell cycle control, apoptosis, activation of genes and induced proteins, and radical detoxification, among others [6]. However, evidence for these hypothesized mechanisms remains scattered and inconclusive. Different studies, using disparate models and diverse protocols have tested individual hypothesis, which cannot be compared to understand entire sequence of events. The present study was therefore, proposed with an aim to test various hypotheses in a singular cellular model using the same sample set and a defined regime for inducing adaptive response. Human peripheral blood mononuclear cells (PBMCs) were chosen as the model system for the study. Human blood to derive PBMCs can be obtained with minimal invasive method and can effectively mimic the *in vivo* conditions. The objectives of the thesis were thus, defined as:

1. Detection of DNA strand breaks in Peripheral Blood Mononuclear Cells (PBMCs) under radioadaptive conditions.
2. Identification and characterization of differentially modulated proteins in human PBMCs under radioadaptive conditions.
3. Understanding the molecular mechanisms of radioadaptive response in human PBMCs.

Organization of Thesis

The thesis is divided into following five chapters:

Chapter 1: Introduction

This chapter begins with a brief introduction to the different sources (natural and man-made) of radiation. Various biological effects of radiation (direct and indirect effects) including IR induced DNA damage, DNA repair pathways, induction of apoptosis and necrosis, activation of MAP kinase signaling is explained. A comprehensive view of IR induced oxidative stress, activation of various antioxidant enzymes and redox specific transcription factors is provided. A major section in this chapter is devoted to explain non-targeted effects of IR, especially RI-AR. Evidences for RI-AR in various cell types and important parameters required for induction of RI-AR are mentioned. Also, a separate section discussing the advanced gel-based and gel-free quantitative proteomics methods to detect protein profiles of PBMCs exposed to radiation is included. The major objectives of the present work are stated at the end of the chapter.

Chapter 2: Materials and Methods

This chapter provides details of experimental materials and protocols of different techniques used in the present study. Blood samples were collected from healthy individuals from Mumbai, India with informed consent. The collection of samples was approved by the Medical Ethics Committee, Bhabha Atomic Research Centre, Mumbai, India. The irradiation of G_0 PBMCs was performed using a ^{60}Co gamma source (Blood Irradiator, 2000, BRIT, India) at a dose rate of 0.3 Gy/min. To study RI-AR, cells were exposed to a low priming dose (PD) of 100 mGy and then, after an adaptive window of 4 h, exposed to a challenge dose (CD) of 2 Gy. These parameters have been shown earlier to give optimal RI-AR in human PBMCs [7].

Subsequently, cells exposed to 100 mGy PD + 2 Gy CD are referred as 'primed cells' and cells exposed to 2 Gy CD alone are referred as 'non-primed cells'. The protocol for PBMCs isolation, *in vitro* irradiation of PBMCs, DNA damage analysis using alkaline comet assay and γH2AX foci detection, cell viability assay, measurement of mitochondrial membrane permeability, and analysis of apoptosis is given in detail. The procedures followed for measurement of cellular redox status by assessing levels of intracellular and mitochondrial ROS, cellular thiols, GSH/GSSG ratio, and antioxidant enzyme activity are included. Detection of nuclear localized redox specific transcription factors using EMSA is explained. The protocol for western blot analysis is included. Protocol for qRT-PCR to quantify mRNA expression of various genes relevant to the current study is included. The detailed procedures used for gel-based (two-dimensional difference gel electrophoresis (2D-DIGE) and gel-free (label free quantification) quantitative proteomic techniques are described. The functional pathway analysis used to identify enriched biological processes and pathways is included. Statistical analysis was performed using student's t-test. $p \leq 0.05$ was considered as significant. Benajami-Hochberg p-value<0.1 was used for DAVID gene ontology and KEGG pathway analysis.

Chapter 3: Role of DNA repair and antioxidant responses in radiation induced-adaptive response.

In this chapter, results obtained for several hypothesized mechanisms of RI-AR, primarily role of DNA damage and oxidative stress, when tested in human G_0 PBMCs, are presented. The results obtained in the present work are then compared and contrasted with published reports in various cell systems. We first measured baseline DNA damage using alkaline comet assay in G_0 PBMCs exposed to increasing doses of γ-rays (0.01 Gy to 4 Gy) and showed a dose dependent increase.

DNA damage at a very low dose of 0.01 Gy did not vary significantly from the sham irradiated control. Next, RI-AR was validated in G_0 PBMCs from 7 individuals since there are conflicting reports in the literature regarding the induction of adaptive response in non-proliferating cells. An 8.3% to 30.8% decrease in % tail DNA, indicative of RI-AR, was seen in primed cells when compared to non-primed cells in five out of seven individuals tested. To avoid inter-individual variability, all further experiments were performed by pooling equal number of PBMCs from the five individuals that showed adaptive response. When dose-effect functions at various time points after CD was followed using alkaline comet assay, there was no difference in residual DNA damage between primed and non-primed cells.

Next, we measured DSBs and followed their repair under RI-AR in human PBMCs using γH2AX foci analysis We showed that low dose radiation exposure not only resulted in significantly lower initial DSBs (10.52 ± 0.69 vs 12.97 ± 0.50 in non-primed cells, p= 0.02) but also faster repair of DSBs in the primed cells. This lower DNA damage was accompanied with a small, but statistically significant, higher survival in the primed cells (93.06 ± 0.00 *vs.* 88.14 ± 0.90 in non-primed cells, p = 0.0007) 24 h post CD. Similarly, primed cells showed a higher mitochondrial membrane potential as compared to non-primed cells (60.67 ± 1.12 vs. 32.86 ± 0.59, $p\leq0.0001$). However, no significant change in apoptosis was observed between primed and non-primed cells. Decrease in DNA damage was accompanied by lower levels of endogenous (41.9 ± 0.36 vs. 58.83 ± 0.42, $p\leq0.001$) and mitochondrial (122.66 ± 4.36 vs. 139.61 ± 4.36, p = 0.009) reactive oxygen species (ROS). We also found increased activity and gene expression of four key antioxidant enzymes catalase, superoxide dismutase, thioredoxin reductase, and glutathione peroxidase in the primed cells. Reduced oxidative stress in primed PBMCs also correlated with

greater nuclear translocation of the redox sensitive transcription factors Nuclear factor kappa B (NF-κB) and Nuclear factor E2-related factor 2 (Nrf2). In addition, primed cells showed early activation of pro-survival ERK MAP kinase.

Chapter 4: Proteomic changes in human PBMCs during radiation induced-adaptive response

Induced protein expression has been proposed as one of the key mechanisms of RI-AR, though it has not been tested rigorously. Global protein expression profile of cellular proteins during RI-AR has been reported in PBMCs isolated from individuals of high level natural background radiation areas using 2-DE [8]. Another 2D-DIGE based study used on human fibroblasts was based on very low priming and challenge dose (≤100 mGy) [9]. In another study, proteins secreted into culture medium when cultured lymphocytes were exposed to adaptive dose of 30 mGy and CD of 1 Gy were studied using LC-MS/MS [10]. None of the published reports therefore, can be compared directly with the present work. To the best of our knowledge, this is the first report on global proteomic analysis in non-cycling human cells during RI-AR using acute irradiation doses. In this chapter, results obtained for total cellular protein expression using gel-based method, 2D-Difference in Gel Electrophoresis (2D-DIGE) and gel free method, label-free LC-MS based quantitative analysis, are presented. The relevance of modulation of key proteins and pathways is presented in the context of other published reports under various stress conditions.

The 2D-DIGE comparative analysis between primed and non-primed cells identified a total of 419±54 protein spots. Out of these 190 protein spots were differentially expressed with a fold change ±1.2. Amongst these, only 2 proteins (WDR1 and ACTG/B) showed significant up-regulation while 38 proteins (e.g. VINC, HSP7C, TBB5, FIBG) showed significant down-regulation (p≤0.05). For

better resolution and greater protein coverage, next we studied expression of proteins using label free quantification technique (gel free method) in the pooled sample. The analysis identified a total of 2532, 2115, 2087 and 2465 proteins in sham irradiated control cells, 100 mGy irradiated cells, non-primed and primed cells, respectively. The DAVID GO analysis identified significant enrichment (Benjamini-Hochberg p-value≤0.1) of 25 different biological processes (BP) in the three dose groups Primed cells showed unique enrichment of transcription regulation (e.g. MED13l, TCF20, CUX1, MMS19), ubiquitination (e.g. RNF6, RNF2, RNF40, USP4, USP6) and chromatin remodeling (e.g. SUPT5H, SUPT6H, SMARCA4, CHD1) related processes. On the other hand, protein phosphorylation related processes (e.g. WNK4, CDC42BPG, CDC42BPA, CIR) were enriched only in non-primed cells. Signal transduction (e.g. PLCB1, MAST1, DOCK4) and cytoskeletal organization related processes (e.g. ITGA11, PDCHA1, MYH10, COL5A6) were enriched in both primed and non-primed cells. The KEGG pathway analysis identified enrichment of 34 KEGG pathways common to the three dose groups (Benjamini-Hochberg p-value≤0.1), relative to sham irradiated control cells. Among the common enriched pathways were cell-matrix interaction and cell signaling related pathways. The number of proteins involved in each KEGG pathway and their relative protein expression differed among the three treatment groups. Primed cells showed distinct enrichment of proteins of HIF-1 signaling pathway (e.g. HIF1A, TLR4, PIK3CB, IGF1R), Ubiquitin mediated proteolysis (e.g. CBL, UBE3A, UBE2O, TRIP12) and RNA transport (e.g. PAIP1, EIF4G3, PABPC3). Enrichment of a crucial pathway for DNA damage repair – Fanconi anemia pathway (e.g. FANCA, FANCI, FANCM, BLM) was observed only in 100 mGy irradiated cells, albeit with p<0.05. Pathways like Ras signaling (e.g. RASA3, PLCG2, INSR, PIK3CB) and phosphatidylinositol

signaling system (e.g. PLCB1, PIK3C2A, PIK3C2B, PI4KA) were enriched only in non-primed cells. Pathways like Rap1 signaling (e.g. INSR, IGF1R, PFN1, THBS1), PI3K-AKT signaling (e.g. PIK3CB, EGFR, INSR, LAMC1), regulation of actin cytoskeleton (e.g. ACTN1, ACTB, DOCK1, PFN1) and focal adhesion (e.g. ACTG1, ACTN1, ROCK1, ITGB4) were enriched in both primed and non-primed cells. The expression value for few proteins when correlated with their gene expression levels using qRT-PCR showed poor correlation. The multivariate principal component analysis (PCA) clearly differentiated the three treatment groups based on protein expression relative to sham-irradiated controls.

Chapter 5: Conclusion and future perspective

Our data established proof-of-concept that radiation-induced adaptive response can be induced in quiescent non-proliferating human PBMCs in the G_0 stage. This has important implications for *in vivo* situations where cells in the G_0 phase are irradiated chronically, like the radiation occupational workers and individuals residing in the high-level natural background radiation areas of the world. We tested an integrated set of multiple probable mechanisms of RI-AR in the same sample set. We established that RI-AR in human PBMCs involves reduced initial DNA damage, faster repair of DSBs, lower ROS, upregulated antioxidant defense and concerted activation of redox sensitive transcription factors NF-κB and Nrf2. Label free quantitative proteomic analysis provided large-scale determination of gene and cellular function at the protein level, including several proteins involved in cellular redox homeostasis, which supported the results shown in chapter III. Bioinformatic analysis further revealed significant enrichment of proteins involved in transcriptional regulation, ubiquitination and chromatin remodeling processes unique to primed cells.

These mechanistic findings will help understand the precise role of adaptive response in long-term health effects of low dose radiation.

Further studies are required to understand whether RI-AR in human cells is part of a generalized response to low stress and whether exposure to stressors other than radiation can modify such effect. Genetic and epigenetic factors in the human population which may contribute to inter-individual variations in RI-AR also need to be studied in detail. Future studies should also focus on targeted proteomics-based verification of key proteins and pathways identified in the present work for their precise role in RI-AR.

References:
1. Matsumoto et al., J Radiat Res. 2007; 48(2):97-106
2. Olivieri et al., Science 1984; 223:594–597.
3. Shadley J.D, Wolff S. Mutagenesis. 1987; 2:95–96.
4. Azzam et al., Radiat. Res. 1994; 138(1): S28–S31.
5. Manesh et al., Mutat. Res. 2015;780: 55–59.
6. Dimova et al., Genet. Mol. Bio. 2008; 31(1):396–408.
7. Shelke and Das. Mutagenesis, 2015;30(3):365-79.
8. Nishad S and Ghosh A. Mutagenesis. 2018; 33(5-6):359-370
9. Hauptmann et al., Radiat Res. 2016; 185(3):299-312.
10. Rithidech et al., Health Phys. 2012; 102(1):39–53.

<u>**Publications in Refereed Journal:**</u>
   a. <u>Published</u>

   Paraswani N, Thoh M, Bhilwade HN, Ghosh A (2018). Early antioxidant responses via the concerted activation of NF-κB and Nrf2 characterize the gamma-radiation-induced adaptive response in quiescent human peripheral blood mononuclear cells. Mutat Res Genet Toxicol Environ Mutagen. 831:50-61

   b. <u>Accepted:</u>
   c. <u>Communicated:</u>

<u>**Other Publications:**</u>
   a. <u>Book/Book Chapter</u>

b. Conference/Symposium

- **Paraswani N**, Thoh M, Ghosh A (2017) P 015 - Cellular redox status mediates adaptive response to ionizing radiation in human peripheral blood mononuclear cells. Free Radical Biology and Medicine 108 (2017): S22. OCC World Congress and Annual SFRR-E Conference 2017 Metabolic Stress and Redox Regulation. Berlin, Germany; 21-23 June 2017.

- **Paraswani N**, Thoh M, Bhilwade HN, Ghosh A (2016) Possible role of oxidative stress in the radioadaptive response of G_0 human PBMCs to ionizing radiation. SFRR-India 14th annual meeting of the Society for Free Radical Research-India and international conference on translational research in ionizing radiation, free radicals, antioxidants and functional food. Kalyani, West Bengal, India; 7-9 Jan 2016.

- **Paraswani N** and Ghosh A (2016). Adaptive response to low dose ionizing radiation in human peripheral blood mononuclear cells is associated with up-regulation of redox genes. XL All India Cell Biology Conference & International Symposium on Functional Genomics and Epigenomics Jiwaji University, Gwalior. November 17-19 2016.

Signature of Student:

Date:

Doctoral Committee:

S. No.	Name	Designation	Signature	Date
1.	Dr. Santosh Kumar, BARC	Chairman		
2.	Dr. Anu Ghosh, BARC	Guide & Convener		
3.	Dr. Anand Ballal, BARC	Member		
4.	Dr. Sahyog Jamdar, BARC	Member		
5.	Dr. Sorab Dalal, ACTREC	External Member		

CHAPTER 1

INTRODUCTION

Humans are continually exposed to radiation from many sources, majority of which are natural in origin while a small contribution comes from man-made sources. Broadly, radiation is the energy emitted by a source in the form of waves or particles that travels through space or other mediums. Radiation can be classified as ionizing and non-ionizing. Radiation is said to be 'ionizing' when it has sufficient energy to ionize (remove an electron from an atom) or disrupt chemical bonds in molecules. The most common forms of ionizing radiation (IR) are alpha (α)-particle radiation, beta (β)-particle radiation, neutrons, gamma (γ)-rays and x-rays. Non-ionizing radiation has less energy but can still cause excitation (raising an electron to a higher energy level) of molecules and atoms causing them to vibrate faster. Microwaves, visible light, radio waves and ultraviolet (UV) light are some of the common examples of non-ionizing radiation.

For the purposes of this thesis, the word "radiation" is used to mean specifically IR.

1.1 Ionizing radiation

Most ionizing radiation originate from the natural decay of unstable atomic nuclei (radioactivity) but can also be artificially generated e.g., by x-ray machines and particle accelerators. Natural sources of IR that contribute to significant human exposures include cosmic rays, terrestrial radiation from long-lived primordial radionuclide such as potassium-40, uranium-238 and thorium-232 found in earth's crust, and radon-222 emanating from rocks and soil of the earth **(Fig. 1. 1).** The predominant artificial or man-made sources of IR are medical diagnostics, nuclear medicine and radiation therapy **(Fig. 1. 1)** [1].
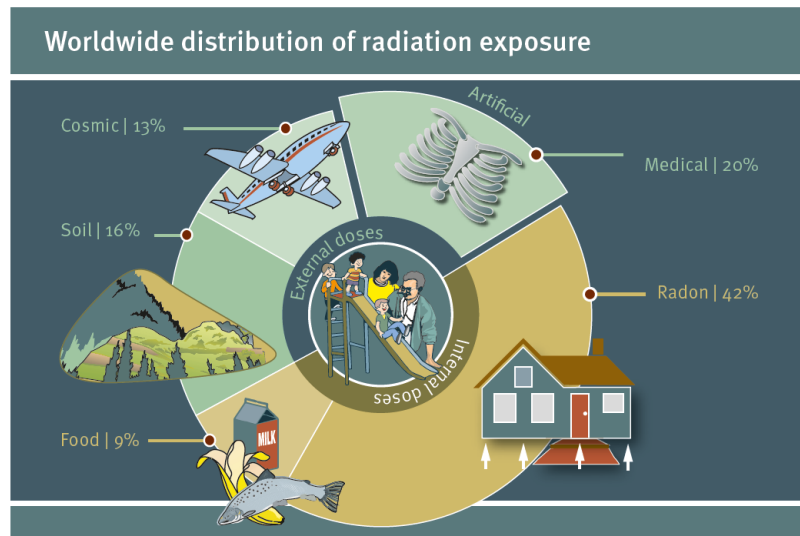
Fig. 1. 1 Different sources of radiation exposure (Adapted from: United Nations Environment Programme (UNEP) booklet).

The intensity of ionizing radiation is measured by the amount of energy deposited per unit mass. The standard unit of absorbed dose is the Gray (Gy), where 1 Gy is defined as 1 J/kg (joule per kilogram). The amount of energy transferred per unit of path length as IR travels through a material is called as linear energy transfer (LET) and is measured in units of keV/µm. Gamma-rays, x-rays and electrons are considered as low-LET radiation, while neutrons, alpha particles and protons are considered high-LET radiation [2]. High LET radiation like α-particles, due to their large +2 charge and fairly large mass, move relatively slowly, travel only a short distance and do not penetrate far into tissues. However, they produce dense ionizations along its path, depositing their energy over a small volume (few cells) and cause extensive damage to these cells. Beta particles, with their smaller size and single negative charge, penetrate deep into tissues. These can thus, affect more cells, but with lesser damage to each cell. Gamma-rays, on the other hand, are low LET, but indirectly ionizing. A γ-ray photon interacts with the atoms of the medium through

which it travels by three primary mechanisms (Photoelectric interaction, Compton scattering and Pair production). This results in the production of high energy electrons. These electrons, due to their smaller +1 or -1 charge and smaller mass result in sparse ionizing collisions. They thus, have a lower rate of energy transfer and are able to travel significant distances in the material before stopping. Gamma radiation is considered primary source of external radiation exposures since it is highly penetrating.

1.2 Biological effects of radiation

In a biological system, IR can deposit a large amount of energy in a small area, and can induce ionization and excitation of atoms and molecules located near its trajectory. Although all major biological molecules like DNA, proteins, lipids and cell membranes are potential targets of radiation exposure, DNA is considered the most critical target for biological damage.

Biological effects of IR also depend on the type of cells affected. Some cells that divide rapidly like the cells lining the stomach cavity, hair follicles, embryonic cells, reproductive cells or bone marrow cells are highly radiosensitive. Non-dividing cells like neurons are considered less radiosensitive.

Biological effects of IR can occur due to two mechanisms: direct effects or indirect effects.

1.2.1 Direct effects of ionizing radiation: In the direct action, the radiant energy interacts directly with the cellular structures. This would result in an ionization and/or excitation leading either to the formation of a radical in the biomolecule which can undergo chain reaction or disruption of atomic structure. Direct action predominantly occurs with high LET radiation such as α particles or neutrons.

4

1.2.2 Indirect effects of ionizing radiation: Indirect effects primarily occur with low LET IR. Since water constitutes nearly 70% of the composition of the cell, transfer of energy to the medium in biological systems predominantly involves ionization of water molecules. These set of discrete physical events are called radiolysis of water and results in formation of free radicals (an atom or molecule with an unpaired number of electrons) which are highly reactive. Time kinetics of radiolysis of water shows that ionization of water occurs in femtoseconds and in picoseconds various free radicals are formed **(Fig. 1. 2).** The free radicals can diffuse and react with each other or with other molecules in the medium to cause cellular damage. Most free radicals which are of concern in biological systems are derived from oxygen. These are collectively called as reactive oxygen species (ROS). Examples of ROS include hydrogen peroxide (H_2O_2), superoxide (O_2^-), and hydroxyl radical ($\cdot OH$).
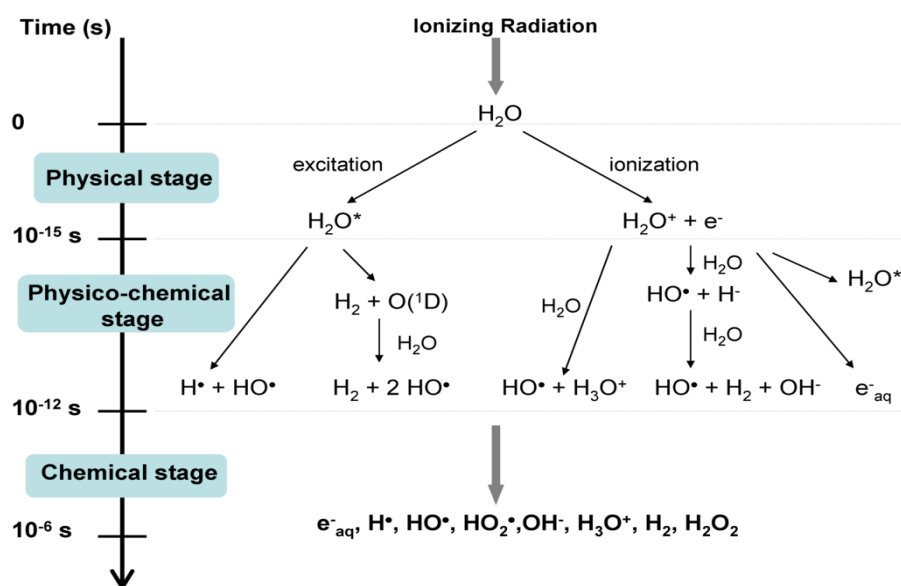
Fig. 1. 2 Indirect effect of IR and radiolysis of water [3].

1.3 DNA Damage Response

The DNA damage response (DDR) is a signal transduction pathway that involves coordinated events mediated through various proteins which function as damage sensors, transducers, mediators and effectors [4]. First, sensors are activated that detect DNA damage and/or chromatin alterations that occur after damage induction. DNA double strand breaks (DSBs) are detected by the MRN (Mre11, RAD50, and NBS1) complex and single strand breaks (SSBs) are detected by the RPA (replication protein A) protein [5]. The signal is then transmitted to transducer proteins, which are usually kinases that amplify the damage signal. These include proteins like ATM (ataxia telangiectasia mutated) and ATR (ataxia telangiectasia and Rad3-related protein), belonging to PI3K (phosphatidylinositol-3 kinase family) which bind to MRN and RPA, respectively. At the end of the cascade are the effector proteins that are involved in specific pathways. The mediator proteins promote interaction between the other proteins.

Upon damage induction by IR, hundreds of molecules of various DDR proteins accumulate on the damage site. These appear as discrete sub-nuclear aggregates by immunofluorescence microscopy, and are referred to as 'ionizing radiation induced foci' (IRIF) [6]. Chromatin architecture plays a key role for the proteins that need to access DNA for repair.

One of the instantaneous downstream targets of ATM is histone H2AX, a variant of histone H2A. Histone H2AX when phosphorylated at Serine 139 is termed as gamma-H2AX (γH2AX). Phosphorylation of H2AX occurs at and around the damaged site covering many mega base-pairs of the chromatin. This can be detected as a distinct spot or a focus when observed under microscope after immunostaining [7].

Gamma-H2AX is considered as a marker of DSBs and is commonly used for studying IR induced DNA strand breaks and repair in human lymphocytes and cell lines [8,9]. Activated ATM also leads to phosphorylation of DNA damage mediator proteins MDC1 (Mediator of DNA damage checkpoint protein 1), 53BP1 (p53-binding protein 1), BRCA1 (Breast cancer type 1 susceptibility protein); effector kinase CHK1 (Checkpoint kinase 1) is then activated. On the other hand, ATR activates TopBP1 (DNA topoisomerase 2-binding protein 1) and CLSPN (Claspin) protein, which in turn activate CHK2 (Checkpoint kinase 2) effector kinase. Apart from this, p53 (Tumor protein p53) is also activated, which can lead to cell cycle arrest, DNA repair or apoptosis depending on the amount of DNA damage. Other proteins like DNA-PK (DNA dependent protein kinase) and PARP (Poly ADP-ribose polymerase) proteins also play an important part in sensing the DNA damage and initiating DNA repair.

1.3.1 DNA repair pathways

Mammalian cells have evolved several mechanisms to repair damaged DNA:

1.3.1.1 Base excision repair (BER): Small base lesions arising from oxidation, methylation or deamination are corrected using BER. The process is initiated by removal of damaged base by DNA glycosylase. This leads to formation of abasic sites, which are then cleaved by AP (apurinic/apyrimidinic) endonuclease, generating single strand breaks. The breaks are repaired by DNA polymerase either by adding a single nucleotide (short-patch BER) or by adding 2-10 nucleotides (long-patch BER).

1.3.1.2 Nucleotide excision repair (NER): NER is primarily used to remove bulky DNA lesions that distort the helical structure. These lesions are recognized by protein complex XPC/hHR23B (Xeroderma pigmentosum, complementation group C/human

homolog of Rad23B). TFIIH complex proteins required for helix unwinding and single strand binding protein RPA are then recruited. After DNA unwinding, incision on either side of the lesion is made by XPG (Xeroderma pigmentosum, complementation group G) and ERCC1-XPF (Excision Repair Cross-Complementation Group 1 and DNA repair endonuclease XPF-also known as Excision Repair Cross-Complementation Group 4 (ERCC4)). The lesion containing DNA fragment (25-32 nucleotide long) is then removed by XPG protein. Resulting gap is filled by DNA polymerase using the complementary strand; the nick is then sealed by DNA ligase and normal nucleotide sequence is restored.

1.3.1.3 Mismatch repair (MMR): MMR recognizes and removes mis-incorporated bases during replication, recombination and DNA repair. Mismatched bases in humans are recognized by MSH2/MSH6 (MutS homolog 2/DNA MutS homolog 6) heterodimer protein. MLH1/PMS2 (MutL homolog 1/ Postmeiotic segregation 2) heterodimer is then recruited at the damage site. The complex slides along the DNA strand and PMS2 creates nick on either side of the mismatch. The cleaved strand is removed by Exo1 (exonuclease I). Resulting gap is then filled by DNA polymerase with the help of other replication accessory proteins like PCNA (Proliferating cell nuclear antigen) and RFC (replication factor C). The gap is sealed by DNA ligase 1.

1.3.1.4 Non-homologous end joining (NHEJ): NHEJ involves joining of two broken ends of DNA without requirement of homologous sequence and is hence, more error prone. It is active throughout the cell cycle, but is found to be more important during G1 phase of the cell cycle when no homology is present. NHEJ is the predominant DSB repair pathway in mammals.

During NHEJ pathway, Ku70 and Ku80 protein heterodimer binds to the damaged ends of DNA. DNA protein kinase catalytic subunit (DNA-PKc) is then recruited at

the DSB site which phosphorylates and activates artemis. Artemis is a nuclease which cleaves damaged DNA overhangs. The DNA ends are then ligated by Ligase IV (a complex of XLF (XRCC4-Like Factor) and XRCC4 (X-Ray Repair Cross Complementing 4) proteins), which has flexibility to ligate across the gaps. This classical NHEJ pathway is backed up by alternative (alt)-NHEJ pathway. The process is mediated through binding of PARP to the damaged DNA ends which then promotes loading of XRCC1/LIG3 (X-Ray Repair Cross Complementing 1/DNA Ligase 3) ligation complex to join the damaged ends.

1.3.1.5 Homologous recombination (HR): HR repairs the damaged DNA using sister chromatid as the template. This pathway mainly operates during late S and G2 phase of the cell cycle. An early event in HR is resection of DNA ends at the DSB site to yield 3'-single stranded DNA (ssDNA) overhangs which are capable of invading duplex DNA containing a homologous sequence. This step involves the MRN complex, which possesses an endonuclease and 3'- 5' exonuclease activity. Resection yields long stretches of single stranded DNA, which is rapidly coated by RPA. Subsequently, RPA is replaced by Rad51, which promotes ATP-dependent invasion of the template strand. A Holliday junction may then be generated, followed by branch migration and finally resolution of the Holliday junction.

Many proteins of the initial DDR and DNA repair thus, overlap or are implicated in both NHEJ and HR repair pathways. Among them are Mre11, BRCA1, H2AX, PARP-1, Rad18, DNA-PKcs, and ATM. Although NHEJ and HR factors are independently recruited to DSBs, pathway choice may be regulated by one or more proteins that act in both pathways [10]. The efficiency of the DNA damage repair processes determines the cellular outcome. Unrepaired or unsuccessful DNA damage

can lead to cell death. Incorrect repair, on the other hand, can lead to mutations and chromosomal aberrations **(Fig. 1. 3).**
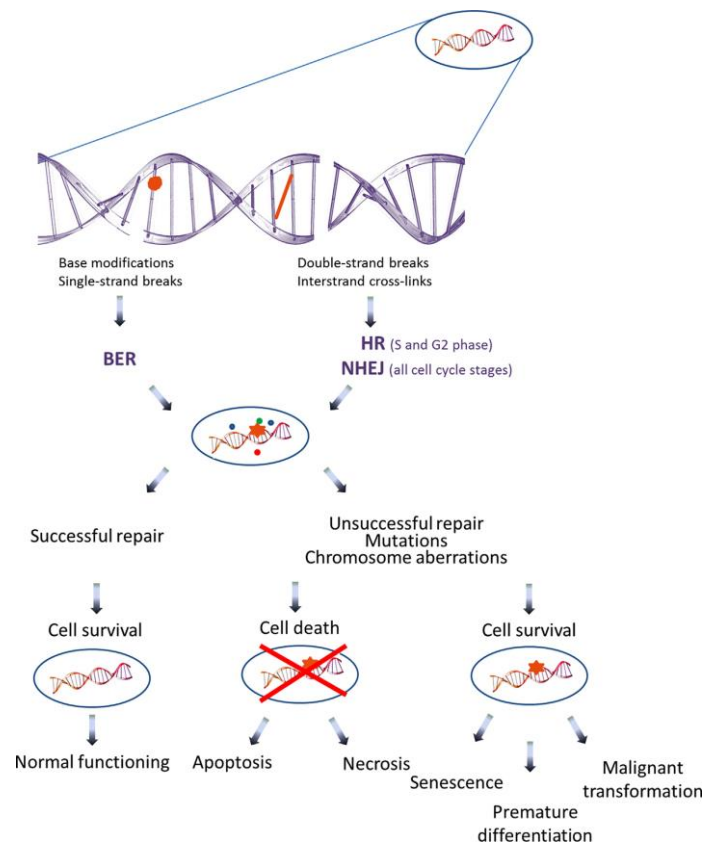
Fig. 1. 3. Radiation induced DNA damage and its related outcomes [11].

1.3.2 Apoptosis

When IR induced DNA lesions are unrepaired or the DNA repair is unsuccessful or if the genome integrity is irreparably compromised, the cell is forced to program itself to death termed as apoptosis. Apoptosis is considered a secondary response to DNA damage, with an aim to maintain genome integrity. Two main pathways of apoptosis are known: intrinsic pathway and extrinsic pathway. Most radiation induced apoptosis is mediated through intrinsic pathway.

1.4 Ionizing radiation induced oxidative stress

There are multiple endogenous and exogenous triggers that can lead to generation of free radicals in the cell. The mitochondrial electron transport chain and various intracellular enzymes like NADPH oxidase, myeloperoxidase etc., are the main generators of endogenous ROS. Radiation, certain drugs, cigarette smoke, heavy metals, pesticides are some of the major exogenous sources of ROS.

At low to moderate concentrations, the ROS molecules promote various physiological processes like cell growth, stress signalling, inflammation, apoptosis and gene expression. However, when steady state levels of ROS are enhanced or when there is an imbalance between the endogenous production of free radicals and the body's antioxidant defense mechanism, it leads to 'oxidative stress'. The oxidative stress can lead to oxidation of important cellular biomolecules like DNA, protein and lipids [12]. The cell contains several enzymatic and non-enzymatic antioxidants to maintain the steady state levels of ROS.

1.4.1 Enzymatic antioxidants

The key enzymatic antioxidants include superoxide dismutase (SOD), catalase (CAT), glutathione peroxidase (GPX) and thioredoxin reductase (TXNRD). These constitute the first line of defense against oxidative stress.

1.4.1.1 Superoxide dismutase (SOD): SOD catalyzes dismutation of superoxide radical into hydrogen peroxide (H_2O_2) and molecular oxygen (O_2).

$$2O_2^{\cdot -} + 2H^+ \xrightarrow{\quad SOD \quad} H_2O_2 + O_2$$

In eukaryotes three forms of SOD are known – SOD1 (Cu/Zn-SOD) found in cytosol, SOD2 (Mn-SOD) found in mitochondrial matrix and SOD3 (Cu/Zn-SOD) found in vascular extracellular space [13].

1.4.1.2 Catalase (CAT): CAT is a ubiquitous enzyme classified into two forms – a heme containing catalase and another non-heme or manganese containing catalase. CAT converts hydrogen peroxide into harmless water and oxygen molecule [14].

$$2H_2O_2 \xrightarrow{\text{CAT}} 2H_2O + O_2$$
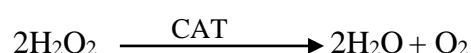
In the cell H_2O_2 can react with iron to produce harmful hydroxyl radical in a reaction termed as Fenton reaction as explained in the reactions below.

$$Fe^{2+} + H_2O_2 \longrightarrow Fe^{3+} + {}^{\bullet}OH + OH^{\bullet}$$

$$Fe^{3+} + H_2O_2 \longrightarrow Fe^{2+} + {}^{\bullet}OOH + H^+$$
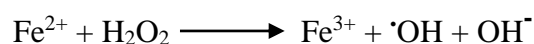
CAT thus, plays an important role in dismutation of highly damaging H_2O_2.

1.4.1.3 Glutathione peroxidase (GPX): Glutathione peroxidase (GPX) is a selenium dependent hydroperoxidase that converts glutathione (GSH) into oxidized glutathione (also called glutathione disulfide, GSSG). In the process, H_2O_2 is reduced to H_2O

$$2GSH + H_2O_2 \longrightarrow GSSG + 2H_2O$$
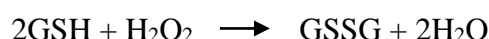
The GPX reaction is coupled to GR, which reduces oxidised GSH, i.e. GSSG with the help of NADPH to maintain reduced glutathione (GSH) levels. NADPH is then regenerated by Glucose-6-phosphate dehydrogenase (G-6-PDH) enzyme by reducing $NADP^+$ **(Fig. 1. 4).**

$$GSSG + NADPH + H^+ \longrightarrow 2GSH + NADP^+$$

$$O_2^{\cdot-} \xrightarrow{\textbf{SOD}} H_2O_2 \xrightarrow[\text{GSH} \quad \text{GSSG}]{\textbf{GPX}} H_2O$$

CAT → H_2O + O_2

GR

$NADP^+$ NADPH

G-6-PDH
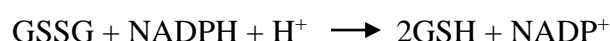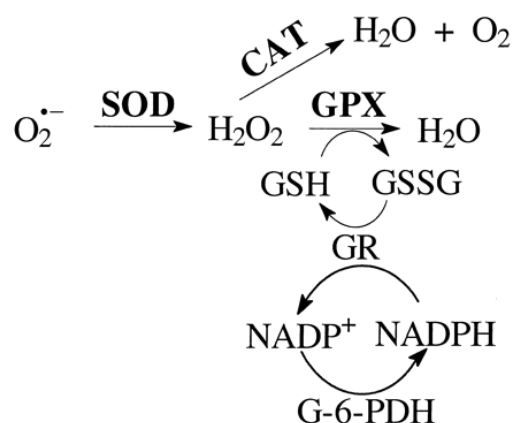
Fig. 1. 4. Detoxification of ROS molecules by antioxidant enzymes [15].

There are at least eight iosforms of GPX enzymes known in humans: GPX1 – GPX8 [16].

1.4.1.4 Thioredoxin reductase (TXNRD): Thioredoxin (TXN) is a class of small redox proteins (~12 kDa) that acts as antioxidants by facilitating reduction of oxidised proteins by cysteine thiol-disulphide exchange. TXNs are kept in reduced form by a selenoenzyme and NADPH dependent flavoprotein thioredoxin reductase (TXNRD) **(Fig. 1. 5).** TXNRD, TXN and NAPDH together form thioredoxin based antioxidant system. In humans, three types of thioredoxin reductase are found: TXNRD1 (cytosolic), TXNRD2 (mitochondrial) and TXNRD3 (testis specific). TXN is required as a reducing agent by the thiol-based antioxidant enzyme Peroxiredoxin (PRDX, a family of peroxidases) that catalyses dismutation of H_2O_2 into H_2O. PRDX1 is induced in macrophages by oxidized low-density lipoprotein and functions not only as an antioxidant and a reducer of ROS, but also activates p38 MAPK and enhances cell survival [17]. PRDX2 blocks H_2O_2 and TNF-α-induced upregulation of Nuclear factor kappa-light-chain-enhancer of B cells (NF-κB) [17].
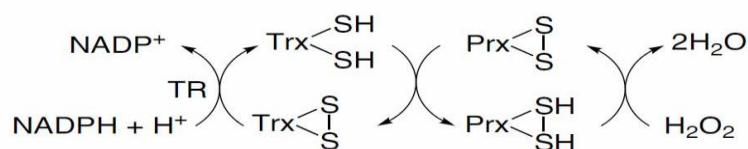
Fig. 1. 5. Thioredoxin based antioxidant mechanism. TR: TXNRD

1.4.2 Non-enzymatic antioxidants

The most abundant non-enzymatic endogenous antioxidant in the cell is Glutathione (GSH). It is generally present in its reduced form (GSH), and can donate an electron to oxidise molecules and neutralize them. Ratio of GSH and its oxidised counterpart glutathione (GSSG) is a widely used indicator to study oxidative stress in the cell [18].

The other prominent non-enzymatic antioxidants which scavenge free radicals in the cell are ascorbate (vitamin C) [19] and vitamin E [20].

Ionizing radiation is an important exogenous source of cellular oxidative stress.

1.4.3 Activation of redox specific transcription factors

Upon radiation stress, consequences like cell death and survival are determined through activation of several transcription factors. Among these are the two key transcription factors, Nuclear factor kappa-light-chain-enhancer of B cells (NF-κB) and NF-E2-related factor 2 (Nrf2) which regulate transcription and cell survival in response to oxidative stress.

1.4.3.1 Nuclear factor kappa-light-chain-enhancer of B cells (NF-κB) was initially identified as a DNA binding protein in activated B cells. The NF-κB family in mammals consists of five related members: p50, p52, RelA (p65), RelB and c-Rel.

The Rel/NF-κB family of molecules forms homodimers and heterodimers. Under normal conditions, NF-κB is sequestered in the cytoplasm by the inhibitory proteins named as IκBs (Inhibitor of kappa B), which include IκBα, IκBβ, IκBε, and Bcl-3, p100 and p105. These inhibitory proteins mask the nuclear localization signal of NF-κB, thus keeping it in inactive state in the cytoplasm.

During oxidative stress or in response to stimuli, IκBα protein is rapidly phosphorylated by IκB kinase complex (IKK) on Ser 32 and Ser 36, ubiquitinated and subsequently degraded by the 26s proteasome [21]. Free NF-κB then translocates into the nucleus to bind to the consensus sequence in the promoter/enhancer region of target genes. NF-κB plays a vital role in antioxidant responses, inflammatory response, anti-apoptosis function and cell survival [21].

The target genes of NF-κB transcription factor includes enzymes involved in antioxidant response such as MnSOD, CuSOD, ferritin heavy chain (FHC), TXN1, TXN2), NADPH quinine oxidoreductase 1 (NQO1) and, Glutathione S-transferase (GST) [22]. Enhanced cell death and diminished expression of MnSOD was observed when IR induced activation of NF-κB was blocked indicating important role of NF-κB in cell survival [23].

1.4.3.2 Nuclear factor erythroid-2-related factor 2 (Nrf2), a 66-kDa protein was first isolated from hypersensitive site 2 located in the beta-globin locus control region. Like NF-κB, Nrf2 also is a major regulator of genes involved in antioxidant response and cell survival. Under homeostatic conditions, Nrf2 is sequestered in the cytoplasm by Kelch like ECH associated protein 1 (KEAP1), a cysteine-rich protein which acts as an adaptor for a Cul3-based E3 ubiquitin ligase complex that promotes ubiquitination and subsequent proteasome mediated degradation of Nrf2. During

oxidative stress, cysteine residues in the Keap1 protein are oxidised, because of which it loses its E3 ubiquitin ligase activity and hence, cannot degrade Nrf2. Then, Nrf2 is released from KEAP1 and rapidly translocates into the nucleus [24]. In the nucleus, it heterodimerizes with small Maf proteins and activates target genes for cytoprotection by binding to antioxidant response element (ARE) on DNA [25].

Downstream target genes of Nrf2 include NADPH quinine oxidoreductase 1 (NQO1), alcohol dehydrogenase (ADH), aldehyde dehydrogenase (ALDH), cytochrome P450s (CYPs), superoxide dismutase (SOD), glutathione peroxidase (GPX), glutathione reductase (GR) and many more [26]. Elevated ROS levels leading to increased DNA damage and tumorigenesis in absence of Nrf2 has been reported [27], indicating importance of antioxidant activity of Nrf2. Activation of Nrf2 has been shown to reduce intracellular ROS levels in fibroblasts [28], bronchial and breast epithelial cells [29], and squamous lung cancer cells [30].

1.5 Mitogen-Activated Protein Kinase signaling

Mitogen-Activated Protein Kinase (MAPK) is activated in response to various stimulants like growth factors, hormones, cytokines, and external stress like radiation. MAPKs belong to serine/threonine kinase family and follow a triple kinase cascade. Three different types of MAPKs are known in humans: ERK1/2 (extracellular signal regulated kinase), JNK/SAPK (c-Jun N-terminal kinase/stress-activated protein kinases) and p38 MAPK. ERK has been more often related with activation by growth factors, leading to proliferation and survival, while JNK and p38 have been shown to be induced by stress responses and cytokines, and can mediate differentiation and cell death [31]. Ionizing radiation, however, is known to activate all three MAPK either

leading to cell proliferation or cell death depending upon the cell type [32–34]. Besides this, MAPK pathways are also known to be activated by ROS [35].

1.6 Dose-response models for assessment of radiation risk

Estimation of radiation risk in humans has been derived from epidemiological studies on atomic bomb survivors of Hiroshima and Nagasaki, studies on individuals with exposures from medical or environmental sources, and occupational radiation workers [36–39].

These epidemiological studies provide convincing evidence about health effects of radiation at high doses (>100 mGy). However, at lower doses (<100 mGy) even the largest epidemiological studies have insufficient statistical power. Thus, we have to rely on mathematical extrapolations from estimates made at higher doses.

Many dose-response models have been proposed to estimate radiation risks at low doses. These range from hormesis model (protective at very low doses) to dose threshold model (no risk until a certain dose is reached) to a linear model without threshold. Among these, the linear no threshold model (LNT) remains the most widely accepted by radiation protection agencies worldwide **(Fig. 1. 6).**

1.7 Non-targeted effects of ionizing radiation

Over the last two decades, new evidences have emerged in radiation biology that challenges the validity of LNT model. Several new findings have shown that cells respond differentially, qualitatively and quantitatively, to radiation at low and high doses. There is also increasing evidence that unique biological processes dominate radiation effects at low doses compared to high doses [40]. These include

17

non-targeted effects (NTEs) like adaptive response, bystander effects, genomic instability and low dose hypersensitivity [41–43]. Both protective as well as deleterious responses of NTEs have been demonstrated in various biological models [44,45]. The NTEs are inherently non-linear responses and thus, considered very important in the low-dose region of the survival curve.

Despite extensive research, major gaps still exist in our understanding of the likely mechanisms of NTEs and their relevance to human health. There is also a lack of general consensus on their impact on human radiation protection principles and practices.
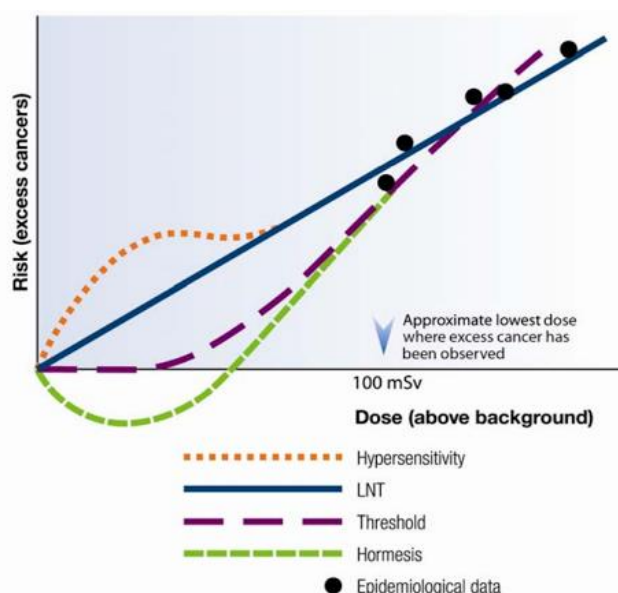
Fig. 1. 6. Different models for health risk from exposure to low doses of IR (Adapted from: Canadian Nuclear Safety Commission, 2013, www.nuclearsafety.gc.ca).

1.8 Radiation-induced adaptive response

Since the origin of earth, living organisms have evolved and adapted to reduce the harmful impact of different stresses, including radiation. Radiation induced-adaptive response (RI-AR) is defined as a phenomenon induced by relatively low 'priming' or 'adaptive' dose of radiation that protects cells against deleterious effects

18

due to subsequent high 'challenge' dos**e** of radiation. This induction of resistance is a conserved response that appeared early in evolution and has subsequently been observed in all forms of life from single-cell prokaryotes and eukaryotes to multicellular organisms [46].

Earliest evidence of adaptive response was reported by Mitchel and Morrison (1984) in *Saccharomyces cerevisiae* where prior exposure to sublethal dose of γ-radiation induced resistance against a subsequently higher dose of γ-radiation [47]. The induction of adaptive response to IR in human cells was first demonstrated by Olivieri *et al* (1984) [48]. The authors showed that human lymphocytes labelled with radioactive thymidine when exposed to a high dose of 1.5 Gy x-rays showed lesser chromosome aberrations as compared to the unlabelled cells exposed only to 1.5 Gy x-rays. Subsequently, RI-AR has been demonstrated in various cell systems and animal models, both *in vitro* and *in vivo* using various indicators of cellular damage, such as cell lethality, chromosomal aberrations, micronuclei induction, mutation induction, DNA damage and altered gene/protein expressions [49–52].

On the other hand, Shadley *et al* (1987), Wang *et al* (1991), Hain *et al* (1992), Mortazavi *et al* (2003) and Joksic and Petrovic (2004) reported lack of adaptive response in pre-irradiated lymphocytes [53–57]. Others reported lack of radioadaptive response in cultured human lymphocytes [55,58]. Conflicting reports are found in the literature regarding the induction of AR in the G_0 phase of the cell cycle in human lymphocytes. Many reports suggest that cells need to be in the sensitive 'S' phase of cell cycle to show AR [59]. On the other hand, there were a few studies which showed AR in G_0 lymphocytes irradiated *in vitro* [50,60–62].

Several studies have demonstrated RI-AR in individuals exposed to occupational or environmental sources. Lymphocytes isolated from hospital workers occupationally exposed to x-rays and γ-rays showed lower frequency of dicentrics after *in vivo* irradiation of 2 Gy than the lymphocytes from unexposed individuals [63]. In a similar study, peripheral blood lymphocytes isolated from 41 temporary nuclear plant workers when challenged with an *in vitro* dose of 3.5 Gy ^{60}Co γ-rays showed significantly smaller numbers of micronuclei as compared lymphocytes from non-exposed individuals [64]. In another study, micronuclei frequency was found to be lower in the radiation worker group as compared to control group when exposed with a challenge dose of 1 and 2 Gy [65].

Similar results have been obtained in individuals residing in several high level natural radiation areas (HLNRAs) of the world like Kerala, India and Ramsar, Iran. Human PBMCs (Peripheral blood mononuclear cells) isolated from individuals residing in HLNRA of Kerala, India, when challenged with a high dose radiation showed adaptive response for induction of micronuclei, DNA strand breaks and several radiation-responsive proteins as compared to individuals from NLNRA (normal level natural radiation areas) [52,62,66,67]. The peripheral blood samples from individuals residing in HLNRA of Ramsar, Iran also showed lower induction of micronuclei frequency and chromosome aberrations when challenged with a high dose, as compared to subjects from control areas [49,68,69]. On the other hand, challenge dose exposure to lymphocytes from children chronically exposed to radiation doses from Chernobyl accident fallout elicited no radioadaptive response when measured with chromosome and chromatid aberrations [70].

Few evidences also exist for cross-adaptive response where low levels of stressors other than IR, like other type of radiation and chemicals or heat, can also

induce RI-AR. Irradiation of mouse CH310T(1/2) fibroblast cells with low dose γ irradiation resulted in adaptive response against subsequent exposure to micro-beam α-particle radiation [71]. Similarly, human lymphocytes showed adaptive response to challenge dose of 0.25 Gy neutron [252]Cf radiation when primed with 0.01 Gy [137]Cs γ-rays [61]. Non-ionizing (radiofrequency) radiation also has been showed to induce RI-AR in combination with mitomycin C and x-rays in human [72] and ionizing radiation (γ-rays) in mice PBMCs [73]. Cross-resistance between IR and chemical mutagens is also reported [74–77].

1.8.1 Dose thresholds and time window for RI-AR

The regime of RI-AR includes exposure of cells first to a low dose named as 'priming dose' (PD). After an adaptive window of few hours, cells are then exposed to a subsequently high dose named as 'challenge dose' (CD). Shadley and Wiencke (1989) measured chromatid deletions in human lymphocytes with two priming doses - 10 mGy and 500 mGy of x-rays [78]. They found that lower dose of 10 mGy offered protection against the effects of a 1.5 Gy challenge dose but not 500 mGy, suggesting an upper dose threshold for RI-AR. However, their study also showed that priming dose of 500 mGy delivered at a dose rate < 10 mGy/min could still induce an adaptive response against the 1.5 Gy challenge dose, Many other studies reported similar observation with priming dose in the range of 1-100 mGy and with lower dose rates [53,60,74,79].

Like upper dose thresholds, available data also indicates existence of lower dose thresholds for adaptive response. Wolff *et al* (1988) reported protection of human lymphocytes with x-rays doses as low as 10 mGy against chromosome breaks induced by various chemical mutagens and cross-linking agents [74]. Recent work by

Nishad and Ghosh (2018) showed evidence of adaptive response in human PBMCs exposed to continuous low dose exposures in the range 15.60 ± 3.04 mGy/y, indicating that the lower dose limit for RI-AR was below this dose [52]. For the challenge dose, most studies report an adaptive response in the range 2 – 6 Gy [50,52,62,80]. Various studies have also shown that induction of AR is not immediate but takes 4-6 hours to become fully active [53,54,81]. Thus, the biological responses induced by RI-AR are dependent on four critical parameters (i) priming dose, (ii) adaptive window, (iii) challenge dose and (iv) dose rate.

1.8.2 Postulated mechanisms of RI-AR

Little is currently known about the precise molecular mechanisms of RI-AR. Most postulated mechanisms are also part of general defense system against various other biotic and abiotic stresses **(Fig. 1. 7).** Many reports suggest that the induction of adaptive response occurs via IR-induced ROS [82–85]. Experiments with inhibitors like 3-aminobenzamide and cycloheximide indicate a role for repair enzymes like poly-ADP-ribose polymerase-1 (PARP1) and protein synthesis in adaptive response [75,81,86]. Various other mechanisms like activation of cell signalling, apoptosis, gene transcription, induction of new proteins, and antioxidant responses have been postulated to be involved in RI-AR [87].
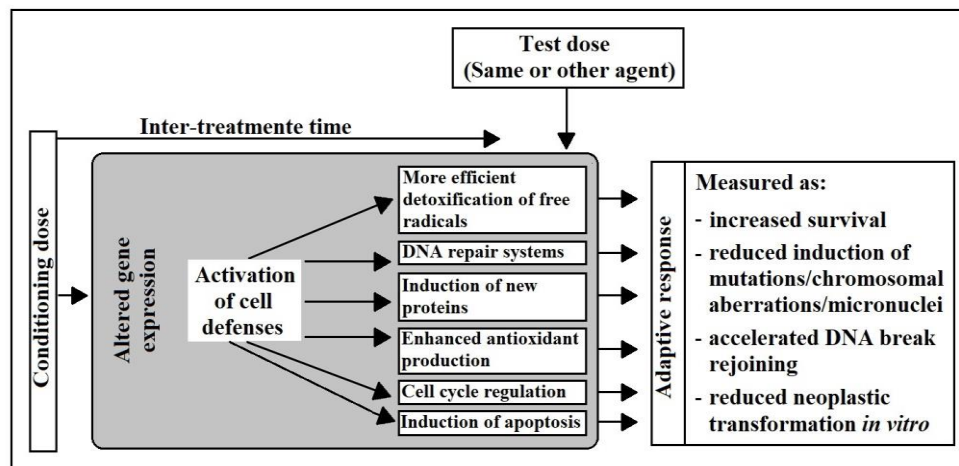
Fig. 1. 7. Postulated mechanisms for adaptive response to general stressors (Adapted from: Dimova *et al* 2008 [87]).

1.9 Radiation Proteomics

The term "proteome" describes the entire protein complement expressed by a genome or a tissue at a given time [88]. Proteomics aims to first identify and characterize all proteins expressed by genomes and subsequently describe different pathways and networks to decipher the functional significance of proteins.

The proteome is neither as uniform nor as static as the genome. Proteins are continually being synthesized, modified, and degraded in a cell. Moreover, the protein expression profile is not only cell-type, developmental stage or tissue specific but also dependent on what signals the cell receives from its environment. Proteomics thus, not only provides insight into the ability of cells to respond to changes in cellular state e.g. differentiation, oncogenesis, inflammation etc. but also the preparedness of cell to respond to changes in external stimuli like temperature, radiation, hypoxia, apoptosis signals, disease states etc.

The proteome is much more complex than genome and transcriptome. This is because one gene does not essentially produces one protein. Variations in proteins

occur due to one of the RNA processing mechanism known as alternate splicing, where one gene can produce multiple proteins. Other mechanism which adds to complexity of proteome are the post-translational modifications (PTMs) of the proteins. More than 200 different PTMs are known [89]. While the number of genes encoding protein in human genome is ~ 21,000 [90], the total number of human protein products, including proteins arising from splice variants and essential PTMs, have been found to be approximately 1 million [91,92]. Hence, studying proteins can allow greater understanding of the complexity of cell than the study of genome alone.

Traditionally, researchers study proteins individually one by one. However, proteomics allows study of several proteins at a single time. Simultaneously, comparison of two proteomes can be performed to find differentially expressed proteins. This approach is useful in diagnosis, biomarker discovery and drug designing. Characterization of PTMs on proteins, understanding protein-protein interactions, generating a 3D proteome map marking cellular localization of different proteins are few important applications of proteomics.

Quantitative proteomics that help to detect absolute or relative small changes in protein or peptide abundance in response to changes in cellular state are performed using gel-based (two-dimensional electrophoresis) and gel-free (label-based or label-free) techniques [93]. Each technique has its own advantages and pitfalls and a combination of these may provide a better coverage of the cell proteome.

1.10 Gel based quantitative proteomics

The most widely used gel based quantitative proteomics platforms are the two-dimensional gel electrophoresis (2-DE) and the two-dimensional difference gel electrophoresis (2D-DIGE).

1.10.1 Two-Dimensional Gel Electrophoresis (2-DE)

Two-dimensional gel electrophoresis (2-DE) also known as 2D-PAGE (polyacrylamide gel electrophoresis) is the most widely used technique for proteomics. Here, the separation of proteins is based on two different physicochemical properties and in two different dimensions. In the first dimension, the complex mixture of proteins is separated based on their net charge or pI value using isoelectric focussing (IEF). In the second dimension, proteins are separated based on their molecular weight through sodium dodecyl sulfate polyacrylamide gel electrophoresis (SDS-PAGE). For IEF commercially available immobilized pH gradient strips (IPG) with different pH ranges within a single strip are used. When electric potential is applied across the IPG strip, positively charged proteins move towards negative end of the gel and vice-versa. At its isoelectric point, the point where net charge on protein is zero, protein stops moving and focuses into a sharp band on the strip. Carrier ampholytes, a mixture of low molecular weight molecules with zwitterionic character, are included in the sample buffer to overcome protein precipitation. The IPG strip is then subjected to reduction and alkylation in a process called as equilibration and placed on SDS-PAGE gel. In presence of electric field, the charged proteins move from the IPG strip into the gel. **Fig. 1. 8** represents a schematic diagram of 2-DE.

The separated proteins are visualized as distinct spots by in-gel staining with various agents like coomassie brilliant blue (CBB), silver stain or SYPRO Ruby. Each protein appears as distinct spot on the gel after staining. CBB has a detection limit of about 10 ng protein/spot while silver stain and SYPRO Ruby can detect ~1 ng protein/spot.

Various commercially available softwares e.g. PDQuest 2-D (Bio-Rad, CA, USA), ImageMaster 2D Platinum (GE Healthcare, Uppsala, Sweden), Delta2D (DECODON, GmbH, Germany), Melanie (GeneBio, GE, Switzerland), Progenesis same spots (Nonlinear Dynamics, Waters, NC, UK) etc. are used for image analysis. Once the differentially regulated protein spots are identified, spots are picked either manually or by a robotic arm. The identification of proteins is then performed using mass spectrometry (MS). In MS, molecules are first converted into gaseous ions. These ions are then separated according to mass/charge ratio under high vacuum and detected in proportion of their abundance. Result is displayed as a mass spectrum which is a plot of ion abundance versus mass/charge ratio. Ions provide information regarding the nature and the structure of their precursor molecule.
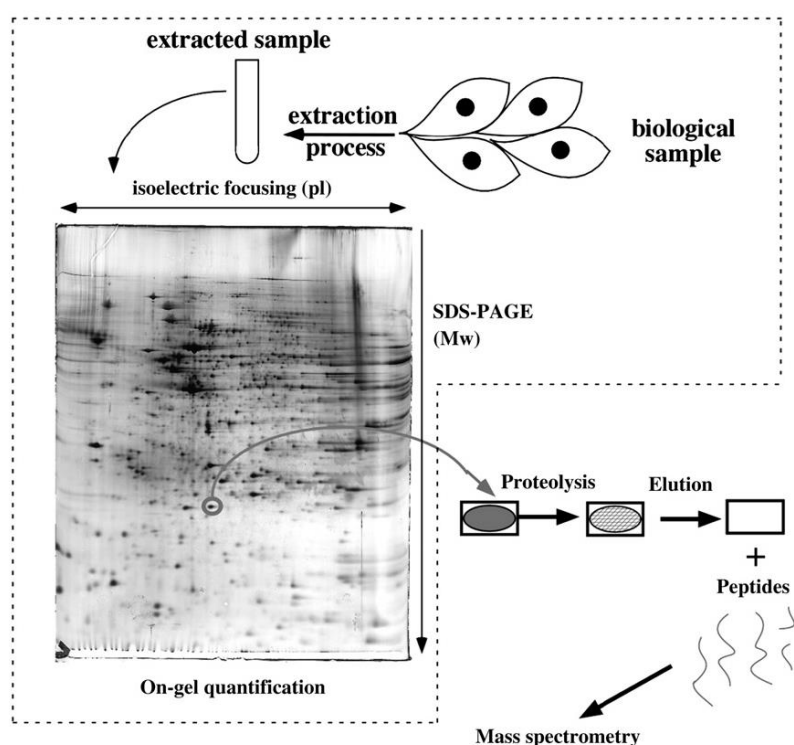
Fig. 1. 8. Scheme of 2-dimensional gel electrophoresis (Adapted from: Rabilloud and Lelong 2011 [94]).

1.10.2 Two-dimensional difference gel electrophoresis (2D - DIGE)

2D - DIGE is an advanced form of 2-DE which allows separation of two or more samples in a single gel using differential fluorescence tags. Here, small quantities of protein samples from different treatment groups are labelled with fluorescent cyanine dyes (CyDyes) – Cy2, Cy3 and Cy5. CyDyes are spectrally distinct, resolvable and photostable molecules. They contain a NHS ester active group, which covalently binds to the lysine residue of a protein via an amide linkage. All the three CyDyes have similar mass and charge and co-migrate to the same position on 2-DE gel. This thus, enables co-separation of different protein samples on a single gel minimizing gel-to-gel variations. An internal standard, usually labelled with Cy2 dye, is used to reduce further inter-gel variations and allow easier matching between repetitive gels. A flow chart for 2D-DIGE is illustrated in **Fig. 1. 9**.
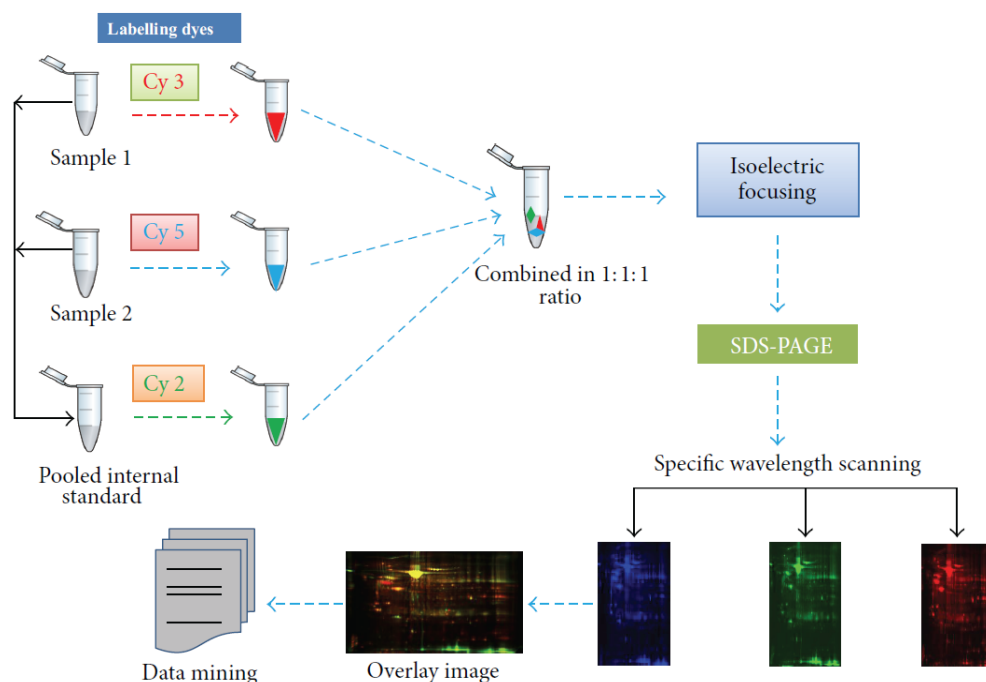
Fig. 1. 9. Steps involved in 2D-DIGE (Adapted from: Paul *et al* 2013 [95])

1.10.3 Relevance of gel-based proteomics

2D-DIGE helps to overcome several limitations of 2-DE like requirement of large sample amount, gel-to-gel variations and the necessity of running multiple gels for each sample (reviewed in [96]). In addition, the sensitivity of 2D-DIGE minimal labeling is unparalleled since it can detect as low as 0.1 ng of protein per 2D spot, though labelling of lysine and cysteine acids limit the protein coverage on gels. Also, manual excision of protein spots for identification with mass spectrometry is difficult. Both 2-DE and 2D-DIGE are highly labour-intensive techniques and does not resolve well the low abundance, highly acidic, basis, hydrophobic and membrane proteins. However, 2-DE and 2D-DIGE are still considered the heart of proteomics and provide a robust snapshot of total cellular proteins along with their PTMs.

1.11 Gel free quantitative proteomics

The gel-free quantitative proteomics or the shotgun proteomic approach uses liquid chromatography (LC) coupled to tandem mass spectrometry (MS) to separate and identify the peptides obtained from the enzymatic digest of an entire protein extract.

Several gel-free based proteomics technologies are now known which allow high-throughput profiling and help overcome coverage limitations of 2-DE. These include label based and label-free approaches.

1.11.1 Labeling-based quantification

The label-based methods rely on the labeling of samples with stable-isotope or isobar tags followed by quantitative analysis in a mass spectrometer. The labels are introduced into proteins or peptides either using metabolic labeling or chemical

isotope tags. Both labeled and unlabelled peptides show the same chromatographic and ionization properties but can be characterized from each other by a mass-shift signature. In metabolic labeling, labeled isotopic or heavy amino acids (^{13}C- arginine, ^{15}N-lysine) are introduced into cellular proteins through the growth medium, while in chemical labeling, isotopic or isobaric tags are introduced into the cellular proteins through a chemical reaction. Chemical labeling offers several advantages over metabolic labeling, such as high labeling efficiency due to covalent linkage with target proteins. This has high relevance for clinical applications as it can be used to label any protein sample derived from multiple sources such as cells, tissue samples or biological fluids. The most popular metabolic proteomic quantitative technique is SILAC (Stable Isotopic Labeling of Amino Acids in Cell Culture) method [97,98]. The major chemical labeling methods used for quantification include isotopic (ICAT: Isotope-Coded Affinity Tags) [98,99] and isobaric (iTRAQ: Isobaric Tags for Relative and Absolute Quantification; TMT: Tandem mass tag) [98,100,101] approaches. Label based techniques are considered time consuming and suffer from few limitations like high cost of labelling reagents, additional steps for sample processing leading to loss of sample and variable labelling efficiency.

1.11.2 Label-free quantification

Label-free method offers a rapid and low-cost alternative to other quantitative proteomic approaches. It can be used for both relative and absolute quantitation and are ideal for large-sample analyses in clinical screening or biomarker discovery experiments with all type of biological (cells, tissues and biological fluids) samples.

Here, label-free samples are separately collected, prepared and analyzed with LC based tandem MS methods. Due to this, label-free quantitation experiments need

to be more rigorously controlled for any experimental variations than the stable isotope methods. Protein quantitation is performed using either ion peak intensity or spectral counting. In spectral counting, numbers of fragment ion spectra (MS/MS) of each protein in multiple runs of different samples are compared to obtain relative abundance. In the second method, peak intensity or chromatographic peak area of peptide precursor ions from different samples is measured and compared to obtain relative abundance [102]. For relative quantitation, direct MS m/z values for all ions are detected and their signal intensities at a particular time recorded. Each detected ion generates a monoisotopic mass peak. Chromatographic peaks of identified peptides are extracted and aligned with peaks from other samples **(Fig. 1. 10).** After alignment, peak intensities or area under curve (AUC) for each peak is computed. AUC values are then compared to calculate relative protein abundance. There is a strong correlation between the signal intensity from electrospray ionization and ion concentration, and therefore the relative peptide levels between samples can be determined directly from these peak intensities [101].

The label-free method has been found to be more error prone as comparison only between similar ions is required to calculate relative abundance. Also, this technique is replicate dependent. However, it allows quantification of all peptides in the sample unlike the labelled techniques where only labelled peptides are detected.
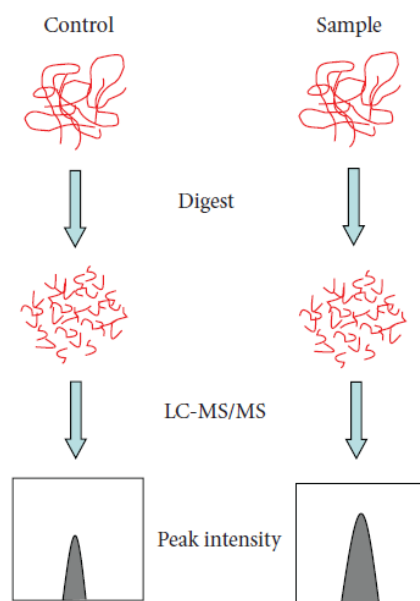
Fig. 1. 10. Label-free quantification of proteins (Adapted from: Zhu *et al* 2010 [102]).

1.12 Cellular system used in this study: Peripheral blood mononuclear cells (PBMCs)

PBMCs are considered an excellent cell type to be used for human studies. These form an important part of the humoral immune system and can be obtained readily from human blood with minimal invasive method. They also show low inter-individual variation as compared to other biofluids. Also, since PBMCs are G_0 non-proliferating cells, their biological responses are considered closer to the *in vivo* system. They are considered to be highly radiosensitive and therefore, can be used as sensitive indices of radiation induced molecular events.

1.13 Objectives of the thesis

There is inherent variability in cellular responses to low-dose radiation exposure. Recent data on the non-targeted effects of radiation, including radiation induced adaptive response (RI-AR), further add to the uncertainties about the

magnitude of risk at these low doses. Evidences for various mechanisms that might be responsible for effects such as RI-AR remain sketchy and have not been tested in a singular cell system. This work therefore, proposed to study complete chain of molecular processes modulated during RI-AR in PBMCs derived from the same set of human samples.

The specific objectives of the thesis are:

1. Detection of DNA strand breaks in Peripheral Blood Mononuclear Cells (PBMCs) under radioadaptive conditions.

2. Identification and characterization of differentially modulated proteins in human PBMCs under radioadaptive conditions.

3. Understanding the molecular mechanisms of radioadaptive response in human PBMCs.

CHAPTER 2

MATERIALS AND METHODS

2.1 Collection of blood samples

Peripheral blood was drawn from seven random adults (coded from S1 to S7) by venepuncture in EDTA vacutainer tubes (Becton Dickinson, Mountain View, CA, USA). The blood sample in tubes was mixed well to prevent coagulation. Samples were processed within 30 min of withdrawal. This work was approved by Medical Ethics Committee, Bhabha Atomic Research Centre, Mumbai. A minimum 15-day gap between two withdrawals was maintained for repeat collection of blood from the same individual. All subjects were informed of the objectives of the study and their consent was taken before blood withdrawal. All the donors were non-smoker healthy volunteers in the age group 22-35 years from Mumbai (India) region and had similar lifestyles.

2.2 Isolation of peripheral blood mononuclear cells

Human PBMCs were isolated by density gradient centrifugation using Histopaque-1077 (Sigma-Aldrich Corp MO, USA) according to the manufacturer's instructions. The Histopaque solution was removed from 4°C and transferred to a 15 ml sterile conical polypropylene centrifuge tube under aseptic conditions using a sterile Pasteur pipette. To prevent clumping of cells during separation, the Histopaque solution in the centrifuge tube was cooled down to room temperature (RT). An equal volume of blood sample was layered carefully on the Histopaque solution using a sterile Pasteur pipette. Mixing of the blood sample with Histopaque medium while layering was avoided as it may not lead to separation of PBMCs as a sharp band in the gradient. Centrifugation was carried out at 3000 rpm for 30 min at RT. To prevent the disruption of the gradients formed, centrifugation was performed without applying brake at the end. After centrifugation, the upper layer containing plasma and

platelets was removed using a Pasteur pipette and discarded in 0.1% Sodium hypochlorite solution. The next opaque interface layer (also called as a buffy layer) containing PBMCs **(Fig. 2. 1)** was carefully aspirated and transferred to a sterile 15 ml conical centrifuge tube kept on ice. The cells were then mixed gently with 4 to 5 volumes of isotonic phosphate buffered saline (PBS) and centrifuged at 1600 rpm for 10 min at RT to remove Histopaque medium, plasma, and platelets. The cells were washed once again with isotonic PBS at 800 rpm for 10 min. The cells were then suspended in complete Roswell Park Memorial Institute (RPMI)-1640 medium supplemented with 10% heat-inactivated fetal calf serum, 100 U/ml penicillin and 100 mg/ml streptomycin.
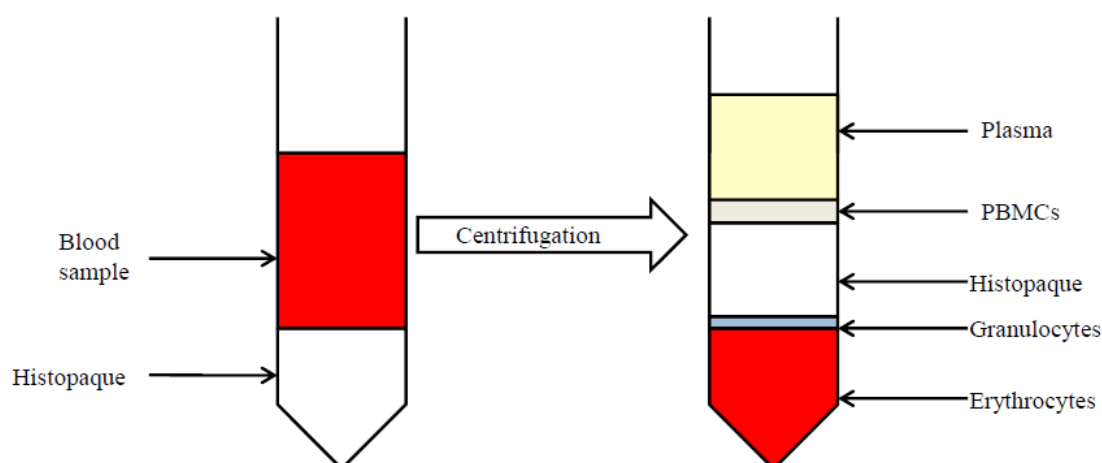
Fig. 2. 1. Isolation of PBMCs from human blood sample using density gradient centrifugation.

2.3 Trypan blue dye exclusion assay

Trypan blue dye exclusion assay was used to assess cell viability. Trypan blue is a diazo dye that selectively penetrates cell membrane of dead cells, staining them blue. Live cells however, possess intact cell membranes that exclude the dye. Cell suspension was mixed with 0.4% trypan blue solution in equal volume and 10 µl of

this was filled on one side of hemocytometer counter with the cover slip already in place. Hemocytometer was then placed on the stage of inverted bright field microscope (Carl Zeiss, AG, Switzerland). Total cells from the four outer and one middle square were counted under 100X magnification and average number of cells were calculated. A separate count of dead cells observed was maintained simultaneously. Viability index was calculated as (Number of live cells in treatment/Number of live cells in control) x 100.

2.4 Irradiation of PBMCs

Irradiation was done at RT using a ^{60}Co γ-ray source (Blood Irradiator, 2000, BRIT, India) at a dose rate of 0.3 Gy/min. In this study, RI-AR was established using a low PD of 100 mGy and a subsequent high CD of 2 Gy. Adaptive window was set to 4 h. Cells were placed in ice before and soon after irradiation. For irradiation, PBMCs were suspended in 1X PBS and were equally divided into 4 different groups (number of cells per group was different for each assay and has been specified in the text). The first group of cells were sham irradiated which served as the experimental control (set I). The second group was irradiated only with a low dose of 100 mGy to study low dose effects (set II). The third group was sham irradiated along with first group of cells, then incubated for 4 hours at 37ºC before irradiation with a high CD of 2 Gy, hereafter these cells were referred to as 'non-primed cells' (set III). The cells from the fourth group were first irradiated with a PD of 100 mGy, incubated for 4 hours at 37ºC and were then irradiated with a CD of 2 Gy, hereafter these cells were referred to as the 'primed cells' (set IV). After irradiation, cells were processed either within 5 min (henceforth, referred to as 0 min time point) or were incubated in

complete RPMI-1640 media at 37ºC in a humidified 5% CO_2 atmosphere for the required time, as specified for different assays.

2.5 Phytohemagglutinin (PHA) induced proliferation of human PBMCs

After irradiation, PBMCs (0.5×10^6) from each treatment group were cultured in complete RPMI-1640 medium for 24 and 72 h either in absence or presence of 10µg/ml PHA in a 24 well plate at 37°C in a humidified 5% CO_2 atmosphere. In case of non-primed and primed cells, PHA was added immediately after exposure to CD.

2.6 Alkaline comet assay

Alkaline single-cell gel electrophoresis (comet) assay was performed as described by [103], with few modifications. For this, clean glass slides (75mm x 25mm, Blue star, MU India) were pre-coated with 1% normal agarose prepared in 0.9% saline. A cell suspension containing 2.5×10^4 cells in 50 µl was mixed with 400µl of warm 0.8% low melting agarose prepared in 0.9% saline and spread on the pre-coated glass slides. A coverslip (60 mm x 24 mm, HiMedia, MU, India) was placed on the slide to ensure even spread of the agarose and allowed to solidify for 5 min at 4ºC. The slides were then immersed in chilled lysis solution (2.5 M NaCl, 100 mM $Na_2.EDTA$, 1% Triton X-100, 10% DMSO and 10 mM Tris pH 10) for 1 h at 4°C. After lysis, slides were subjected to DNA unwinding and expression of alkali-labile sites for 20 min in ice-cold electrophoresis buffer (300 mM NaOH, 1 mM $Na_2.EDTA$, pH 13). Electrophoresis was carried out at 25 V, 300 mA for 30 min at ~1.4 V/cm. Following electrophoresis, slides were dipped in neutralizing buffer (0.4 M Tris HCl, pH 7.5) for 5 min and stored in a wet chamber at 4°C until imaging. For visualization, slides were stained with SYBR Green II (Sigma-Aldrich Corp. MO,

USA) solution at a concentration of 1:10,000 in TE buffer (10 mM Tris HCl, 1 mM EDTA, pH 7.5). All chemicals used for comet assay were from Sigma-Aldrich Corp. MO, USA. For each dose point, duplicate slides were prepared. Fifty cells from duplicate slides of each dose point were examined randomly using a fluorescence microscope (Carl Zeiss, AG, Switzerland) equipped with a 3CCD camera (Sony Corp. MI, Japan) at a magnification of 400x. Images were analyzed using Comet Assay Software Project (CASP) software [104]. The extent of DNA damage was measured quantitatively and expressed as % DNA in the comet tail. Basal damage was defined as damage in the sham irradiated cells.

2.7 Immunofluorescence of phospho-histone H2AX foci

PBMCs ($0.1x10^6$) were allowed to adhere on poly L-lysine coated coverslips (12 mm round Corning^{TM} NY USA) for 1 h and irradiated as explained above. The cells were fixed immediately after irradiation using 4% paraformaldehyde for 20 min, washed twice with 1X PBS and permeabilized with 0.5% Triton X-100/PBS for 3 min. For immunodetection, cells were blocked with 5% bovine serum albumin (BSA) for 1 h followed by incubation with rabbit anti γH2Ax (S139) antibody (#2577S Cell Signaling Technology Inc. MA, USA) at 1:100 dilution for 2 h and visualized with Alexa Fluor 488 goat anti-rabbit IgG secondary antibody (#7074 Cell Signaling Technology Inc. MA, USA) at 1:200 dilution. Coverslips were mounted on a microscopic glass slide using ProLong Gold antifade mounting media containing DNA-intercalating agent 4′,6-diamidino-2-phenylindol dihydrochloride (DAPI) for detection of nuclear DNA (#P36935 Molecular Probes, OR, USA). Images were captured with an epifluorescence microscope (Carl Zeiss, AG, Switzerland). For each

dose/time point, coverslips were made in triplicate and foci from 30 cells of each coverslip were counted.

2.8 Mitochondrial membrane potential (MMP) assay

A dual emission dye 5,50,6,60-tetrachloro-1,10,3,30-tetraethylbenzimidazolylcarbocyanine iodide (JC-1) was used to measure radiation induced change in MMP ($\Delta\Psi$m). In the cells with healthy mitochondria JC-1 forms J-aggregates and emits red fluorescence. In the cells with unhealthy mitochondria loss of membrane potential prevents JC-1 from forming aggregates and so it remains in the monomeric form which emits green fluorescence. A decrease in red/green fluorescence intensity ratio thus, indicates loss of membrane potential. For this study, $1x10^6$ PBMCs were irradiated and incubated in complete RPMI-1640 medium in a humidified 5% CO_2 atmosphere at 37ºC. After incubation, PBMCs were incubated with JC1 (5µM) for 10 min at 37°C in the dark. Cells were washed once with 1X PBS and JC-1 fluorescence was measured using a flow cytometer (Partec, GmbH Germany) by acquiring 20,000 cells. Data was analyzed using FlowJo software (Treestar Inc, Ashland, USA) and the ratio of red/green fluorescence was calculated.

2.9 Apoptosis assay

2.9.1 Propidium iodide staining

Apoptosis during RI-AR was studied using PI flow cytometric assay [105]. G_0 PBMCs ($1x10^6$) were irradiated and incubated in triplicate in 24 well plates at 37°C in a humidified 5% CO_2 atmosphere. After incubation, cells were washed once with 1X PBS and gently suspended in 1 ml PI/RNaseA solution (0.1% Sodium Citrate, 0.1% Triton X-100, 100µg/ml RNase A and 50mg/L Propidium Iodide (Sigma-

Aldrich Corp MO, USA) in 1x PBS. The cells were incubated at room temperature for 15 min in dark. Fluorescence was measured on Partec Cyflow space flow cytometer (GmbH Germany) by acquiring 20,000 cells in triplicates for each dose point and data was analyzed using FlowJo software (Tree Star Software, San Carlos, California, USA).

2.9.2 Annexin V-FITC and propidium iodide dual staining

Flipping of phosphatidylserine (PS) from inner leaflet of plasma membrane to outer leaflet is observed at early stages of apoptosis. Annexin-V has high affinity for PS; therefore, labelling Annexin-V with a fluorochrome helps in detection of cells undergoing apoptosis. Further, to differentiate between early and late apoptotic cells, Propidium Iodide (PI) stain is used. As the membrane permeability is compromised at later stages of apoptosis, PI can easily enter into the cell and bind DNA. Hence, late apoptotic cells are stained with both Annexin-V and PI. Cells undergoing necrosis take up only PI. Live cells exclude both Annexin-V and PI.

After irradiation, PBMCs ($1x10^6$) were incubated at 37°C in a humidified 5% CO_2 atmosphere (Eppendorf, Hamburg, Germany). The cells were harvested after incubation and washed once with 1X PBS. Cell pellet was then suspended in 100 µl of Annexin-V-FLUOS labeling solution as per the manufacturer's instructions (Roche diagnostics GmbH, Germany) for 15 min in dark. After incubation 900 µl of 1X PBS was added to each tube and 20,000 cells, were acquired on a flow cytometer (Partec, GmbH Germany). Each sample was analyzed in triplicate. Data was analysed using FlowJo (Treestar Inc, Ashland, USA). Unlabelled cells, cells stained only with Annexin-V FITC and only PI were used as control for setting the gates for the following populations: Annexin-V$^-$/PI$^-$ (live cells), Annexin-V$^+$/PI$^-$ (early apoptotic cells), Annexin-V$^+$/PI$^+$ (late apoptotic cells), Annexin-V$^-$/PI$^+$ (necrotic cells).

2.10 Measurement of intracellular ROS

Intracellular ROS levels were measured using oxidation sensitive probe Dichloro-dihydrofluorescein diacetate (H$_2$DCF-DA). H$_2$DCF-DA is a cell permeable dye which is rapidly cleaved by esterases to form H$_2$DCF. The oxidation of H$_2$DCF in presence of ROS forms a fluorescent product DCF whose fluorescence intensity is considered to be directly proportional to ROS levels in the cell.

PBMCs (1x10^5) were incubated with 20μM H$_2$DCF-DA for 20 min at 37°C before irradiation for set I and set II. In set III (non-primed cells) and set IV (primed cells) cells, the dye was added 20 min before exposure to CD. Immediately after irradiation, the fluorescence of DCF formed due to oxidation of H$_2$DCF-DA was measured by acquiring 20,000 cells on a flow cytometer (Partec, GmbH Germany) and data was analysed using FlowJo software (Treestar Inc, Ashland, USA).

2.11 Measurement of mitochondrial ROS

Mitochondrial ROS levels were measured using MitoSOX™ Red, a novel fluorogenic dye specifically targeted to mitochondria in live cells. MitoSOX™ Red reagent is rapidly oxidized by superoxide molecules which produces red fluorescence. To measure mitochondrial ROS, PBMCs (1x10^5) were incubated with MitoSOX™ red (5μM) for 20 min at 37°C before irradiation for set I and set II. In set III (non-primed cells) and set IV (primed cells) cells, the dye was added 20 min before exposure to CD. MitoSOX™ red fluorescence was measured immediately after irradiation using λ_{ex} of 485 nm and λ_{em} of 535 nm in a multiwell plate reader (Synergy H1 Hybrid, Biotek, USA).

2.12 Estimation of total thiols and intracellular thiols

For determination of total thiol levels, $3x10^6$ cells (per dose point) were lysed after respective treatments in a buffer containing 100 mM Tris-HCl, pH 7.5 and 1mM EDTA. Estimation was done using thiol detection kit (Cayman Chemical, MI, USA) as per the manufacturer's instructions.

Intracellular thiol levels were detected using a widely-used probe - monobromobimane (MBB). MBB reacts with thiols and forms thiol-bimane fluorescent adduct, which can be measured at $\lambda_{ex/em}$ of 394nm/490nm. For this, PBMCs ($1x10^6$) were incubated with 20 µM MBB (Thermo Fisher Scientific, USA) for 20 min at 37°C for set I and set II cells. In set III (non-primed cells) and set IV (primed cells) cells, the dye was added 20 min before exposure to CD. Before measuring fluorescence, cells were washed once with 1X PBS at 4°C. Cells were then re-suspended in 1X PBS and kept on ice during acquiring. Fluorescence was measured on Partec Cyflow Space flow cytometer (GmbH Germany) by acquiring 20,000 cells.

2.13 Measurement of intracellular GSH/GSSG

GSH/GSSG was measured by conventional enzyme recycling method as described by Rahman *et al* (2007) [106]. Here, GSH reacts with sulfhydryl reagent DTNB [5, 5'-dithio-bis (2-nitrobenzoic acid)] to form GS-TNB adduct which is reduced to GSSG by GR in presence of NADPH, recycling back GSH. In this process, a yellow derivative 5'-thio-2-nitrobenzoic acid (TNB) is released. The absorbance of TNB is measured at 412 nm. The rate of formation of TNB is considered to be directly proportional to the concentration of GSH. For this method, irradiated cells ($3x10^6$) were lysed by repeated freezing and thawing followed by

centrifugation at 12000 g for 10 min at 4ºC. After centrifugation, 20 µl of supernatant was mixed with a freshly prepared mixture of DTNB and GR (1:1) and absorbance was measured at 412 nm in a multiwell plate reader (Synergy H1 Hybrid, Biotek, USA) after addition of NADPH. For measuring GSSG, the cell extract was first treated with 2-vinylpyridine, which covalently reacts with GSH (but not with GSSG). With the help of GR, the GSSG present in the cell was recycled to GSH. This GSH was then measured by DTNB reduction method.

2.14 Estimation of protein concentration

Bicinchoninic acid assay (BCA) was used to estimate total protein concentration in the samples as per the manufacturer's instructions (Bangalore Genei India Pvt. Ltd., Bangalore, India). Bovine serum albumin (BSA) standards ranged from 50 µg/ml to 1000 µg/ml. BCA working reagent (BWR) was prepared in 50:1, reagent A:B ratio. In a 96 well plate, 20 µl of each standard and protein sample, and BWR (200 µl) was added. Plate was incubated for 30 min at 37°C in dark. Absorbance was measured at 540 nm using microplate plate reader (Synergy H1 Hybrid, Biotek, VT, USA) and a standard curve of BSA was plotted **(Fig. 2. 2)**.
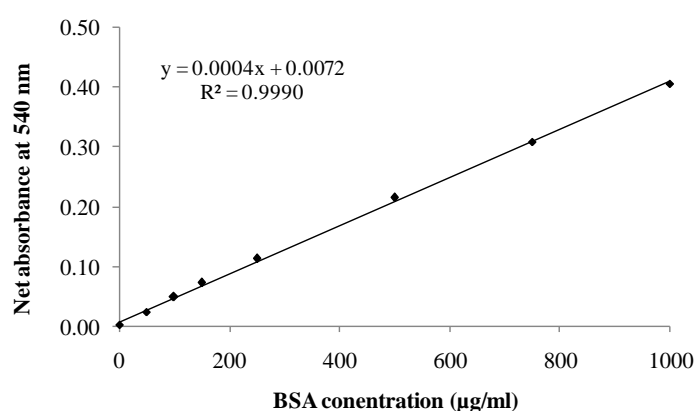
Fig. 2. 2. A representative standard curve for different dilutions of BSA (0 to 1000 µg/ml).

2.15 Measurement of antioxidant enzyme activity

PBMCs ($2x10^6$) were irradiated as explained and activities of antioxidant enzymes like superoxide dismutase (SOD), catalase, glutathione peroxidase (GPX) and thioredoxin reductase (TrxR) were measured. Enzyme activities obtained were expressed as units/µg protein.

2.15.1 Superoxide dismutase (SOD): SOD activity was measured using the SOD assay kit II as per the manufacturer's instructions (Calbiochem). The method uses tetrazolium salt which forms yellow formazan dye in presence of superoxide radicals generated by xanthine oxidase. SOD scavenges these superoxide radicals and reduces the formation of formazan dye. The absorbance of the formazan dye formed was then measured at 450 nm using microplate reader (Synergy H1 Hybrid, Biotek, VT, USA) and SOD activity was determined using the SOD standard curve.

2.15.2 Catalase (CAT): Catalase catalyzes the conversion of two molecules of H_2O_2 to molecular H_2O and O_2. Catalase activity was measured using Catalase assay kit (Calbiochem) as per the manufacturer's instructions. In this assay, detoxification of H_2O_2 is performed using peroxidatic activity of catalase using methanol. The formaldehyde formed is measured spectrophotometrically using purpald as chromogen, which upon oxidation gives purple colour. Colour change was measured at 540 nm using a microplate reader (Synergy H1 Hybrid, Biotek, VT, USA).

2.15.3 Glutathione peroxidase (GPX): GPX is a selenocysteine-containing enzyme that utilizes glutathione (GSH) as a substrate to reduce hydroperoxides in order to reduce oxidative damage in the cell. The oxidized glutathione formed in this process is recycled back to GSH by GR in the presence of NADPH. In this study, GPX activity was determined using glutathione peroxidase assay kit (Calbiochem) as per the manufacturer's instructions. The decrease in NADPH absorption was measured at

340 nm using a microplate reader (Synergy H1 Hybrid, Biotek, VT, USA) which is directly proportional to the GPX activity in the sample.

2.15.4 Thioredoxin reductase (TRxR): Activity of TRxR enzyme was determined using thioredoxin assay kit (Sigma-Aldrich Corp MO, USA), utilizing DTNB as substrate as per the manufacturer instructions. Reduction of DTNB with NADPH to TNB in presence of thioredoxin reductase gives a yellow colour. Increase in absorption due to the reduction of DTNB was monitored at 412 nm for 3 min with 30 sec intervals using microplate reader (Synergy H1 Hybrid, Biotek, VT, USA). To rule out reduction by other cellular enzymes like GR or GPX, DTNB reduction was also monitored in the presence of aurothiomalate - thioredoxin reductase inhibitor.

2.16 Isolation of total RNA

Total RNA ($2x10^6$ cells) was isolated using HiPurA^{TM} Total RNA Mini-prep Purification Spin kit (HiMedia Laboratory Pvt. Ltd, Mumbai, India) as per the manufacturer's instructions. Cells were harvested by centrifugation at 2500 rpm, 4°C for 5 min and washed with 1X PBS. Cell pellet thus obtained was suspended in 350 µl of RNA lysis solution and vortexed for 2 min for complete homogenization. The lysate was then transferred into a HiShredder column placed in a 2-ml collection tube and centrifuged for 2 min at 14000 rpm. Equal volume of 70% ethanol was added to the cleared lysate and transferred into a HiElute Miniprep Spin column placed in a 2-ml collection tube. The tube was then centrifuged for 30 sec at 14000 rpm. Pre-wash solution (700 µl) was added to the HiElute Miniprep Spin column and centrifuged at 14000 rpm for 30 sec. Flow through was discarded and the column was washed twice with wash solution (500 µl) for 2 min at 14000 rpm. Then the column was placed in a new 1.5 ml collection tube and 30 µl of elution solution (RNase-Free water) was

added, and centrifuged at 14000 rpm for 2 min. The elute containing total RNA was stored at -80°C until further use.

Total RNA was quantified using Picodrop (Pico 100, Picodrop Ltd, HI, UK) and its purity was determined with A_{260}/A_{280} ratio. The integrity of RNA was checked by running 1μg of total RNA on 1% agarose gel containing ethidium bromide. Total RNA samples showing distinct bands of 28S and 18S rRNA with 2:1 ratio were used for cDNA preparation **(Fig. 2. 3).**
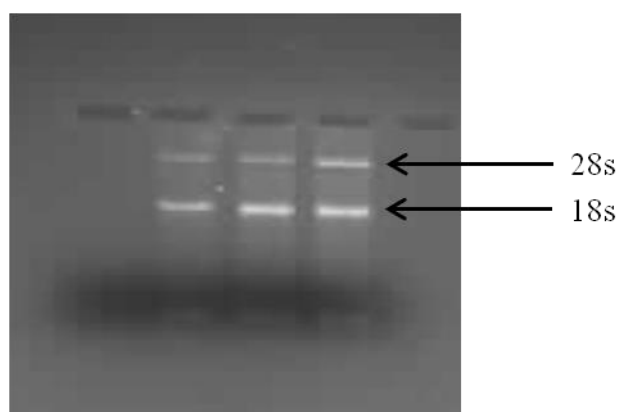
Fig. 2. 3. Total RNA separated on 1% agarose gel.

2.17 cDNA preparation

Transcriptor High Fidelity cDNA synthesis kit (Roche Diagnostics Pvt Ltd, GmbH, Germany) was used to prepare cDNA as per the manufacturer's instructions. RNA sample (1 μg) served as a template for the synthesis of cDNA using reverse transcriptase enzyme. Random hexamer primer (60 μM) was mixed with template RNA in a sterile, nuclease free, thin walled PCR tube placed on ice. The template-primer mixture was denatured by heating for 10 min at 65°C in a thermocycler (Techne ST UK). This step helps in denaturation of RNA secondary structures. After 10 min, the tubes were immediately placed on ice. A mixture containing 1X buffer, 20 U RNase inhibitor, 5 mM DTT, dNTPs (1 mM each) and reverse transcriptase

enzyme (10 U) was added to template-primer mixture. One cycle of 50°C/30 min followed by heating to 85°C/5 min was performed on thermocycler. cDNA was stored at -20°C until further use.

2.18 Real-time quantitative PCR

Quantitiative real-time polymerase chain reaction (qPCR) was performed on LightCycler 480 instrument (Roche Diagnostics Pvt. Ltd., GmbH, Germany) using 2X SYBR Green I master mix (Roche Diagnostics Pvt. Ltd.) and gene specific forward and reverse primers **(Table 2. 1).** The reactions were performed in total volume of 12.5 µl in duplicates with no-template control for each primer pair in a 96-well plate. All the consumables used in qPCR were procured from Roche Diagnostics Pvt. Ltd., GmbH, Germany). All the primer sets were designed using Universal Probe Library software (Probe Finder Version 2.50, Roche Diagnostic Pvt. Ltd., GmbH, Germany) and procured from Integrated DNA Technologies Inc. USA. PCR cycling was programmed for 45 cycles with denaturation at 95°C for 10 sec, annealing at 59°C for 30 sec and extension at 72°C for 30 sec with a pre-incubation for 5 min at 95°C. The fluorescence of SYBR Green I was measured once per cycle to monitor template amplification. Uniformity of the PCR product was studied using melting curve analysis following threshold dependent cycling where fluorescence of SYBR Green I was measured during a linear temperature transition from 60°C to 95°C at 0.1°C/sec melt rate. After this, the amplified products were cooled down to 40°C. A representative melting curve image for the amplified product of GAPDH and MnSOD gene is given in **Fig. 2. 4** and **Fig. 2. 5**, respectively. The amplification of each gene was repeated independently in triplicate. The change in gene expression levels were calculated using the $2^{-\Delta\Delta ct}$ method [107] and normalized using glyceraldehyde 3-

phosphate dehydrogenase (GAPDH) as a reference gene. The relative change in the expression was plotted with respect to the control.
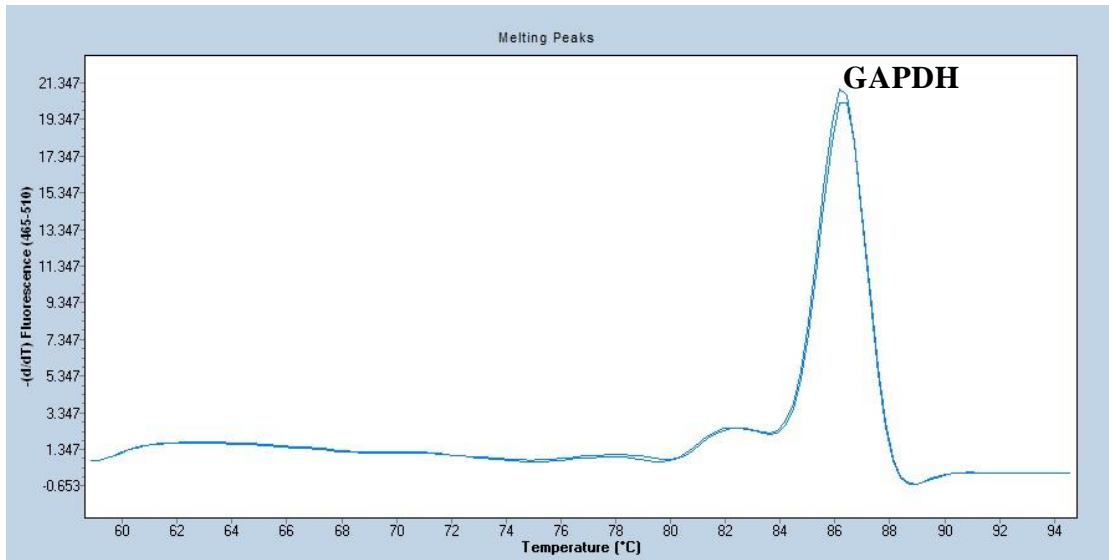
Fig. 2. 4. Representative melting curve for the RT-PCR product GAPDH gene
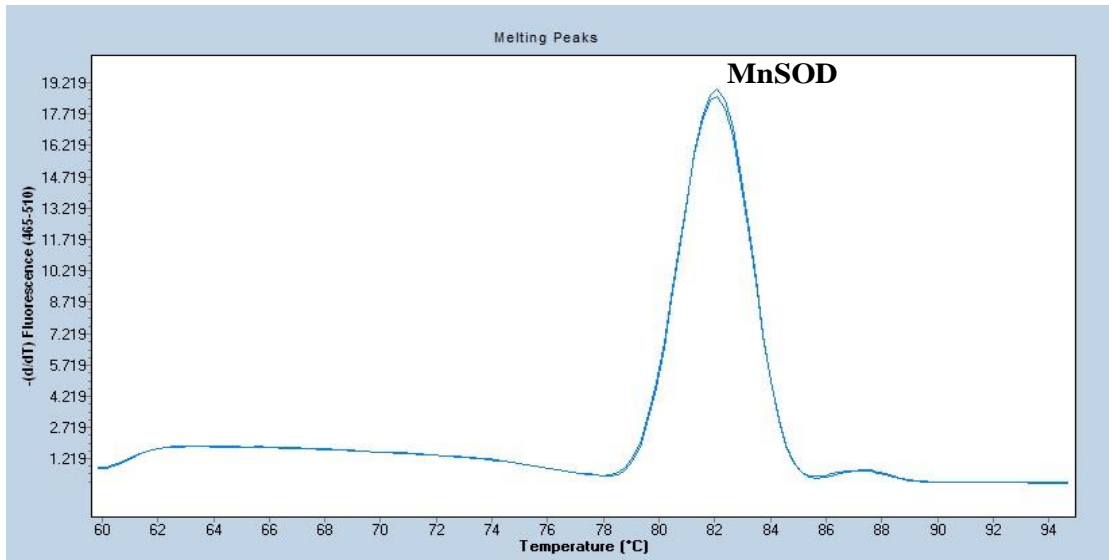
Fig. 2. 5. Representative melting curve for the RT-PCR product MnSOD gene.

Gene Name	Primer sequence
GAPDH	F: 5'CCCCGGTTTCTATAAATTGAGC 3' R: 5'CACCTTCCCCATGGTGTCT 3'
MnSOD	F: 5'AATCAGGATCCACTGCAAGG 3' R: 5' TAAGCGTGCTCCCACACAT 3'
CAT	F: 5'TCATCAGGGATCCCATATTGTT 3' R: 5'CCTTCAGATGTGTCTGAGGATTT 3'
GPX1	F: 5'CAACCAGTTTGGGCATCAG 3' R: 5'TCTCGAAGAGCATGAAGTTGG 3'
TXNRD1	F: 5'TCCTTATTTTGTGCTTGAACTTGA 3' R: 5'CAATTCCGAGAGCGTTCC 3'
IFNG	F: 5'GTTTTGGGTTCTCTTGGCTGTTA 3' R: 5'AAAAGAGTTCCATTATCCGCTACATC 3'
TNFA	F: 5'CCCCAGGGACCTCTCTCTAATC 3' R: 5'GGTTTGCTACAACATGGGCTACA 3'
HMOX1	F: 5'CAGTCAGGCAGAGGGTGATAG 3' R: 5'AGCTCCTGCAACTCCTCAAA 3'
PRDX6	F: 5'TCAATAGACAGTGTTGAGGACCA 3' R: 5'TTTCTGTGGGCTCTTCACAA 3'
MED13L	F:5'AACGCAAGGGAACATAGGC3' R:5'CTCCGTGGGAATTCCTATTCT3'
TCF20	F:5'CCTCAGCACAGAGCAGTCG3' R:5'TTCTCATCTCCACAGTCTCACC3'
KDM5A	F:5'GAGACATATGGCTACGACATGAA3' R:5'GATTGGGTTCAAGACTACTAGAGGA3'
RNF20	F:5'CCCGGAAGCTAAACAGTGG3' R:5'TCTCCTGTGCGAGGAAAGA3'
EGF	F:5'GGCCGTAGATTCTATTGGACA3' R:5'TTTTGGAACGTTTCCCATTTA3'
BRWD3	F:5'GGACGGGAAAATTGTAAAGATG3' R:5'TTGCTGCCCAATTACCTGTT3'
RBM25	F:5'TGATGATAGAGATGACCCCAAAT3' R:5'TCACGCAACCTTTTCTGAAG3'
ITGA11	F:5'TCAGCAAATCCATCTTCCTACA3' R:5'TGTCCCGCTCATTACTGTCA3'
BLM	F:5'TGGAGGGTTACTACCAAGAATCTG3' R:5'ATGGTTTCCATCTTTTTCCATC3'
CHD4	F:5'CACTTCCAGAGATCCCCAAC3' R:5'TTCTGCACTTTGCCCTTCA3'
DICER1-F	F:5'TTTGATCCCCCTGTGAATTG3' R:5'GCCAGCATGCAGTCTTTTG3'
DUOX2	F:5'GGAGAACAGCCCCATTTCTT3' R:5'TGTGTACAGCCGGGGAGT3'

Table 2. 1. Primer sequences used for RT-qPCR.

2.19 Western blot analysis

Whole cell protein extracts from $2x10^6$ cells were prepared using RIPA buffer (50 mM Tris pH 8, 150 mM NaCl, 0.5% Deoxycholate, 0.1% SDS, 1% NP40) containing 1X protease inhibitor (Roche Diagnostics Pvt Ltd, GmbH, Germany). Protein concentrations were estimated using BCA method as explained earlier. Approximately 40 µg of protein sample per treatment was separated on a 4-12% Novex Bis-Tris gel (Invitrogen CarlsBAD, CA) using MES SDS running buffer (50 mM MES, 50 mM Tris base, 0.1% SDS, 1 mM EDTA, pH 7.3). Electrophoresis was carried out at RT for 2 hours at 120 V. Proteins were then blotted on to a PVDF membrane (Sigma-Aldrich Corp MO, USA) using transfer buffer (39 mM glycine, 48 mM Tris base, 0.037% SDS, 20% methanol, pH 8.3) by electroblotting at 25 V overnight in cold room. The membrane was then blocked using 5% BSA prepared in 1X TBST (50 mM Tris-HCl, 150 mM NaCl, pH 7.4, 0.05% tween 20) for 1 hour at RT. Primary antibodies for pERK (#4370 Cell Signaling Technology Inc. MA USA), Total ERK (#4695 Cell Signaling Technology Inc. MA, USA), phospho p38 (M8177 Sigma-Aldrich Corp MO, USA), total p38 (#8690 Cell Signaling Technology Inc. MA, USA), phospho SAPK/JNK (#9255 Cell Signaling Technology Inc. MA, USA) were used. With subsequent washings, appropriate secondary antibodies coupled with horseradish peroxidase (Santa Cruz Biotechnology, Inc. TX, USA) were used for detection. Bands were visualized using Super Signal West Dura Chemiluminescent substrate (Thermo Scientific Inc. MA, USA) and image was captured using G:BOX chemi XX6 system (Syngene CA, UK). Public domain ImageJ software (developed at National Institutes of Health, https://imagej.nih.gov/ij/) was used for densitometry analysis.

2.20 Electrophoretic mobility shift assay (EMSA)

PBMCs (3×10^6) were incubated with 100 µl of cytoplasmic extraction buffer (10 mM HEPES pH 7.9, 10 mM KCl, 0.1 mM EDTA, 0.1 mM EGTA, 1X protease inhibitor cocktail) for 45 min in ice. After incubation, 6 µl of 10% NP-40 was added to the tube. The tube was vortexed for 30 sec and then centrifuged at 14000 rpm for 1 min at 4°C to obtain the nuclear pellet. The pellet was suspended in 30 µl of nuclear extraction buffer (20 mM HEPES pH 7.9, 400 mM NaCl, 1 mM EDTA, 1 mM EGTA, 1 X protease inhibitor cocktail) and incubated on ice for 30-40 min. The tube was intermittently vortexed. Centrifugation at 14000 rpm for 10 min at 4°C was done to obtain the nuclear extract. Protein concentration was estimated and 8 µg of extract was incubated with 16 fmol of either ^{32}P-end-labeled NF-κB (5′-TTG TTA CAA GGG ACT TTC CGC TGG GGA CTT TCC AGG GAG GCG TGG-3′) or Nrf2 (5'-TGG GGA ACC TGT GCT GAG TCA CTG GAG-3') oligonucleotides in the presence of 2 µg of poly (2′-deoxyinosinic–2′-deoxycytidylic acid) in binding buffer (20 mM Hepes, pH 7.9, 0.4mM EDTA, 0.4 mM DTT and 5% glycerol) for 30 min at 37 °C. The DNA–protein mixture was then run on 7.6% native polyacrylamide gel. The gel was dried and exposed on a phosphor screen (Fujifilm 20 x 25 cm) and the bands were visualized using a phosphor Image scanner (Fuji BAS-5000, TO, Japan). To check the specificity of consensus sequence of NF-kB and Nrf2, a competition test was performed with mutant, cold competitor and mutant competitor.

2.21 Statistical analysis

Data are represented as mean ± standard error of mean (SEM) from three replicates. For each assay two independent experiments were carried out. Statistical analysis was performed using student's t-test where $p \leq 0.05$ was considered as significant.

2.22 Proteomics analysis

2.22.1. Protein lysate preparation

PBMCs ($4x10^6$) were suspended in 200 µl lysis buffer (10 mM Tris base containing 1X protease inhibitor cocktail) and lysed using sonication (Misonix S-4000 sonicator NY, USA). For this, probe of sonicator was cleaned with 70% (V/V) ethanol and dried thoroughly using a clean tissue. Sonicator tip was suspended well below the surface of the liquid in the sample tube and not touching the sides. Sample tube was placed in a beaker containing ice-water to keep it cold during sonication. Sonication was carried out on ice using 10 sec pulse 'ON' and 30 sec pulse 'OFF' for 15 cycles. Samples were centrifuged at 14,000 g for 40 min. Protein concentration was determined using BCA method as explained earlier. These samples were stored at -80°C until further use.

2.22.2 Two-dimensional fluorescence Difference Gel Electrophoresis (2D-DIGE)

2.22.2.1 Minimal CyDye labeling

The CyDye were reconstituted in dimethylformamide (DMF) as per the manufacturer's instructions (GE Healthcare). Proteins were labelled using CyDye DIGE fluor kit (CyDye™ DIGE Fluor Minimal Labeling Kit). Concentration of protein sample used for labelling was 100 µg. Final concentration of 600 pmoles/µl of each CyDye was used. Protein lysate from non-primed and primed cells was labelled with Cy3 and Cy5 dye, respectively. Internal standard was prepared and labelled with Cy2 dye.

Before labelling, the pH of protein lysates was adjusted to pH 8.0 using 100 mM NaOH. All the reactions were performed in dark and on ice. Protein lysate (100 µg) of non-primed cells was mixed with 1 µl of diluted Cy3 dye (600 pmoles).

Protein lysate (100 µg) of primed cells was mixed with 1 µl of diluted Cy5 dye (600 pmoles). An internal standard was prepared by pooling 25 µg of each sample and labelled with Cy2 dye. Protein samples were then kept in ice for 30 min in dark. The reaction was stopped by adding 10 mM lysine. Next, equal volume of 2X sample buffer containing 2% w/v DTT, 2% v/v IPG buffer pH 3-10 NL was added to each sample. Labelled samples (Cy2, Cy3 and Cy5) were then pooled and IEF was performed.

2.22.2.2 IEF and SDS-PAGE

The labelled proteins were separated first using IEF [105] with minor modifications. All labelled samples were mixed with an equal volume of 2X rehydration buffer and pooled. The samples were then loaded onto the IPG strip of length 18 cm, pH 4-7 for rehydration. IEF was performed overnight at 20°C on an IPGphor II system (GE Healthcare, Bucking-hamshire, UK) at a constant current of 50µA/strip and in a step-wise increasing voltage program until 80,000 Vh was reached. The strips were stored at -80°C until further use. For second dimension, IPG strips were equilibrated in an equilibration buffer (6M urea, 2% SDS, 0.05M Tris-Cl pH 6.8, 20% glycerol) containing 2% DTT first and then in 2.5% iodoacetamide for 15 min each. Electrophoresis was carried out on 12% SDS-PAGE overnight at 85 V at 4°C for 16 h.

2.22.2.3 Image scanning, spot detection and analysis

Gels were scanned immediately following the SDS-PAGE using Typhoon TRIO (GE Healthcare). The general workflow during analysis has three main steps: spot detection, alignment, and statistical analysis of spots. In this study, protein spots

identification and abundance from the scanned images was analysed using Dymension 3 software (Syngene, Cambridge, UK). Two sets of gel (for each CyDye) were used for analysis. All the gel images were cropped together prior to loading into the software to make sure that the region of interest analyzed (ROI) was identical. Therefore, gel images were first cropped, then loaded and grouped using the multiplexed experimental wizard. Protein spots from the ROI (those from internal standard as well as both treatments) were detected automatically. Default spot detection settings were used with blur radius of 1.2, peak limit threshold of 0.01 and a splitting threshold of 0.001. Detection confidence ratio and separation confidence ratio was set at 20 as per the manufacturer's recommendation. Noise filtering and background correction was performed automatically by using the following parameters: Raw Volume/Height >10, Height >5. Gels were then automatically warped to improve the matching. Pool matching i.e. matching of all the spots across the gels was carried out by automatic gel alignment. Statistical analysis was automatically done when pool matching was carried out. The intensity change of the differential protein expression was obtained after spot matching under multiplexed matching results tab. Dymension accepts only those spots which appear in all the internal standard gels. Proteins spots with changes in expression levels of at least 1.2-fold at 95% confidence level ($p \leq 0.05$) when compared with non-primed cells were selected for further analysis.

2.22.3 Label-free proteomics

2.22.3.1 Trypsin digestion

For trypsin digestion, 100 µg of protein sample (prepared as explained in section 2.22.1.1) from each treatment group was first subjected to reduction using 100

mM DTT made in 50 mM ammonium bicarbonate (NH_4HCO_3). The tubes were incubated at 56 °C for 1 h. The samples were cooled to RT and then alkylated with 250 mM Iodoacetamide in 50 mM NH_4HCO_3 at room temperature in dark for 45 min. The treated protein samples were then digested with trypsin (solubilised in 50 mM NH_4HCO_3) overnight at 37 °C. The trypsin digestion was then stopped by adding 1 µl of 100% Formic acid at 37˚C for 45 min. The samples were centrifuged at 10,000g for 10 min and the supernatant was collected into a separate tube. The supernatant was then vacuum-dried and dissolved in 0.1% formic acid. The digested sample was centrifuged at 10,000g. To ensure complete digestion, 1 µl of digested sample was loaded on SDS-PAGE. Injection volume of 10 µl per digested sample was used for separation of tryptic peptides on C18 UPLC (ultra performance liquid chromatography) column. Separation was carried out in triplicates for each sample.

2.22.3.2 Reverse phase LC-MS/MS

Liquid chromatography was performed on nanoACQUITY UPLC® chromatographic system (Waters, Manchester, UK). The tryptic peptides were separated using nanoACQUITY UPLC® chromatographic system (Waters, Manchester, UK). Here the peptides were separated by reverse-phase chromatography. Solvent A containing 0.1% v/v aqueous formic acid and solvent B containing 0.1% v/v formic acid in acetonitrile were used for nano separations. LC separation of tryptic peptides was first performed on a Symmetry C18 5 µm trapping column (180 µm x 20mm) for 1 min, where tryptic peptides were trapped and desalted. This column was placed in line with a ACQUITY UPLC BEH C18 analytical column (75 µm x 150mm) with particle size of 1.7 µm for reverse phase separation of peptides. A gradient elution program was run for the chromatographic

separation with mobile phase A (0.1% formic acid in water), and mobile phase B (0.1% formic acid in acetonitrile) as follows:

S.No	Time	Flow	%A	%B	Curve
1	Initial	0.300	98.0	2.0	Initial
2	1.00	0.300	98.0	2.0	6
3	30.00	0.300	50.0	50.0	6
4	32.00	0.300	50.0	50.0	6
5	40.00	0.300	20.0	80.0	6
6	45.00	0.300	20.0	80.0	6
7	50.00	0.300	98.0	2.0	6
8	55.00	0.300	98.0	2.0	6
9	60.00	0.300	98.0	2.0	6

Peptides were eluted from the analytical column with a linear gradient of 1 to 40% solvent B over 55.5 min at a flow rate of 300 nl/min followed by a 7.5 min rinse of 80% solvent B. The column was immediately re-equilibrated at initial conditions (1% solvent B) for 20min. The column temperature was maintained at 40°C. Each sample was injected in triplicate with blank injections between each sample.

Peptide fractions were then analysed on a Synapt G2 High Definition MS System (HDMSE System, Waters) equipped with an electrospray ionization (ESI) source was used for mass spectrometric detection. Sample analysis was performed in positive mode. The operation parameters were as follows:

Experimental Instrument Parameters

- Polarity   ES+
- Analyser   Resolution Mode
- Capillary (kV)   3.5000
- Source Temperature (°C)   150
- Sampling Cone   45
- Extraction Cone   4.5

- Source Gas Flow (mL/min)   30
- Desolvation Temperature (°C)   350
- Cone Gas Flow (L/Hr)   30
- Desolvation Gas Flow (L/Hr)   800

Acquisition:

```
Acquisition Time
Start time              : 0 min
End Time                : 60 min
Source                  : ES
Acquisition Mode
Polarity                : Positive
Analyzer Mode           : Resolution
```

TOF MS:

```
Da Range
Start                   : 50Da
End                     : 1500Da
Scanning Conditions
Scan Time               : 0.5 Sec
Data Format             : Continuum
```

Collision Energy:
```
Function-1 Low Energy
Trap Collision Energy               : On – 6V
Transfer Collision Energy           : On – 6V
Function-2 High Energy
Ramp Trap Collision Energy          : On – 20V to 45V
Ramp Transfer Collision Energy      : Off
```

Cone Voltage:

```
Cone Voltage  : 40V
```

2.22.3.3 Protein identification

The protein identification and label-free relative protein quantification was done using Protein Lynx Global Server v2.5.3 (PLGS, Waters, India) against homosapiens UniProt database. A peptide tolerance of 30 ppm, fragment tolerance of 70 ppm, and missed cleavage of 1 was allowed. Each run was performed in

triplicates. Parameters used during protein identification included minimum 3 fragment ions matched per peptide, minimum 7 fragment ions matched per protein and minimum 2 peptide matched per protein. One missed cleavage, a fixed carbamidomethyl modification and variable oxidation modification was allowed. During the database search, the protein false positive rate was set to 4%. For protein quantification, expression levels of proteins were normalized by auto-normalization function of PLGS Expression^E software (Waters, Manchester, UK). To perform comparative proteomic analysis, normalized peak intensity of the peptides identified from different treatments was compared with the sham irradiated control. For this, peptides identified in at least 2 out of 3 injections were considered. Next, expression value of different proteins identified in primed cells, non-primed cells and cells exposed to 100 mGy was normalized with sham irradiated control to obtain a relative expression value.

2.22.3.4 Functional pathway analysis

To determine the functions of significantly modulated proteins identified, Gene ontology (GO) analysis was performed on total proteins identified using an open source software DAVID (Database for Annotation, Visualization and Integrated Discovery) version 6.8 (http://david.ncifcrf.gov/). This analysis classified the total proteins into different GO terms which are grouped into three independent categories - biological process, cellular component, and molecular function. The biological pathways modulated were predicted using Kyoto Encyclopedia of Genes and Genomes (KEGG) module. The biological processes and KEGG pathways were considered significantly enriched using Benjamini-Hochberg $p \leq 0.1$.

CHAPTER 3

ROLE OF DNA REPAIR AND ANTIOXIDANT RESPONSES IN RADIATION INDUCED-ADAPTIVE RESPONSE

3.1 Baseline DNA damage in G_0 PBMCs with IR

To assess the validity of the cell system used for the present work we first studied DNA damage in unstimulated human G_0 PBMCs over a range of doses of γ-radiation from 0.01 Gy to 4 Gy in two healthy individuals (labelled S1 and S2). Cells were processed for alkaline comet assay immediately after irradiation to capture instant DNA damage and compared to sham irradiated cells which served as the control (0 Gy). The strand breaks were quantified in terms of percentage of DNA in comet tail (% tail DNA). The relationship between the % tail DNA and the IR dose delivered was linear, and both S1 and S2 showed a similar dose dependent increase. The experiment was repeated twice with the same individuals. For S1, the average % tail DNA varied from 1.3 ± 0.09 at 0.01 Gy to 19.4 ± 0.37 at 4 Gy; for S2, the average % tail DNA varied from 1.6 ± 0.09 at 0.01 Gy to 21.8 ± 0.61 at 4 Gy **(Fig. 3. 1).** The R^2 values, which represent goodness of fit, were 0.88 for S1 and 0.91 for S2 **(Fig. 3. 1).** DNA breaks at the very low dose of 0.01 Gy did not vary significantly from that observed in sham irradiated control.
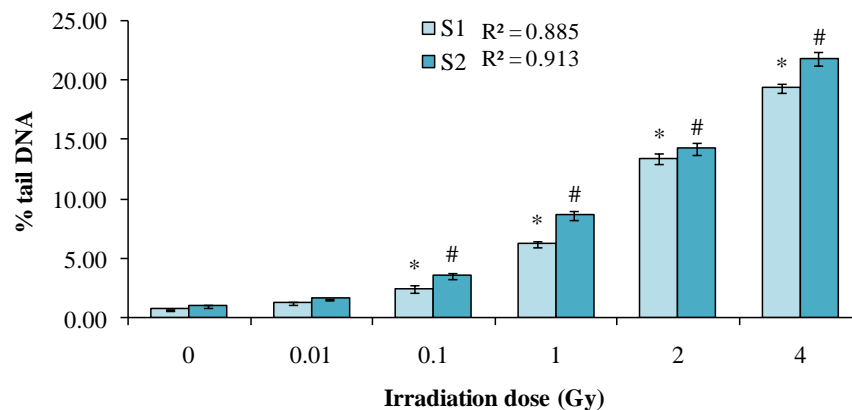
Fig. 3. 1 Dose response of DNA damage in human PBMCs exposed to γ-rays. PBMCs from two individuals (S1 and S2) were irradiated with various doses from 0.01 Gy to 4 Gy. Alkaline comet assay was performed immediately after irradiation.

DNA strand breaks were measured as % tail DNA. *Sham irradiated control *vs* irradiated for individual S1; [#] sham irradiated *vs* irradiated for individual S2.

3.2 Initial induction of DNA strand breaks and repair of DSBs in RI-AR

When cells are exposed to a small priming dose (PD) typically in the range of 1–200 mGy, followed by a larger challenge dose (CD) in the range of 1–10 Gy after a short time, RI-AR is induced. For non-proliferating G_0 PBMCs, a PD of 100 mGy, a CD of 2 Gy and a time interval of 4 h between these two doses has been shown to give optimal RI-AR [50,108]. Hence, for the present work, all studies on RI-AR were carried out using these parameters. Initially, seven individuals (coded S1-S7) were screened for RI-AR using this protocol and comet assay was performed immediately after CD (0 min, as specified in section 2.4). Pre-exposure (priming) of PBMCs with a low dose of 100 mGy before exposure to a high dose 2 Gy (challenge) after 4 h, resulted in a significantly reduced % tail DNA ($p < 0.05$), as compared to the cells exposed to 2 Gy CD alone, indicative of the phenomena of adaptive response. However, this RI-AR was observed only in five (S1-S5) out of seven individuals screened, consistently in two independent experiments, each with three technical replicates ($p \leq 0.05$). The decrease in % tail DNA in comets in samples S1-S5 however, varied widely ranging from 8.3% to 30.8%. Pre-exposure with low dose radiation resulted in no change in DNA damage in samples S6 and S7 indicating absence of adaptive response. These two samples were thus, excluded from all further experiments **(Fig. 3. 2A)**.
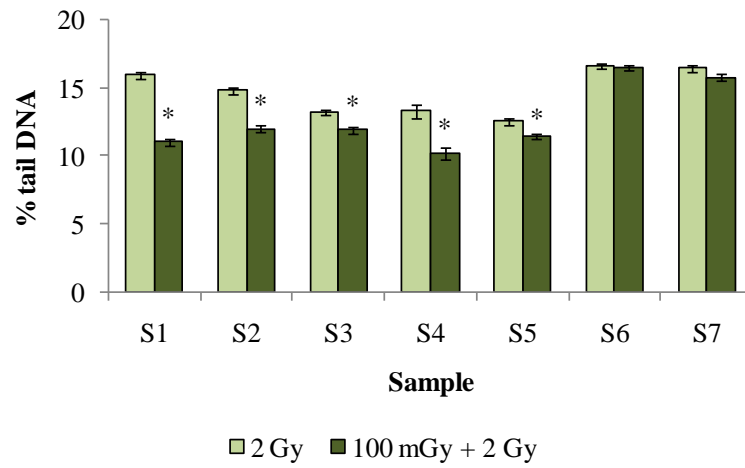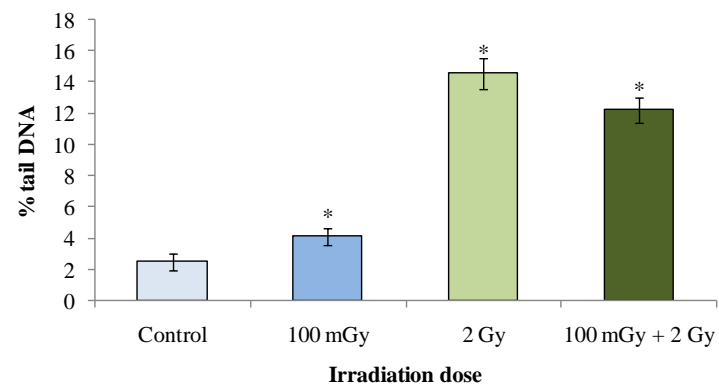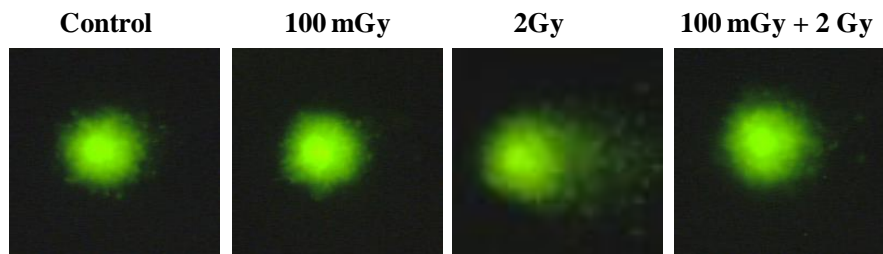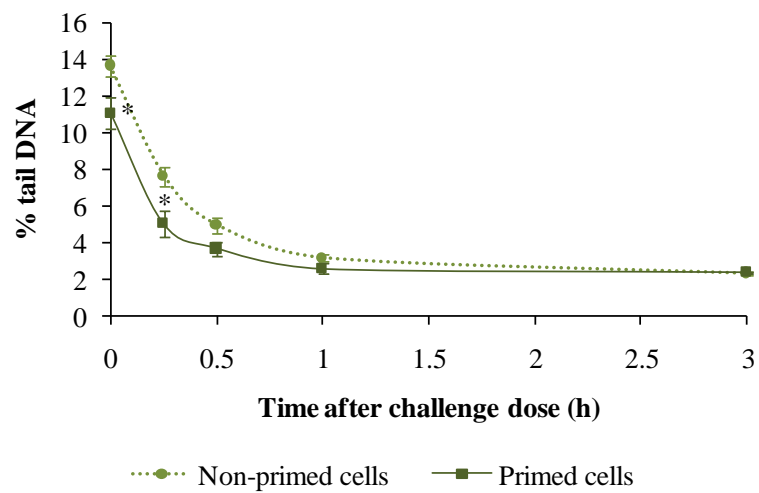
Fig. 3. 2 Pre-exposure of human PBMCs to a small priming dose of 100 mGy decreased DNA damage upon subsequent irradiation with 2 Gy. Cells exposed to 100 mGy priming dose were irradiated with 2 Gy challenge dose after 4 h of adaptive window and analyzed immediately for induction of DNA strand breaks using alkaline comet assay. (A) DNA strand breaks assessed using alkaline comet assay in seven individuals (S1–S7). Statistical significance: *2 Gy *vs* 100 mGy + 2 Gy. (B) Average % tail DNA observed in pooled PBMCs from five individuals (S1-S7) which showed RI-AR. Statistical significance: *sham irradiated control *vs* irradiated, [#]2 Gy *vs* 100 mGy + 2 Gy. (C) Representative images of comet tails observed under fluorescence microscope. (D) Residual DNA damage observed using alkaline comet assay after 15, 30, 60 and 180 min of exposure to CD. *Non-primed cells *vs* primed cells.

In order to avoid inter-individual variability and provide uniform pre-analytical conditions during sample preparation, all further experiments were performed by pooling equal number of freshly isolated PBMCs from five individuals (S1-S5) which showed RI-AR. The % tail DNA in the primed aliquot of pooled samples, when measured immediately after CD, was 12.23 ± 0.81 as compared to 14.58 ± 0.97 in the non-primed cells, indicative of a ~16% decrease in initial induction of DNA damage due to pre-exposure to low dose radiation ($p = 0.04$) **(Fig. 3. 2B)**. Representative images of DNA damage as visualized by alkaline comet assay in the primed and non-primed cells is given in **Fig. 3. 2C**. DNA breaks at the very low dose of 100 mGy showed marginal but significant increase from that observed in sham irradiated control.

We next followed DNA repair by analysing residual comet tails 15, 30, 60 and 180 min after CD in primed and non-primed cells. As shown in **Fig. 3. 2D**, the

primed cells showed a significantly reduced (p = 0.04) % tail DNA in the comets (5.1 ± 0.73) at the end of first 15 min of repair after CD as compared to non-primed cells (7.7 ± 0.51). At 30 min, % tail DNA was still lower in primed cells (3.7 ± 0.40) than non-primed cells (5.0 ± 0.44); however, the difference was non-significant. At the end of 180 min, both primed cells and non-primed cells showed similar residual damage (2.4 ± 0.10 *vs* 2.4 ± 0.06, respectively).

We next determined γH2AX foci number during RI-AR in the pooled sample. To capture instant damage by IR, primed and non-primed cells were fixed with paraformaldehyde immediately after challenge dose and immunostained for γH2AX (**Fig. 3. 3A** and **Fig. 3. 3B**). Similar to our observation with total DNA damage as measured with alkaline comet assay, the initial number of γH2AX foci per cell in primed cells (5.9 ± 0.70) were also significantly lower (p < 0.001) than in the non-primed cells (10.7 ± 0.64), when measured immediately after CD. Irradiation of PBMCs with low dose of radiation (100 mGy PD alone) resulted in only 0.5 ± 0.23 γH2AX foci per cell, which was same as the basal level observed in sham irradiated controls **(Fig. 3. 3A).**

A
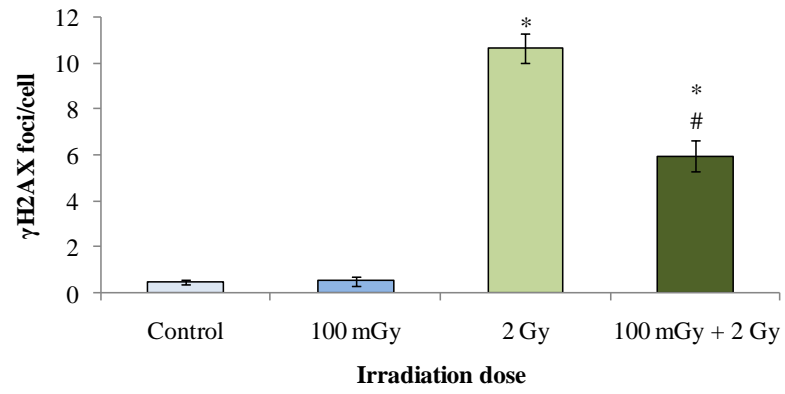
B
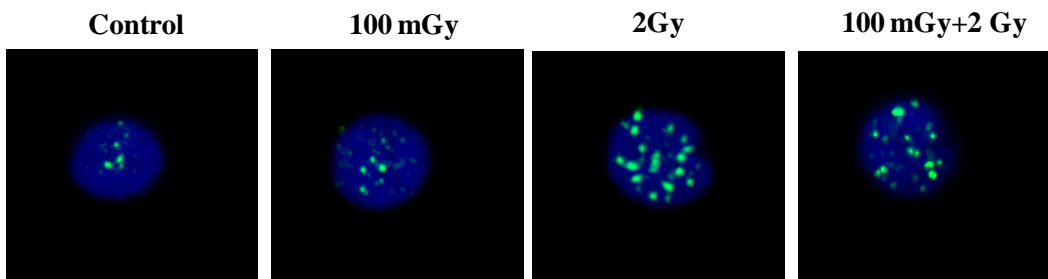
C
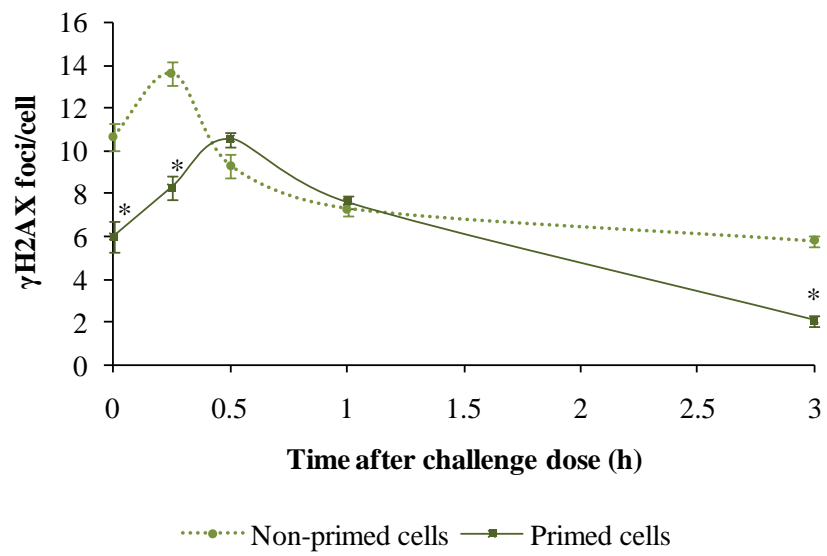
D
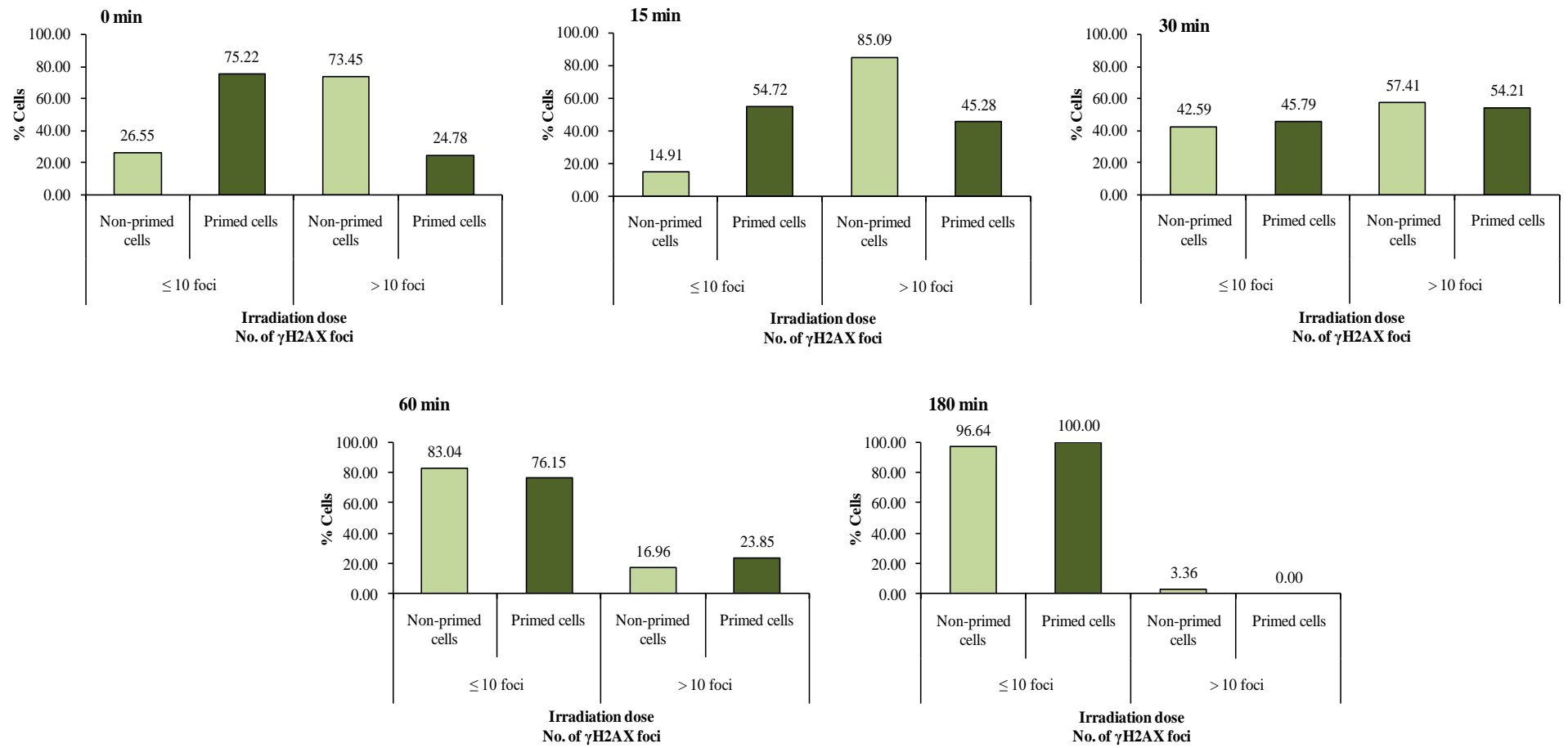
Fig. 3. 3. Pre-exposure of human PBMCs to a small priming dose of 100 mGy lead to a decrease in DSBs upon subsequent irradiation with 2 Gy. Cells exposed to 100 mGy priming dose were irradiated with 2 Gy challenge dose after 4 h of adaptive window and analyzed immediately for induction of DSBs using γH2AX assay. (A) Average number of γH2AX foci/cell in PBMCs pooled from five individuals (S1–S5) which showed RI-AR. Statistical significance: *sham irradiated control *vs* irradiated, [#]2 Gy *vs* 100 mGy + 2 Gy. (B) Representative images of DAPI stained cells (blue colour) with γH2AX foci (green colour). (C) Effect of pre-exposure to a small priming dose on the repair of DSBs after 15, 30, 60 and 180 min of exposure to CD. *Non-primed cells *vs* primed cells. (D) Distribution of γH2AX foci (≤10 foci and >10 foci) in non-primed and primed cells at 0 min, 15 min, 30 min, 60 min and 180 min after CD.

When followed at different times (15, 30, 60 and 180 min) after CD, the number of γH2AX foci/cell in non-primed cells peaked at 15 min post-irradiation with CD (13.6 ± 0.52) followed by a decay phase **(Fig. 3. 3C)**. Simultaneously, the number of γH2AX positive cells with >10 foci peaked to 85.1% 15 min after CD, increasing from 73.5% seen immediately after CD **(Fig. 3. 3D)**. After 180 min, 3.4% non-primed cells were found to be γH2AX positive with 5.8 ± 0.26 γH2AX per cell **(Fig. 3. 3C)**. The primed cells on the other hand, showed a slower increase both in γH2AX positive cells with >10 foci and γH2AX foci per cell and reached the maximum level 30 min after CD, later than the non-primed cells **(Fig. 3. 3C** and **Fig. 3. 3D)**. Both the nuclear damage parameters however, were significantly lower than the non-primed cells at the peak. The highest values detected after 30 min were 54.2% γH2AX positive cells with 10.6 ± 0.34 γH2AX per cell. By 180 min, primed cells showed only 2.1 ± 0.22

γH2AX foci per cell which was significantly (p < 0.001) lesser than non-primed cells (5.79 ± 0.26) at same time point **(Fig. 3. 3C)**.

Thus, for the cell model employed here, pre-exposure of PBMCs with LDR resulted not only in lesser initial DNA damage but also in more efficient repair of more deleterious DSB lesions.

We also measured mRNA expression of two DNA damage response genes ATM and P53 immediately after irradiation with CD (0 min) in non-primed and primed cells. ATM and P53 are considered critical players in DNA damage response. Relative to sham irradiated controls, both the non-primed and primed cells showed a significantly higher ~2.5-fold increase for both the genes. Thus, there was no effect of prior exposure to LDR on the gene expression of these two genes in PBMCs. The transcript levels with 100 mGy LDR alone resulted in still higher ~3.5-fold increase for both the genes, relative to sham irradiated control.

3.3 Cell survival and mitochondrial membrane potential in RI-AR

Next, to verify the cytotoxic effect of priming dose if any, cellular outcomes in terms of viability as well as apoptosis were investigated.

Cells were allowed to recover for 24 and 72 h after CD, with and without PHA, and cell viability and proliferation were measured with trypan blue dye exclusion assay. A viability index was calculated which represents the ratio of number of live cells in irradiated group to the number of live cells in control, expressed as percentage. As shown in **Table 3. 1**, in the absence of PHA, primed cells consistently showed cell viability >90% which was significantly higher (p < 0.05) than the non-primed cells, though 7% and 9% lower than the sham irradiated cells at

24 h and 72 h, respectively. Cell viability remained uniformly high at all the time points in PBMCs irradiated with low dose of 100 mGy.

Viability index				
		100mGy	2Gy	100 mGy + 2 Gy
Without PHA	24 h	100.90 ± 0.45	88.14 ± 0.09*	93.06 ± 0.86*#
	72 h	100.21 ± 0.47	78.61 ± 0.05*	91.05 ± 2.33*#
With PHA	24 h	90.19 ± 2.11*	90.64 ± 1.26*	86.42 ± 1.02*
	72 h	96.51 ± 1.02*	88.92 ± 2.41*	90.67 ± 2.72*

Table 3. 1. Effect of low dose exposure on the viability of PBMCs incubated with and without PHA for 24 h and 72 h. *Sham irradiated *vs* irradiated; #2 Gy *vs* 100 mGy + 2 Gy.

We next asked whether pre-exposure to low dose radiation can modify phytohemagglutinin (PHA)-induced cell proliferation of human PBMCs. For this, post-irradiation, PBMCs were allowed to proliferate for 24 and 72 h in the presence of PHA and the total cell count was calculated. In the initial 24 h post radiation, the proliferation was slow and did not differ much among the three irradiated groups when compared with sham irradiated controls **(Fig. 3. 4)**. Non-primed cells showed 43% increase in cells while primed cells showed 51% increase against 56% increase in sham irradiated controls **(Fig. 3. 4)**. PBMCs irradiated with low dose of 100 mGy showed the smallest rate of proliferation with only 34% increase. When measured 72 h post CD, significant differences were found between the three treatment groups **(Fig. 3. 4).** PHA induced primed and non-primed cells showed significantly slower proliferative response than the sham irradiated and 100 mGy cells. As shown in **Fig. 3. 4** growth of primed cells was delayed by ~24 h while non-primed cells showed a delay of ~36 h relative to control, indicating the proliferative advantage of low dose

priming. On the other hand, low dose radiations of 100 mGy caused late stimulation in proliferation of PBMCs and exceed the sham irradiated controls by ~6 h.
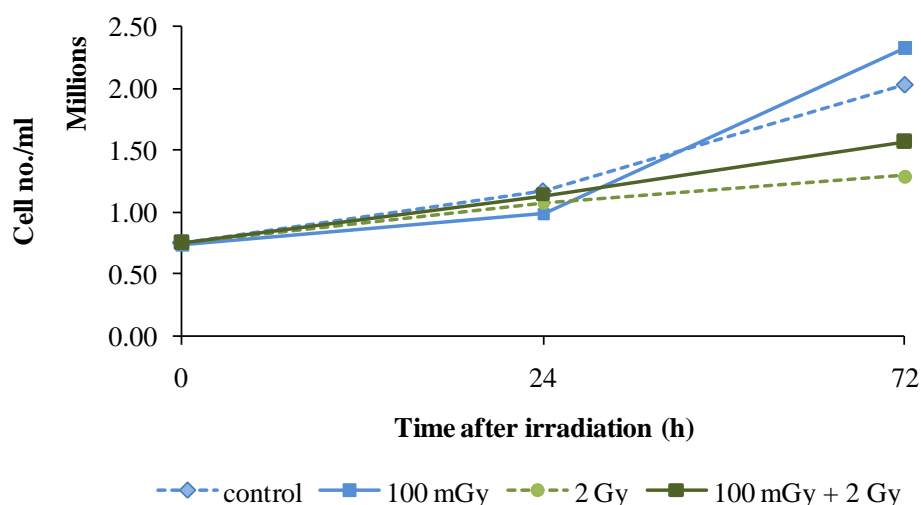
Fig. 3. 4. PHA-induced cell proliferation of human PBMCs. After irradiation, PBMCs were allowed to proliferate for 24 and 72 h in presence of PHA (10 µg/ml). Total number of cells were then counted using haemocytometer.

An important index of cell viability is the inner mitochondrial transmembrane potential ($\Delta\Psi$m). Changes in $\Delta\Psi$m are integral to physiological cell functioning and life–death transition. We therefore, evaluated $\Delta\Psi$m 24 h post-irradiation with CD using JC-1, a lipophilic cationic dye. This probe forms aggregates in mitochondria with high $\Delta\Psi$m and after excitation at 488 nm emit orange/red fluorescence at 590 nm. In cells undergoing membrane depolarization, loss of membrane potential prevents JC-1 from forming aggregates and the monomers emit in the green region of the spectrum (with a maximum at 527 nm). A decrease in red/green fluorescence intensity thus, indicates membrane depolarization. Changes in fluorescence were measured using a flow cytometer.

Fig. 3. 5A shows a representative flow cytometric dot plot demonstrating distribution of JC-1 aggregates and monomers in upper right and lower right quadrant, respectively. Sham irradiated as well as 100 mGy irradiated cells showed high red/green fluorescence ratio **(Fig. 3. 5B)**, indicating high $\Delta\Psi_m$. Irradiation of cells with 2 Gy alone in non-primed cells caused significant decrease in $\Delta\Psi_m$ to 32.9 $\pm$ 0.34 (p < 0.001) as compared to sham irradiated controls cells **(Fig. 3. 5B)**. On the other hand, cells that were pre-exposed to a priming dose showed significantly higher $\Delta\Psi_m$ as compared to the non-primed cells (60.7 $\pm$ 0.65, p < 0.001), though it was still lower than the sham irradiated control cells.

A
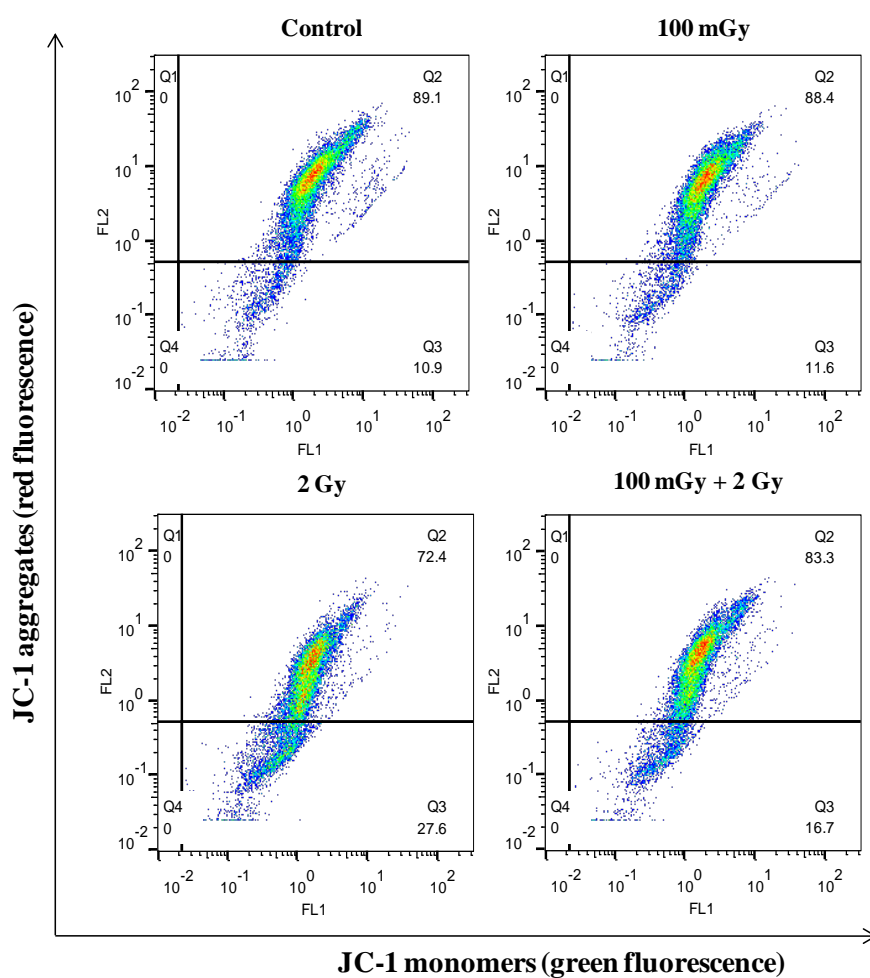
B
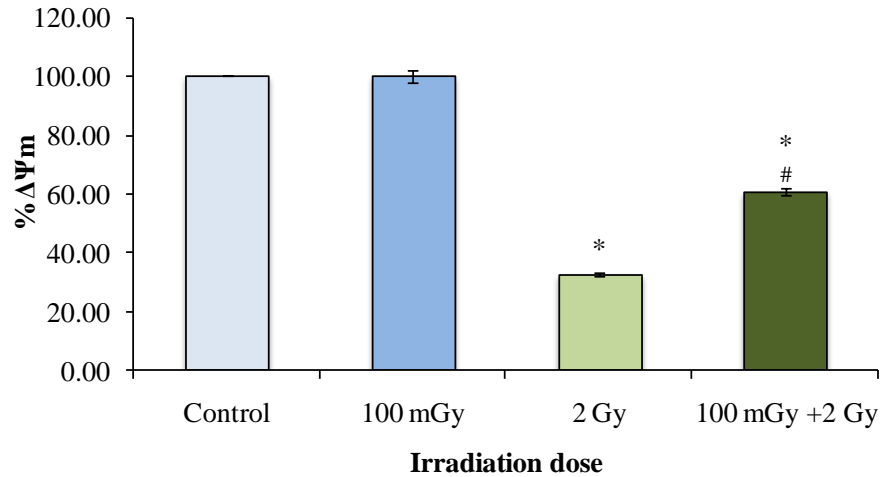
Fig. 3. 5 Primed human PBMCs showed lesser decrease of mitochondrial membrane potential ($\Delta\Psi$m) when challenged with 2 Gy. Cells were harvested and incubated with JC-1 for 15 min at 37°C in dark. JC-1 fluorescence was measured using flow cytometer. (A) Representative flow cytometric dot plot showing % cells with green fluorescence (FL1 channel) in lower right quadrant (Q3) and red fluorescence (FL2 channel) in upper right quadrant (Q2). (B) Ratio of red to green fluorescence (FL1/FL2) normalized with sham irradiated control plotted against dose. Statistical significance: *sham irradiated control *vs* irradiated, #2 Gy *vs* 100 mGy + 2 Gy.

3.4 Radiation-induced apoptosis in RI-AR

An increase in cell survival, as seen under non-cycling conditions, may be related not only to DNA strand breaks and repair but also with apoptosis. Effect of pre-exposure to LDR on apoptosis was studied using PI staining and annexin V-PI staining, 24 h post CD, with flow cytometry.

3.4.1 PI staining

Primed and non-primed cells were followed in the subG1 phase of the cell cycle as characteristic of apoptosis, 24 h after CD, using PI, a membrane impermeant

dye that is generally excluded from viable cells. The assay helps to detect necrotic or late apoptotic cells, which are characterized by loss of the integrity of the plasma and nuclear membrane. Both non-primed and primed cells showed significantly higher apoptosis as compared to sham irradiated control cells (54% in non-primed *vs* 56% in primed, $p < 0.01$) **(Fig. 3. 6A).** Prior exposure to LDR had no effect on apoptosis with no significant difference between primed and non-primed cells. Cells exposed to the low dose of 100 mGy did not show any significant change in apoptosis as compared to sham irradiated control cells.

3.4.2 Annexin V-FITC/PI dual staining

Apoptosis was also assessed with the more sensitive Annexin V-FITC/PI dual staining as it allows easy discrimination between viable cells (Annexin V− / PI−), early apoptotic cells (Annexin V+ / PI−), late apoptotic/necrotic cells (Annexin V+ / PI+) and late necrotic cells (Annexin V− / PI+). The results observed were same as seen with PI assay. PBMCs exposed to 2 Gy CD alone (non-primed cells) showed a significant increase in early apoptosis relative to sham irradiated control (10.3 ± 0.14 *vs* 3.3 ± 0.48, p=0.03). Cells pre-exposed to 100 mGy (primed cells) showed a similar increase relative to sham irradiated cells (9.6 ± 0.66, $p = 0.012$) **(Fig. 3. 6B)** Thus, there was no statistical difference between primed and non-primed cells. PBMCs irradiated with low dose of 100 mGy alone showed a small statistically insignificant increase in early apoptosis relative to control ($p = 0.07$).

A

B
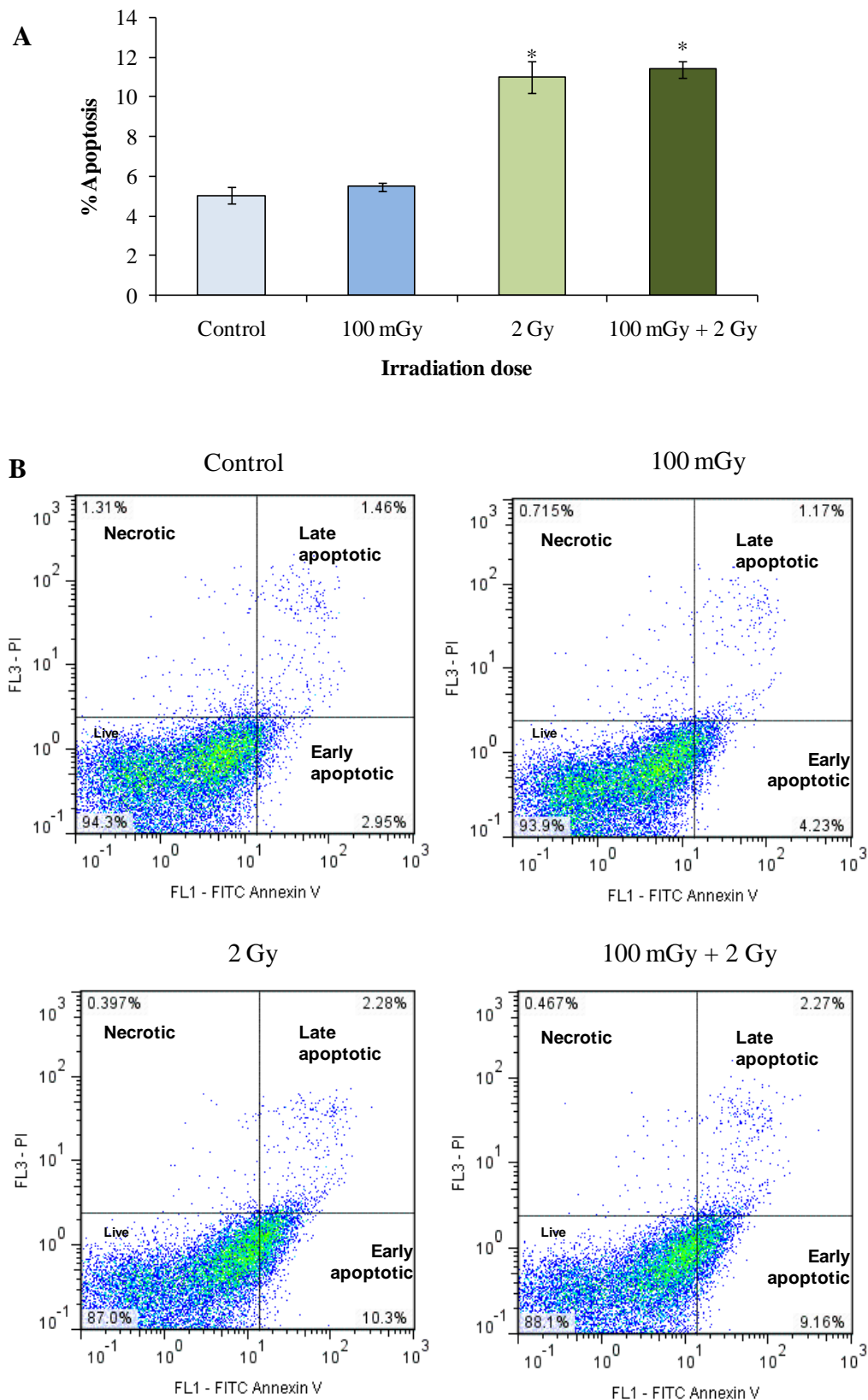
Fig. 3. 6. Pre-exposure to a low priming dose does not alter apoptosis. Human PBMCs were incubated for 24 h after irradiation. (A) Estimation of apoptosis by PI

staining and flow cytometry. *sham irradiated control *vs* irradiated. (B) Estimation of apoptosis by annexin V-FITC and PI dual staining. All dot plots are a representation of equal cell populations (n=20,000) from a single analysis. The lower left, lower right, upper right and upper left quadrants represents the populations of live, early and late apoptotic, and necrotic cells, respectively.

3.5 Levels of intracellular and mitochondrial ROS in RI-AR

It has been well established that in the target tissue, IR predominantly interacts with water molecules to generate water radiolysis products, including free radicals. The ROS generated by radiation is the primary contributor to DNA damage in the cell. Here we explored the role of ROS in RI-AR of human PBMCs. Intracellular ROS was measured using H_2DCF-DA on a flow cytometer **(Fig. 3. 7A and Fig. 3. 7B)** and visualized using a fluorescent microscope **(Fig. 3. 7C)**. Mitochondrial (mt) ROS was analysed with mitoSOX fluorescence on a spectrophotometer **(Fig. 3. 7D)**.

Irradiation of non-primed cells with 2 Gy showed a significant increase in the levels of intracellular ROS immediately after radiation, with a change in DCF fluorescence intensity from 36.3 ± 1.70 in sham irradiated control to 58.8 ± 0.42 ($p < 0.001$). On the other hand, cells primed with LDR showed a smaller increase in DCF fluorescence to 41.8 ± 0.36, though it was still significantly higher than the control cells ($p = 0.01$) **(Fig. 3. 7A and Fig. 3. 7B)**. Irradiation of cells with low dose of 100 mGy showed no change in DCF fluorescence, as compared to sham irradiated cells.

A

B

C

| Control | 100 mGy | 2 Gy | 100 mGy + 2 Gy |

D
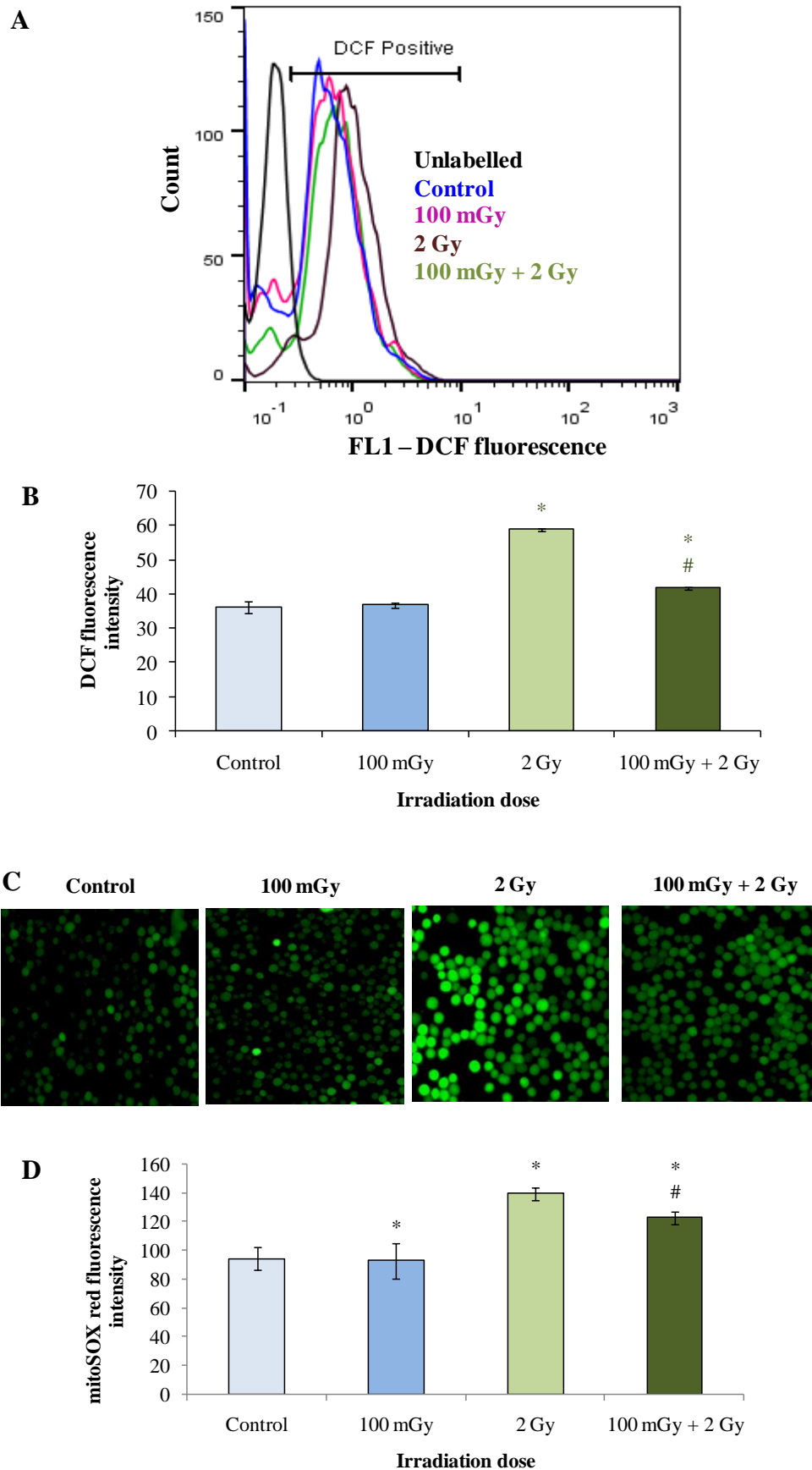
Fig. 3. 7. Primed cells showed decreased levels of ROS. Human PBMCs were incubated with H_2DCF-DA for 20 min at 37°C in dark to measure endogenous ROS. Fluorescence was measured after immediate exposure to IR (A) Representative flow cytometric histogram showing endogenous ROS levels. (B) Corresponding bar graph showing endogenous ROS levels. (C) DCF fluorescence observed under fluorescence microscope. (D) Human PBMCs were incubated with mitoSOX red to measure mitochondrial ROS. Fluorescence was measured after immediate exposure to IR. *sham irradiated control *vs* irradiated, #2 Gy *vs* 100 mGy + 2 Gy.

A similar trend was observed for mt ROS. The mitoSOX red fluorescence in the 2 Gy irradiated cells increased to 139.6 ± 4.36 from 94.3 ± 8.08 in sham irradiated control immediately after radiation (p = 0.002). Cells primed with LDR showed a smaller increase to 122.6 ± 4.36 (p = 0.01) as compared to sham irradiated control cells **(Fig. 3. 7D)**. mtROS levels in cells irradiated with 100 mGy alone was similar to sham irradiated cells.

3.6 Active redox regulation in RI-AR

The intracellular redox status is a balance between oxidative stress and endogenous thiol levels which protect cells from oxidative damage. Therefore, we next studied modulation of thiols in response to low priming dose.

Basal and IR induced levels of total thiols and intracellular thiols in human PBMCs were analyzed immediately (0 min) and 60 min, post IR exposure. Total thiol levels were measured with Cayman's total thiol detection kit. Intracellular thiol levels were measured using thiol specific probe monobromobimane (MBB).

The levels of total thiols remain unchanged in the all irradiated cells when compared with sham irradiated cells at both the time points **(Fig. 3. 8A)**. There was no significant difference in the thiol levels between non-primed and primed cells.

Intracellular thiols, on the other hand, showed a significant decrease ($p < 0.05$) in all irradiated samples immediately after irradiation (0 min) and the levels continued to be low even after 60 min **(Fig. 3. 8B)**. Interestingly, primed cells required lesser utilization of intracellular thiols than non-primed cells ($p = 0.05$), immediately after IR **(Fig. 3. 8B)**, probably since IR-induced ROS levels were also low in the primed cells.

A

B
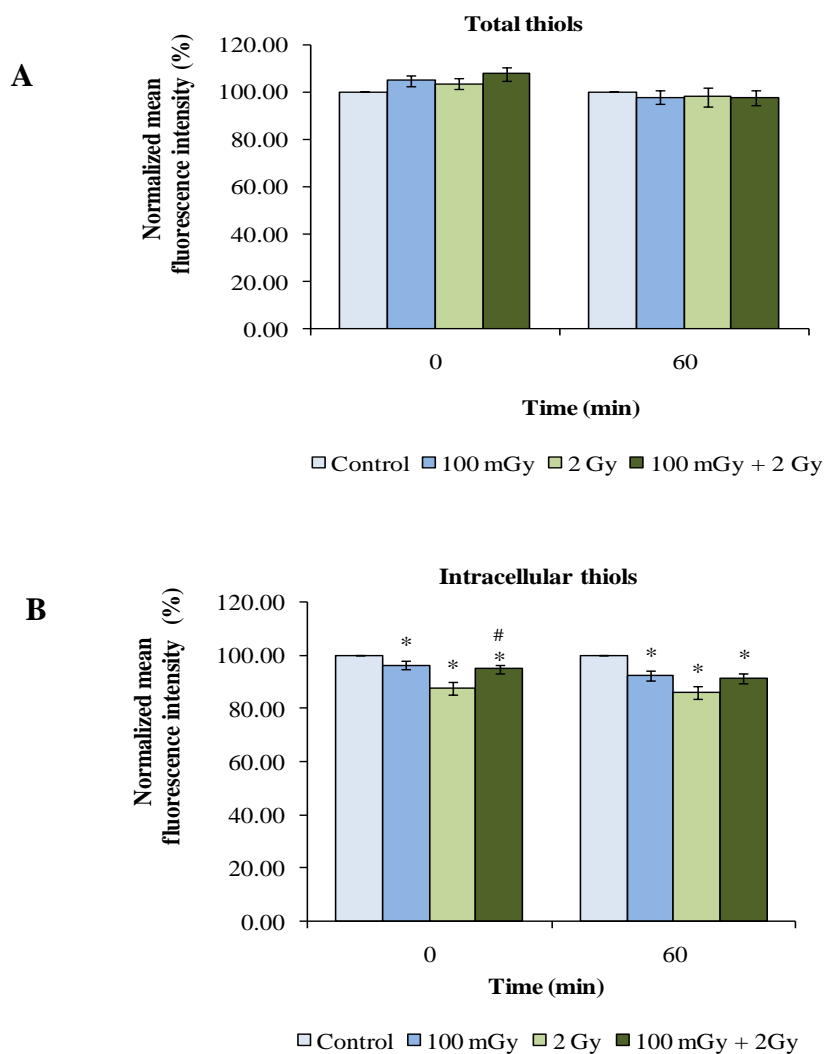
Fig. 3. 8. Primed cells showed modulation of thiols. Cells were harvested 0 and 60 min post IR exposure and thiol levels were measured. (A) Total thiol levels measured by Cayman total thiol detection kit using the manufacturer's instructions. (B) Intracellular thiol levels measured using MBB staining and flow cytometry. Values were normalized to sham irradiated control. *sham irradiated control *vs* irradiated, [#]2 Gy *vs* 100m Gy + 2 Gy.

Reduced glutathione (GSH) is considered to be a key thiol-disulfide redox buffer of the cell and its ratio with oxidised glutathione (GSSG) may be used as an indicator of oxidative stress. Levels of GSH and GSSG were measured immediately (0 min) and 60 min post exposure to CD. When measured immediately after exposure to IR, non-primed and primed cells showed a decrease of ~26% and ~40% respectively (p ≤ 0.05) in GSH levels **(Fig. 3. 9A).** Similar trend was observed 60 min post exposure to CD with a decrease of ~33% and ~35% in non-primed and primed cells respectively (p ≤ 0.05).

This robust utilization of GSH was companied with a significantly lower GSH/GSSG ratio both in non-primed and primed cells as compared to sham irradiated cells at both the studied time points. However, the decrease was steeper in primed cells than the non-primed cells immediately after CD **(Fig. 3. 9B).** This indicated a shift of intracellular redox state more towards more oxidizing conditions.

A

B
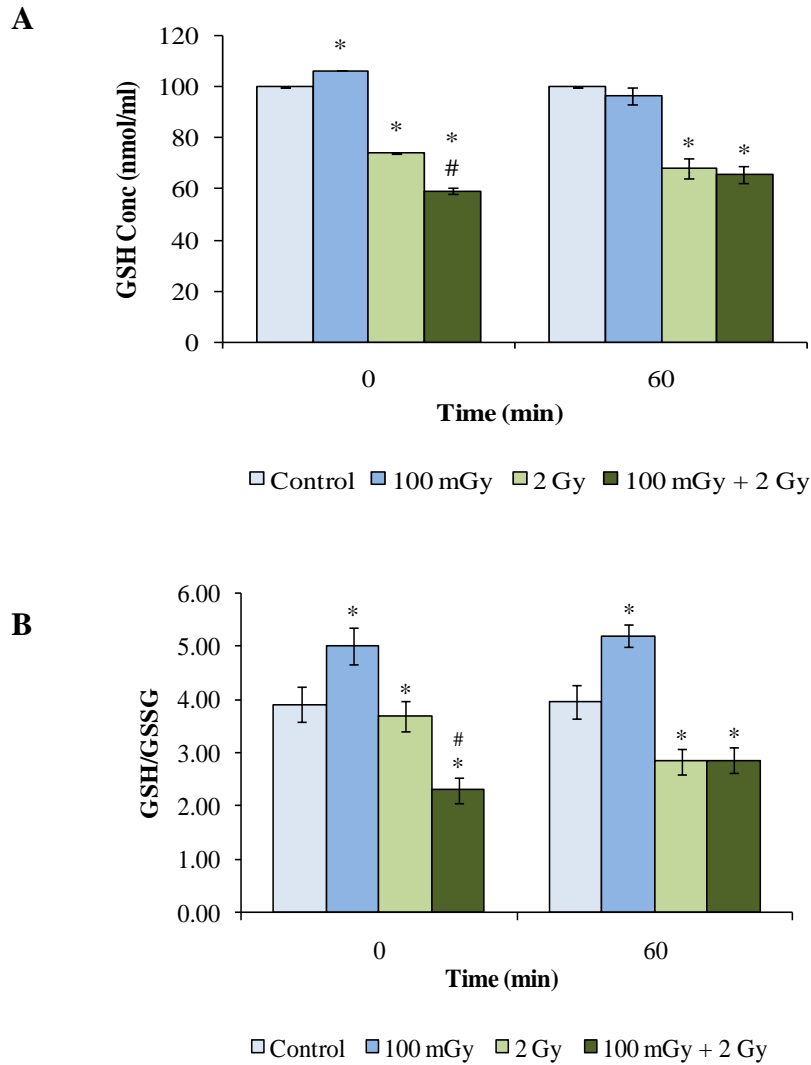
Fig. 3. 9. Primed cells showed modulation of GSH levels and GSH/GSSG ratio. Cells were harvested 0 and 60 min post IR and concentration of GSH and GSSG was measured spectrophotometrically and ratio of GSH to GSSG was calculated. (A) Concentration of GSH measured at indicated time points. (B) Bar graph represents GSH/GSSG ratio. *sham irradiated control *vs* irradiated, #2 Gy *vs* 100 mGy + 2 Gy.

Primed cells however, showed a small recovery in GSH/GSSG ratio when measured 60 min after CD, while the ratio decreased further in non-primed cells (**Fig. 3. 9B**). In both the cases, the ratio was still lower than the control cells. Cells irradiated with low dose of 100 mGy alone showed a significantly increased levels of

GSH early after irradiation (0 min) **(Fig. 3. 9A)**. These cells also showed a significantly higher ($p < 0.05$) GSH/GSSG ratio at both the time points when compared with sham irradiated control cells **(Fig. 3. 9B)**.

3.7 Early activation of antioxidant enzymes in RI-AR

Modulation of overall redox state and the extent to which ROS accumulates in a cell is governed by an extensive network of cellular antioxidant defense system working as a whole. Since the primed cells showed lower levels of ROS, it was argued that this could reflect an early activation of potent antioxidant system in these cells. Therefore, we measured coordinated changes in activity and transcript levels of four key antioxidant enzymes: catalase (CAT), superoxide dismutase (SOD), thioredoxin reductase (TXNRD1) and glutathione peroxidase (GPX), 0 min and 60 min post irradiation.

3.7.1 Gene expression

Gene expression was monitored with RT-qPCR using GAPDH as the reference gene. The MIQE guidelines of 2009 [109] mandates validation of the reference gene(s) for the cell system and the specific conditions used for an experiment. Therefore, we first compared Cq values for GAPDH gene in human PBMCs from three samples selected randomly from the five individuals used in this study. qPCR was performed at 0 and 60 min time points under all the three irradiation conditions and compared with sham irradiated cells. Stable expression of GAPDH was seen in all the treatment groups, indicating its suitability for RT-qPCR in human PBMCs **(Fig. 3. 10).**
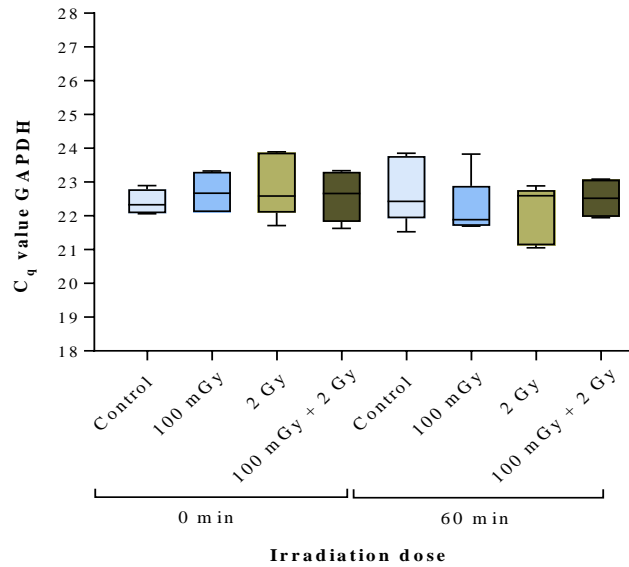
Fig. 3. 10. Quantification cycle values (Cq) of reference gene GAPDH measured in all the treatment groups in human G_0 PBMCs. Each box represents Cq values for three individuals, at the respective dose (sham irradiation, 100 mGy, 2 Gy and 100 mGy+2 Gy) and time points (0 and 60 min). The boxes indicate the 5/95 percentiles, black line across the box represents median values and whiskers indicate the value range.

When gene expressions were compared at 0 min, primed cells showed higher expression for MnSOD (~2.77 fold *vs* ~1.99 fold; p = 0.0006) and CAT genes (~3.09 fold *vs* ~2.04 fold; p = 0.043) **(Table 3. 2A)**. By 60 min post CD, expression for both MnSOD and CAT had reduced significantly in both primed and non-primed cells **(Table 3. 2B)**. On the other hand, expression for GPX1 increased after 60 min but was lower in primed cells as compared to non-primed cells (~1.09 *vs* ~1.28; p = 0.046). Similarly for TXNRD1, non-primed cells showed a significantly higher expression as compared to primed cells (~2.63 *vs* ~0.75; p = 0.0004) after 60 min. Irradiation with 100 mGy alone resulted in statistically significant upregulation of CAT mRNA levels immediately after CD (6.9 fold; p = 0.0004) **(Table 3. 2A)**, and

MnSOD (2.1 fold; $p < 0.0001$) and GPX1 levels (2.4 fold; $p < 0.0001$) 60 min after CD, compared to sham irradiated controls **(Table 3. 2B).**

A

Gene	0 min			
	100 mGy	2 Gy	100 mGy + 2 Gy	p value
MnSOD	0.14 ± 0.01	1.99 ± 0.15	2.77 ± 0.20	**5.9E-03**
GPX1	0.11 ± 0.01	0.31 ± 0.02	0.43 ± 0.04	**6.9E-03**
CAT	6.94 ± 0.96	2.04 ± 0.05	3.09 ± 0.62	**4.3E-02**
TXNRD1	0.38 ± 0.10	0.85 ± 0.04	0.62 ± 0.13	**4.5E-02**

B

Gene	60 min			
	100 mGy	2 Gy	100 mGy + 2 Gy	p value
MnSOD	2.14 ± 0.01	1.09 ± 0.09	0.60 ± 0.02	**3.1E-06**
GPX1	2.40 ± 0.10	1.28 ± 0.03	1.09 ± 0.11	**4.6E-02**
CAT	0.61 ± 0.12	0.39 ± 0.06	0.20 ± 0.03	**9.0E-03**
TXNRD1	0.70 ± 0.01	2.83 ± 0.32	0.75 ± 0.05	**3.9E-04**

Table 3. 2. Relative expression of antioxidant genes in human PBMCs measured at (A) 0 and (B) 60 min after irradiation. The significant p-values for non-primed *vs* primed cells are represented in bold.

3.7.2 Enzyme activity

Pre-exposure to a low dose priming dose resulted in higher activity of all four-studied antioxidant enzymes as compared to the activity in non-primed cells **(Fig. 3. 11A-D)**. While TrxR activity peaked immediately after CD **(Fig. 3. 11D)**, activity of CAT, MnSOD and GPX peaked after 60 min in primed cells **(Fig. 3. 11A-D)**. At 0 min after CD, TrxR activity was 147% ($p = 0.0095$) in primed cells as compared to non-primed cells and persisted to slightly higher level after 60 min (16.1%, $p = 0.30$), The CAT enzyme activity was 67.7% higher in primed cells as compared to non-primed cells ($p = 0.007$) when estimated 60 min post CD, though there was no

significant difference from sham irradiated cells or non-primed cells immediately (0 min) after irradiation **(Fig. 3. 11B)**. When MnSOD activity was assessed, primed cells showed a modest 19.5% (p = 0.13) increased activity immediately after CD and increased further (~117%, p = 0.039) by 60 min relative to non-primed cells **(Fig. 3. 11A)**. When comparison was made for GPX activity, it was found to be lower in primed cells (by 16.9%, p = 0.0024) at 0 min, but increased significantly (55.7% *vs* non-primed cells; p < 0.0001) 60 min post CD **(Fig. 3. 11C)**. The non-primed cells showed significant increase from sham irradiated cells only for GPX activity at 0 min post CD (p < 0.01). With only low dose (100 mGy) irradiation, CAT activity showed a significant increase after 0 min (19.6%; p = 0.036) and MnSOD (79%, p = 0.03) at 60 min post CD, while TrxR showed a significant decrease after 60 min (37%; p = 0.001).
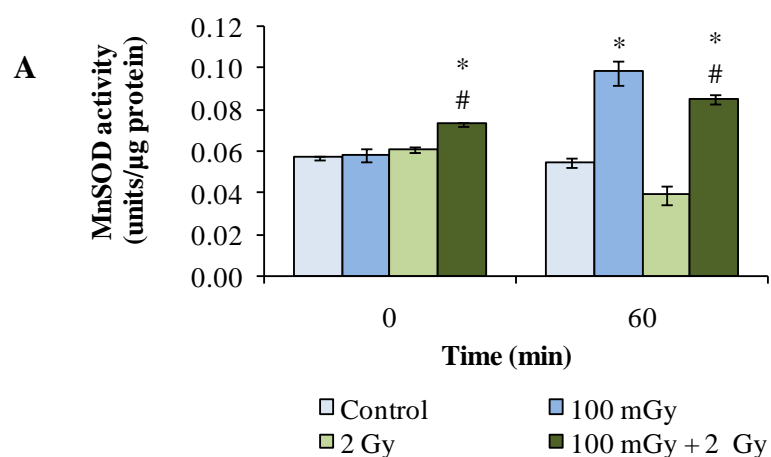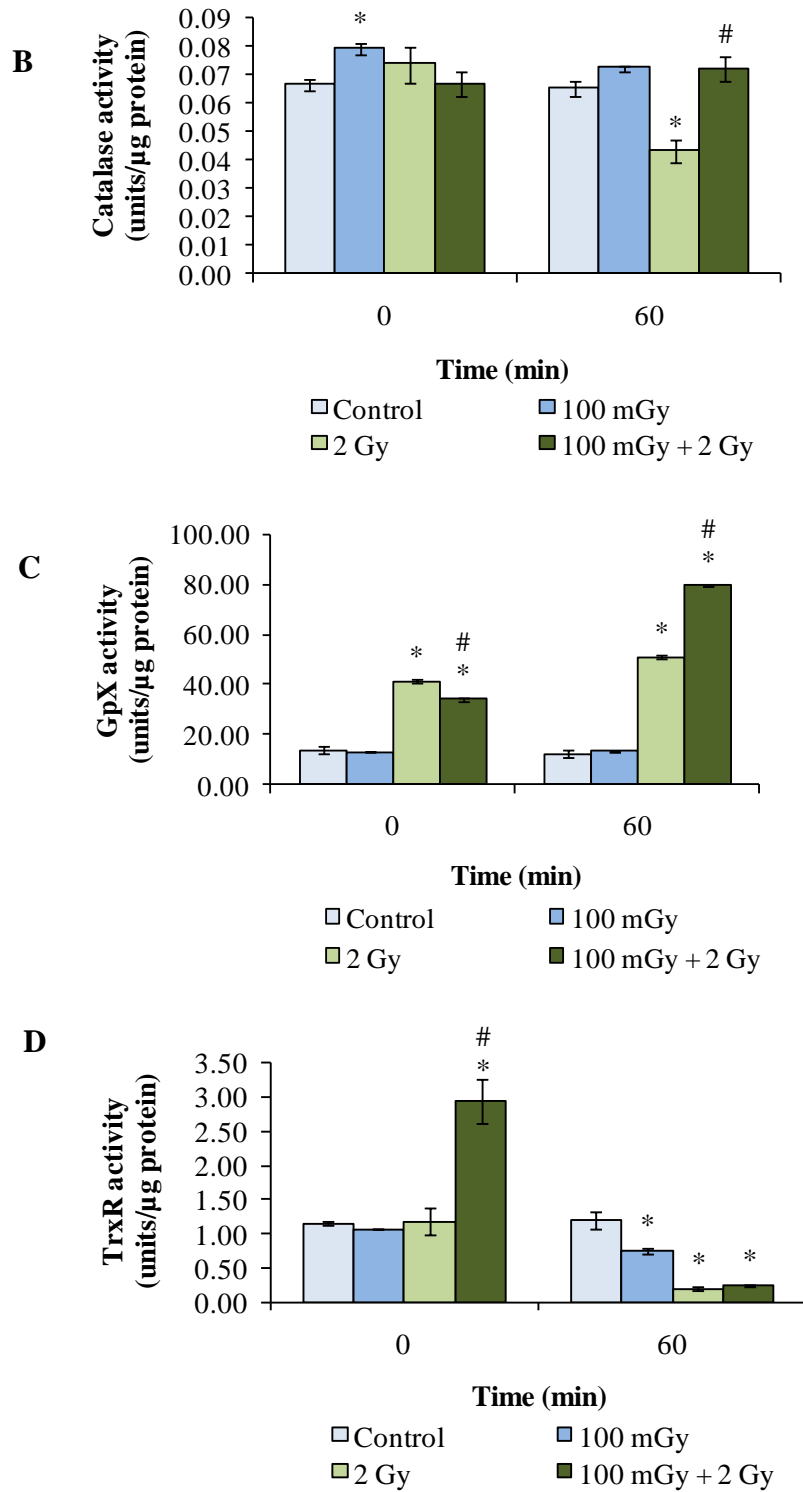
Fig. 3. 11. Pre-exposure to a low PD enhanced the activity of antioxidant enzymes (A) MnSOD, (B) catalase, (C) glutathione peroxidase, (D) thioredoxin reductase at indicated time points. *sham irradiated control *vs* irradiated, #2 Gy *vs* 100 mGy + 2 Gy.

To the best of our knowledge, our data shows for the first-time the gene expression patterns of antioxidant genes in conjunction with the enzyme activity to understand RI-AR in the same human samples.

3.8 Increased binding of NF-κB and Nrf2 in RI-AR

The transcription factors nuclear factor-erythroid-2-related factor 2 (Nrf2) and nuclear factor-κB (NF-κB) are known to be the major components that regulate cellular redox homeostasis in response to various stress stimuli, including IR. They are known to be critical mediators of antioxidant program in the cell. They bind to the ARE in the promoter region of various antioxidant and detoxification genes, thereby regulating their basal as well as coordinated expression in a cell and stimulus specific manner.

To study whether the reduced ROS levels and increased antioxidant activity in primed cells are mediated through DNA binding of Nrf2 and NF-κB in G_0 PBMCs, EMSA was performed. All the treatment groups showed an immediate and significant binding of NF-κB when compared to sham irradiated control cells (**Fig. 3. 12A**). When comparison was made between primed and non-primed cells, a higher binding was seen in primed cells immediately after CD which persisted till 60 min (**Fig. 3. 12A**). On the other hand, Nrf2 showed a highly specific, immediate and transient binding only in primed cells analysed immediately after CD (**Fig. 3. 12B**). Nrf2 did not show any appreciable binding for non-primed and 100 mGy irradiated cells (**Fig. 3. 12B**). Specificity of NF-κB and Nrf2 binding oligonucleotide was confirmed by performing competition assay (**Fig. 3. 12C & D**). No signal was observed with mutant and cold competitor oligonucleotide.
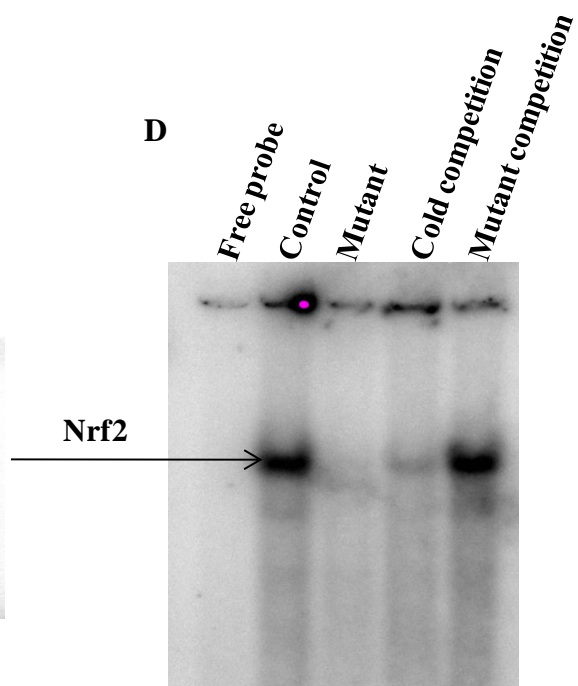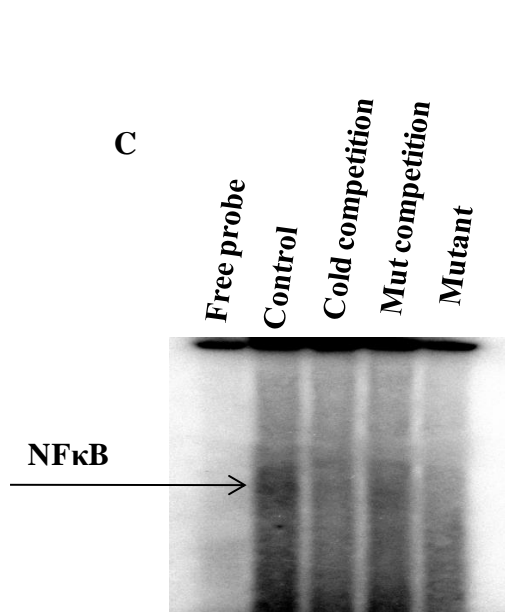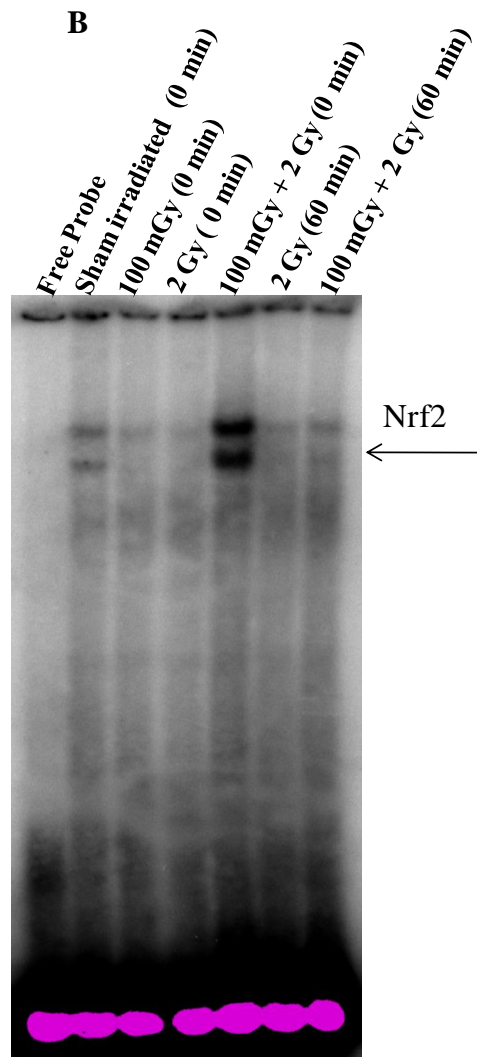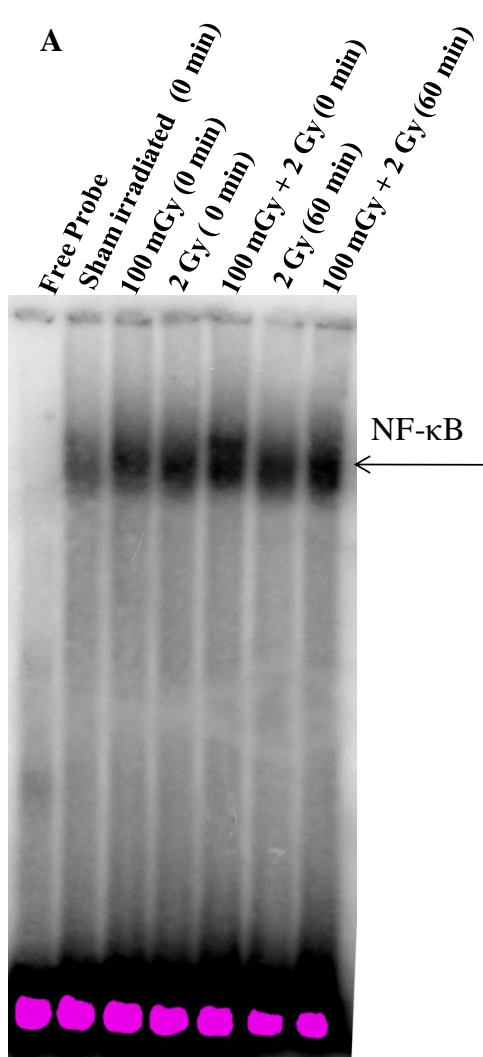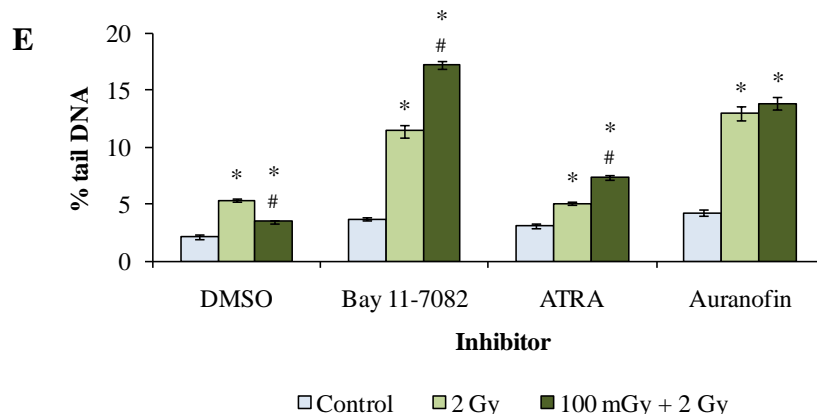
Fig. 3. 12. Pre-exposure to a low PD lead to increased DNA binding of NF-κB and Nrf2. Nuclear extracts of non-primed and primed cells were prepared immediately (0 min) and 60 min after irradiation and electrophoretic mobility shift assay (EMSA) was performed using ^{32}P labelled probe for (A) NF-κB and (B) Nrf2. Competition assay for (C) NF-κB and (D) Nrf2 sequence specificity confirmation (E) Abrogation of RI-AR in presence of inhibitors for Nf-κB (Bay 11-7082), Nrf2 (ATRA) and thioredoxin reductase (Auranofin) observed using alkaline comet assay. DMSO – No inhibitor control. *sham irradiated control *vs* irradiated, #2 Gy *vs* 100 mGy + 2 Gy.

To further evaluate the role of these two transcription factors in RI-AR, DNA damage using alkaline comet assay was measured by treating the PBMCs with chemical inhibitor of Nrf2 - ATRA (5 µM) and inhibitor of NF-κB/IKK – Bay 11-7082 (2.5 µM) separately for 2 h before irradiation with priming dose. In both the cases, chemical inhibition resulted in complete abrogation of adaptive response. Binding of transcription factors to DNA is a Trx-dependent process [110]. Treatment of PMBCs with a thioredoxin reductase inhibitor (Auranofin, 0.1 µM) resulted in a similar loss of RI-AR (**Fig. 3. 12E**).

We also performed RT-qPCR for four downstream target genes of NF-κB and Nrf2: IFNG (interferon-γ), TNFA (tumor necrosis factor-α), HMOX1 (heme oxygenase 1) and PRDX6 (peroxiredoxin 6). Primed cells showed significantly higher expressions of IFNG, TNFA and PRDX6 as compared to non-primed cells when analysed immediately after CD **(Table 3. 3A)**. On the other hand, HMOX1 expression showed a down-regulation both in primed and non-primed cells as compared to the sham-irradiated control **(Table 3. 3A)**.

A Gene	0 min			
	100 mGy	2 Gy	100 mGy + 2 Gy	p value
IFNG	1.47 ± 0.35	3.24 ± 0.17	8.47 ± 1.85	**3.2E-02**
TNFA	1.48 ± 0.26	1.52 ± 0.59	3.29 ± 0.62	**2.3E-02**
HMOX1	0.94 ± 0.04	0.85 ± 0.03	0.92 ± 0.01	**2.3E-02**
PRDX6	0.55 ± 0.02	0.75 ± 0.04	1.42 ± 0.17	**2.7E-03**

B Gene	60 min			
	100 mGy	2 Gy	100 mGy + 2 Gy	p value
IFNG	0.56 ± 0.15	1.72 ± 0.17	1.25 ± 0.30	0.08
TNFA	1.14 ± 0.13	1.32 ± 0.48	1.19 ± 0.48	0.76
HMOX1	1.05 ± 0.06	1.01 ± 0.01	0.90 ± 0.04	**5E-03**
PRDX6	0.92 ± 0.03	0.83 ± 0.13	0.93 ± 0.19	0.53

Table 3. 3. Mean fold change of gene expression in human PBMCs for NF-κB dependent genes (IFNG, TNFA) and Nrf2 dependent genes (HMOX1, PRDX6) measured (A) 0- and (B) 60-min post-irradiation using SYBR green. The significant 'p' values (p ≤ 0.05) for primed *vs* non-primed cells are represented in bold.

3.9 Early activation of MAP kinase enzymes in RI-AR

Radiation is known to activate the MAPK family of signal transduction proteins [33,111]. To understand how priming with low dose might affect intracellular signaling in general in human PBMCs, total cellular proteins were

extracted from the cells and the three MAPK proteins - ERK, p38 and SAPK/JNK - were assessed by Western blotting. Activation of these MAPK proteins is dependent on phosphorylation at specific sites, which was assayed by probing with phosphorylation site-specific antibodies. GAPDH was used as the loading control.

Western blot analysis showed that adaptive dose of 100 mGy directed rapid and early increase in phosphorylation of the MAP kinase signaling proteins after exposure to CD **(Fig. 3. 13)**. Phosphorylated-p38 (p-p38) was activated strongly as early as 5 min post radiation in both primed and non-primed cells. Primed cells showed a higher, but transient expression, while the activation persisted till 15 min post CD in non-primed cells. p-ERK, on the other hand, was activated at 15 min post CD in both primed and non-primed cells. While the expression for primed cells peaked transiently at 15 min, non-primed cells showed a delayed peak at 60 min. Similarly, pSAPK/JNK showed an early activation at 15 min post CD in the primed cells which persisted till 60 min, while activation in non-primed cells trailed at 30 min post CD and continued till 60 min. Thus, primed PBMCs presented distinct kinetics of activation of MAPK as opposed to non-primed cells.
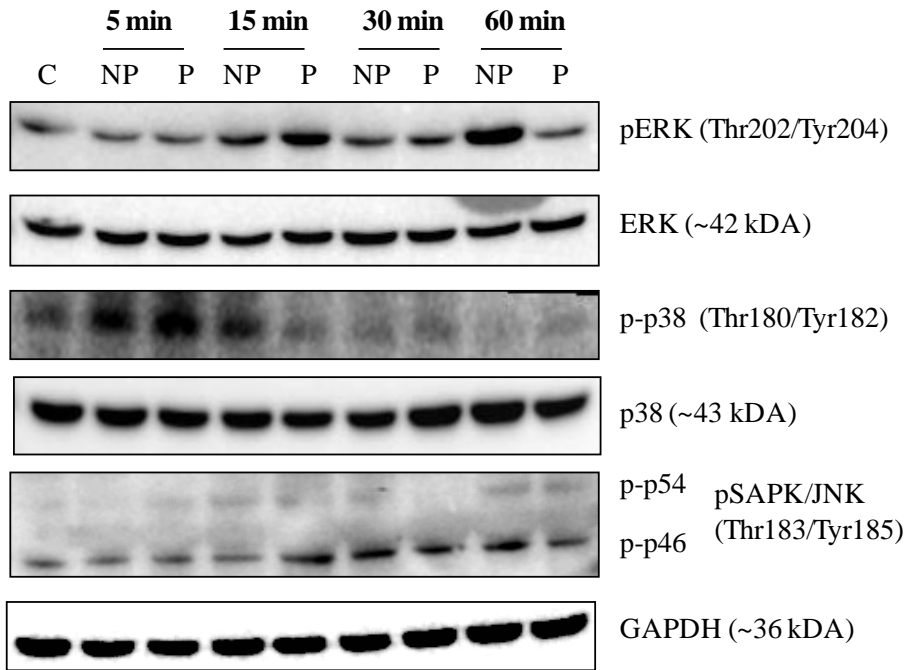
Fig. 3. 13. Early activation of MAP kinase enzymes in primed cells. Protein extracts were prepared 5, 15, 30 and 60 minutes after exposure to CD and western blotting was performed using GAPDH as loading control. A representative blot for pERK, ERK, p-p38, p38, pSAPK/JNK and GAPDH is given.

3.10 Discussion

The scientific community has long been concerned with how biological systems respond to and tolerate exposure to low doses of ionizing radiation. A wealth of evidence now indicates that when cells are pre-exposed to low doses of radiation (referred to variously in the literature as the conditioning, inducing, priming as adaptive dose) or other DNA damaging agents, they develop higher resistance to a subsequent high dose of these agents (called the challenge dose). This response to low dose exposure has been referred to as an adaptive response. The first important observation from mammalian cells studies in support of these processes was provided by Oliveri *et al* [48]. Ten years later, the low dose radiation induced-adaptive response (RI-AR) phenomenon was, for the first time, officially introduced by the United Nations Scientific Committee on the Effects of Atomic Radiation (UNSCEAR) in its 1994 report to the United Nations (UN) General Assembly [112]. Subsequently, more evidence of RI-AR has been described in proliferating cultured lymphocytes [78,113] and in other mammalian cell types such as bone marrow cells [114,115] and fibroblasts [116,117]. Evidence of RI-AR has also been described in studies using laboratory animals [51], occupational workers exposed to chronic low doses of radiation [63,64] as well as in human populations exposed to high level natural background radiation [67–69]. Presence of RI-AR is not clearly evident from the animal studies in terms of extended life-span or a reduced tumor induction.

Interpretation of these experiments is further complicated by variations in the susceptibility of different animal strains. Most epidemiological cancer surveys on human populations exposed to low dose radiation lack the required statistical power to reach a decisive conclusion on the existence or absence of RI-AR. New research that can provide consistent evidence is therefore, required.

The responses of mammalian cells to low dose radiation are complex and involve multi-step processes. The entire chain of molecular processes involved in the development of RI-AR in human cells has not been studied systematically, though many individual links have been postulated. There have been suggestions that adaptive response can be considered as a consequence of DNA damage and cellular repair is likely to play a key role by mechanisms similar to those involved in the generalized stress response. Other cellular mechanisms too, have been proposed. This includes cell cycle control, activation of genes and induced proteins specifically that initiate DNA repair and radical detoxification to reduce potential for damage [112]. A comprehensive testing of these hypotheses in a singular cellular model that can effectively mimic the *in vivo* conditions is nevertheless, essential. In recent years, it has been suggested that the conventional estimates of the risks of stochastic effects of low doses of radiation using the linear no-threshold (LNT) model may be an over-estimation since it does not take into account the radioadaptive ability of cells. This has also led to concerns that an over-emphasis on LNT even in the low dose region may lead to apprehensions in the public mind about radiation and may limit its applications for societal benefits. A better understanding of the mechanisms of RI-AR might help resolve whether adaptive response can modify the incidence of late effects such as cancer induction in humans after low doses of radiation. This could further

help to develop improved cancer treatment regimens, risk assessment and risk management strategies, and better radiation protection, e.g. for radiation workers.

Validation of RI-AR in G_0 PBMCs

PBMCs, which are recognized as quiescent cells (G_0 state), have been widely used for basic research and clinical studies to investigate the biological effect of IR since these cells show high radiation sensitivity. They form a subset of white blood cells and can be easily isolated from whole blood, although the non-cycling nature of quiescent cells makes obtaining sufficient quantities of cells for many biological assays particularly challenging. PBMCs provide a reliable representation of physiological or pathological processes of the body. They also hold the advantage of lower inter-individual variations as compared to other biofluids.

We first validated the cellular system of G_0 PBMCS adopted for the present study by measuring baseline DNA damage using alkaline comet assay with increasing exposures to IR ranging from 0.01 Gy to 4 Gy. Since for most mutagens the strongest effect has been reported immediately after treatment [118], we measured DNA damage within the first 5 min after irradiation (hereafter called 0 min time point). The strand breaks were quantified in terms of percentage of DNA in comet tail (% tail DNA) as it is considered the preferred metric or the primary end point [119]. Comet assay has been used widely to understand IR induced DNA damage in various cellular systems such as chinese hamster ovary (CHO) cells [120], tumor cells [121,122], germ cells [123] and human lymphocytes [66,124], for both high dose exposures as well as for exposures below 1 Gy [125]. Alkaline comet assay detects DNA SSBs either induced directly or formed as a result of BER and alkali-labile sites, DNA-DNA/DNA-protein cross-linking, and transient repair sites [126]. We

observed a consistent dose dependent increase in the average % tail DNA with increasing radiation dose.

RI-AR is characterized by a narrow range for the priming and challenge dose and a specific "adaptive window" between the priming and challenge dose [127,128]. Next, proof-of-concept for adaptive response was established in non-proliferating G_0 PBMCs using a PD of 100 mGy, a CD of 2 Gy and a time interval of 4 h between these two doses using alkaline comet assay to measure DNA damage. Adaptive response was observed in five out of seven samples screened during this work and a decrease in % tail DNA ranging from 8.3% to 30.8% in comets was observed.

Inter-individual donor variability in adaptive response and variability in human cell lines has been reported by many researchers [56,129–133]. The question why lymphocytes from some individuals do not respond to the priming dose remains unresolved. In fact, some reports suggest a synergistic effect with the subsequent challenge in lymphocyte cultures [55,56]. Several theories have been proposed. One possibility is that the variability in AR or differences in sensitivity to radiation may depend on genetic constitution of the cell [55,56,134]. In case of culture cells, physiological state of the cell like the pH of the media, presence of growth factors etc., might contribute to the variability [129,131]. Another possibility is that the nutritional status or immunocompetence of an individual may influence radiation response. Another explanation that has been put forward is that adaptive response occurs only at precise time in the cell cycle. For asynchronous cell populations, there is variability in the cell cycle transition times. As the intrinsic cellular radiosensitivity varies in different stages of cell cycle, the time of administering CD may be crucial.

There is a difference of opinion in literature as to whether or not the RI-AR occurs if the priming dose is given in the resting or early (G_0/G1) stages of the cell

cycle. Some studies reported that RI-AR can be induced only when priming dose was administered to mitogen stimulated lymphocytes in G1 [54,135] or S phase [53,114] but not when administered in G_0 stage [53,54,136]. This important point needs to be resolved since it has important implications for the situations where cells are chronically irradiated *in vivo* and the cells are presumed to be in the G_0 phase. This includes lymphocytes of workers occupationally exposed to low doses of radiation or individuals residing in the high level natural background radiation areas of the world. The results from this study provide additional evidence that RI-AR can be induced in quiescent human lymphocytes in the G_0 stage and support several such studies [65,67,114,137–139].

Since the main objective of the present work was to understand mechanism of RI-AR, all further experiments were carried out by pooling equal number of freshly extracted PBMCs from five individuals (S1-S5) to minimize variability within and between assays. The pooled sample showed 16% lesser % tail DNA in comets when primed with 100 mGy as compared to non-primed cells. Thus, low dose radiation appears to offer protection from initial DNA damage. This is in contrast to results shown by Ikushima *et al* 1996 [140].

Mechanisms of radiation-induced adaptive response

DNA repair

In their seminal publication regarding RI-AR, Wolff *et al* (1998) suggested the role of DNA repair in RI-AR and *de novo* synthesis of factors involved in DNA repair during induction of RI-AR [141]. Subsequent work by several authors proposed involvement of several DNA repair proteins such as PARP, DNA-PK, ERCC5, ATM, NHEJ and BER pathway proteins in induction of RI-AR [142].

To test the role of DNA repair in RI-AR, we used alkaline comet assay to study dose-effect functions at various time points after CD to follow DNA repair. In continuance to lower initial DNA damage, primed cells showed lower % tail DNA in comets at 15 min post irradiation with CD also (5.06 ± 0.73 in primed *vs* 7.65 ± 0.51 in non-primed, p = 0.04). However, by 30 min after CD, both primed and non-primed cells showed similar % tail DNA in comet and most damage was repaired by 60 min. Thus, there was no difference in residual DNA damage between primed and non-primed cells as measured by comet assay.

Though single strand breaks are one of the more frequent DNA lesions produced by IR, DNA double strand breaks (DSBs) are the principal cytotoxic lesion for IR. In fact, in his paper in 1996, Wolff (1996) suggested that DNA double strand breaks *per se* can initiate an adaptive response, though the number of DSBs at low priming dose will be very low [141,143]. We therefore, next measured DSBs and followed their repair under RI-AR in human PBMCs.

Any form of DNA damage that forms a DSB is always followed by the phosphorylation of the histone H2AX at Ser-139 (named γH2AX), The number of γH2AX foci is considered a highly sensitive reflection of DSBs formation in 1:1 manner. Similarly, loss of γH2AX signal is a marker of DNA double strand breaks repair. Gamma H2AX is required for the stabilization of DNA repair proteins on the chromatin and plays a role in both NHEJ and HR repair pathways. We observed that similar to the lower % tail DNA in comets; the initial DNA double strand breaks were also lower in primed cells, both at 0 min and 15 min post CD. When repair of γH2AX was followed at different times after CD, significant differences were observed. In non-primed cells, the number of γH2AX foci reached peak levels 15 min after CD exposure. The number of foci decreased to approximately one-half their maximum at

60 min post CD and maintained a steady state thereafter so that 180 min post CD almost 5.79 ± 0.26 foci/cell remained. The primed cells showed a slower increase and delayed maxima at 30 min post-CD; nevertheless, the number of foci/cells was significantly lower than the peak for non-primed cells. These cells showed a steady repair thereafter so that after 180 min post CD only 2.05 ± 0.22 foci/cell remained. Thus, clearly primed cells showed a faster and better repair of DSBs than the non-primed cells. Our results thus, for the first time suggest that RI-AR in human PBMCs is characterized not only by protection from initial DNA damage, both SSBs and DSBs, but also better repair of DSBs (but not SSBs) resulting in lesser residual damage in primed cells.

Earlier Kumar *et al* (2015) showed that the lymphocytes of individuals from high-level natural radiation areas which are exposed to low dose chronic radiation, when challenged with high dose, showed better repair in the first 15 min of repair as compared to individuals from control areas [66]. Ikushima *et al* (1996) showed no change in initial damage but lesser residual DSBs during RI-AR in cultured Chinese hamster cells [140]. Wojcik *et al (*1996) demonstrated an increase in DSB repair capacity in the primed PHA-stimulated human lymphocytes [144]. There are also reports where no change in DNA repair of both SSBs and DSBs between primed and non-primed cells was observed [145–147].

A biphasic nature of repair of DNA DSBs in human PBMCs where an initial phase of fast repair is followed by a slow phase has been reported [148,149]. *In vitro* studies have reported that IR induced γH2AX foci formation reaches a peak at 15 – 30 min post irradiation [150,151] and then declines with a half life of several hours [152,153]**.**

Cell survival, recovery of mitochondrial membrane potential and apoptosis

Since priming with low dose radiation resulted in lower initial DNA damage and better DSB repair, it was argued that this should then result in increased survival at later times. To evaluate cytotoxic effect if any, of priming dose, cellular outcomes first in terms of viability was evaluated 24 and 72 h post-irradiation with CD. Lower DNA damage in primed cells correlated with a relatively small, but statistically significant, higher survival in G_0 PBMCs at both the time points indicating that pre-exposure of cells to LDR may provide a distinct survival advantage. There are only a few studies which have shown cell survival as the endpoint under radioadaptive conditions. While some described a survival adaptive response [116,154,155] others did not observe any such advantage [138,156,157].

Reduced DNA damage and increased survival also correlated with higher mitochondrial membrane potential in primed cells relative to non-primed cells. Stable levels of $\Delta\Psi m$ are thought to be a prerequisite for normal cell functioning [158]. Thus, higher mitochondrial membrane potential observed in the primed cells may help in maintenance of cellular health and viability. Earlier reports have shown that pre-treatment of human leukemic cells with small doses of H_2O_2 [159] and mouse myoblast cells with x-rays [160] offered higher levels of mitochondrial membrane potential. There are also reports which showed that exposure to low grade mild stress agents like starvation or As_2O_3 can protect neuronal cells by maintaining mitochondrial membrane potential [161]. To the best of our knowledge, ours is the first study to demonstrate that pre-exposure to a small priming radiation dose stabilizes membrane potential in primary human cells as a mechanism of RI-AR.

An increase in cell survival, as seen for primed cells, may be related not only to lower DNA strand breaks and better repair but also with apoptosis. Radiation

induced programmed cell death or apoptosis has been proposed as a protective mechanism by resting lymphocytes to remove misrepaired or incomplete repaired cells and thus, may help reduce genetic instability and potential carcinogenic risk [162–164]. Cregan *et al* (1999) compared apoptosis 24 h after irradiation with a 2 Gy challenge dose in cells that were primed with 100 mGy adapting dose 6 h earlier. All donors showed either an increased or no change in apoptosis [165]. Few other studies too, have reported higher apoptosis in primed cells than the non-primed cells [166–169], whereas Ibuki and Goto (1994) reported that adaptive dose exposure prevents cells from undergoing apoptosis [170].

In the present study, we did not observe any difference in apoptosis between primed and non-primed cells 24 h post-irradiation with CD. Nevertheless, in addition to 24 hr, we need to follow apoptosis at other time points like 6, 48 and 72 hr also to make a definite conclusion.

Also, whether this pre-conditioning mediated cytoprotection against apoptosis is mediated by the increased expression of anti-apoptotic genes or other agents like ROS scavengers or chaperones need to be studied further.

Reactive oxygen species (ROS) and oxidative stress

An alternate mechanism that has been hypothesized to explain RI-AR relates to the role of reduced ROS and oxidative stress in cells that are pre-conditioned with low dose radiation. It is well established that a primary biological effect of absorption of IR by living cells under ambient oxygen is ionization and excitation of water molecules leading to formation of water radiolysis products, including ROS, in a process termed indirect action of radiation. IR induced changes in both cellular ROS [171] as well as mitochondrial ROS [172] has also been well established. ROS play

multiple roles that greatly depend on their concentrations. Physiologically relevant concentrations of ROS participate in the regulation of key signaling transduction cascades essential for cellular health and survival. However, aberrant yield of ROS and high nuclear concentration can cause oxidative stress and alter biochemical reactions [84]. A redox imbalance thus, created can lead to further consequences like induced DNA damages, gene mutations and alterations in signal transduction.

In this study, we tested the role of oxidative stress in RI-AR. An exposure to relatively high dose of 2 Gy resulted in an immediate increase in both intracellular and mitochondrial ROS levels. PBMCs primed with low dose of 100 mGy showed a smaller increase as compared to non-primed cells, which was still higher than the sham irradiated controls. We propose that this small increase in ROS in primed cells contribute to radioadaptive response in human PBMCs by various modes: (i) by directly inducing DNA damage that initiate RI-AR; (ii) the small DNA damage induced by ROS may regulate certain genes/proteins that allow DNA repair and promote protection; (iii) by promoting antioxidant response that confers RI-AR; (iv) by inducing certain proteins (e.g. transcription factors) that induce cellular events to enhance survival and promote overall cellular health.

Some support for this hypothesis has come from animal studies where exposure to low dose IR offered protection against diabetic induced renal damage by decreasing oxidative stress [173]. Pramojanee *et al* (2012) showed reduced ROS production during detoxification of osteoblastic cells exposed to low dose dental irradiation [174]. In one study, NO radicals were shown to act as initiator of RI-AR in a human glioblastoma cell line [175]. Some studies have observed a preconditioning role for mitochondrial ROS in cardiomyocytes [176], ischemic tolerance in the brain

[177] and 'mitohormesis' in general [178]. Adaptive response to oxidative stress has also been demonstrated with pre-exposure of cells to other stressors like H_2O_2 [179].

Mobilization of antioxidant system

Since the primed cells showed lower levels of ROS as compared to non-primed cells, this could reflect an early induction of radical detoxification system and mobilization of antioxidant enzymes (thiol/non-thiol) in these cells. We observed that the primed cells showed an early differential modulation of intracellular thiols, but no significant change in total thiol levels. On the other hand, the non-primed PBMCs showed higher utilization of intracellular thiols as compared to the primed cells, in trend with higher ROS levels in these cells.

The redox pair glutathione (GSH) and glutathione disulphide (GSSG) represents the most important redox buffer system for radical detoxification. When the GSH/GSSG ratio was followed, robust mobilization of glutathione for restoration of reduced cellular environment was indicated in cells pre-conditioned with low dose. Lesser utilization of intracellular thiols but higher utilization of GSH indicated that restoration of reduced cellular environment in primed cells may be GSH dependent. A similar decrease in GSH/GSSG ratio at early time points post-irradiation have been reported for mouse splenic lymphocytes [180] and Jurkat (human T-cell lymphoma) cells [181]. In addition to its well-defined role as a free radical scavenger, recent reports suggest several pleiotropic functions of glutathione in processes like signal transduction and apoptosis [182]. The survival responses to GSH depletion include the transcriptional activation of genes encoding cytoprotective proteins through the two transcriptional activators, NF-κB [183] or the Nrf2 [184].

We next evaluated the role of antioxidant enzymes in maintaining cellular homeostasis during RI-AR. Low dose radiation mediated upregulation of gene expression of several antioxidant genes like GPX1, CAT, SOD etc have been reported in literature [185,186]. Antioxidant enzymes like MnSOD and CAT have been associated with adaptive response in breast cancer cell line MCF-7, Human Umbilical Vein Endothelial Cells (HUVEC) and skin keratinocytes, and also in dividing cells like human lymphoblastoid cells and mouse embryonic fibroblasts [185,187–189].

An enhanced antioxidant level in the blood plasma of chronically exposed radiation health workers has also been reported [190–192]. However, most reports have been limited to assays on individual enzymes and either activity or expression, except for one report of UV induced small 1.3 to1.5-fold increase in CAT, MnSOD and GPX activity in PBMCs [193]. For our work, we evaluated coordinated changes in activity of four major antioxidant enzymes, namely CAT, MnSOD, GPX1 and TXNRD1 and also monitored their mRNA expression in primed and non-primed cells.

When the activities of antioxidant enzymes were compared between primed and non-primed cells, all four antioxidant enzymes showed higher expression in primed cells, supporting the hypothesis that the reduced ROS and increased protection in these cells may be mediated through early augmentation of antioxidant activity. Up-regulation of MnSOD and CAT after low dose exposure of 100 mGy highlighted the important radio-protective role of these two enzymes in human PBMCs. This ability of IR to elicit an antioxidant response in quiescent human cells may have important implications for radioprotection in humans, especially in the low dose region. In an earlier study that is in agreement with our data, Kumar *et al* (2016) showed enhanced antioxidant levels in the blood plasma of radiation health workers

with chronic radiation exposure [192]. On the other hand, Hafer *et al* (2010) reported that antioxidants like DMSO and L-ascorbic acid could uniquely protect dividing yeast cells but not non-dividing cells from radiation-induced DNA deletions [194]. Another study demonstrated a statistically significant decrease of CAT activity and no change for SOD enzymes in lymphoblastoid cells exposed to a very low dose of 20 mGy alone [187].

When transcript levels were studied using qPCR, at both TRXR1 and GPX1 gene loci, mRNA expression diverged from enzyme activity. Mammalian thioredoxin reductases are ubiquitously expressed homodimeric enzymes belonging to the pyridine nucleotide disulfide oxidoreductase family. It contains a C-terminal selenocysteine involved in catalytic activity. In mammals, three different isoforms of TrxR encoded by three separate genes have been found: cytosolic (TrxR1), mitochondrial (TrxR2, also called TR3 or TRβ), and testis-specific (TGR) [195]. Several splice variants of TrxR1 and TrxR2 have been also identified [196]. Similarly, at least eight different isoforms of glutathione peroxidase superfamily (GPX 1-8) have been identified in humans [16]. For both TrxR and GPX, activity was tested as a whole in cell lysates, while for transcript levels specifically, only TXNRD1 and GPX1 gene expression was quantified. Thus, the possibility that the other TXNRD and GPX genes might be involved in RI-AR of human PBMCs and may ultimately contribute to the increase in enzymatic activity observed in primed cells, cannot be excluded. Overall, our results highlight a strong possibility that low dose of radiation induce an adaptive increase in the antioxidant defense mechanism.

Activation of redox-sensitive transcription factors

Next, we tested the hypothesis that a small transient increase in ROS may directly influence regulatory proteins, such as redox-sensitive transcription factors. These factors may then condition the pro-survival cellular adaptive response through induced expression of several genes. For our work, we studied two such pleiotropic mediators of stress-induced gene expression – NF-kB and Nrf2. Acute exposure of human PBMCs either to 100 mGy or 2 Gy alone resulted in activation of NF-κB but not Nrf2. A large number of studies report that NF-κB and NRF2 signaling pathways are predominantly opposite. Various mechanisms have been postulated to explain this antagonism. These include feedback suppression, homology between KEAP1 and IκB, post-translational modulation of NF-κB by Nrf2 and competition for CREB [197].

Interestingly, we observed an early activation of both NF-κB and Nrf2 in the primed PBMCs irradiated with 100 mGy PD and 2 Gy CD. This correlated well with immediate increase post-IR in the expression of antioxidant genes, as shown in section 3.7a. Adaptive response was completely abrogated in presence of ATRA, chemical inhibitor Nrf2, and in presence of Bay 11-7082, chemical inhibitor of NF-kB. This further confirmed the role of these two transcription factors in RI-AR. In response to oxidative stress, TR is known to regulate activation of prosurvival signaling factors like NF-κB and AP-1 [198]. As a consequence, treatment of PBMCs with thioredoxin inhibitor auranofin resulted in a similar loss of adaptive response.

IR induced binding of Nrf2 to DNA has been demonstrated in Jurkat cells [181] *albeit* 6 h post irradiation. In the present study, the enhanced binding observed almost immediately after irradiation of PBMCs, may indicate a context-dependent as well as cell-type dependent activation of these transcription factors. There are several

reports that show that both NF-κB [199–201] and Nrf2 [85,202] form essential part of dynamic adaptive cellular program that counteract against intrinsic and extrinsic stresses through transactivation of expression of cytoprotective genes which promote cell survival. Crosstalk between Nrf2 and nuclear factor kappaB (NF-κB) has also been reported in the regulation of critical redox regulators like glutathione [203].

The role of these two transcription factors in RI-AR of PBMCs was further validated by examining gene expression of their downstream targets IFNG, TNFA and PRDX6. Primed cells showed higher expression of all these genes when compared with non-primed cells. Expression of HMOX1, target for Nrf2, was marginally higher in primed cells, but was less than the sham irradiated control for both primed and non-primed cells. Similar trend for the expression of HMOX1 was earlier shown with murine splenic lymphocytes [180]. Thus, this study showed for the first time the vital role of redox sensitive transcription factors NF-kB and Nrf2 in RI-AR of human PBMCs. For radioadaptive response in certain cell lines, a cooperative function of ATM, ERK and NF-κB has been proposed [199,200].

CHAPTER 4

PROTEOMIC ANALYSIS DURING RADIATION INDUCED- ADAPTIVE RESPONSE

Induced protein expression has been proposed as one of the key mechanisms of RI-AR, though it has not been tested rigorously.

In the present study, differential protein expression in primed and non-primed PBMCs were studied using two different proteomics methods: (1) Gel based method: Two–dimensional difference in gel electrophoresis (2D-DIGE) and (2) Gel free method: Quantitative label-free analysis. For both the methods, PBMCs extracted from the same five individuals (S1-S5) as studied in Chapter 3 were used. For inducing adaptive response irradiation of PBMCs was performed at room temperature using ^{60}Co γ-rays (Blood irradiator, 2000, BRIT, India) at a dose rate of 0.4 Gy/min. A PD of 100 mGy was given 4 h prior to a CD of 2 Gy, same as was used in Chapter 3. After irradiation, cells were incubated in RPMI-1640 media at 37°C in a humidified, 5% CO_2 atmosphere for 1 h before extraction of proteins.

4.1 Global proteome analysis using gel based 2D-DIGE

For the 2D-DIGE based separation of samples, we used the typical three-dye approach. The protein lysate from non-primed cells was labelled with Cy3 and lysate from primed cells was labelled with Cy5. The internal standard was prepared by mixing equal amount of protein from primed and non-primed cells. This protein extract was labelled with Cy2. Use of internal standard allowed more accurate alignment since it represents all the spots among the groups and replicates. Each gel therefore, consisted of protein lysate from non-primed cells (Cy3), primed cells (Cy5) and internal standard (Cy2). After IEF, images were acquired using Typhoon TRIO (GE Healthcare, USA). Cy2 images were scanned with 488 nm/520 nm, Cy3 images were scanned with 532 nm/580 nm and Cy5 images were scanned with 633 nm/670

nm. Triplicate gels were then aligned using internal standard and analyzed using Dymension 3 (Syngene, Cambridge, UK) software.

A total of 419 ± 54 protein spots were identified on the master DIGE gel, out of which 190 protein spots (~45%) were matched on all the three replicates. To have an idea about the spot-wise variations of the selected proteins, we calculated coefficient of variation (% CV) for each spot. The CV of Cy3 labeled spots (non-primed cells) was found to vary from 0.12% to ~81% with a high ~96% of spots showing CV less than 50%. The CV of Cy5 labeled spots (primed cells) ranged between 1.5% to 109.6% with 75% of protein spots showing CV less than 50% (**Fig. 4. 1**). A CV threshold of 50% is usually employed to filter out the highly variable and uninformative proteins. After spot matching, protein spots labelled with Cy3 and Cy5 dye were normalized with Cy2 dye (internal control). The expression of proteins from primed cells (Cy5 labelled) was then compared with non-primed cells (Cy3 labelled) to identify the differentially expressed proteins. Proteins with a relative expression change of ± 1.2 fold in spot intensity, and P-value of ≤ 0.05 were considered significant. In biological systems even subtle changes in protein concentration may regulate cellular and molecular functions [204]. To avoid missing-out such proteins with subtle, yet functionally relevant changes in expression, a lower fold change cut off of 1.2-fold was chosen.
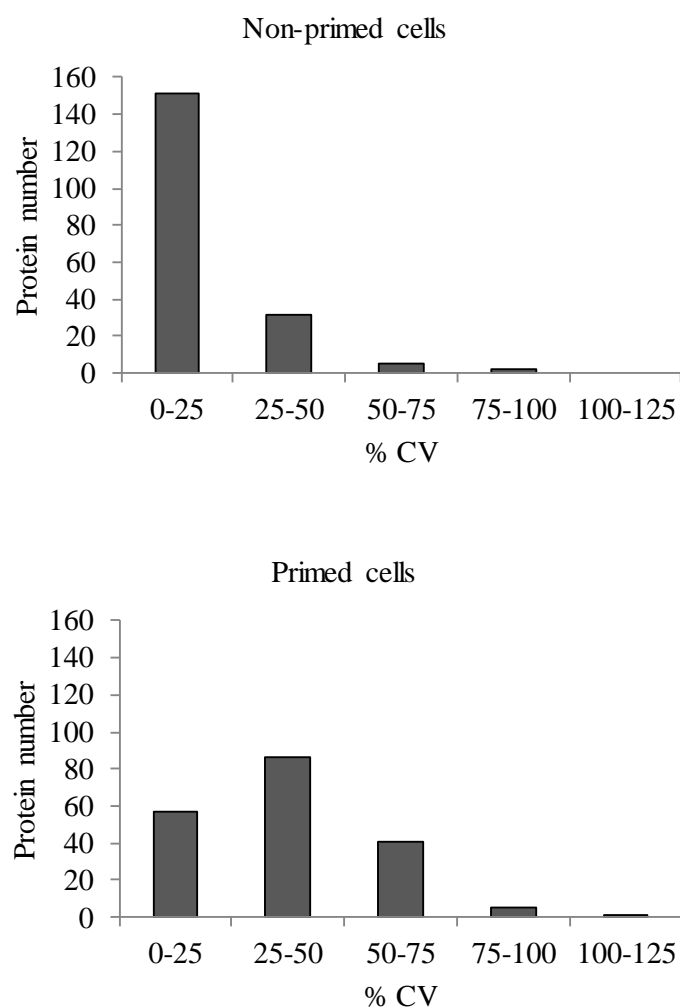
Fig. 4. 1. % CV for the differentially modulated proteins in the non-primed and primed cells.

The analysis revealed 40 protein spots to be significantly altered in primed cells as compared to the non-primed cells. Among these, 2 spots (spot 57 and spot 96) were over-expressed while the remaining 38 spots were under-expressed. Representative images of 2D-DIGE gels are shown in **Fig. 4. 2**. The highly reproducible protein map from a representative 2D-DIGE gel is shown in **Fig. 4. 3**. **Fig. 4. 4** shows a 3D image of significantly altered spots in primed and non-primed cells.
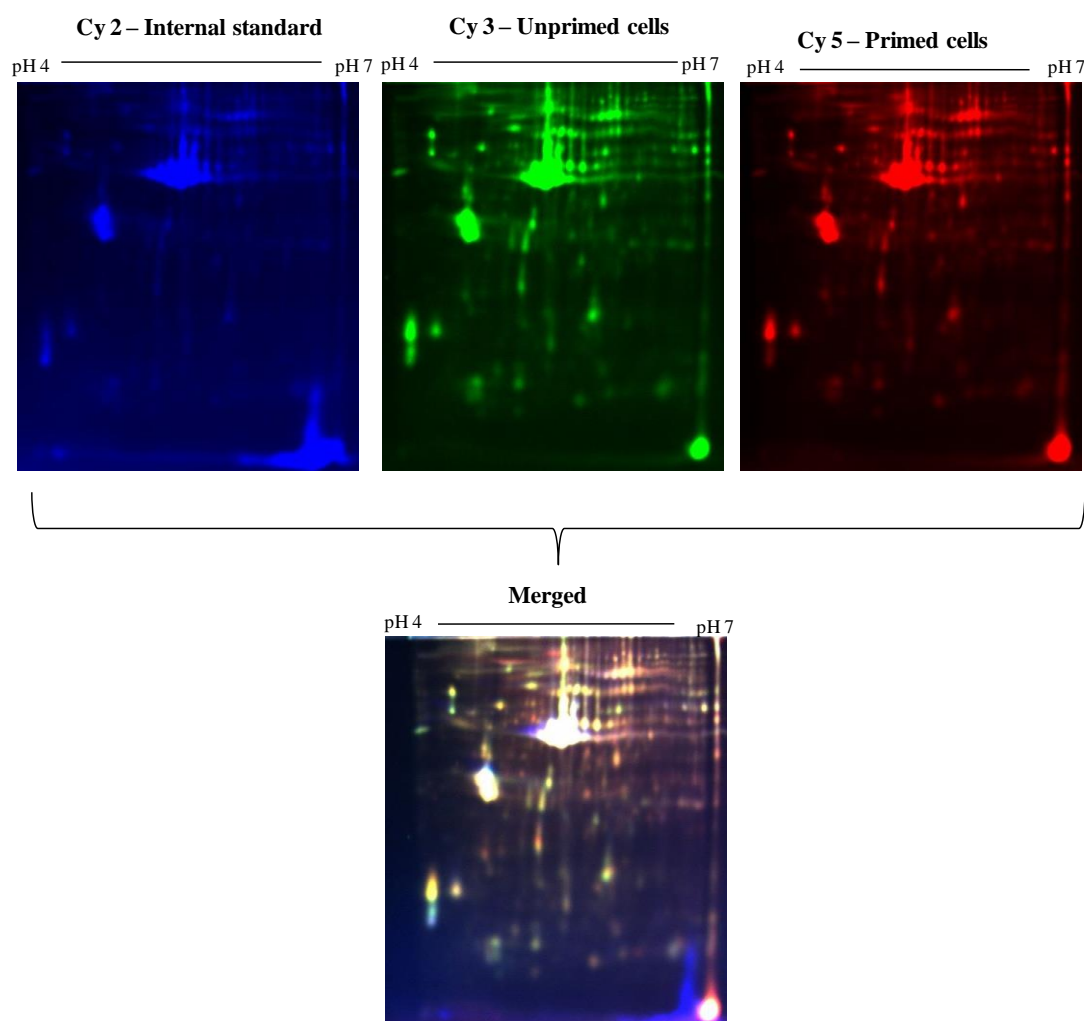
Fig. 4. 2. Analysis of human PBMCs by 2D-DIGE. Representative 2D-DIGE gel images for non-primed cells (Cy 3 labelled), primed cells (Cy 5 labelled) and internal standard (Cy2 labelled). Superimposition of three colour images gives a merged image. The range of the horizontal dimension is isolecetric point for IEF (pI 4 to 7); the range of the vertical dimension is molecular weight (from ~ 97 to 8 KDa).

In the preparative gels with colloidal Coomassie, most differentially expressed spots could not be visualized, probably due to low abundance. In the absence of an automated spot-picker for fluorescent gels, we used the available protein maps of PBMCs for protein identification. The pI and molecular weight coordinate data derived from DIGE gels was transposed onto the PBMC proteome map derived in our

lab [105] **(Fig. 4. 5)** and the PBMC map generated by Vergara *et al* 2008 [205].

Extensive matching with these two published PBMC maps allowed us to identify 28

differentially expressed protein spots **(Table 4. 1),** which contained 2 proteins up-

regulated and 26 proteins down-regulated. The two proteins that were over-expressed

in primed cells were identified as WDR1 and ACTG/B. Proteins under-expressed in

primed cells included cytoskeletal proteins like VINC, VIME, FIBG, CAPZA1, actin

(ACTG) and tubulin (TBB) isoforms; redox proteins PRDX-2 and CLIC1; apoptosis

related proteins 14-3-3 isoforms, BID; cell signaling proteins GDIR, GDIA, GMFG;

and molecular chaperone HSP7C.
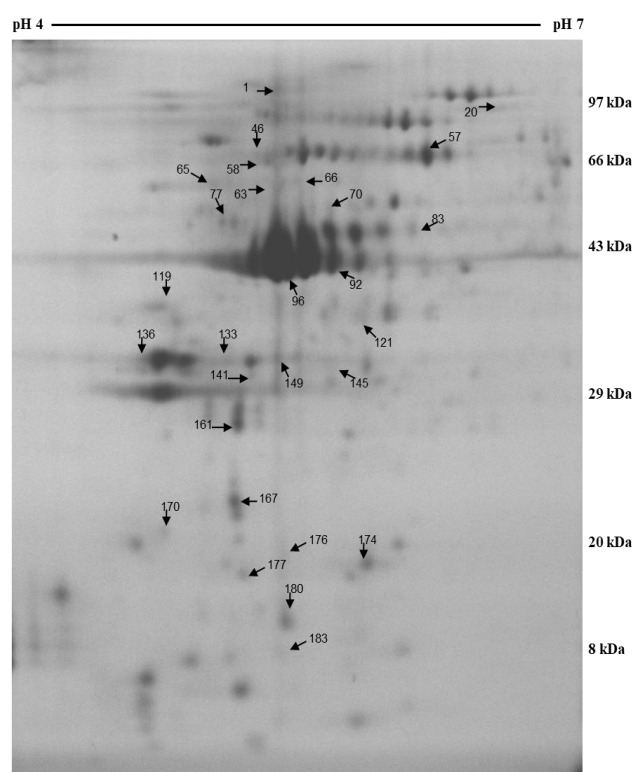
Fig. 4. 3. A representative 2D-DIGE image (grey scale). Differentially expressed

proteins are marked with arrow and spot numbers assigned using Dymension. The

range of the horizontal dimension is isolecetric point for IEF (pI 4 to 7); the range of

the vertical dimension is molecular weight (from ~ 97 to 8 KDa).
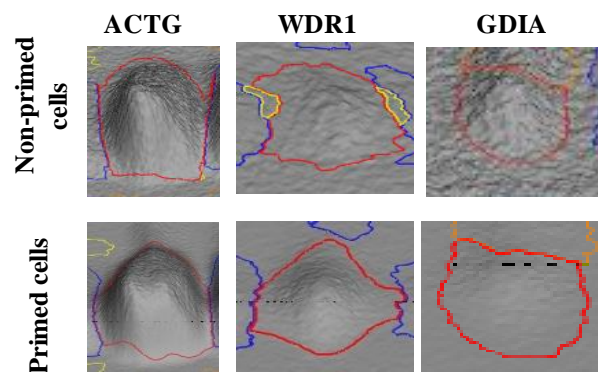
Fig. 4. 4. Magnified 3D image of three significantly altered spots in non-primed and primed cells.
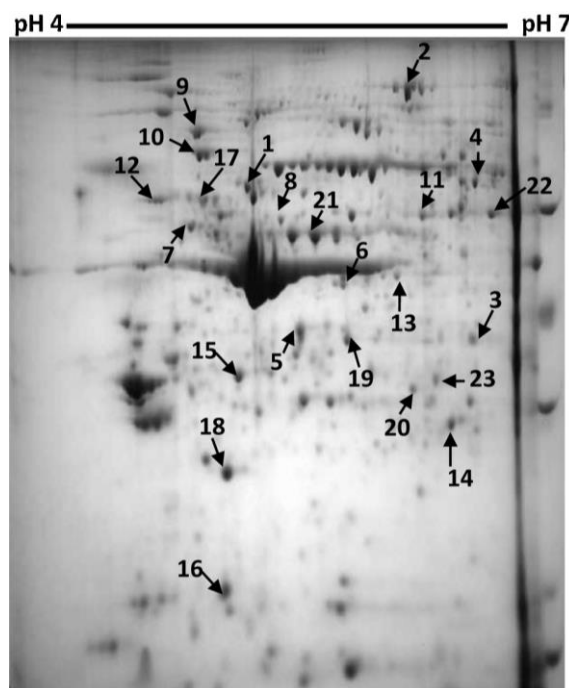
Fig. 4. 5. Representative 2-DE image of proteins from Nishad and Ghosh 2016 [105]

Spot No.	Entry name	Accession no.	Protein name	Measured		Theoretical		Fold change	P Value
				pI	MW (kDa)	pI	MW (Da)		
1	VINC	P18206	Vinculin (Metavinculin)	5.5	101	5.5	124.1	0.59	0.024
20	TRFE	P02787	Serotransferrin precurosr (Transferrin)	6.5	82	6.8	77	0.39	0.018
46	F13A	P00488	Coagulation factor XIII A chain precursor	5.4	69	5.7	83.1	0.43	0.001
57	WDR1	O75083	WD repeat protein 1	6.2	66	6.2	66	1.42	0.039
58	HSP7C	P11142	Heat shock cognate 71kDa protein	5.3	66	5.4	70.8	0.47	0.018
63	TBB1	Q9H4B7	Tubulin beta-1 chain	5.4	58	5.1	50.3	0.51	0.043
65	VIME	P08670	Vimentin	5.1	57	5.1	53.5	0.46	0.045
66	TBB5	P07437	Tubulin beta-5 chain	5.6	56	4.8	49.6	0.61	0.041
70	FIBG	P02679	Fibrinogen gamma chain precursor	5.7	53	5.4	51.5	0.65	0.021
77	PRS6A	P17980	26S protease regulatory subunit 6A	5.2	50	5.1	50.3	0.58	0.027
83	KPYM	P14618	Pyruvate kinase isozymes M1/M2	6.1	46	8	57.8	0.63	0.03
92	ACTG/B	P63261/P60709	Actin gamma/ actin beta	5.7	40	5.3	41.7	0.82	0.036
96	ACTG/B	P63261/P60709	Actin gamma/ actin beta	5.5	40	5.3	41.7	1.4	0.001
119	RSSA	P08865	40S ribosomal protein SA (p40)	5	31	4.8	32.7	0.45	0.044
121	ACTG/B	P63261/P60709	Actin gamma/ actin beta	5.7	30	5.3	41.7	0.49	0.003
133	1433G	P61981	14-3-3 protein gamma	5.2	24	4.8	28.1	0.53	0.016

136	1433T	P27348	14-3-3 protein theta	4.7	23	4.7	27.7	0.5	0.022
141	CLIC1	O00299	Chloride intracellular channel protein 1	5.3	22	5.1	26.7	0.45	0.049
145	LDHB	P07195	L-lactate dehydrogenase B chain	5.6	21	5.7	36.7	0.59	0.044
149	CAZA1	P52907	F-actin capping protein alpha-1 subunit	5.4	21	5.4	32.7	0.58	0.029
161	GDIR	P52565	Rho GDP-dissociation inhibitor 2	5.3	18	5.1	22.8	0.74	0.026
167	GDIA	P31150	Rab GDP dissociation inhibitor alpha	5.3	12	5	50.5	0.74	0.015
170	TCTP	P13693	Translationally-controlled tumor protein	4.9	10	4.8	19.5	0.42	0.031
174	PRDX2	P32119	Peroxiredoxin-2	5.9	9	5.7	21.8	0.58	0.041
176	BID	P55957	BH3-interacting domain death agonist	5.5	9	5.3	21.9	0.49	0.019
177	LGUL	Q04760	Lactoylglutatione lyase, chain A	5.3	8	5.2	20.1	0.61	0.05
180	GMFG	O60234	Glia maturation factor gamma	5.5	7	5.2	16.8	0.69	0.028
183	IF5A1	P63241	Eukaryotic translation initiation factor 5A-1	5.5	6	5.1	16.7	0.32	0.037

Table 4. 1. List of differentially expressed proteins in primed cells. The spot numbers are as labeled on Fig. 3.

Using the UniProt/SwissProt protein database the 28 identified proteins were broadly classified into eight groups according to their general biological functions: cell matrix adhesion proteins (TBB1, TBB5, three isoforms of actin, VINC, VIME, WDR1, TCTP), cell signaling proteins (GD1R, GD1A, GMFG), Cell redox homeostasis proteins (PRDX2, CLIC1), apoptosis proteins (LGUL,1433G, 133T, BID), proteins involved in cellular metabolic processes (KPYM, LDHB,CAZA1), extracellular proteins (F13A, FIBG), molecular chaperone (HSP7C), and proteins involved in cellular processes (IF5A1,RSSA,PRS6A) **(Fig. 4. 6)**. Of these, the cell matrix adhesion proteins formed the largest group with nine proteins.
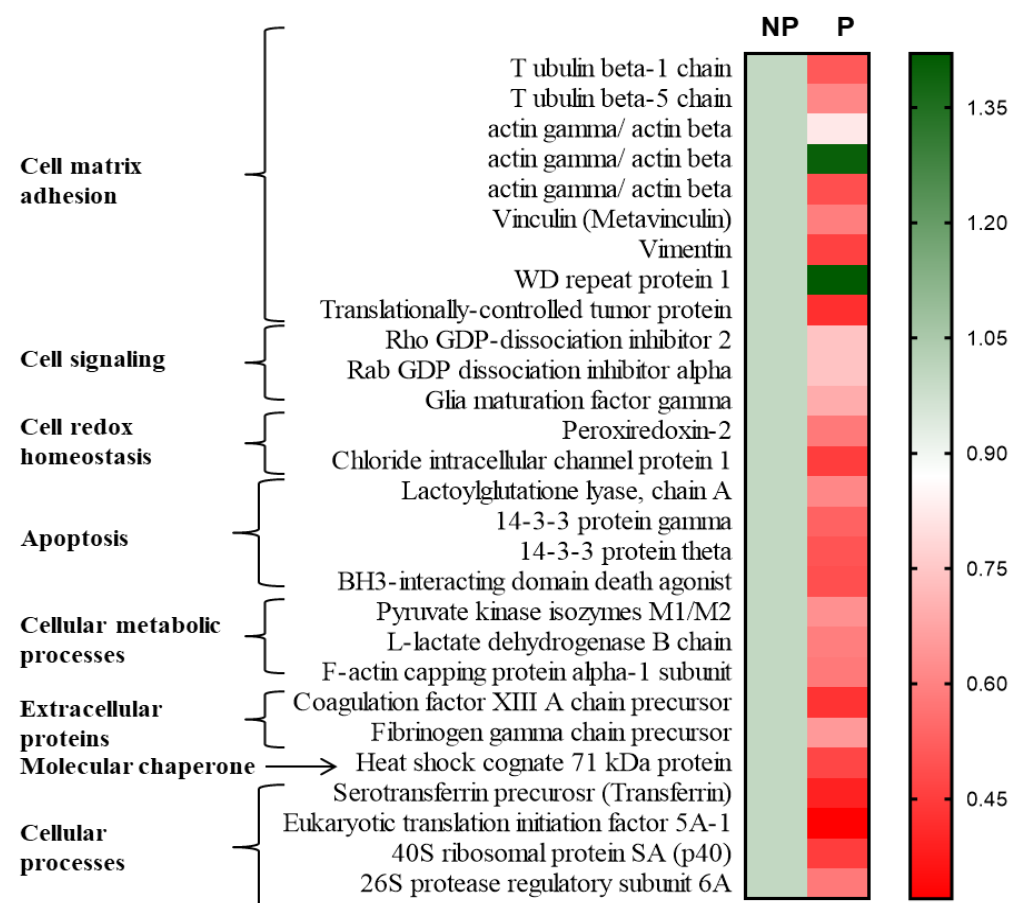
Fig. 4. 6. Heat map showing differentially expressed proteins in 2D-DIGE (fold change ±1.2 fold and $P \leq 0.05$) in the non-primed and primed cells. Relative spot

intensity of differentially regulated proteins in non-primed cells (NP) and primed cells (P) is shown in each column. Rows represent individual proteins grouped according to their biological function.

4.2 Global proteome analysis using label-free analysis

To study protein expression using label-free technique, approximately 100 µg of tryptic protein lysate, in triplicate, from each treatment group was separated by nanoscale liquid chromatography (nanoLC) using nanoACQUITY UPLC system (Waters, Manchester, UK) coupled to Quadrupole-Time of Flight (Q-TOF) mass spectrometer [SYNAPTG2 High Definition MS (HDMS) system, Waters Corporation]. LC-MS data was processed using ProteinLynx Global Server v.2.4 software (PLGS, Waters Corp.). Protein identification was performed using UniProt Homo sapiens annotated database.

Overall, we were able to identify a total of 5739 proteins in the entire data set of sham irradiated, 100 mGy, 2 Gy and 100 mGy +2 Gy irradiated samples. Of these, 2532 proteins were identified in sham irradiated control cells, 2071 in 100 mGy irradiated cells and 2056 and 2422 proteins in non-primed and primed cells, respectively. The label-free analysis identified ~14 times more proteins as compared to 2D-DIGE. Protein sequence coverage and distribution of number of peptides across the samples is shown in **Fig. 4. 7** and **Fig. 4. 8**. The three treatment groups showed average sequence coverage of ~22 % while almost 63% of the proteins were represented by ≥ 10 peptides.
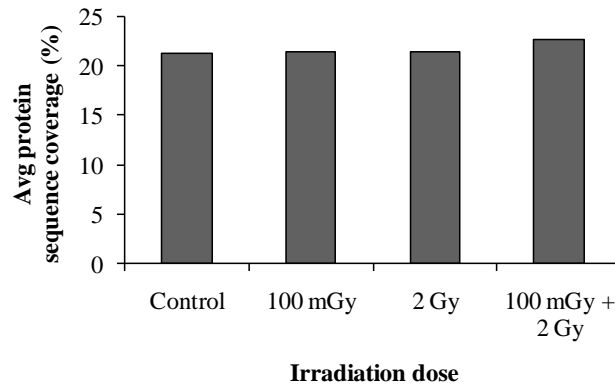
Fig. 4. 7. Sequence coverage of proteins identified using label-free analysis.
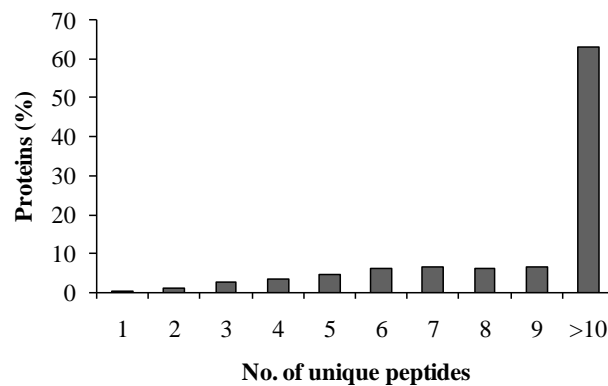
Fig. 4. 8. Number of peptides for proteins identified using label-free analysis.

4.2.1 Biological interpretation of identified proteins

For biological interpretation, the proteins identified in each treatment group were functionally annotated using DAVID according to the biological processes, molecular function, cellular component, and KEGG pathways.

4.2.1.1 Gene ontology (GO) based on biological processes

The DAVID GO analysis identified 34 biological processes (BP) significantly enriched (Benjamini-Hochberg p-value ≤ 0.1) in three treatment groups (100 mGy, non-primed cells and primed cells) as compared to the sham irradiated control cells

List of biological processes enriched in 100 mGy irradiated cells, non-primed cells and primed cells is given in **Annexure I, Annexure II** and **Annexure III** respectively. Out of these, only three processes were common between all the three groups **(Fig. 4. 9A).** Five biological processes were common between non-primed and primed cells **(Fig. 4. 9B)**, while ten processes were unique to each.
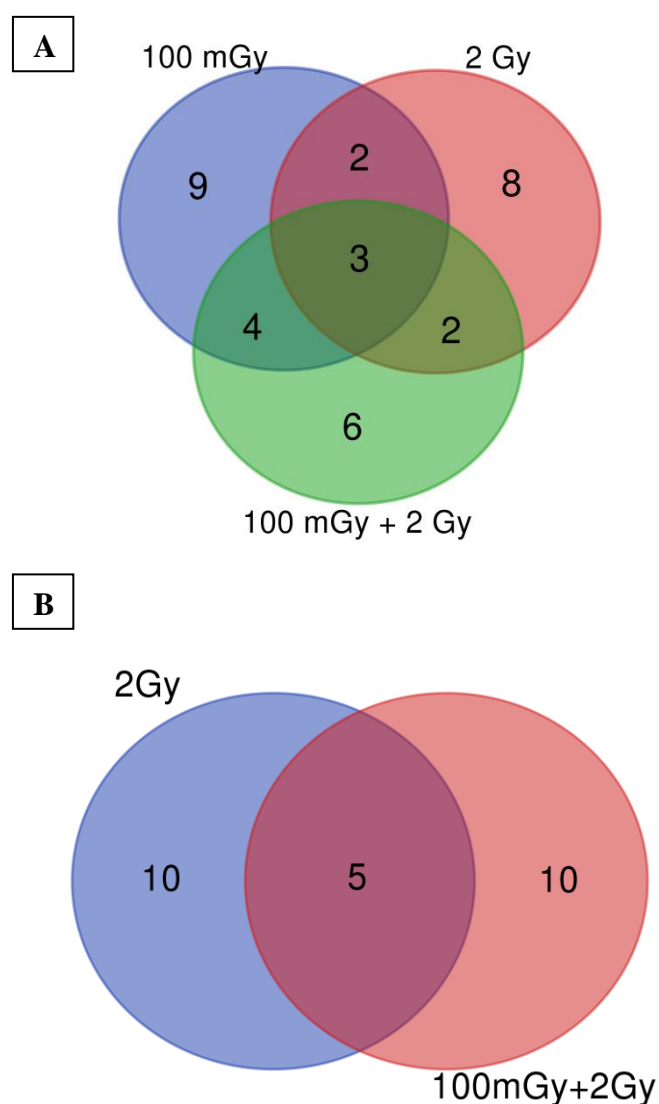
Fig. 4. 9. Biological processes significantly enriched (A) in the three treatment groups and (B) in the non-primed and primed cells.

4.2.1.1.1 Key radiation related biological processes enriched in non-primed and primed cells

The biological processes enriched after radiation in non-primed and primed cells were compared. These can be broadly grouped into four major categories: (1) DNA repair, chromatin remodeling and transcriptional regulation, 2) Post translational modifications, (3) Signaling networks and (4) Cytoskeletal organization **(Fig. 4. 10)**.
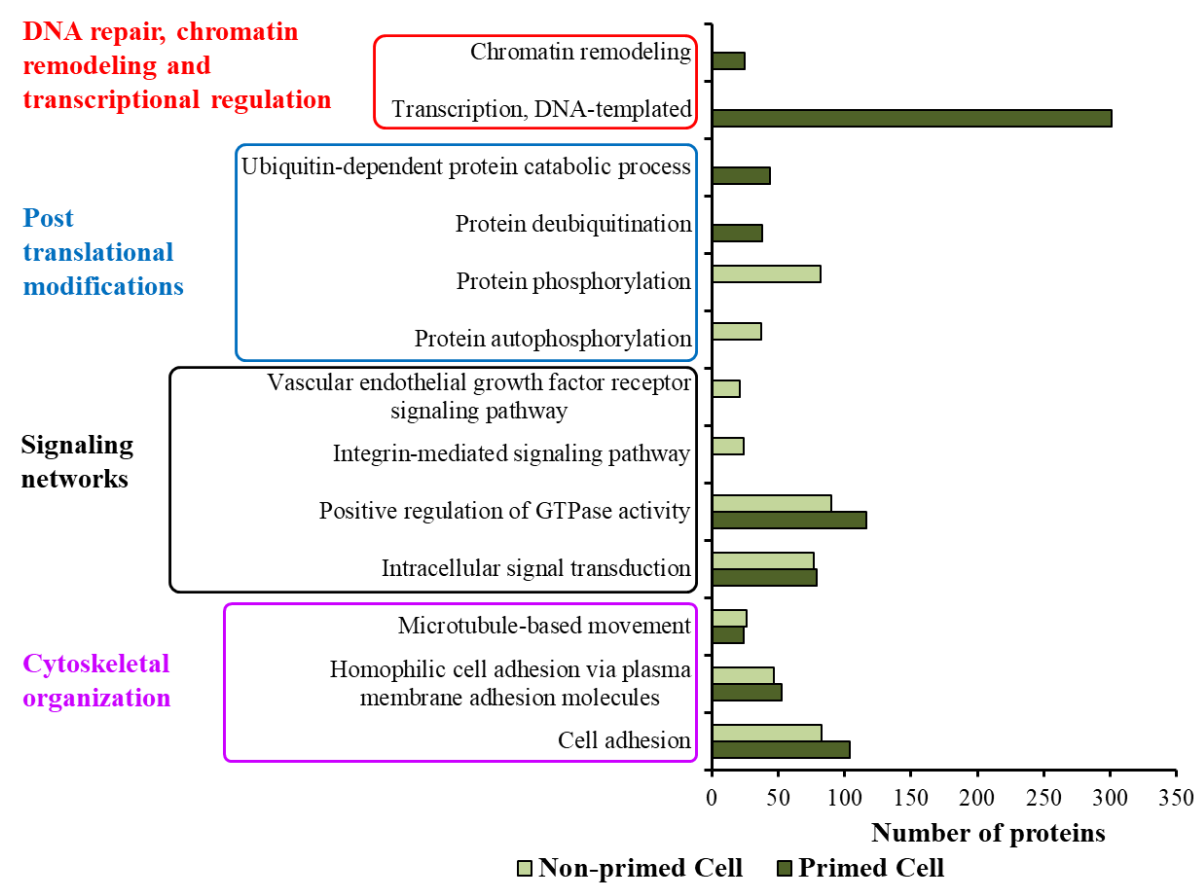
Fig. 4. 10. Key radiation related biological processes enriched in non-primed and primed cells.

4.2.1.1.1a Proteins involved in DNA repair, chromatin remodeling and transcriptional regulation

A large number of proteins involved in DNA repair, chromatin remodelling and transcriptional regulation were identified only in primed cells, but not in non-primed cells. This included biological processes with GO:0006351~transcription, DNA-templated (301 proteins) and GO:0006338~chromatin remodelling (25 proteins). Many of these proteins were zinc finger transcription factors (e.g. ZNF778, ZNF862, ZNF546, ZNF600, ZNF100, ZNF518A, ZNF638), while some were transcription factors which function as critical mediator of oxidative stress (e.g. FOXO1, HIF1). Some of the identified proteins are found associated with basal transcription machinery (e.g. MED13L, SUPT6H, TCF20, IWS1, MED12L) and transcription elongation (SUPT5H, SUPT6H). Some of these transcriptional regulation proteins are also known to be involved in DNA repair (e.g. CUX1, CUX2, MMS19) and DNA damage response protein (e.g. TP53BP1). A large number of proteins associated with histone modifications (e.g. PRDM2, KMT5B, WHSC1L1, SETD1A, DNMT1, KDM5B, KDM3B, PHF2, KDM5C, PHF8, BRPF1, KAT6A, HDAC6), chromatin-remodeling complexes (e.g. CHD1, CHD2, CHD4, CHD5, CBX8, RSF1 BAZ1A, ARID1B, INO80, ESR1), SWI/SNF chromatin remodeling complexes (SMARCA4 and RERE - Arginine-glutamic acid dipeptide repeats protein) were also identified. Cells irradiated with 100 mGy also showed enrichment of GO:0006351 (301 proteins) and GO:0006338 (25 proteins).

4.2.1.1.1b Proteins involved in post translational modifications

Enrichment of biological processes like GO:0016579~protein deubiquitination (38 proteins) and GO:0006511~ubiquitin-dependent protein catabolic process (44

proteins) was observed only in primed cells. On the other hand, enrichment of processes like GO:0006468~protein phosphorylation (82 proteins) and GO:0046777~protein autophosphorylation (37 protiens) was unique to non-primed cells. Primed cells showed specific enrichment of proteins with E3 ubiquitin-protein ligase function (e.g. CUL4B, UBE3A, RNF6, RNF20, RNF40, UBR3) and deubiquitinase enzymes (e.g. USP4, USP6, USP32, USP42, USP49). Among the proteins involved in phosphorylation were serine threonine protein kinases (e.g. WNK4, CDC42BPG, CDC42BPA, CIR, PRKD3, MAP3K6, IKBKB, MAST1), receptor tyrosine kinases (e.g. INSR, INSRR) and non-receptor tyrosine-protein kinases (e.g. ABL1). Like primed cells, cells exposed only to 100 mGy showed specific enrichment of GO:0016579 (32 proteins) and GO:0006511 (44 proteins) but not GO:0006468 and GO:0046777 processes.

4.2.1.1.1c Proteins involved in cell signaling pathways

Primed cells showed specific enrichment of GO:0035556~intracellular signal transduction (79 proteins) and GO:0043547~positive regulation of GTPase activity (116 proteins). Among the important proteins detected in primed cells were PRKCQ, DGKK, PLCB1 DLGS JAK2 EGF, and EGFR. Several guanine nucleotide exchange factors like ARFGEF2, ARFGEF18, DAB2IP, DOCK4 DOCK1, DOCK2, DOCK8, DOCK11, and many Rho GTPase activating proteins such as ARHGAP32, ARHGAP5, DCL1, ARHGAP25, ARHGAP31, ARHGAP2 were also observed. In contrast, non-primed cells showed enrichment of four such biological processes GO:0035556~intracellular signal transduction (77 proteins), GO:0043547~positive regulation of GTPase activity (70 proteins), GO:0007229~integrin-mediated signaling pathway (24 proteins), GO:0048010~vascular endothelial growth factor receptor

signaling pathway (21 proteins). Among the key proteins observed in in non-primed cells were WNK4, MAST1, CDC42BPG, CDC42BPA, MAP3K4, ADCY10, ITGA11, ROCK2, VEGFC, HSP90AA1. The guanine nucleotide exchange factors detected in non-primed cells included DOCK2, DOCK3, DOCK4, DOCK9, DOCK11, RAPGEF2. Again, the cells irradiated only with low dose of 100 mGy showed enrichment of GO:0035556 (80 proteins) and GO:0043547 (116 proteins) but not GO:0007229 and GO:0048010 seen in non-primed cells.

4.2.1.1.1d Proteins involved in cytoskeletal organization

Biological processes GO:0007018~microtubule-based movement, GO:0007155~cell adhesion, GO:0007156~homophilic cell adhesion via plasma membrane adhesion molecules were enriched in both primed and non-primed cells as well as in 100 mGy exposed cells. Other processes like GO:0031032~actomyosin structure organization (6 proteins) were enriched in primed cells only, while enrichment of GO:0007010~cytoskeleton organization, GO:0030198~extracellular matrix organization and GO:0007160~cell-matrix adhesion was unique to non-primed cells. Some of the notable proteins detected under this category included integrins like ITGA11, ITGAL, ITGB4, ITGB3, protocadherins like PCDHA1, PCDHA4, PCDHA6 and cytoskeletal proteins like TNS1, TNS3, MYO9B, CDC42BPB, CDC42BPG, MAST1 and MAST2.

4.2.1.2 Classification of differentially expressed proteins based on molecular function

In the molecular function ontology, 66 categories were significantly enriched (Benjamini-Hochberg p-value ≤ 0.1). Out of these, 18 categories were common

between all the three groups **(Fig. 4. 11)**. The binding to protein, RNA, DNA and chromatin was the major category with 85% proteins from 100 mGy, and ~78% proteins from non-primed cells and primed cells each belonging to this molecular function **(Fig. 4. 12)**.
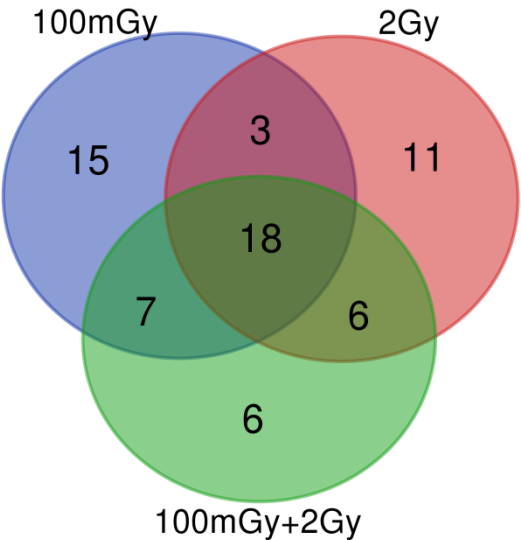
Fig. 4. 11. Molecular function categories enriched in the three treatment groups.
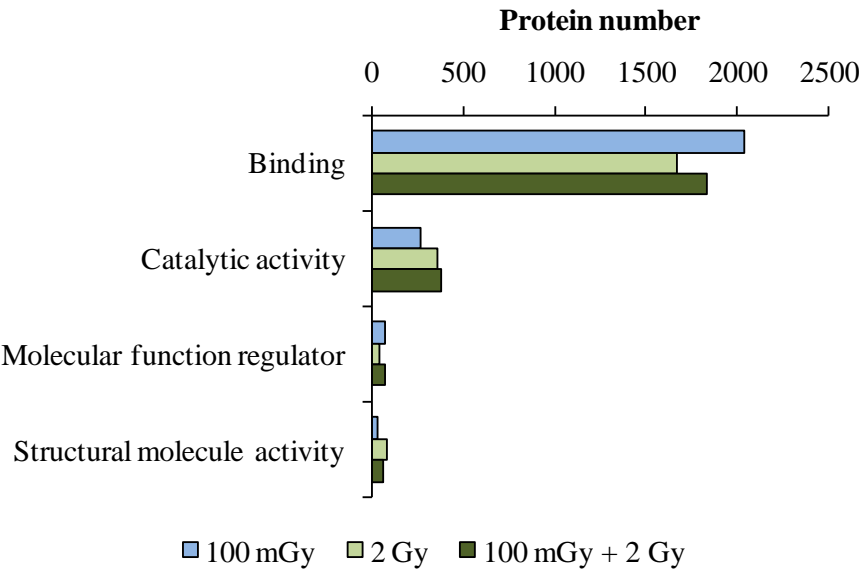
Fig. 4. 12. Key molecular function categories critical for cellular radiation response enriched in the three treatment groups.

Significant enrichment of molecular function GO:0003700~transcription factor activity, sequence-specific DNA binding was seen only in primed cells (47 proteins) and cells exposed to low dose of 100 mGy (134 proteins), but not in non-primed cells. There were 12 transcription factors that were common between both the groups (PAXBP1, ZNF33B, ZSCAN2, ZHX2, ZNF564, ARID4A, KDM5B, ZNF33A, TCF20, ZNF382, PRDM15, KDM5A). Few transcription factors like KLF2, KLF3, PBX4 REST, TADA2A, HIF1A, SUPT6H, NFKB1 were found only in primed cells. Other factors such as BCL6, HMGB1, FOXP2, HSF1, GLI3, TAF4, RERE were significantly enriched only in cells exposed to 100 mGy only. The other MF categories represented were catalytic activity, molecular function regulator and structural molecule activity **(Fig. 4. 12)**.

4.2.1.3 Classification of differentially expressed proteins based on cellular component

Enrichment of 71 cellular component categories was observed in three groups. Out of these, 15 categories were common between all the three groups **(Fig. 4. 13).** The localization to cytoplasm was the major category enriched **(Fig. 4. 14).** Almost 45% of all proteins detected in each group localized to cytoplasm. Approximately 21% and 16% of proteins localized to membrane and intracellular component, respectively. A smaller percentage of proteins localized to cytoskeleton, microtubule and chromosome **(Fig. 4. 14)**.
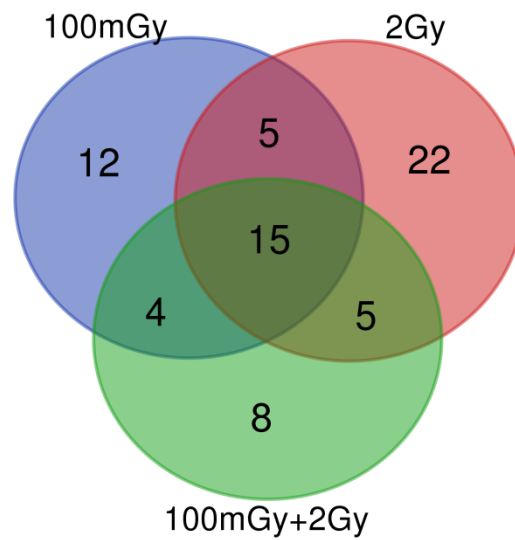
Fig. 4. 13. Distribution of cellular component categories in the three treatment groups.
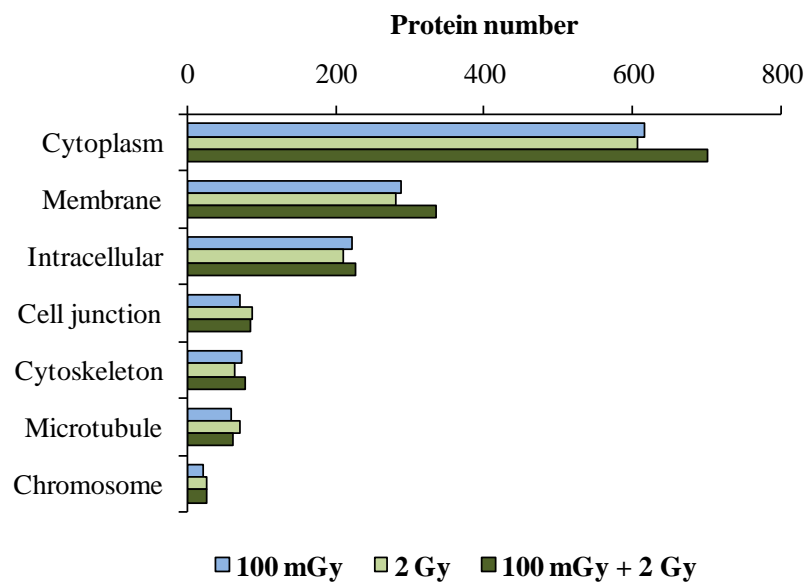
Fig. 4. 14. Key cellular component categories critical for cellular radiation response enriched in the three treatment groups.

4.2.2 Functional pathway analysis using KEGG

The KEGG pathway analysis identified enrichment of 43 pathways after irradiation (Benjamini-Hochberg p-value ≤ 0.1). List of pathways identified for 100 mGy irradiated cells, non-primed cells and primed cells is given in **Annexure IV, Annexure V** and **Annexure VI**, respectively. Out of these, 8 pathways were shared among the three groups while 16 pathways were shared between the non-primed and primed cells **(Fig. 4. 15).** Exposure to low dose of 100 mGy showed significant enrichment of 16 KEGG pathways. The non-primed cells showed significant enrichment of 27 pathways and primed cells showed significant enrichment of 28 pathways **(Fig. 4. 15).** Among these, there were few pathways that may play a critical role in cellular response to radiation (represented in **Fig. 4. 16**).
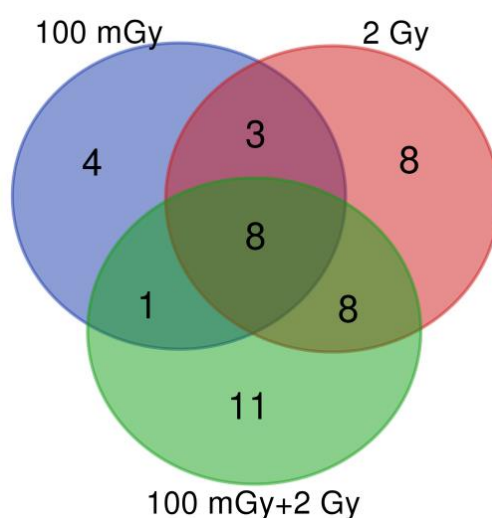
Fig. 4. 15. Venn diagram showing distribution of KEGG pathways in the three treatment groups.
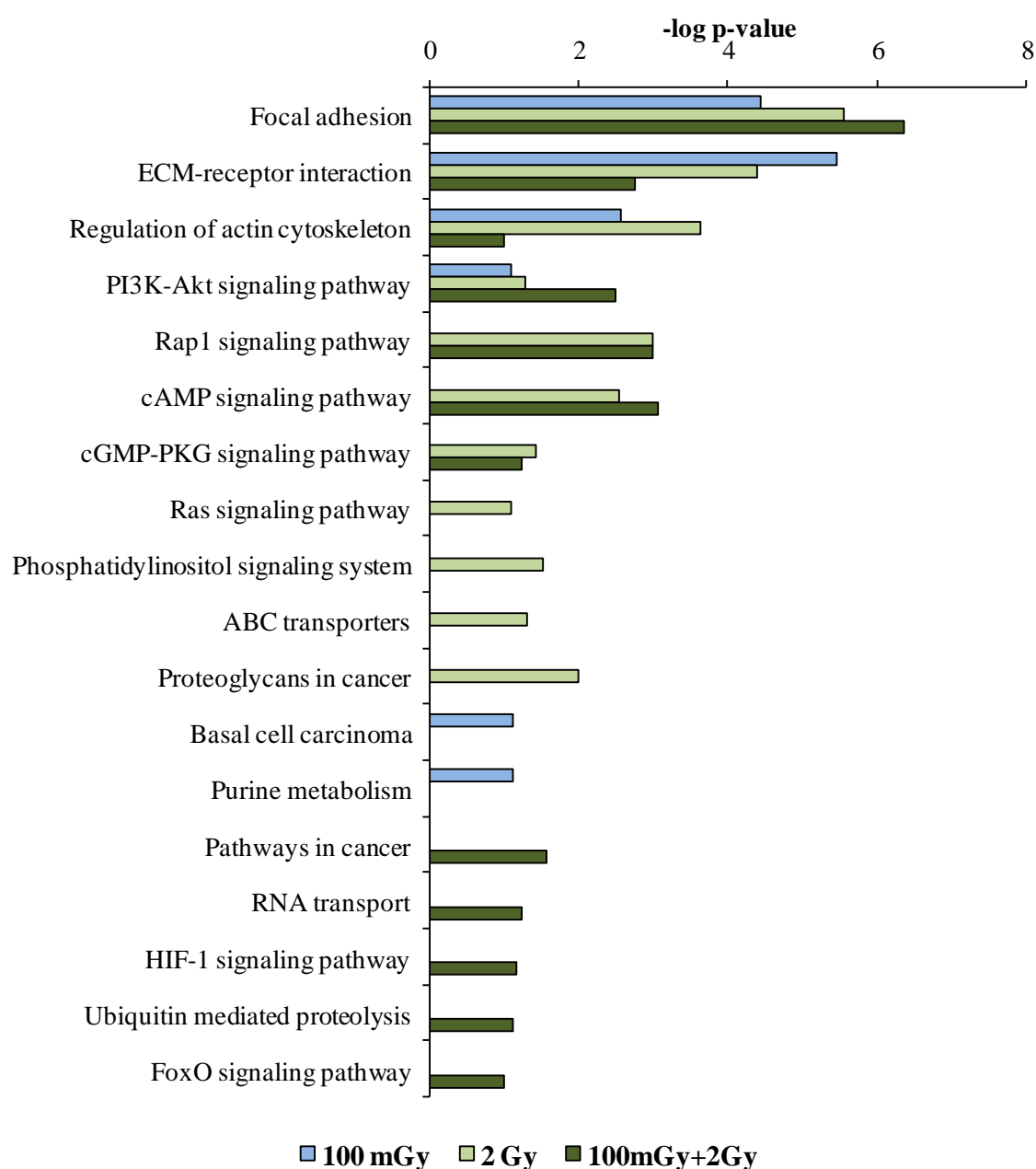
Fig. 4. 16. Key KEGG pathways critical for cellular radiation response enriched in the three treatment groups.

4.2.2.1 Key radiation related KEGG pathways

Many important pathways like hsa04510:focal adhesion, hsa04512:ECM-receptor interaction, hsa04151:PI3K-Akt signaling pathway and hsa04810:regulation of actin cytoskeleton showed significant enrichment in all the three treatment groups.

For focal adhesion, 44, 50 and 56 proteins from 100 mGy irradiated cells, non-primed cells and primed cells, respectively were altered. Few proteins like THBS1, LAMC1, ITGB4, VCL, IGF1R were detected in all three groups as were different isoforms of actin, collagen, laminins and integrins. Several proteins of the pathway however, showed a dose specific expression: VAV1, XIAP, TNR were detected only in cells exposed to 100 mGy; SRC, VEGFC, PAK5 were detected only in the non-primed cells and AKT1, AKT2, AKT3, PXN, COMP, BIRC3 were detected only in the primed cells. For ECM-receptor interaction pathway, 28, 27 and 25 proteins from 100 mGy irradiated cells, non-primed cells and primed cells respectively, showed modulation. Some proteins like COL6A6, COL4A2, COL11A1, TNN were represented in all three groups. Other proteins like TNR, GP9 were unique to 100 mGy irradiated cells; proteins such as DAG1, CD36, SV2B were detected only in the non-primed cells while proteins like COMP, SV2A were detected only in the primed cells. Few proteins like collagen, laminins, thrombospondin, integrins showed several isoforms. For PI3-AKT pathway 49 proteins were altered in cells exposed to 100 mGy, 52 proteins in the non-primed cells and 65 proteins in the primed cells. Proteins like EGF, EGFR, IGF1R, COL4A2, PIK3CB, KIT, BRCA1 were detected in all the three groups. Few proteins showed dose-specific modulation: IRS1, TNR, YWHAE were detected only in cells exposed to 100 mGy; NFKB1, HSP90AA1 were detected in only in the non-primed and primed cells; AKT1, AKT2, AKT3, TLR4, CHUK, JAK2, CREB3L4 were detected only in the primed cells. Regulation of actin cytoskeleton pathway was represented by 39 proteins from cells exposed to 100 mGy, 45 proteins from the non-primed cells and 37 proteins from the primed cells. Proteins like APC2, ACTN1, VCL, EGF, INSRR, ITGB4, ITGA11 were found in all the three groups. Examples of some proteins that showed dose-specific alteration were: VAV1,

ABI2, FGFR3, FGFR4 in 100 mGy irradiated cells, ROCK2, PIK3CB, SRC in non-primed cells and SOS1, PXN, ARHGAP35, PIK3CD in primed cells. Different isoforms of actin, integrin proteins were found in each group.

There were several other pathways that were enriched only in specific treatment groups. Pathways like hsa05200:pathways in cancer, hsa03013:RNA transport, hsa04066:HIF-1 signaling pathway, hsa04068:FoxO signaling pathway and hsa04120:ubiquitin-mediated proteolysis pathway were enriched only in the primed cells. Other pathways like hsa04014:Ras signaling pathway, hsa04070:Phosphatidylinositol signaling system, hsa02010:ABC transporters and hsa05205:Proteoglycans in cancer were enriched only in the non-primed cells. Cells irradiated with low dose of 100 mGy showed specific enrichment of pathways like hsa05217:Basal cell carcinoma and hsa00230:Purine metabolism.

There were few pathways that were enriched in both non-primed and primed cells, but not in cells irradiated with low dose of 100 mGy. This included hsa04015:Rap1 signaling pathway, hsa04024:cAMP signaling pathway and hsa04022:cGMP-PKG signaling pathway. For the Rap1 signaling pathway 43 proteins from the non-primed cells and 47 proteins from the primed cells were altered. Proteins like PIK3CB, DOCK4, RAPGEF6, SIPA1L2, MET, KIT were detected in both the groups. Proteins like SRC, VEGFC, PLCB3 were unique to the non-primed cells and proteins like AKT1, AKT2, AKT3, RAP1GAP were unique to the primed cells. For cAMP signaling pathway, 39 and 45 proteins were significantly modulated in the non-primed and primed cells, respectively. Proteins like ADCY9, ADCY10, GLI3, NFKB1, ROCK1, ROCK2, PIK3CB were detected in both the treatment groups. Others like PLD2, NFATC1 (in non-primed cells) and AKT1, AKT2, AKT3, CREB3L4 (in primed cells) showed dose specific expression. cGMP-

PKG signaling pathway comprised of 29 and 31 proteins from the non-primed and primed cells, respectively. Proteins such as ADCY7, CACNA1F, CACNA1D, ROCK1, ROCK2, INSR, PLCB were found in both groups, ADCY1, ADCY5 ATP1A2 and ATP1A4 expressed only in the non-primed cells and, ADCY6, ADCY8, ADCY9, ATP2B4, ATP2B3, ATP2B2 expressed specifically in the primed cells.

A critical DNA repair related KEGG pathway- Fanconi anemia (FA) pathway (hsa03460) was enriched only in the cells irradiated with 100 mGy. FA pathway is not only involved in the repair of DNA interstrand crosslinks (ICLs) in the genome, but it also coordinates the repair of DNA strand breaks through proteins of other major repair pathways. Seven proteins (FANCA, FANCI, FANCM, BLM, PALB2, ATRIP, REV1) were differentially expressed in these cells when compared to sham irradiated controls.

4.3 mRNA expression of selected radiation responsive proteins

The expression levels of 13 selected radiation responsive proteins were correlated at the mRNA level using RT-PCR. The selected candidate genes belonged to several important biological processes such as transcription (MED13L RNF20 TCF20, RBM25); chromatin modification (KDM5A, BRWD, CHD4); DNA repair (BLM) and cell signaling (EGF, ITGA11). Other proteins studied included LRRC37A2 belonging to the family of proteins with leucine rich repeats, DICER1 which is a double-stranded RNA-specific endoribonuclease and DUOX2, a dual oxidase enzyme. RT-PCR analysis was performed with the SYBR green based method. Endogenous reference gene GAPDH was used to normalize the expression of target genes. Gene expression levels were analyzed at the same time point as label-

free analysis (1 h post-irradiation). The gene expression pattern for most genes correlated poorly with the protein expression data. The mRNA expression trend matched to a certain extent with the protein expression trend of the three treatment groups only for three genes (KDM5A, LRRC37A2 AND RNF20) (**Table 4. 2**).

Gene expression values				
Gene	Control	100 mGy	2 Gy	100 mGy + 2 Gy
MED13L	1	5.13 ± 0.86	1.39 ± 0.31	4.62 ± 0.60
KDM5A	1	0.78 0.17	2.26 ± 0.12	2.34 ± 0.51
LRRC37A2	1	1.00 ± 0.02	0.81 ± 0.01	0.82 ± 0.002
RNF20	1	0.39 ± 0.01	0.88 ± 0.02	1.12 ± 0.02
TCF20	1	1.06 ± 0.63	0.39 ± 0.09	1.23 ± 0.08
EGF	1	0.72 ± 0.30	0.98 ± 0.14	1.09 ± 0.38
BRWD	1	1.34 ± 0.42	0.47 ± 0.11	2.33 ± 0.08
RBM25	1	1.99 ± 0.22	0.37 ± 0.00	2.72 ± 0.00
ITGA11	1	0.26 ± 0.02	0.35 ± 0.08	0.84 ± 0.71
BLM	1	0.44 ± 0.13	0.97± 0.02	1.19 ± 0.64
CHD4	1	1.13 ± 0.07	2.35 ± 0.08	3.17 ± 0.35
DICER1	1	0.72 ± 0.15	1.35 ± 0.01	1.31 ± 0.03
DUOX2	1	2.4 ± 0.08	4.3 ± 0.83	3.6 ± 0.95

Table 4. 2. mRNA expression of selected radiation responsive proteins.

4.4 Discussion

Proteins are considered the functional blocks of the cells. While the cellular genome remains largely stable, the proteins in any cell change dynamically in response to the environment. Thus, a more complete understanding of molecular responses of cells to stressors like IR can be gained through the study of cellular proteome. Traditional proteomic quantitation has relied extensively on high-resolution protein separation by 2D gels. In this context, 2-DE still remains a reliable and efficient method for the separation of several hundred different proteins on one gel based on mass and charge. The gel-based methods are thus, hugely useful for applications like definitive protein expression profiling to compare and contrast expression of any two samples [52,105]. Unfortunately, 2-DE implies some inherent limitations such as low dynamic range and gel-to-gel variability. The improved process of 2D-DIGE overcomes many of these problems associated with traditional 2-DE and allows more accurate and sensitive quantitative proteomics. The process is based on pre-electrophoretic labelling of samples with fluorescent CyDyes (Cy2, Cy3, and Cy5). Also, the post-translational modifications can be easily identified as a shift on the gel. Furthermore, it allows visualization of intact proteins and not as fragments in the MS. Over the last few years, rapid technical developments in the field of MS have allowed the evolution of proteomics into a more powerful bioanalytical platform. In particular, label-free proteomics has emerged as a capable high-throughput method for quantitative proteomics studies.

In the present study, an integrated approach of gel based 2D-DIGE and gel-free LC-MS based process was followed to understand proteomic responses with low dose radiation that can lead to radio-adaption.

There are only few studies where proteomic analysis using 2D-DIGE has been used to understand radiation induced alterations. In a study on endothelial cells, Sriharshan *et al* (2012) showed modulation of 27 proteins 4 h post-irradiation and 18 proteins 24 h post-irradiation with 2.5 Gy of γ-rays (Cs-137) [206]. In another report, proteomic analysis on blood plasma from three radiological accident victims showed alterations in the expression of 18 protein spots when compared with blood plasma from control group individuals [207]. Among the identified proteins were haptoglobin, serotransferrin/transferrin, fibrinogen and ubiquitin-60S ribosomal protein L40. Another study with 2D-DIGE identified post translational modifications in human serum proteins in a man overexposed to a gammagraphy radioactive source of 192Ir (3.3 TBq) [208]. Besides this, 2D-DIGE has also been used to develop biomarkers for esophageal cancer [209], gastric cancer [210], liver cancer [211] and sarcomas [212]. In a study on radioadaptive response, very low priming dose of 40 mGy and a low challenge dose of ≤100 mGy was used to study adaptive changes in the proteome of cultured human fibroblasts (VH10) and human adipose-derived stem cells (ADSC) using 2D-DIGE [213]. A study from our group described global expression of cellular proteins during RI-AR in PBMCs isolated from individuals living in high level natural background radiation areas using traditional 2-DE [52]. There is only one report on proteome profiling for RI-AR using label-free analysis. The study identified the proteins in the medium collected from human lymphocyte cultures exposed to a priming low dose of 30 mGy ^{137}Cs γ-rays followed by a challenging dose of 1 Gy ^{137}Cs γ-rays after 4 h [214]. However, none of the above reports can be compared directly with the present work either due to differences in irradiation conditions used to induce adaptive response or due to the cellular system employed. To the best of our knowledge, the present work is the first report in G_0

non-cycling human cells exposed to *in vitro* radiation to study global proteome changes during RI-AR.

There are many reports however, on the use of label-free based proteomics method for clinical studies. Hyung *et al* (2011) studied serum samples from 96 breast cancer patients and identified 13 novel biomarker candidates [215]. Similarly, serum protein levels in brain cancer patients undergoing radiotherapy were identified using label-free approach to discover candidate biomarkers leading to radiation-induced skin lesions. A significant modulation of 25 proteins was seen before the emergence of skin lesions [216]. In another study on blood plasma from 30 breast cancer patients, a correlation between alterations in protein glycosylation, lipid metabolism, and the progression of breast cancer was shown using label-free approach [217]. Label-free quantitative proteomics have also been used to identify biomarkers from blood plasma for discriminating pulmonary TB (PTB) from latent infection (LTBI). A total of 31 proteins were found to be significantly modulated in PTB patients when compared with LTBI individuals and healthy controls [218]. Studies have also been performed to identify proteins from other biofluids like bile and urine using label-free approach [219,220]. It has also been successfully used to identify modulated proteins from normal and cancer cells cultured *in vitro* [221–224]. There is at least one report on label-free proteomics for human PBMCs derived from HIV-infected patients [225].

In the present study, we identified 28 proteins differentially expressed in primed cells relative to non-primed cells using gel based 2D-DIGE method. The identified proteins were clustered into eight major groups based on their biological function using information available in Uniprot/Swissprot database: Among them, the cell adhesion proteins formed the largest group with nine proteins. Radiation

mediated induction of several adhesion molecules which may contribute to inflammatory reactions and tissue injury has been reported [226]. Radiation induced alterations of cytoskeletal proteins like actin and tubulin have also been reported in several cell models, including PBMCs [105,227–229].

Though, there are several advantages of using 2D-DIGE as a quantitative method, it nevertheless retains some of the major limitations of 2-DE. It also involves high cost involved in fluorescent labelling of proteins and imaging of gels. The label-free method on the other hand, offers a high through-put cost effective and reproducible method of quantitative proteomics [230]. Li *et al* (2012) performed a comparative study of label-free quantification with other gel-free proteomics techniques like SILAC, iTRAQ and TMT [231]. The authors showed that label-free approach has the highest proteome coverage for protein identification as compared to other gel-free techniques. Similar conclusions were drawn by Merl *et al* (2012) through studies on primary retinal Muller cells using a combination of label-free quantification and SILAC [232]. Trinh *et al* (2013) and Latosinska *et al* (2015) reported higher sequence coverage and higher number of differentially expressed proteins using label-free approach when compared with iTRAQ [233,234]. In the present study, we identified a total of 5739 proteins in human PBMCs using label-free proteomics based on peptide ion intensity measurement, which is in agreement with most published studies. Thus, with label-free analysis, the number number of proteins identified in human PBMCs increased ~22 times when compared with earlier reports on 2-DE [52,105,205]. In this report, a poor overlap was seen between proteins identified by 2D-DIGE and label-free analysis, with only five proteins common between the two methods (VINC, ACTB/G, ACTB/G, HSP7C and TRFE). As quality control, an assessment of experimental variation among the three technical

replicates of label-free analysis was performed by calculating % coefficient of variation (% CV). More than 60% of the identified proteins showed a CV ≤ 30%, indicating good assay reproducibility, minimum variation between the experimental replicates and good stability of expression. The data quality was further assured since ~99% of the proteins detected showed sequence coverage of more than 5%, while ~90% proteins were represented by ≥5 peptides.

To identify potential pathways and functions affected during RI-AR, functional annotation of the differentially expressed proteins was performed with DAVID Bioinformatics Resource. GO annotation classified the proteins into 34 biological processes, 66 molecular function categories and 71 cellular component categories. The GO term enrichment analysis indicated that the proteins modulated during RI-AR primarily associated with processes like DNA damage repair, chromatin modifications, transcriptional regulation, post translational modifications, cytoskeletal organization and cell signaling. More than 77% of the proteins belonged to the molecular function of protein, RNA, DNA and chromatin binding. Almost 45% of the enriched proteins were localized to cytoplasm.

This study showed that in response to genotoxic stress like IR, cells evoke an integrated network of DNA damage repair and transcriptional regulation. This may play an important role in RI-AR as we observed a specific enrichment of GO:0006351~transcription, DNA-templated biological process in primed and 100 mGy irradiated cells but not in non-primed cells. This also formed the largest group of proteins (326 proteins) in the primed cells. A large number of proteins belonging to DNA repair, regulation of transcription, chromatin remodelling and chromatin modification were included in this group. Some of the important DNA damage repair proteins that showed over-expression were CUX1, CUX2, MMS19 CHD2 and

SMARCA5. Several studies have reported an important role of Cut homeobox 1 (CUX1) transcription factor in regulating a large number of genes and microRNAs involved in varied cellular processes like DNA replication and DDR [235,236]. CUX1 protein is rapidly recruited to the sites of DNA damage [237]. It was shown to be essential not only for the expression of ATM and ATR checkpoint kinases in the absence of genotoxic stress, but also for activation of these kinases after treatment with DNA damaging agents. It was further seen that CUX1-deficient cells showed defects in ATM/ATR-mediated DDR signaling, cell cycle checkpoint control and cell survival following exposure to UV or IR [236]. Ramdzan *et al* (2014, 2015) reported a role for CUX1 in the repair of oxidative DNA damage [238,239]. The authors showed that Cut repeats of CUX1 bind to 8-oxoguanine DNA glycosylase (OGG1), an enzyme involved in BER process and stimulates its glycosylase and AP-lyase enzymatic activities. CUX2 protein was shown to play a similar role in the repair of oxidative DNA damage [240]. The nucleotide excision repair protein homolog MMS19 plays a key role in the cytosolic biogenesis of Fe–S proteins that are specifically involved in DNA repair and DNA metabolism. MMS19 has been reported to interact with a subset of cellular iron-sulfur proteins such as ERCC2/XPD, FANCJ and RTEL, and thus, acts as a key player in nucleotide excision repair, homologous recombination repair, DNA replication and RNA polymerase II transcription [241–243].

The architecture of the chromatin and the level of condensation can greatly affect the sensitivity of the DNA to damage. Chromatin remodelling is considered necessary for various DNA processes including, transcription, chromatin assembly, replication, recombination and DNA repair. Epigenetic regulation or involvement of chromatin modifications and chromatin remodelling activities for the induction of RI-

AR has been proposed [244]. The gene sets and pathways for histone modification were observed in low dose (5 cGy) primed normal human fibroblasts by Hou *et al* (2015) [117]. Our study showed changes in abundance for several histone modifying enzymes and proteins involved in chromatin remodelling complexes. The chromatin remodelling enzyme CHD1 (chromodomain helicase DNA binding protein 1) detected in our study is an important protein required for DNA-damage signalling. The chromodomain helicase DNA binding proteins, in general, are known to affect transcription through their ability to remodel chromatin and modulate histone deacetylation [245]. Zhou *et al* 2018 showed that targeted disruption of CHD1 gene in human cells leads to a defect in DSB repair via homologous recombination, resulting in hypersensitivity to IR [246]. It also exhibits transcriptional regulatory activity and influences the DNA damage response by affecting the transcriptional activity of p53 [245]. Under the GO:0006338~chromatin remodelling biological process, several proteins of the SWI/SNF chromatin-remodelling family, which are the ATP-dependent chromatin-remodelling enzymes, showed modulation in expression. These included SMARCC1, SMARCC2, SMARCA1, SMARCA4, SMARCA5 and ARID1. Proteins like DEK, SUPT5H, SUPT6H, CHD1, TADA2A involved in positive regulation of transcription by RNA pol II enzyme, and histone deacetylases HDAC4 and HDAC5 were also found to be modulated. Similarly, our study also found enrichment of proteins involved in several PTMs, indicating important role of active PTM under radiation stress. PTMs like ubiquitylation, phosphorylation, acetylation and methylation on the histone proteins are known to regulate chromatin reorganization during the different processes requiring DNA as a substrate [247]. Histone PTMs are suggested to be one of the many molecular candidate biomarkers for IR induced damage [248].

Our study also detected enrichment of several zinc finger (ZnF) domain-containing proteins that have been implicated in telomere maintenance and DNA repair, and chromatin-remodelling in damaged DNA [249]. ZnF domain is one of the most abundant DNA-binding motifs found in eukaryotic transcriptional factors [250]. Goldberg *et al* (2006) showed increase in gene expression of zinc finger proteins in skin tissue of men exposed to therapeutic radiation [251].

Primed cells also showed enrichment of several proteins involved in protein ubiquitination and deubiquitination. Ubiquitination regulates multiple cellular events in eukaryotes through modification of intracellular proteins with 76-amino acid polypeptide ubiquitin which are then destined for proteolysis or activity alteration. The primed cells showed modulation of several such enzymes, among which were the E3 ubiquitin ligase RNF6 reported to be involved in cell signaling [252], the cullin family ubiquitin ligase protein CUL4B which plays an important role in establishing the cellular DNA repair threshold [253], and RNF20 and RNF 40 which catalyze monoubiquitylation of histone H2B on lysine120 in the mammalian cells in response to DNA damage [254,255]. RNF20 and RNF40 have also been reported to be a putative tumour suppressor proteins [256,257].

Ubiquitin specific proteases (USP) a subclass of deubiquitinating enzymes was also found to be modulated in primed cells. Deubiquitination is a highly regulated process which is involved in various cellular functions like gene expression, cycle regulation and DNA repair. USP4, USP7, USP11, USP17L2, USP28, USP47 and USP49 involved in DNA damage response were modulated [258,259]. Khoronenkova *et al* (2012) reported a role for USP7 in BER of lesions induced by oxidative damage [260]. USP4, USP6 involved in cell signaling [261,262], USP42, USP47, USP53 involved in maintenance of cell junctions [263], USP22, USP42,

USP49 involved in gene expression regulation [264–266] and USP22 involved in cell cycle progression [264] were also found to be modulated in our dataset.

Various kinases involved in signal transduction pathways like the MAP kinase pathway, phosphatidylinositol mediated signaling pathway and I-kappaB kinase signaling were found to be modulated in both primed and non-primed cells. MAPKs and PI3K are known to be activated by a wide range of environmental stresses and transmit extracellular signals to changes in gene expression through signal responsive transcription factors like AP-1, ATF-2, and TCF/Elk-1 [111,267,268]. Among the three MAPK subfamilies, our data showed enrichment of proteins involved in positive regulation of JNK cascade in non-primed cells. Apart from this, proteins involved in integrin mediated signaling pathway and vascular endothelial growth factor receptor signaling pathway were also found to be enriched only in non-primed cells

Proteins involved in positive regulation of GTPase activity, guanine exchange factors (GEF) and GTPase activating proteins (GAP), were found to be enriched in both primed and non-primed cells. The downstream proteins of GEF and GAP are involved in actin cytoskeletal organization, regulation of cell shape and protein transport. Rho guanine nucleotide exchange factor 18 (ARHGEF18) that acts as a GEF for ROS inducer Rho GTPase protein Rac1 was found to be up-regulated in primed cells.

We also observed differential modulation of proteins involved in cytoskeletal organization in both primed and non-primed cells. The cytoskeleton and their associated family proteins of eukaryotic cells are important for a multitude of cellular functions including maintenance of cell shape, cell motility and mitosis. These proteins also associate with chromatin remodeling enzymes and all three RNA

polymerases, thus indicating their role in gene transcription [269]. The radiation stress induced modulation of cytoskeletal proteins has been reported in several cell models [227,229,270,271]. Lately, a role for tubulin protein in the transport of DNA repair proteins in response to DNA damage was reported [272]. Proteomic studies from our lab have earlier reported wide ranging modulation of proteins involved in cytoskeletal organization after exposure to acute and chronic dose in human PBMCs [52,105].

To further characterize the functions of radiation modulated proteins, the KEGG pathway mapping based on KEGG orthology terms was performed. The analysis identified statistical enrichment (Benjamini-Hochberg corrected p-value $\leq$ 0.1) of 43 pathways in different radiation groups.

Three cell-matrix adhesion related pathways namely focal adhesion, ECM-receptor interaction and regulation of actin cytoskeleton were found to be significantly altered in all the three groups. Cell-matrix adhesion refers to the interaction of a cell with the extracellular matrix. This interaction is mediated through integrin - dependent junctions at specific membrane areas termed as focal adhesion (FA) points. At the FA points, a multi-protein adhesion assembly of fibronectin, collagen and fibrin from the cell-extracellular matrix interacts with the actin cytoskeleton within the cell through transmembrane receptors of the integrin family. The FA points serve as active regions of many signal transduction molecules like the Src-family kinases, guanine nucleotide exchange factors, Ras-family proteins and MAP kinases. FA points therefore, not only help to maintain cell-matrix adhesions but also play an important role in various intracellular processes like cell motility, cell differentiation, cell proliferation, regulation of gene expression and cell survival [273,274]. At the cell membrane surface, integrins, receptor tyrosine kinases, GPCRs

and cadherins receive extracellular signals, which then influence the activity of Rho GTPase by modulating activity of guanine nucleotide exchange factors (GEFs) and GTPase activating proteins (GAP). Rho GTPases in turn activate ROCK proteins, which lead to reorganization of the actin cytoskeleton [275]. Our work showed that several FA proteins with predominantly a structural role (e.g. integrins, actins, actinins, lamins, vinculin, tenascin), and several others which are involved in signal transduction (EGFR, EGF, ROCK1, ROCK2, DOCK1, ARHGAP5, PIK3CB) were altered after radiation. Primed cells showed an over-expression of phosphatidylinositol-4,5-bisphosphate 3-kinase catalytic subunit beta (PIK3CB) which generates PI(3,4,5)P3 known to be involved in actin dependent cellular processes [276] and also activates downstream pro-survival PI3K-AKT signaling pathway. In line with this, modulation of pro-survival PI3K-AKT signaling pathway was observed in all the three treatment groups. The IR activated PI3K-Akt signaling has been widely reported in different cell types [277,278].

The KEGG pathway analysis revealed specific response for several other signalling processes in the three groups. Rap1 signaling pathway, cAMP signaling pathway, cGMP-PKG signaling pathway were modulated both in primed and non-primed cells, but were not enriched in the 100 mGy irradiated group.
Rap1 proteins are members of the Ras superfamily of small molecular weight GTPases. Activated Rap1 regulates several signalling pathways, including MAPK cascade [279] and is also involved in integrin-based cell matrix adhesion and regulation of cytoskeleton remodelling [280]. cAMP signaling pathway is also an important process that regulates a multitude of cellular responses including metabolism, gene expression, growth, differentiation, proliferation and apoptosis. cAMP signaling system has also been reported to modulate apoptosis in cancer cells

[281] and regulate ATM [282] in response to DNA damage. The cGMP is the intracellular second messenger that mediates the action of nitric oxide (NO) and regulates a broad array of physiologic processes. Activation of the cGMP/PKG pathway is antineoplastic in several cancer types [283]. Studies on diabetic osteoblasts have revealed a pro-survival role of NO/cGMP/PKG signalling through potent antioxidant effects [284]. Here, our work reports an important role for this pathway in radiation response of human PBMCs.

There were four KEGG pathways that were enriched only in non-primed cells: hsa04014:Ras signaling pathway, hsa04070:Phosphatidilinositol signaling system, hsa02010:ABC transporters and hsa05205:Proteoglycans in cancer. Ras signaling is known to be activated as a part of general stress response in the cell and is a significant contributor to radiation resistance [285]. Phosphatidilinositol signaling system essentially involves signal transduction via small lipid molecules called as phosphoinositides (mono, di and triphosphates of phosphatidilinositol). Phosphoinositides mediate pre-survival PI3-AKT signaling. These molecules also play a role in regulating various cell activities like actin-cytoskeletal reorganization, vesicle trafficking, cell division and stress response [286,287]. ABC transporters protect the cells against oxidative stress generated from various reactive oxygen species. ABC transporters eliminate the toxic compounds after they are detoxified by conjugation to GSH, glucuronide, and sulphate [288]. Proteins involved in cell matrix adhesion and cell-cell adhesion, WNT pathway and PI3-AKT signaling pathway were represented in proteoglycans in cancer KEGG pathway.

Enrichment of five pathways namely HIF1 signaling pathway, FoxO signalling pathway, Ubiquitin mediated proteolysis pathway, RNA transport and pathways in cancer were found only in primed cells.

A specific over-expression of pro-survival transcription factor HIF-1α was seen in primed cells. This protein functions as a master regulator of adaptive response to hypoxia, and activates various target genes to limit oxygen consumption and push the cell into survival mode [289]. It also induces non-transcriptional activities like hypoxic inhibition of DNA replication even in quiescent fibroblasts [290]. Increased ROS and nitric oxide production are known to stabilize HIF [267,291,292]. The HIF signaling is thus, regulated by cellular redox status and it can modify the downstream pro-survival or pro-death factors depending on the cellular stress conditions [267]. It is thus, considered a critical player in the survival strategy of stressed cells [293].

The FoxO transcription factor modulates expression of multiple genes involved in cellular processes like cell cycle, DNA damage repair, apoptosis, oxidative stress response, and cell differentiation. In response to oxidative or nutrient stress stimuli, stress-activated JNK and the energy sensing AMP-activated protein kinase (AMPK) phosphorylate and activate FoxO. In general, FoxO family plays a central role in redox signaling by upregulating antioxidant enzymes catalase and MnSOD through FoxO1a, thus, providing resistance against oxidative stress [294]. The other major proteins detected and modulated in FoxO signaling pathway included the three growth factor receptors - TGF-beta receptor type-2 (TGFBR2), Insulin receptor (INSR), Insulin-like growth factor 1 receptor (IGF1R) were over-expressed. Increased expression of IGF1R signaling has been reported to promote radioresistance [295].

Primed cells also showed enrichment of KEGG pathway: pathways in cancer. This group included proteins from different signaling pathways, cell-matrix adhesion pathways, DNA damage response pathways essential for radioresistance, cell survival and proliferation.

Proteins involved in RNA transport and translation were also found to be enriched in primed cells. Radiation-induced translational control of gene expression is a fundamental component of cellular radio-response. Radiation-induced gene expression has long been hypothesized as a critical component of the adaptive response protecting against cell death both in prokaryotes [296] as well as eukaryotes [297]. Mazan-Mamczarz *et al* (2011) showed that irradiation of lymphocytes altered the mRNAs bound to HuR antigen after 1 Gy [298]. Thus, radiation-induced translational control of gene expression may be a novel means of radiation induced-adaptive response of human PBMCs and needs to be probed in greater detail.

Basal cell carcinoma KEGG pathway was enriched only in cells exposed to low dose of 100 mGy. This KEGG pathway represented proteins majorly involved in Hedgehog signaling pathway and Wnt signaling pathway, vital pathways for regulating the developmental processes and cell proliferation in multicellular organisms. Low dose radiation activation of Wnt signaling pathway has been described [299]. However, deregulation of proteins involved in both of these pathways may lead to basal cell carcinoma and various other cancers [300,301].

Similarly, the 100 mGy irradiated cells showed specific enrichment of purine metabolism KEGG pathway indicating that low dose radiation may be involved in alteration of basal cellular processes. Alteration of enzymes involved in purine metabolism has been reported earlier with a high dose of 10 Gy of IR in ATCL8 cell line [302].

We also observed an enrichment of Fanconi anemia pathway (FAP) in cells irradiated with 100 mGy but at Student t-test $p < 0.05$. Three FAP proteins (FANCA, BLM, PALB2) showed an over-expression. Three other proteins that form the FAP nuclear complex were modulated: FANCA was over-expressed, FANCM was under-

expressed while FANCI was unchanged. FAP proteins are mainly involved in coordinating repair of DNA strand breaks through proteins of all the major DNA repair pathways. In non-replicating cells, these proteins promote alternate end joining repair over classical NHEJ. They are also involved in processing of transcription associated R-loops and stabilization of replication forks [303–307]. Additional cytoprotective roles of FAP proteins from cell death induced by ROS and pro-inflammatory cytokines is also reported [273].

The present work strongly suggests reduced ROS levels and coordinated activation of antioxidant enzymes as the key mechanism of radiation induced-adaptive response in human PBMCs. In chapter 3, activity and expression of four key antioxidant enzymes, CAT, SOD, TXNRD1 and GPX were studied in detail. Interestingly, label-free analysis identified several other proteins, along with CAT, that are involved in maintenance of the cell redox homeostasis but only in primed cells and not in non-primed or 100 mGy irradiated cells. This included proteins like HIF1A, FOXO1, NFATC1, NOS2, KLF2 and CHUK. Several of the vital cell signaling proteins like AKT1, AKT2, AKT3, TLR4, HSP90B1, PLK1, CREB3L4 which are known to be activated in response to oxidative stress were also detected **(Table 4. 3).**

Accession no.	Protein Name	Description	Function
P31749	AKT1	RAC-alpha serine/threonine-protein kinase	Metabolism, proliferation, cell survival, growth and angiogenesis
P31751	AKT2	RAC-beta serine/threonine-protein kinase	Metabolism, proliferation, cell survival, growth and angiogenesis
Q9Y243	AKT3	RAC-gamma serine/threonine-protein kinase	Ubiuitin dependent proteolysis, FOXO signaling pathway, Insulin signaling pathway,proliferation, cell survival, growth
P04040	CAT	Catalase	catalyzes detoxification of hydrogen peroxide
O15111	CHUK	Inhibitor of nuclear factor kappa-B kinase subunit alpha	Negative feedback of NF-kappa-B canoncial signaling pathway
Q8TEY5	CREB3L4	Cyclic AMP-responsive element-binding protein 3-like protein 4	cAMP signaling pathway, Unfolded protein response, transcription activation
Q12778	FOXO1	Forkhead box protein O1	FOXO signaling pathway, Insulin signaling pathway
Q16665	HIF1A	Hypoxia-inducible factor 1-alpha	HIF1 signaling pathway, DNA-binding transcription factor activity
P14625	HSP90B1	Endoplasmin	Molecular chaperone that functions in the processing and transport of secreted protein
Q9Y5W3	KLF2	Krueppel-like factor 2	FOXO signaling pathway, transcription factor
P35228	NOS2	Nitric oxide synthase, inducible	Produces nitric oxide (NO), NO mediates tumoricidal and bactericidal action
P53350	PLK1	Serine/threonine-protein kinase	Protein tyrosine kinase activity, cell proliferation, regulation of mitotic exit, cytokinesis
O00206	TLR4	Toll-like receptor 4	NF-kappa-B activation, cytokine secretion and the inflammatory response

Table 4. 3. Cell redox homeostasis proteins detected in primed cells using label-free analysis.

In summary, an integrated approach based on gel based 2D-DIGE and gel-free, label-free quantitative proteomics enabled an exhaustive analysis of changes in protein expression with radiation and contribution of these to radiation-induced adaptive response of human PBMCs.

CHAPTER 5

KEY CONCLUSIONS AND FUTURE DIRECTIONS

Radiation induced-adaptive response is a biological phenomenon in which resistance to a high challenge dose is induced by a small preceding radiation dose. RI-AR has been observed in various cell lines *in vitro* and *in vivo* using various end points. The molecular mechanisms governing this response have yet not been completely elucidated. There have been suggestions that RI-AR involves similar processes like that to other common environmental stressors like metal toxicity, heat shock, pesticides etc. However, different studies have used diverse protocols on independent models; which makes understanding entire sequence of events difficult. The present study, thus attempts to understand the molecular processes involved in RI-AR in a singular cellular model (human PBMCs) using the same sample set and a defined regime for inducing adaptive response.

With the help of two different methods to assess DNA damage and repair - alkaline comet assay and γH2AX assay, we first demonstrated that PBMCs primed with a low dose of radiation show lesser initial damage and better repair of DSBs than non-primed cells. This indicated that RI-AR in human PBMCs is associated with higher efficiency of repair of DSBs. Decreased DNA damage lead to better survival and higher mitochondrial membrane potential in primed cells. Further, primed cells showed low levels of ROS that corresponded with early activation of antioxidant enzymes like CAT, SOD, TXNRD1 and GPX. We further showed increased binding of transcription factors Nrf2 and NFκB in the primed cells that occurred early after irradiation. Pre-exposure to low dose radiation also showed early activation of pERK pro-survival signaling molecule. We thus, hypothesize that RI-AR in human PBMCs is mediated through reduced oxidative stress and increased antioxidant activity in primed cells.

Additionally, we used an integrated approach of gel based 2D-DIGE and gel-free LC-MS based label-free analysis to identify proteomic responses during radioadaptation. Number of proteins identified using label-free analysis in each treatment group were almost 14 times more than the number of proteins identified using 2D-DIGE. Both the proteomics methods showed good assay reproducibility and minimum variation between the experimental replicates. 2D-DIGE analysis identified 28 differentially expressed protein spots out of which 2 were up-regulated (WDR1 and ACTG/B) and 26 were down-regulated (e.g. VINC, VIME, FIBG, ACTG, TBB) in primed cells when compared with non-primed cells. A poor overlap was seen between proteins identified by 2D-DIGE and label-free analysis with only five proteins common between the two methods: P18206 (VINC), P63261 (ACTB/G), P60709 (ACTG/B), P11142 (HSP7C) and P02787 (TRFE). Label-free quantitative proteomic analysis identified 2422 proteins in the primed cells. DAVID analysis identified significant enrichment of 34 biological processes (Benjamini-Hochberg p-value $\leq$ 0.1) in the three treatment groups. Enrichment of proteins involved in transcriptional regulation, ubiquitination and chromatin remodeling processes were unique to primed cells. Functional pathway analysis using KEGG identified enrichment of 18 pathways in the three treatment groups (Benjamini-Hochberg p-value $\leq$ 0.1) that may play a critical role in cellular response to radiation. Several key proteins involved in cellular redox homeostasis (CAT, HIF1A, FOXO1, NFATC1, NOS2, KLF2 and CHUK) were detected only in primed cells. Important cell signaling proteins like AKT1, AKT2, AKT3, TLR4, HSP90B1, PLK1, CREB3L4 which are known to be activated in response to oxidative stress were also unique to the primed cells. These findings again supported our hypothesis that increased

activity of antioxidant enzymes lead to rapid scavenging of ROS and consequently less cellular damage in the primed cells.

The present work identified a large list of unique proteins in primed PBMCs. In the follow-up approach, candidate redox sensitive transcription factors and other antioxidant proteins will be verified using functional assays and targeted proteomics. This will help develop biomarkers of radio-adaptation in human cells. Furthermore, we used only a small fixed period of time between the adapting and challenging dose (4 h) and studied protein expression only at one time point after irradiation (1 h). Characterization of radiation-sensitive proteins at later time points will be interesting and should help better understanding of the long-term implications of radiation-induced adaptive response. This will have huge implications for radiation occupational workers and space astronauts on manned missions.

We are aware of various limitations of our current knowledge of RI-AR. The physiological, genetic and epigenetic factors which may contribute to interindividual variation and affect development of RI-AR have not been tested. Various studies have used contrasting PD and CD in varied cellular systems, indicating different systems might respond to different dose regimes for RI-AR induction. Thus, the hypothesized mechanisms need to be rigorously tested in other cellular systems and animal models to validate their universality. Additionally, development of RI-AR in individuals with dysfunctional repair and immune system is not known and should be tested. New research in the field of low dose radiation is highly pertinent in the modern world. The contribution of non-targeted effects like radioadaptive response, especially in this low dose range, will have important implications for defining an appropriate dose-response model for radiation protection.

REFERENCES

[1] UNSCEAR, Sources, Effects and Risks of Ionizing Radiation 2010 Report, 2010.

[2] G.A. Hall EJ, Radiobiology for the Radiologist, 7th Ed, Lippincott Williams & Wilkins, Philadelphia, PA, 2012.

[3] S. Le Caër, Water Radiolysis: Influence of Oxide Surfaces on H2 Production under Ionizing Radiation, Water. 3 (2011) 235–253. doi:10.3390/w3010235.

[4] A. Marechal, L. Zou, DNA damage sensing by the ATM and ATR kinases., Cold Spring Harb. Perspect. Biol. 5 (2013). doi:10.1101/cshperspect.a012716.

[5] X. Li, H. Xu, C. Xu, M. Lin, X. Song, F. Yi, Y. Feng, K.A. Coughlan, W.C.-S. Cho, S.S. Kim, L. Cao, The yin-yang of DNA damage response: roles in tumorigenesis and cellular senescence., Int. J. Mol. Sci. 14 (2013) 2431–2448. doi:10.3390/ijms14022431.

[6] J. Vignard, G. Mirey, B. Salles, Ionizing-radiation induced DNA double-strand breaks: A direct and indirect lighting up, Radiother. Oncol. 108 (2013) 362–369. doi:https://doi.org/10.1016/j.radonc.2013.06.013.

[7] Kai Rothkamm, Stephen Barnard, JayneMoquet, Michele Ellender, Zohaib Rana, DNA Damage Foci:Meaning and Significance, Environ. Mol. 56 (2015) 491–504.

[8] L.J. Kuo, L.-X. Yang, Gamma-H2AX - a novel biomarker for DNA double-strand breaks., In Vivo. 22 (2008) 305–9. doi:0258-851X/2008.

[9] L. Beels, J. Werbrouck, H. Thierens, Dose response and repair kinetics of γ-H2AX foci induced by in vitro irradiation of whole blood and T-lymphocytes with X-and γ-radiation, Int. J. Radiat. Biol. 86 (2010) 760–768. doi:10.3109/09553002.2010.484479.

[10] M. Shrivastav, L.P. De Haro, J.A. Nickoloff, Regulation of DNA double-

strand break repair pathway choice., Cell Res. 18 (2008) 134–147. doi:10.1038/cr.2007.111.

[11]   C. Arena, V. Micco, E. Macaeva, R. Quintens, Space radiation effects on plant and mammalian cells, Acta Astronaut. 104 (2014) 419–431. doi:10.1016/j.actaastro.2014.05.005.

[12]   Halliwell B and Gutteridge JMC, Free radicals in biology and medicine, 4th ed., Oxford University Press, New York, 2007.

[13]   T. Fukai, M. Ushio-Fukai, Superoxide dismutases: role in redox signaling, vascular function, and diseases., Antioxid. Redox Signal. 15 (2011) 1583–1606. doi:10.1089/ars.2011.3999.

[14]   C. J. Weydert, J. J. Cullen, Measurement of Superoxide Dismutase, Catalase, and Glutathione Peroxidase in Cultured Cells and Tissue, Nat. Protoc. 5 (2011) 51–66. doi:10.1038/nprot.2009.197.MEASUREMENT.

[15]   S. Li, T. Yan, J.-Q. Yang, T.D. Oberley, L.W. Oberley, The Role of Cellular Glutathione Peroxidase Redox Regulation in the Suppression of Tumor Cell Growth by Manganese Superoxide Dismutase, Cancer Res. 60 (2000) 3927 LP – 3939. http://cancerres.aacrjournals.org/content/60/14/3927.abstract.

[16]   S. Toppo, S. Vanin, V. Bosello, S.C.E. Tosatto, Evolutionary and structural insights into the multifaceted glutathione peroxidase (Gpx) superfamily, Antioxidants Redox Signal. (2008). doi:10.1089/ars.2008.2057.

[17]   J.P. Conway, M. Kinter, Dual Role of Peroxiredoxin I in Macrophage-derived Foam Cells, J. Biol. Chem. . 281 (2006) 27991–28001. doi:10.1074/jbc.M605026200.

[18]   O. Zitka, S. Skalickova, J. Gumulec, M. Masarik, V. Adam, J. Hubalek, L. Trnkova, J. Kruseova, T. Eckschlager, R. Kizek, Redox status expressed as

GSH:GSSG ratio as a marker for oxidative stress in paediatric tumour patients, Oncol. Lett. 4 (2012) 1247–1253. doi:10.3892/ol.2012.931.

[19]   T.H. Wideman, A.J. Zautra, R.R. Edwards, NIH Public Access, 154 (2014) 2262–2265. doi:10.1016/j.pain.2013.06.005.Re-Thinking.

[20]   L. Packer, S.U. Weber, G. Rimbach, Molecular Aspects of α-Tocotrienol Antioxidant Action and Cell Signalling, J. Nutr. 131 (2001) 369S-373S. doi:10.1093/jn/131.2.369S.

[21]   M.S. Hayden, S. Ghosh, Signaling to NF- ☐ B, (2004) 2195–2224. doi:10.1101/gad.1228704.bone.

[22]   M.J. Morgan, Z. Liu, Crosstalk of reactive oxygen species and NF-κB signaling, Cell Res. 21 (2011) 103–115. doi:10.1038/cr.2010.178.

[23]   G. Guo, Y. Yan-Sanders, B.D. Lyn-Cook, T. Wang, D. Tamae, J. Ogi, A. Khaletskiy, Z. Li, C. Weydert, J.A. Longmate, T.-T. Huang, D.R. Spitz, L.W. Oberley, J.J. Li, Manganese Superoxide Dismutase-Mediated Gene Expression in Radiation-Induced Adaptive Responses, Mol. Cell. Biol. 23 (2003) 2362–2378. doi:10.1128/MCB.23.7.2362-2378.2003.

[24]   D.D. Zhang, G.M. Habib, S.-C. Lo, M. Hannink, Z. Sun, M.W. Lieberman, Ubiquitination of Keap1, a BTB-Kelch Substrate Adaptor Protein for Cul3, Targets Keap1 for Degradation by a Proteasome-independent Pathway, J. Biol. Chem. 280 (2005) 30091–30099. doi:10.1074/jbc.m501279200.

[25]   K. Taguchi, H. Motohashi, M. Yamamoto, Molecular mechanisms of the Keap1-Nrf2 pathway in stress response and cancer evolution, Genes to Cells. 16 (2011) 123–140. doi:10.1111/j.1365-2443.2010.01473.x.

[26]   S. Wu, H. Lu, Y. Bai, Nrf2 in cancers: A double-edged sword., Cancer Med. 8 (2019) 2252–2267. doi:10.1002/cam4.2101.

[27] D.A. Frohlich, M.T. McCabe, R.S. Arnold, M.L. Day, The role of Nrf2 in increased reactive oxygen species and DNA damage in prostate tumorigenesis., Oncogene. 27 (2008) 4353–4362. doi:10.1038/onc.2008.79.

[28] S.T. Mathew, P. Bergstrom, O. Hammarsten, Repeated Nrf2 stimulation using sulforaphane protects fibroblasts from ionizing radiation., Toxicol. Appl. Pharmacol. 276 (2014) 188–194. doi:10.1016/j.taap.2014.02.013.

[29] M. El-Ashmawy, O. Delgado, A. Cardentey, W.E. Wright, J.W. Shay, CDDO-Me protects normal lung and breast epithelial cells but not cancer cells from radiation., PLoS One. 9 (2014) e115600. doi:10.1371/journal.pone.0115600.

[30] M.E. Abazeed, D.J. Adams, K.E. Hurov, P. Tamayo, C.J. Creighton, D. Sonkin, A.O. Giacomelli, C. Du, D.F. Fries, K.-K. Wong, J.P. Mesirov, J.S. Loeffler, S.L. Schreiber, P.S. Hammerman, M. Meyerson, Integrative radiogenomic profiling of squamous cell lung cancer., Cancer Res. 73 (2013) 6289–6298. doi:10.1158/0008-5472.CAN-13-1616.

[31] M. Rincon, R.A. Flavell, R.J. Davis, Signal transduction by MAP kinases in T lymphocytes., Oncogene. 20 (2001) 2490–2497. doi:10.1038/sj.onc.1204382.

[32] R.K. Schmidt-Ullrich, P. Dent, S. Grant, R.B. Mikkelsen, K. Valerie, Signal transduction and cellular radiation responses., Radiat. Res. 153 (2000) 245–257. doi:10.1667/0033-7587(2000)153[0245:stacrr]2.0.co;2.

[33] P. Dent, A. Yacoub, P.B. Fisher, M.P. Hagan, S. Grant, MAPK pathways in radiation responses, Oncogene. (2003). doi:10.1038/sj.onc.1206701.

[34] H.S. Park, G.E. You, K.H. Yang, J.Y. Kim, S. An, J.-Y. Song, S.-J. Lee, Y.-K. Lim, S.Y. Nam, Role of AKT and ERK pathways in controlling sensitivity to ionizing radiation and adaptive response induced by low-dose radiation in human immune cells., Eur. J. Cell Biol. 94 (2015) 653–660.

doi:10.1016/j.ejcb.2015.08.003.

[35] Y. Son, Y. Cheong, N. Kim, H. Chung, D.G. Kang, H. Pae, Mitogen-Activated Protein Kinases and Reactive Oxygen Species : How Can ROS Activate MAPK Pathways ?, 2011 (2011). doi:10.1155/2011/792639.

[36] D.L. Preston, D.A. Pierce, Y. Shimizu, Age-time patterns for cancer and noncancer excess risks in the atomic bomb survivors., Radiat. Res. 154 (2000) 733–735.

[37] M.P. Little, Radiation: a dose of the bomb., Nature. 424 (2003) 495–496. doi:10.1038/424495a.

[38] J.A. Siegel, J.S. Welsh, Does Imaging Technology Cause Cancer? Debunking the Linear No-Threshold Model of Radiation Carcinogenesis., Technol. Cancer Res. Treat. 15 (2016) 249–256. doi:10.1177/1533034615578011.

[39] E.J. Grant, A. Brenner, H. Sugiyama, R. Sakata, A. Sadakane, M. Utada, E.K. Cahoon, C.M. Milder, M. Soda, H.M. Cullings, D.L. Preston, K. Mabuchi, K. Ozasa, Solid Cancer Incidence among the Life Span Study of Atomic Bomb Survivors: 1958-2009., Radiat. Res. 187 (2017) 513–537. doi:10.1667/RR14492.1.

[40] A. Mezentsev, S.A. Amundson, Global Gene Expression Responses to Low- or High-Dose Radiation in a Human Three-Dimensional Tissue Model, Radiat. Res. 175 (2011) 677–688. doi:10.1667/rr2483.1.

[41] M.C. Joiner, B. Marples, P. Lambin, S.C. Short, I. Turesson, Low-dose hypersensitivity: current status and possible mechanisms, Int. J. Radiat. Oncol. 49 (2001) 379–389. doi:10.1016/S0360-3016(00)01471-1.

[42] H. Matsumoto, A. Takahashi, T. Ohnishi, Radiation-induced adaptive responses and bystander effects., Biol. Sci. Sp. = Uchū Seibutsu Kagaku.

(2004). doi:10.2187/bss.18.247.

[43] M. Kadhim, S. Salomaa, E. Wright, G. Hildebrandt, O. V Belyakov, K.M. Prise, M.P. Little, Non-targeted effects of ionising radiation--implications for low dose risk, Mutat. Res. 752 (2013) 84–98. doi:10.1016/j.mrrev.2012.12.001.

[44] J.J. Burtt, P.A. Thompson, R.M. Lafrenie, Non-targeted effects and radiation-induced carcinogenesis: a review., J. Radiol. Prot. 36 (2016) R23-35. doi:10.1088/0952-4746/36/1/R23.

[45] Unscear, Non-targeted and delayed effects of exposure to ionizing radiation, UNSCEAR 2006 Report, Vol. II. (2006) Annex C.

[46] R.E.J. Mitchel, Low doses of radiation are protective in vitro and in vivo: evolutionary origins., Dose. Response. 4 (2006) 75–90. doi:10.2203/dose-response.04-002.Mitchel.

[47] R.E.J. Mitchel, D.P. Morrison, An Oxygen Effect for Gamma-Radiation Induction of Radiation Resistance in Yeast, Radiat. Res. 100 (1984) 205–210. http://www.jstor.org/stable/3576534.

[48] G. Olivieri, J. Bodycote, S. Wolff, Adaptive response of human lymphocytes to low concentrations of radioactive thymidine, Science (594-597). (1984). doi:10.1126/science.6695170.

[49] S. Tapio, V. Jacob, Radioadaptive response revisited, Radiat. Environ. Biophys. (2007). doi:10.1007/s00411-006-0078-8.

[50] S. Shelke, B. Das, Dose response and adaptive response of non-homologous end joining repair genes and proteins in resting human peripheral blood mononuclear cells exposed to γ radiation, Mutagenesis. (2015). doi:10.1093/mutage/geu081.

[51]   M. Nenoi, B. Wang, G. Vares, In vivo radioadaptive response: a review of studies relevant to radiation-induced cancer risk, Hum. Exp. Toxicol. 34 (2015) 272–283. doi:10.1177/0960327114537537.

[52]   S. Nishad, A. Ghosh, Comparative proteomic analysis of human peripheral blood mononuclear cells indicates adaptive response to low-dose radiation in individuals from high background radiation areas of Kerala, Mutagenesis. (2018). doi:10.1093/mutage/gey036.

[53]   J.D. Shadley, V. Afzal, S. Wolff, Characterization of the Adaptive Response to Ionizing Radiation Induced by Low Doses of X Rays to Human Lymphocytes, Radiat. Res. (1987). doi:10.2307/3576936.

[54]   Z.Q. Wang, S. Saigusa, M.S. Sasaki, Adaptive response to chromosome damage in cultured human lymphocytes primed with low doses of X-rays, Mutat. Res. - Fundam. Mol. Mech. Mutagen. (1991). doi:10.1016/0027-5107(91)90120-D.

[55]   J. Hain, R. Jaussi, W. Burkart, Lack of adaptive response to low doses of ionizing radiation in human lymphocytes from five different donors, Mutat. Res. Lett. 283 (1992) 137–144. doi:10.1016/0165-7992(92)90146-9.

[56]   S.M.J. Mortazavi, T. Ikushima, H. Mozdarani, Variability of chromosomal radioadaptive response in human lymphocytes, Iran J Radiat Res. 1 (2003).

[57]   G. Joksić, S. Petrović, Lack of adaptive response of human lymphocytes exposed in vivo to low doses of ionizing radiation, J. Environ. Pathol. Toxicol. Oncol. (2004). doi:10.1615/JEnvPathToxOncol.v23.i3.30.

[58]   A. Bosi, G. Olivieri, Variability of the adaptive response to ionizing radiations in humans, Mutat. Res. - Fundam. Mol. Mech. Mutagen. (1989). doi:10.1016/0027-5107(89)90102-4.

[59] A. Sannino, O. Zeni, M. Sarti, S. Romeo, S. B Reddy, M. Belisario, T. Prihoda, , Vijayalaxmi, M.R. Scarfi, Induction of adaptive response in human blood lymphocytes exposed to 900 MHz radiofrequency fields: Influence of cell cycle, Int. J. Radiat. Biol. 87 (2011) 993–999. doi:10.3109/09553002.2011.574779.

[60] L. Cai, S.Z. Liu, Induction of cytogenetic adaptive response of somatic and germ cells in vivo and in vitro by low-dose x-irradiation, Int. J. Radiat. Biol. 58 (1990) 187–194. doi:10.1080/09553009014551541.

[61] N. Gajendiran, K. Tanaka, T.S. Kumaravel, N. Kamada, Neutron-induced Adaptive Response Studied in Go Human Lymphocytes Using the Comet Assay, J. Radiat. Res. 42 (2001) 91–101. doi:10.1269/jrr.42.91.

[62] V. Jain, D. Saini, P.R.V. Kumar, G. Jaikrishan, B. Das, Efficient repair of DNA double strand breaks in individuals from high level natural radiation areas of Kerala coast, south-west India., Mutat. Res. 806 (2017) 39–50. doi:10.1016/j.mrfmmm.2017.09.003.

[63] J.F. Barquinero, L. Barrios, M.R. Caballín, R. Miró, M. Ribas, A. Subias, J. Egozcue, Occupational exposure to radiation induces an adaptive response in human lymphocytes, Int. J. Radiat. Biol. (1995). doi:10.1080/09553009514550231.

[64] H. Thierens, A. Vral, M. Barbé, M. Meijlaers, A. Baeyens, L. De Ridder, Chromosomal radiosensitivity study of temporary nuclear workers and the support of the adaptive response induced by occupational exposure, Int. J. Radiat. Biol. (2002). doi:10.1080/0955300021000034710.

[65] H. Gourabi, H. Mozdarani, A cytokinesis-blocked micronucleus study of the radioadaptive response of lymphocytes of individuals occupationally exposed

to chronic doses of radiation, Mutagenesis. 13 (1998) 475–480. doi:10.1093/mutage/13.5.475.

[66] P.R.V. Kumar, M. Seshadri, G. Jaikrishan, B. Das, Effect of chronic low dose natural radiation in human peripheral blood mononuclear cells: Evaluation of DNA damage and repair using the alkaline comet assay., Mutat. Res. 775 (2015) 59–65. doi:10.1016/j.mrfmmm.2015.03.011.

[67] E.N. Ramachandran, C. V. Karuppasamy, V.A. Kumar, D.C. Soren, P.R.V. Kumar, P.K.M. Koya, G. Jaikrishan, B. Das, Radio-adaptive response in peripheral blood lymphocytes of individuals residing in high-level natural radiation areas of Kerala in the southwest coast of India, Mutagenesis. 32 (2017) 267–273. doi:10.1093/mutage/gew057.

[68] M. Ghiassi-Nejad, S.M.J. Mortazavi, J.R. Cameron, A. Niroomand-Rad, P.A. Karam, Very high background radiation areas of Ramsar, Iran: Preliminary biological studies, Health Phys. (2002). doi:10.1097/00004032-200201000-00011.

[69] S. Mohammadi, M. taghavi dehaghani, M.R. Gharaati, R. masoomi jahandizi, M. Ghiassi-Nejad, Adaptive Response of Blood Lymphocytes of Inhabitants Residing in High Background Radiation Areas of Ramsar- Micronuclei, Apoptosis and Comet Assays, J. Radiat. Res. 47 (2006) 279–285. doi:10.1269/jrr.0575.

[70] L. Padovani, M. Appolloni, P. Anzidei, B. Tedeschi, D. Caporossi, P. Vernole, F. Mauro, Do human lymphocytes exposed to the fallout of the Chernobyl accident exhibit an adaptive response? 1. Challenge with ionizing radiation, Mutat. Res. Mol. Mech. Mutagen. 332 (1995) 33–38. doi:https://doi.org/10.1016/0027-5107(95)00120-5.

[71] S.G. Sawant, G. Randers-Pehrson, N.F. Metting, E.J. Hall, Adaptive response and the bystander effect induced by radiation in C3H 10T(1/2) cells in culture., Radiat. Res. 156 (2001) 177–180.

[72] A. Sannino, O. Zeni, S. Romeo, R. Massa, G. Gialanella, G. Grossi, L. Manti, Vijayalaxmi, M.R. Scarfì, Adaptive response in human blood lymphocytes exposed to non-ionizing radiofrequency fields: resistance to ionizing radiation-induced damage., J. Radiat. Res. 55 (2014) 210–217. doi:10.1093/jrr/rrt106.

[73] B. Jiang, J. Nie, Z. Zhou, J. Zhang, J. Tong, Y. Cao, Adaptive response in mice exposed to 900 MHz radiofrequency fields: primary DNA damage., PLoS One. 7 (2012) e32040. doi:10.1371/journal.pone.0032040.

[74] S. Wolff, V. Afzal, J.K. Wiencke, G. Olivieri, A. Michaeli, Human lymphocytes exposed to low doses of ionizing radiations become refractory to high doses of radiation as well as to chemical mutagens that induce double-Strand breaks in DNA, Int. J. Radiat. Biol. (1988). doi:10.1080/09553008814550401.

[75] Vijayalaxmi, W. Burkart, Effect of 3-aminobenzamide on chromosome damage in human blood lymphocytes adapted to bleomycin, Mutagenesis. 4 (1989) 187–189. doi:10.1093/mutage/4.3.187.

[76] I. Domínguez, N. Panneerselvam, P. Escalza, A. Natarajan, F. Cortés, Adaptive response to radiation damage in human lymphocytes conditioned with hydrogen peroxide as measured by the cytokinesis-block micronucleus technique, Mutat. Res. 301 (1993) 135–141. doi:10.1016/0165-7992(93)90036-U.

[77] F. Cortés, I. Domínguez, M.J. Flores, J. Piñero, J.C. Mateos, Differences in the

adaptive response to radiation damage in G0 human lymphocytes conditioned with hydrogen peroxide or low-dose X-rays, Mutat. Res. 311 (1994) 157—163. doi:10.1016/0027-5107(94)90084-1.

[78]   J.D. Shadley, J.K. Wiencke, Induction of the Adaptive Response by X-rays is Dependent on Radiation Intensity, Int. J. Radiat. Biol. 56 (1989) 107–118. doi:10.1080/09553008914551231.

[79]   M.S. Sasaki, On the Reaction Kinetics of the Radioadaptive Response in Cultured Mouse Cells, Int. J. Radiat. Biol. 68 (1995) 281–291. doi:10.1080/09553009514551211.

[80]   H. Yu, N. Liu, H. Wang, Q. Shang, P. Jiang, Y. Zhang, Different responses of tumor and normal cells to low-dose radiation, Contemp. Oncol. (Poznań, Poland). 17 (2013) 356–362. doi:10.5114/wo.2013.35289.

[81]   J.H. Youngblom, J.K. Wiencke, S. Wolff, Inhibition of the adaptive response of human lymphocytes to very low doses of ionizing radiation by the protein synthesis inhibitor cycloheximide, Mutat. Res. 227 (1989) 257–261.

[82]   L.E. Feinendegen, V.P. Bond, C.A. Sondhaus, H. Muehlensiepen, Radiation effects induced by low doses in complex tissue and their relation to cellular adaptive responses, Mutat. Res. Mol. Mech. Mutagen. 358 (1996) 199–205. doi:https://doi.org/10.1016/S0027-5107(96)00121-2.

[83]   L. De Saint-Georges, Low-dose ionizing radiation exposure: understanding the risk for cellular transformation., J. Biol. Regul. Homeost. Agents. 18 (2004) 96–100.

[84]   E.I. Azzam, J.P. Jay-Gerin, D. Pain, Ionizing radiation-induced metabolic oxidative stress and prolonged cell injury, Cancer Lett. 327 (2012) 48–60. doi:10.1016/j.canlet.2011.12.012.

[85]   N. Chen, L. Wu, H. Yuan, J. Wang, ROS/autophagy/Nrf2 pathway mediated low-dose radiation induced radio-resistance in human lung adenocarcinoma A549 cell, Int. J. Biol. Sci. 11 (2015) 833–844. doi:10.7150/ijbs.10564.

[86]   J.K. Wiencke, V. Afzal, G. Olivieri, S. Wolff, Evidence that the [H]thymidine-induced adaptive response of human lymphocytes to subsequent doses of x-rays involves the induction of a chromosomal repair mechanism, Mutagenesis. (1986). doi:10.1093/mutage/1.5.375.

[87]   E.G. Dimova, P.E. Bryant, S.G. Chankova, "Adaptive response" - Some underlying mechanism and open questions, Genet. Mol. Biol. (2008). doi:10.1590/S1415-47572008000300002.

[88]   M.R. Wilkins, J.-C. Sanchez, A.A. Gooley, R.D. Appel, I. Humphery-Smith, D.F. Hochstrasser, K.L. Williams, Progress with Proteome Projects: Why all Proteins Expressed by a Genome Should be Identified and How To Do It, Biotechnol.   Genet.   Eng.   Rev.   13   (1996)   19–50. doi:10.1080/02648725.1996.10647923.

[89]   G. Duan, D. Walther, The Roles of Post-translational Modifications in the Context of Protein Interaction Networks, PLoS Comput. Biol. (2015). doi:10.1371/journal.pcbi.1004049.

[90]   M. Pertea, A. Shumate, G. Pertea, A. Varabyou, Y. Chang, A.K. Madugundu, A. Pandey, S. Salzberg, Thousands of large-scale RNA sequencing experiments yield a comprehensive new human gene list and reveal extensive transcriptional noise, BioRxiv. (2018). doi:10.1101/332825.

[91]   M.R. Wilkins, E. Gasteiger, A.A. Gooley, B.R. Herbert, M.P. Molloy, P.A. Binz, K. Ou, J.C. Sanchez, A. Bairoch, K.L. Williams, D.F. Hochstrasser, High-throughput mass spectrometric discovery of protein post-translational

modifications., J. Mol. Biol. 289 (1999) 645–657. doi:10.1006/jmbi.1999.2794.

[92] J. Godovac-Zimmermann, L.R. Brown, Perspectives for mass spectrometry and functional proteomics, Mass Spectrom. Rev. 20 (2001) 1–57. doi:10.1002/1098-2787(2001)20:1<1::AID-MAS1001>3.0.CO;2-J.

[93] G. Baggerman, E. Vierstraete, A. De Loof, L. Schoofs, Gel-based versus gel-free proteomics: a review., Comb. Chem. High Throughput Screen. 8 (2005) 669–677. doi:10.2174/138620705774962490.

[94] T. Rabilloud, C. Lelong, Two-dimensional gel electrophoresis in proteomics: A tutorial, J. Proteomics. (2011). doi:10.1016/j.jprot.2011.05.040.

[95] D. Paul, A. Kumar, A. Gajbhiye, M.K. Santra, R. Srikanth, Mass spectrometry-based proteomics in molecular diagnostics: Discovery of cancer biomarkers using tissue culture, in: Omi. Clin. Pract. Genomics, Pharmacogenomics, Proteomics, Transcr. Clin. Res., 2014. doi:10.1201/b17137.

[96] I. Miller, Application of 2D DIGE in animal proteomics., Methods Mol. Biol. 854 (2012) 373–396. doi:10.1007/978-1-61779-573-2_26.

[97] M. Mann, Functional and quantitative proteomics using SILAC., Nat. Rev. Mol. Cell Biol. 7 (2006) 952–958. doi:10.1038/nrm2067.

[98] O. Chahrour, D. Cobice, J. Malone, Stable isotope labelling methods in mass spectrometry-based quantitative proteomics., J. Pharm. Biomed. Anal. 113 (2015) 2–20. doi:10.1016/j.jpba.2015.04.013.

[99] W.A. Tao, R. Aebersold, Advances in quantitative proteomics via stable isotope tagging and mass spectrometry., Curr. Opin. Biotechnol. 14 (2003) 110–118. doi:10.1016/s0958-1669(02)00018-6.

[100] T.J. Griffin, H. Xie, S. Bandhakavi, J. Popko, A. Mohan, J. V Carlis, L.

Higgins, iTRAQ reagent-based quantitative proteomic analysis on a linear ion trap mass spectrometer., J. Proteome Res. 6 (2007) 4200–4209. doi:10.1021/pr070291b.

[101] V.C. Wasinger, M. Zeng, Y. Yau, Current Status and Advances in Quantitative Proteomic Mass Spectrometry, Int. J. Proteomics. (2013). doi:10.1155/2013/180605.

[102] W. Zhu, J.W. Smith, C.-M. Huang, Mass spectrometry-based label-free quantitative proteomics., J. Biomed. Biotechnol. 2010 (2010) 840518. doi:10.1155/2010/840518.

[103] N.P. Singh, M.T. McCoy, R.R. Tice, E.L. Schneider, A simple technique for quantitation of low levels of DNA damage in individual cells, Exp. Cell Res. 175 (1988) 184–191. doi:https://doi.org/10.1016/0014-4827(88)90265-0.

[104] R.C. Chaubey, H.N. Bhilwade, R. Rajagopalan, S. V Bannur, Gamma ray induced DNA damage in human and mouse leucocytes measured by SCGE-Pro: a software developed for automated image analysis and data processing for Comet assay., Mutat. Res. 490 (2001) 187–197. doi:10.1016/s1383-5718(00)00166-2.

[105] S. Nishad, A. Ghosh, Dynamic changes in the proteome of human peripheral blood mononuclear cells with low dose ionizing radiation, Mutat. Res. - Genet. Toxicol. Environ. Mutagen. (2016). doi:10.1016/j.mrgentox.2016.01.001.

[106] I. Rahman, A. Kode, S.K. Biswas, Assay for quantitative determination of glutathione and glutathione disulfide levels using enzymatic recycling method, Nat. Protoc. 1 (2007) 3159–3165. doi:10.1038/nprot.2006.378.

[107] S. Nishad, A. Ghosh, Gene expression of immediate early genes of AP-1 transcription factor in human peripheral blood mononuclear cells in response to

ionizing radiation, Radiat. Environ. Biophys. 55 (2016) 431–440. doi:10.1007/s00411-016-0662-5.

[108] S.M. Toprani, B. Das, Radio-adaptive response of base excision repair genes and proteins in human peripheral blood mononuclear cells exposed to gamma radiation, Mutagenesis. (2015). doi:10.1093/mutage/gev032.

[109] S.A. Bustin, V. Benes, J.A. Garson, J. Hellemans, J. Huggett, M. Kubista, R. Mueller, T. Nolan, M.W. Pfaffl, G.L. Shipley, J. Vandesompele, C.T. Wittwer, The MIQE Guidelines: Minimum Information for Publication of Quantitative Real-Time PCR Experiments, Clin. Chem. 55 (2009) 611–622. doi:10.1373/clinchem.2008.112797.

[110] M.J. Morgan, Z. Liu, Crosstalk of reactive oxygen species and NF-κB signaling, Cell Res. 21 (2011) 103–115. doi:10.1038/cr.2010.178.

[111] A. Munshi, R. Ramesh, Mitogen-Activated Protein Kinases and Their Role in Radiation Response, 73104 (n.d.) 401–408. doi:10.1177/1947601913485414.

[112] UNSCEAR (1994) Report to the General Assembly. Annex B: Adaptive responses to radiation in cells and organisms. United Nations, New York.

[113] N. Assadi, E. Zabihi, M. Khosravifarsani, S. Khafri, H. Akhavanniaki, M. Amiri, A. Shabestani-Monfared, Radioadaptive response in human lymphocyte cells., Int. J. Mol. Cell. Med. (2014).

[114] L. Cai, S.-Z. Liu, Induction of Cytogenetic Adaptive Response of Somatic and Germ Cells in Vivo and in Vitro by Low-dose X-irradiation, Int. J. Radiat. Biol. 58 (1990) 187–194. doi:10.1080/09553009014551541.

[115] Z. Farooqi, P.C. Kesavan, Low-dose radiation-induced adaptive response in bone marrow cells of mice., Mutat. Res. 302 (1993) 83–89. doi:10.1016/0165-7992(93)90008-j.

[116] E.I. Azzam, S.M. de Toledo, R.E.J. Mitchel, G.P. Raaphorst, Radiation-induced radioresistance in a normal human skin fibroblast cell line, 1992.

[117] J. Hou, F. Wang, P. Kong, P.K.N. Yu, H. Wang, W. Han, Gene profiling characteristics of radioadaptive response in AG01522 normal human fibroblasts, PLoS One. 10 (2015) 1–25. doi:10.1371/journal.pone.0123316.

[118] T. Nikolova, F. Marini, B. Kaina, Genotoxicity testing: Comparison of the γH2AX focus assay with the alkaline and neutral comet assays, Mutat. Res. - Genet. Toxicol. Environ. Mutagen. 822 (2017) 10–18. doi:10.1016/j.mrgentox.2017.07.004.

[119] T.S. Kumaravel, A.N. Jha, Reliable Comet assay measurements for detecting DNA damage induced by ionising radiation and chemicals, Mutat. Res. - Genet. Toxicol. Environ. Mutagen. 605 (2006) 7–16. doi:10.1016/j.mrgentox.2006.03.002.

[120] Q. Hu, R.P. Hill, Radiosensitivity, Apoptosis and Repair of DNA Double-Strand Breaks in Radiation-Sensitive Chinese Hamster Ovary Cell Mutants Treated at Different Dose Rates, Radiat. Res. (1996). doi:10.2307/3579379.

[121] F. Galardi, C. Oakman, M.C. Truglia, S. Cappadona, A. Biggeri, L. Grisotto, L. Giovannelli, S. Bessi, A. Giannini, L. Biganzoli, L. Santarpia, A. Di Leo, Inter- and intra-tumoral heterogeneity in DNA damage evaluated by comet assay in early breast cancer patients, The Breast. 21 (2012) 336–342. doi:https://doi.org/10.1016/j.breast.2012.02.007.

[122] H. Kim, Q. Lin, Z. Yun, The hypoxic tumor microenvironment in vivo selects tumor cells with increased survival against genotoxic stresses, Cancer Lett. 431 (2018) 142–149. doi:https://doi.org/10.1016/j.canlet.2018.05.047.

[123] G.A. Haines, J.H. Hendry, C.P. Daniel, I.D. Morris, Germ Cell and Dose-

Dependent DNA Damage Measured by the Comet Assay in Murine Spermatozoaa after Testicular X-Irradiation1, Biol. Reprod. (2002). doi:10.1095/biolreprod.102.004382.

[124] A. Allione, B. Pardini, C. Viberti, M. Oderda, M. Allasia, P. Gontero, P. Vineis, C. Sacerdote, G. Matullo, The prognostic value of basal DNA damage level in peripheral blood lymphocytes of patients affected by bladder cancer, Urol. Oncol. Semin. Orig. Investig. 36 (2018) 241.e15-241.e23. doi:https://doi.org/10.1016/j.urolonc.2018.01.006.

[125] N.P. Singh, Microgels for estimation of DNA strand breaks, DNA protein crosslinks and apoptosis, Mutat. Res. - Fundam. Mol. Mech. Mutagen. (2000). doi:10.1016/S0027-5107(00)00075-0.

[126] X. Pu, Z. Wang, J.E. Klaunig, Alkaline comet assay for assessing DNA damage in individual cells, Curr. Protoc. Toxicol. (2015). doi:10.1002/0471140856.tx0312s65.

[127] J.D. Shadley, S. Wolff, Very low doses of x-rays can cause human lymphocytes to become less susceptible to ionizing radiation, Mutagenesis. (1987). doi:10.1093/mutage/2.2.95.

[128] B.E. Leonard, Adaptive response: Part II. Further modeling for dose rate and time influences, Int. J. Radiat. Biol. (2007). doi:10.1080/09553000701326995.

[129] G. Olivieri, A. Bosi, Possible causes of variability of the adaptive response in human lymphocytes, Mutat. Res. Mutagen. Relat. Subj. (1990). doi:10.1016/0165-1161(90)90109-2.

[130] J.D. Shadley, Chromosomal Adaptive Response in Human Lymphocytes, Radiat. Res. (1994). doi:10.2307/3578750.

[131] Vijayalaxmi, B.Z. Leal, T.S. Deahl, M.L. Meltz, Variability in adaptive

response to low dose radiation in human blood lymphocytes: consistent results from chromosome aberrations and micronuclei, Mutat. Res. Lett. (1995). doi:10.1016/0165-7992(95)90020-9.

[132] K.J. Sorensen, C.M. Attix, A.T. Christian, A.J. Wyrobek, J.D. Tucker, Adaptive response induction and variation in human lymphoblastoid cell lines, Mutat. Res. - Genet. Toxicol. Environ. Mutagen. (2002). doi:10.1016/S1383-5718(02)00110-9.

[133] K. Schlade-Bartusiak, A. Stembalska-Kozlowska, M. Bernady, M. Kudyba, M. Sasiadek, Analysis of adaptive response to bleomycin and mitomycin C, Mutat. Res. - Genet. Toxicol. Environ. Mutagen. (2001). doi:10.1016/S1383-5718(01)00288-1.

[134] I. Kalina, G. Némethová, Variability of the adaptive response to low dose radiation in peripheral blood lymphocytes of twins and unrelated donors, Folia Biol. (Praha). (1997).

[135] J.D. Shadley, G. Dai, Cytogenetic and survival adaptive responses in G1 phase human lymphocytes, Mutat. Res. - Fundam. Mol. Mech. Mutagen. (1992). doi:10.1016/0027-5107(92)90056-8.

[136] J.E. Moquet, J.S. Prosser, A.A. Edwards, D.C. Lloyd, Sister-chromatid exchanges induced by mitomycin C after acute or chronic exposure of human lymphocytes to a low dose of X-rays, Mutat. Res. Lett. (1989). doi:10.1016/0165-7992(89)90098-5.

[137] H. Tuschl, H. Altmann, R. Kovac, A. Topaloglou, D. Egg, R. Gunther, Effects of low-dose radiation on repair processes in human lymphocytes., Radiat. Res. 81 (1980) 1–9.

[138] B.J.S. Sanderson, A.A. Morley, Exposure of human lymphocytes to ionizing

radiation reduces mutagenesis by subsequent ionizing radiation, Mutat. Res. Mutagen. Relat. Subj. 164 (1986) 347–351. doi:10.1016/0165-1161(86)90027-0.

[139] S. Shelke, B. Das, Dose response and adaptive response of non-homologous end joining repair genes and proteins in resting human peripheral blood mononuclear cells exposed to ?? radiation, Mutagenesis. 30 (2015) 365–379. doi:10.1093/mutage/geu081.

[140] T. Ikushima, H. Aritomi, J. Morisita, Radioadaptive response: Efficient repair of radiation-induced DNA damage in adapted cells, Mutat. Res. - Fundam. Mol. Mech. Mutagen. 358 (1996) 193–198. doi:10.1016/S0027-5107(96)00120-0.

[141] S. Wolff, The Adaptive Response in Radiobiology: Evolving Insights and Implications, Environ. Health Perspect. (1998). doi:10.2307/3433927.

[142] M.S. Sasaki, Y. Ejima, A. Tachibana, T. Yamada, K. Ishizaki, T. Shimizu, T. Nomura, DNA damage response pathway in radioadaptive response, Mutat. Res. - Fundam. Mol. Mech. Mutagen. (2002). doi:10.1016/S0027-5107(02)00084-2.

[143] S. Wolff, Aspects of the adaptive response to very low doses of radiation and other agents, Mutat. Res. - Fundam. Mol. Mech. Mutagen. (1996). doi:10.1016/S0027-5107(96)00114-5.

[144] A. Wojcik, K. Sauer, F. Zölzer, T. Bauch, W.U. Muller, Analysis of DNA damage recovery processes in the adaptive response to ionizing radiation in human lymphocytes, Mutagenesis. (1996). doi:10.1093/mutage/11.3.291.

[145] M. Wojewodzka, M. Kruszewski, I. Szumiel, Effect of signal transduction inhibition in adapted lymphocytes: micronuclei frequency and DNA repair.,

Int. J. Radiat. Biol. 71 (1997) 245–252. doi:10.1080/095530097144111.

[146] P. Cramers, P. Atanasova, H. Vrolijk, F. Darroudi, A.A. van Zeeland, R. Huiskamp, L.H.F. Mullenders, J.C.S. Kleinjans, Pre-exposure to Low Doses: Modulation of X-Ray-Induced DNA Damage and Repair?, Radiat. Res. (2005). doi:10.1667/rr3430.1.

[147] M. Wojewódzka, I. Buraczewska, I. Szumiel, I. Grądzka, DNA double-strand break rejoining in radioadapted human lymphocytes: Evaluation by neutral comet assay and pulse-field gel electrophoresis, Nukleonika. (2006).

[148] P. Schmezer, N. Rajaee-Behbahani, A. Risch, S. Thiel, W. Rittgen, P. Drings, H. Dienemann, K.W. Kayser, V. Schulz, H. Bartsch, Rapid screening assay for mutagen sensitivity and DNA repair capacity in human peripheral blood lymphocytes, Mutagenesis. 16 (2001) 25–30. doi:10.1093/mutage/16.1.25.

[149] D.T. Saha, B.J. Davidson, A. Wang, A.J. Pollock, R.A. Orden, R. Goldman, Quantification of DNA repair capacity in whole blood of patients with head and neck cancer and healthy donors by comet assay, Mutat. Res. Toxicol. Environ. Mutagen. 650 (2008) 55–62. doi:https://doi.org/10.1016/j.mrgentox.2007.10.004.

[150] O.A. Sedelnikova, I. Horikawa, D.B. Zimonjic, N.C. Popescu, W.M. Bonner, J.C. Barrett, Senescing human cells and ageing mice accumulate DNA lesions with unrepairable double-strand breaks., Nat. Cell Biol. 6 (2004) 168–170. doi:10.1038/ncb1095.

[151] L.G. Mariotti, G. Pirovano, K.I. Savage, M. Ghita, A. Ottolenghi, K.M. Prise, G. Schettino, Use of the γ-H2AX assay to investigate DNA repair dynamics following multiple radiation exposures, PLoS One. 8 (2013) 1–12. doi:10.1371/journal.pone.0079541.

[152] E.P. Rogakou, C. Boon, C. Redon, W.M. Bonner, Megabase chromatin domains involved in DNA double-strand breaks in vivo., J. Cell Biol. 146 (1999) 905–916. doi:10.1083/jcb.146.5.905.

[153] F.A. Cucinotta, J.M. Pluth, J.A. Anderson, J. V Harper, P. O'Neill, Biochemical kinetics model of DSB repair and induction of gamma-H2AX foci by non-homologous end joining., Radiat. Res. 169 (2008) 214–222. doi:10.1667/RR1035.1.

[154] D.A. Meyers, M.; Schea, R.A.; Petrowski, A.E.; Seabury, H.; McLaughlin, P.W.; Lee, I.; Lee, S.W.; Boothman, Role of X-ray-inducible genes and proteins in adaptive survival responses, IAEA, Netherlands, 1992. https://inis.iaea.org/search/search.aspx?orig_q=RN:24053350.

[155] D.J. Grdina, J.S. Murley, R.C. Miller, H.J. Mauceri, H.G. Sutton, M.J. Thirman, J.J. Li, G.E. Woloschak, R.R. Weichselbaum, A Manganese Superoxide Dismutase (SOD2)-Mediated Adaptive Response, Radiat. Res. 179 (2013) 115–124. doi:10.1667/RR3126.2.

[156] O. Rigaud, D. Papadopoulo, E. Moustacchi, Decreased deletion mutation in radioadapted human lymphoblasts., Radiat. Res. 133 (1993) 94–101.

[157] S.S. Manesh, T. Sangsuwan, A. Wojcik, S. Haghdoost, Studies of adaptive response and mutation induction in MCF-10A cells following exposure to chronic or acute ionizing radiation, Mutat. Res. - Fundam. Mol. Mech. Mutagen. 780 (2015) 55–59. doi:10.1016/j.mrfmmm.2015.07.008.

[158] L.D. Zorova, V.A. Popkov, E.Y. Plotnikov, D.N. Silachev, I.B. Pevzner, S.S. Jankauskas, V.A. Babenko, S.D. Zorov, A. V Balakireva, M. Juhaszova, S.J. Sollott, D.B. Zorov, Mitochondrial membrane potential., Anal. Biochem. 552 (2018) 50–59. doi:10.1016/j.ab.2017.07.009.

[159] G.A. Santa-Gonzalez, A. Gomez-Molina, M. Arcos-Burgos, J.N. Meyer, M. Camargo, Distinctive adaptive response to repeated exposure to hydrogen peroxide associated with upregulation of DNA repair genes and cell cycle arrest, Redox Biol. (2016). doi:10.1016/j.redox.2016.07.004.

[160] Z. CHEN, K. SAKAI, Enhancement of Radiation-induced Apoptosis by Preirradiation with Low-dose X-rays in Human Leukemia MOLT-4 Cells, J. Radiat. Res. 45 (2004) 239–243. doi:10.1269/jrr.45.239.

[161] D. Bironaite, J.A. Westberg, L.C. Andersson, A. Venalis, A variety of mild stresses upregulate stanniocalcin-1 (STC-1) and induce mitohormesis in neural crest-derived cells, J. Neurol. Sci. 329 (2013) 38–44. doi:10.1016/j.jns.2013.03.011.

[162] S. Kondo, Altruistic cell suicide in relation to radiation hormesis, Int. J. Radiat. Biol. 53 (1988) 95–102. doi:10.1080/09553008814550461.

[163] J.F.R. Kerr, C.M. Winterford, B. V. Harmon, Apoptosis. Its significance in cancer and cancer Therapy, Cancer. (1994). doi:10.1002/1097-0142(19940415)73:8<2013::AID-CNCR2820730802>3.0.CO;2-J.

[164] B. Zhivotovsky, G. Kroemer, Apoptosis and genomic instability, Nat. Rev. Mol. Cell Biol. (2004). doi:10.1038/nrm1443.

[165] S.P. Cregan, D.L. Brown, R.E.J. Mitchel, Apoptosis and the adaptive response in human lymphocytes, Int. J. Radiat. Biol. (1999). doi:10.1080/095530099139548.

[166] D.I. Portess, G. Bauer, M.A. Hill, P. O'Neill, Low-dose irradiation of nontransformed cells stimulates the selective removal of precancerous cells via intercellular induction of apoptosis, Cancer Res. (2007). doi:10.1158/0008-5472.CAN-06-2985.

[167] S.B. Schwarz, P.M. Schaffer, U. Kulka, B. Ertl-wagner, R. Hell, M. Schaffer, The effect of radio-adaptive doses on HT29 and GM637 cells, 6 (2008) 1–6. doi:10.1186/1748-717X-3-12.

[168] R. Lall, S. Ganapathy, M. Yang, S. Xiao, T. Xu, H. Su, M. Shadfan, J.M. Asara, C.S. Ha, I. Ben-Sahra, B.D. Manning, J.B. Little, Z.M. Yuan, Low-dose radiation exposure induces a HIF-1-mediated adaptive and protective metabolic response, Cell Death Differ. (2014). doi:10.1038/cdd.2014.24.

[169] A.B. Abdelrazzak, D.L. Stevens, G. Bauer, P. O'Neill, M.A. Hill, The Role of Radiation Quality in the Stimulation of Intercellular Induction of Apoptosis in Transformed Cells at Very Low Doses, Radiat. Res. 176 (2011) 346–355. doi:10.1667/RR2509.1.

[170] Y. Ibuki, R. Goto, Adaptive response to low doses of gamma-ray in Chinese hamster cells: determined by cell survival and DNA synthesis., Biol. Pharm. Bull. 17 (1994) 1111–1113. doi:10.1248/bpb.17.1111.

[171] M. Yamaguchi, I. Kashiwakura, Role of Reactive Oxygen Species in the Radiation Response of Human Hematopoietic Stem/Progenitor Cells, PLoS One. 8 (2013) e70503. doi:10.1371/journal.pone.0070503.

[172] T. Yamamori, H. Yasui, M. Yamazumi, Y. Wada, Y. Nakamura, H. Nakamura, O. Inanami, Ionizing radiation induces mitochondrial reactive oxygen species production accompanied by upregulation of mitochondrial electron transport chain function and mitochondrial content under control of the cell cycle checkpoint, Free Radic. Biol. Med. 53 (2012) 260–270. doi:10.1016/j.freeradbiomed.2012.04.033.

[173] M. Shao, X. Lu, W. Cong, X. Xing, Y. Tan, Y. Li, X. Li, L. Jin, X. Wang, J. Dong, S. Jin, C. Zhang, L. Cai, Multiple low-dose radiation prevents type 2

diabetes-induced renal damage through attenuation of dyslipidemia and insulin resistance and subsequent renal inflammation and oxidative stress, PLoS One. (2014). doi:10.1371/journal.pone.0092574.

[174] S.N. Pramojanee, W. Pratchayasakul, N. Chattipakorn, S.C. Chattipakorn, Low-dose dental irradiation decreases oxidative stress in osteoblastic MC3T3-E1 cells without any changes in cell viability, cellular proliferation and cellular apoptosis, Arch. Oral Biol. (2012). doi:10.1016/j.archoralbio.2011.09.004.

[175] H. Matsumoto, A. Takahashi, T. Ohnishi, Nitric oxide radicals choreograph a radioadaptive response, Cancer Res. (2007). doi:10.1158/0008-5472.CAN-07-1913.

[176] T.L. Vanden Hoek, L.B. Becker, Z. Shao, C. Li, P.T. Schumacker, Reactive oxygen species released from mitochondria during brief hypoxia induce preconditioning in cardiomyocytes, J. Biol. Chem. (1998). doi:10.1074/jbc.273.29.18092.

[177] M. a Perez-Pinzon, K.R. Dave, A.P. Raval, Role of reactive oxygen species and protein kinase C in ischemic tolerance in the brain., Antioxid. Redox Signal. 7 (2005) 1150–7. doi:10.1089/ars.2005.7.1150.

[178] P.C. Tapia, Sublethal mitochondrial stress with an attendant stoichiometric augmentation of reactive oxygen species may precipitate many of the beneficial alterations in cellular physiology produced by caloric restriction, intermittent fasting, exercise and dietary p, Med. Hypotheses. 66 (2006) 832–843. doi:10.1016/j.mehy.2005.09.009.

[179] D.R. Spitz, W.C. Dewey, G.C. Li, Hydrogen peroxide or heat shock induces resistance to hydrogen peroxide in Chinese hamster fibroblasts, J. Cell. Physiol. (1987). doi:10.1002/jcp.1041310308.

[180] R.S. Patwardhan, R. Checker, D. Sharma, S.K. Sandur, K.B. Sainis, Involvement of ERK-Nrf-2 Signaling in Ionizing Radiation Induced Cell Death in Normal and Tumor Cells, PLoS One. 8 (2013) 1–12. doi:10.1371/journal.pone.0065929.

[181] R.S. Patwardhan, D. Sharma, R. Checker, M. Thoh, S.K. Sandur, Spatio-temporal changes in glutathione and thioredoxin redox couples during ionizing radiation-induced oxidative stress regulate tumor radio-resistance, Free Radic. Res. (2015). doi:10.3109/10715762.2015.1056180.

[182] K. Aquilano, S. Baldelli, M.R. Ciriolo, Glutathione: New roles in redox signalling for an old antioxidant, Front. Pharmacol. (2014). doi:10.3389/fphar.2014.00196.

[183] J.H. Limón-Pacheco, N.A. Hernández, M.L. Fanjul-Moles, M.E. Gonsebatt, Glutathione depletion activates mitogen-activated protein kinase (MAPK) pathways that display organ-specific responses and brain protection in mice, Free Radic. Biol. Med. (2007). doi:10.1016/j.freeradbiomed.2007.06.028.

[184] H.R. Lee, J.M. Cho, D.H. Shin, C.S. Yong, H.G. Choi, N. Wakabayashi, M.K. Kwak, Adaptive response to GSH depletion and resistance to L-buthionine-(S,R)-sulfoximine: Involvement of Nrf2 activation, Mol. Cell. Biochem. (2008). doi:10.1007/s11010-008-9853-y.

[185] V. Lanza, V. Pretazzoli, G. Olivieri, G. Pascarella, A. Panconesi, R. Negri, Transcriptional Response of Human Umbilical Vein Endothelial Cells to Low Doses of Ionizing Radiation, J. Radiat. Res. (2005). doi:10.1269/jrr.46.265.

[186] K. Otsuka, T. Koana, H. Tauchi, K. Sakai, Activation of Antioxidative Enzymes Induced by Low-Dose-Rate Whole-Body γ Irradiation: Adaptive Response in Terms of Initial DNA Damage, Radiat. Res. 166 (2006) 474 –

478. doi:10.1667/RR0561.1.

[187] A. Bravard, C. Luccioni, E. Moustacchi, O. Rigaud, Contribution of antioxidant enzymes to the adaptive response to ionizing radiation of human lymphoblasts, 75 (1999).

[188] G. Guo, Y. Yan-Sanders, B.D. Lyn-Cook, T. Wang, D. Tamae, J. Ogi, A. Khaletskiy, Z. Li, C. Weydert, J.A. Longmate, T.-T. Huang, D.R. Spitz, L.W. Oberley, J.J. Li, Manganese superoxide dismutase-mediated gene expression in radiation-induced adaptive responses., Mol. Cell. Biol. 23 (2003) 2362–78. doi:10.1128/MCB.23.7.2362-2378.2003.

[189] A. Eldridge, M. Fan, G. Woloschak, D.J. Grdina, B.A. Chromy, J. Jian Li, Manganese superoxide dismutase interacts with a large scale of cellular and mitochondrial proteins in low-dose radiation-induced adaptive radioprotection, Free Radic. Biol. Med. 53 (2012) 1838–1847. doi:10.1016/j.freeradbiomed.2012.08.589.

[190] B. Durović, V. Spasić-Jokić, B. Durović, Influence of occupational exposure to low-dose ionizing radiation on the plasma activity of superoxide dismutase and glutathione level, Vojnosanit. Pregl. (2008).

[191] G.L. Russo, I. Tedesco, M. Russo, A. Cioppa, M.G. Andreassi, E. Picano, Cellular adaptive response to chronic radiation exposure in interventional cardiologists, Eur. Heart J. (2012). doi:10.1093/eurheartj/ehr263.

[192] D. Kumar, S. Kumari, S.R. Salian, S. Uppangala, G. Kalthur, S. Challapalli, S.G. Chandraguthi, P. Kumar, S.K. Adiga, Genetic Instability in Lymphocytes is Associated With Blood Plasma Antioxidant Levels in Health Care Workers Occupationally Exposed to Ionizing Radiation, Int. J. Toxicol. 35 (2016) 327–335. doi:10.1177/1091581815625593.

[193] S. Alvarez, A. Boveris, Antioxidant adaptive response in human blood mononuclear cells exposed to UVB, J. Photochem. Photobiol. B Biol. (1997). doi:10.1016/S1011-1344(96)07436-2.

[194] K. Hafer, L. Rivina, R.H. Schiestl, Cell Cycle Dependence of Ionizing Radiation-Induced DNA Deletions and Antioxidant Radioprotection in Saccharomyces cerevisiae , Radiat. Res. (2010). doi:10.1667/rr1661.1.

[195] Q.A. Sun, Y. Wu, F. Zappacosta, K.T. Jeang, B.J. Lee, D.L. Hatfield, V.N. Gladyshev, Redox regulation of cell signaling by selenocysteine in mammalian thioredoxin reductases, J. Biol. Chem. 274 (1999) 24522–24530. doi:10.1074/jbc.274.35.24522.

[196] E.S.J. Arner, Focus on mammalian thioredoxin reductases--important selenoproteins with versatile functions., Biochim. Biophys. Acta. 1790 (2009) 495–526. doi:10.1016/j.bbagen.2009.01.014.

[197] S. V Kostyuk, L.N. Porokhovnik, E.S. Ershova, E.M. Malinovskaya, M.S. Konkova, L. V Kameneva, O.A. Dolgikh, V.P. Veiko, V.M. Pisarev, A. V Martynov, V.A. Sergeeva, A.A. Kaliyanov, A.D. Filev, J.M. Chudakova, M.S. Abramova, S.I. Kutsev, V.L. Izhevskaya, N.N. Veiko, Changes of KEAP1/NRF2 and IKB/NF-κB Expression Levels Induced by Cell-Free DNA in Different Cell Types, Oxid. Med. Cell. Longev. 2018 (2018) 1052413. doi:10.1155/2018/1052413.

[198] W.H. Watson, X. Yang, Y.E. Choi, D.P. Jones, J.P. Kehrer, Thioredoxin and its role in toxicology, Toxicol. Sci. 78 (2004) 3–14. doi:10.1093/toxsci/kfh050.

[199] K. Mokim Ahmed, J.J. Li, NF-κB-mediated adaptive resistance to ionizing radiation, Free Radic. Biol. Med. (2008). doi:10.1016/j.freeradbiomed.2007.09.022.

[200] K.M. Ahmed, D. Nantajit, M. Fan, J.S. Murley, D.J. Grdina, J.J. Li, Coactivation of ATM/ERK/NF-κB in the low-dose radiation-induced radioadaptive response in human skin keratinocytes, Free Radic. Biol. Med. (2009). doi:10.1016/j.freeradbiomed.2009.03.012.

[201] D.J. Grdina, J.S. Murley, R.C. Miller, G.E. Woloschak, J.J. Li, NFκB and Survivin-Mediated Radio-Adaptive Response, Radiat. Res. 183 (2015) 391–397. doi:10.1667/RR14002.1.

[202] T.W. Kensler, N. Wakabayashi, S. Biswal, Cell Survival Responses to Environmental Stresses Via the Keap1-Nrf2-ARE Pathway, Annu. Rev. Pharmacol. Toxicol. 47 (2007) 89–116. doi:10.1146/annurev.pharmtox.46.120604.141046.

[203] H. Yang, N. Magilnick, C. Lee, D. Kalmaz, X. Ou, J.Y. Chan, S.C. Lu, Nrf1 and Nrf2 regulate rat glutamate-cysteine ligase catalytic subunit transcription indirectly via NF-kappaB and AP-1., Mol. Cell. Biol. 25 (2005) 5933–5946. doi:10.1128/MCB.25.14.5933-5946.2005.

[204] G.M. Silva, C. Vogel, Quantifying gene expression: the importance of being subtle., Mol. Syst. Biol. 12 (2016) 885. doi:10.15252/msb.20167325.

[205] D. Vergara, F. Chiriacò, R. Acierno, M. Maffia, Proteomic map of peripheral blood mononuclear cells, Proteomics. (2008). doi:10.1002/pmic.200700726.

[206] A. Sriharshan, K. Boldt, H. Sarioglu, Z. Barjaktarovic, O. Azimzadeh, L. Hieber, H. Zitzelsberger, M. Ueffing, M.J. Atkinson, S. Tapio, Proteomic analysis by SILAC and 2D-DIGE reveals radiation-induced endothelial response: Four key pathways, J. Proteomics. (2012). doi:10.1016/j.jprot.2012.02.009.

[207] R. Nylund, E. Lemola, S. Hartwig, S. Lehr, A. Acheva, J. Jahns, G.

Hildebrandt, C. Lindholm, Profiling of low molecular weight proteins in plasma from locally irradiated individuals, J. Radiat. Res. 55 (2014) 674–682. doi:10.1093/jrr/rru007.

[208] T. Chaze, M.-C. Slomianny, F. Milliat, G. Tarlet, T. Lefebvre-Darroman, P. Gourmelon, E. Bey, M. Benderitter, J.-C. Michalski, O. Guipaud, Alteration of the Serum N-glycome of Mice Locally Exposed to High Doses of Ionizing Radiation, Mol. Cell. Proteomics. 12 (2013) 283–301. doi:10.1074/mcp.M111.014639.

[209] N. Uemura, Y. Nakanishi, H. Kato, S. Saito, M. Nagino, S. Hirohashi, T. Kondo, Transglutaminase 3 as a prognostic biomarker in esophageal cancer revealed by proteomics, Int. J. Cancer. 124 (2009) 2106–2115. doi:10.1002/ijc.24194.

[210] H. Ichikawa, T. Kanda, S. Kosugi, Y. Kawachi, H. Sasaki, T. Wakai, T. Kondo, Laser Microdissection and Two-Dimensional Difference Gel Electrophoresis Reveal the Role of a Novel Macrophage-Capping Protein in Lymph Node Metastasis in Gastric Cancer, J. Proteome Res. 12 (2013) 3780–3791. doi:10.1021/pr400439m.

[211] K. Kimura, H. Ojima, D. Kubota, M. Sakumoto, Y. Nakamura, T. Tomonaga, T. Kosuge, T. Kondo, Proteomic identification of the macrophage-capping protein as a protein contributing to the malignant features of hepatocellular carcinoma, J. Proteomics. 78 (2013) 362–373. doi:https://doi.org/10.1016/j.jprot.2012.10.004.

[212] K. Kikuta, N. Tochigi, T. Shimoda, H. Yabe, H. Morioka, Y. Toyama, A. Hosono, Y. Beppu, A. Kawai, S. Hirohashi, T. Kondo, Nucleophosmin as a Candidate Prognostic Biomarker of Ewing{\textquoteright}s Sarcoma

Revealed by Proteomics, Clin. Cancer Res. 15 (2009) 2885–2894. doi:10.1158/1078-0432.CCR-08-1913.

[213] M. Hauptmann, S. Haghdoost, M. Gomolka, H. Sarioglu, M. Ueffing, A. Dietz, U. Kulka, K. Unger, G. Babini, M. Harms-Ringdahl, A. Ottolenghi, S. Hornhardt, Differential Response and Priming Dose Effect on the Proteome of Human Fibroblast and Stem Cells Induced by Exposure to Low Doses of Ionizing Radiation, Radiat. Res. 185 (2016) 299–312. https://doi.org/10.1667/RR14226.1.

[214] K.N. Rithidech, X. Lai, L. Honikel, P. Reungpatthanaphong, F.A. Witzmann, Identification of proteins secreted into the medium by human lymphocytes irradiated in vitro with or without adaptive environments, Health Phys. 102 (2012) 39–53. doi:10.1097/HP.0b013e31822833af.

[215] S.W. Hyung, M.Y. Lee, J.H. Yu, B. Shin, H.J. Jung, J.M. Park, W. Han, K.M. Lee, H.G. Moon, H. Zhang, R. Aebersold, D. Hwang, S.W. Lee, M.H. Yu, D.Y. Noh, A serum protein profile predictive of the resistance to neoadjuvant chemotherapy in advanced breast cancers, Mol. Cell. Proteomics. (2011). doi:10.1074/mcp.M111.011023-1.

[216] A. Ouerhani, G. Chiappetta, O. Souiai, H. Mahjoubi, J. Vinh, Investigation of serum proteome homeostasis during radiation therapy by a quantitative proteomics approach, Biosci. Rep. (2019). doi:10.1042/bsr20182319.

[217] M.D.P. Lobo, F.B.M.B. Moreno, G.H.M.F. Souza, S.M.M.L. Verde, R. de A. Moreira, A.C. de O. Monteiro-Moreira, Label-free proteome analysis of plasma from patients with breast cancer: Stage-specific protein expression, Front. Oncol. (2017). doi:10.3389/fonc.2017.00014.

[218] H. Sun, L. Pan, H. Jia, Z. Zhang, M. Gao, M. Huang, J. Wang, Q. Sun, R. Wei,

B. Du, A. Xing, Z. Zhang, Label-free quantitative proteomics identifies novel plasma biomarkers for distinguishing pulmonary tuberculosis and latent infection, Front. Microbiol. (2018). doi:10.3389/fmicb.2018.01267.

[219] T.O. Lankisch, J. Metzger, A.A. Negm, K. Vokuhl, E. Schiffer, J. Siwy, T.J. Weismüller, A.S. Schneider, K. Thedieck, R. Baumeister, P. Zürbig, E.M. Weissinger, M.P. Manns, H. Mischak, J. Wedemeyer, Bile proteomic profiles differentiate cholangiocarcinoma from primary sclerosing cholangitis and choledocholithiasis, Hepatology. (2011). doi:10.1002/hep.24103.

[220] J. Metzger, A.A. Negm, R.R. Plentz, T.J. Weismüller, J. Wedemeyer, T.H. Karlsen, M. Dakna, W. Mullen, H. Mischak, M.P. Manns, T.O. Lankisch, Urine proteomic analysis differentiates cholangiocarcinoma from primary sclerosing cholangitis and other benign biliary disorders, Gut. (2013). doi:10.1136/gutjnl-2012-302047.

[221] X.W. Cai, K. Shedden, X. Ao, M. Davis, X.L. Fu, T.S. Lawrence, D.M. Lubman, F.M. (Spring) Kong, Plasma Proteomic Analysis May Identify New Markers for Radiation-Induced Lung Toxicity in Patients With Non-Small-Cell Lung Cancer, Int. J. Radiat. Oncol. Biol. Phys. (2010). doi:10.1016/j.ijrobp.2010.01.038.

[222] S. Raimondo, L. Saieva, M. Cristaldi, F. Monteleone, S. Fontana, R. Alessandro, Label-free quantitative proteomic profiling of colon cancer cells identifies acetyl-CoA carboxylase alpha as antitumor target of Citrus limon-derived nanovesicles, J. Proteomics. (2018). doi:10.1016/j.jprot.2017.11.017.

[223] S.B. Nukala, G. Baron, G. Aldini, M. Carini, A. D'Amato, Mass Spectrometry-based Label-free Quantitative Proteomics to Study the Effect of 3PO Drug at Cellular Level, ACS Med. Chem. Lett. (2019).

doi:10.1021/acsmedchemlett.8b00593.

[224] N.Y. Han, J.Y. Hong, J.M. Park, C. Shin, S. Lee, H. Lee, J.H. Yun, Label-free quantitative proteomic analysis of human periodontal ligament stem cells by high-resolution mass spectrometry, J. Periodontal Res. (2019). doi:10.1111/jre.12604.

[225] L. Zhang, Z. Wang, Y. Chen, C. Zhang, S. Xie, Y. Cui, Z. Wang, Label-free proteomic analysis of PBMCs reveals gender differences in response to long-term antiretroviral therapy of HIV, J. Proteomics. (2015). doi:10.1016/j.jprot.2015.05.033.

[226] U. t. a. Behrends, G. Eißner, G.W. Bornkamm, R.U. Peter, R. Hintermeier-Knabe, E. Holler, S.W. Caughman, K. Degitz, Ionizing Radiation Induces Human Intercellular Adhesion Molecule-1 In Vitro, J. Invest. Dermatol. 103 (1994) 726–730. doi:https://doi.org/10.1111/1523-1747.ep12398607.

[227] A. Turtoi, A. Srivastava, R.N. Sharan, D. Oskamp, R. Hille, F.H.A. Schneeweiss, Early response of lymphocyte proteins after gamma-radiation, in: J. Radioanal. Nucl. Chem., 2007. doi:10.1007/s10967-007-1133-x.

[228] A. Turtoi, R.N. Sharan, A. Srivastava, F.H.A. Schneeweiss, Proteomic and genomic modulations induced by γ-irradiation of human blood lymphocytes., Int. J. Radiat. Biol. 86 (2010) 888–904. doi:10.3109/09553002.2010.486016.

[229] S. Skiöld, S. Becker, U. Hellman, G. Auer, I. Näslund, M. Harms-Ringdahl, S. Haghdoost, Low doses of γ-radiation induce consistent protein expression changes in human leukocytes, Int. J. Low Radiat. (2011). doi:10.1504/IJLR.2011.047188.

[230] K.A. Neilson, N.A. Ali, S. Muralidharan, M. Mirzaei, M. Mariani, G.

Assadourian, A. Lee, S.C. van Sluyter, P.A. Haynes, Less label, more free: Approaches in label-free quantitative mass spectrometry, Proteomics. 11 (2011) 535–553. doi:10.1002/pmic.201000553.

[231] Z. Li, R.M. Adams, K. Chourey, G.B. Hurst, R.L. Hettich, C. Pan, Systematic comparison of label-free, metabolic labeling, and isobaric chemical labeling for quantitative proteomics on LTQ orbitrap velos, in: J. Proteome Res., 2012. doi:10.1021/pr200748h.

[232] J. Merl, M. Ueffing, S.M. Hauck, C. von Toerne, Direct comparison of MS-based label-free and SILAC quantitative proteome profiling strategies in primary retinal Müller cells, Proteomics. (2012). doi:10.1002/pmic.201100549.

[233] H. V. Trinh, J. Grossmann, P. Gehrig, B. Roschitzki, R. Schlapbach, U.F. Greber, S. Hemmi, iTRAQ-Based and Label-Free Proteomics Approaches for Studies of Human Adenovirus Infections, Int. J. Proteomics. (2013). doi:10.1155/2013/581862.

[234] A. Latosinska, K. Vougas, M. Makridakis, J. Klein, W. Mullen, M. Abbas, K. Stravodimos, I. Katafigiotis, A.S. Merseburger, J. Zoidakis, H. Mischak, A. Vlahou, V. Jankowski, Comparative analysis of label-free and 8-plex iTRAQ approach for quantitative tissue proteomic analysis, PLoS One. (2015). doi:10.1371/journal.pone.0137048.

[235] R. Harada, C. Vadnais, L. Sansregret, L. Leduy, G. Bérubé, F. Robert, A. Nepveu, Genome-wide location analysis and expression studies reveal a role for p110 CUX1 in the activation of DNA replication genes, Nucleic Acids Res. 36 (2007) 189–202. doi:10.1093/nar/gkm970.

[236] C. Vadnais, S. Davoudi, M. Afshin, R. Harada, R. Dudley, P.-L. Clermont, E. Drobetsky, A. Nepveu, CUX1 transcription factor is required for optimal

ATM/ATR-mediated responses to DNA damage, Nucleic Acids Res. 40 (2012) 4483–4495. doi:10.1093/nar/gks041.

[237] Z.M. Ramdzan, V. Ginjala, J.B. Pinder, D. Chung, C.M. Donovan, S. Kaur, L. Leduy, G. Dellaire, S. Ganesan, A. Nepveu, The DNA repair function of CUX1 contributes to radioresistance, Oncotarget. (2017). doi:10.18632/oncotarget.14875.

[238] Z.M. Ramdzan, C. Vadnais, R. Pal, G. Vandal, C. Cadieux, L. Leduy, S. Davoudi, L. Hulea, L. Yao, A.N. Karnezis, M. Paquet, D. Dankort, A. Nepveu, RAS Transformation Requires CUX1-Dependent Repair of Oxidative DNA Damage, PLoS Biol. (2014). doi:10.1371/journal.pbio.1001807.

[239] Z.M. Ramdzan, R. Pal, S. Kaur, L. Leduy, G. Bérubé, S. Davoudi, C. Vadnais, A. Nepveu, The function of CUX1 in oxidative DNAdamage repair is needed to prevent premature senescence of mouse embryo fibroblasts, Oncotarget. (2015). doi:10.18632/oncotarget.2919.

[240] R. Pal, Z.M. Ramdzan, S. Kaur, P.M. Duquette, R. Marcotte, L. Leduy, S. Davoudi, N. Lamarche-Vane, A. Iulianella, A. Nepveu, CUX2 protein functions as an accessory factor in the repair of oxidative DNA damage, J. Biol. Chem. (2015). doi:10.1074/jbc.M115.651042.

[241] Y. Yang, L. Queimado, MMS19 is required for NER and transcription in human cells, Cancer Res. 68 (2008) 854. http://cancerres.aacrjournals.org/content/68/9_Supplement/854.abstract.

[242] O. Stehling, A.A. Vashisht, J. Mascarenhas, Z.O. Jonsson, T. Sharma, D.J.A. Netz, A.J. Pierik, J.A. Wohlschlegel, R. Lill, MMS19 assembles iron-sulfur proteins required for DNA metabolism and genomic integrity, Science (80-.). (2012). doi:10.1126/science.1219723.

[243] K. Gari, A.M.L. Ortiz, V. Borel, H. Flynn, J.M. Skehel, S.J. Boulton, MMS19 links cytoplasmic iron-sulfur cluster assembly to DNA metabolism, Science (80-.). (2012). doi:10.1126/science.1219664.

[244] S. Ma, X. Liu, B. Jiao, Y. Yang, X. Liu, Low-dose radiation-induced responses: Focusing on epigenetic regulation, Int. J. Radiat. Biol. (2010). doi:10.3109/09553001003734592.

[245] P. Nagarajan, T.M. Onami, S. Rajagopalan, S. Kania, R. Donnell, S. Venkatachalam, Role of chromodomain helicase DNA-binding protein 2 in DNA damage response signaling and tumorigenesis, Oncogene. (2009). doi:10.1038/onc.2008.440.

[246] J. Zhou, J. Li, R.B. Serafim, S. Ketchum, C.G. Ferreira, J.C. Liu, K.A. Coe, B.D. Price, T. Yusufzai, Human CHD1 is required for early DNA-damage signaling and is uniquely regulated by its N terminus, Nucleic Acids Res. 46 (2018) 3891–3905. doi:10.1093/nar/gky128.

[247] A.K. Williamson, Z. Zhu, Z.-M. Yuan, Epigenetic mechanisms behind cellular sensitivity to DNA damage., Cell Stress. 2 (2018) 176–180. doi:10.15698/cst2018.07.145.

[248] J. Hall, P.A. Jeggo, C. West, M. Gomolka, R. Quintens, C. Badie, O. Laurent, A. Aerts, N. Anastasov, O. Azimzadeh, T. Azizova, S. Baatout, B. Baselet, M.A. Benotmane, E. Blanchardon, Y. Guéguen, S. Haghdoost, M. Harms-Ringhdahl, J. Hess, M. Kreuzer, D. Laurier, E. Macaeva, G. Manning, E. Pernot, J.L. Ravanat, L. Sabatier, K. Tack, S. Tapio, H. Zitzelsberger, E. Cardis, Ionizing radiation biomarkers in epidemiological studies – An update, Mutat. Res. - Rev. Mutat. Res. (2017). doi:10.1016/j.mrrev.2017.01.001.

[249] H.B. Forrester, I.R. Radford, Ionizing radiation-induced chromosomal

rearrangements occur in transcriptionally active regions of the genome, Int. J. Radiat. Biol. (2004). doi:10.1080/09553000400017952.

[250] C.K. Vilas, L.E. Emery, E.L. Denchi, K.M. Miller, Caught with One's Zinc Fingers in the Genome Integrity Cookie Jar., Trends Genet. 34 (2018) 313–325. doi:10.1016/j.tig.2017.12.011.

[251] Z. Goldberg, D.M. Rocke, C. Schwietert, S.R. Berglund, A. Santana, A. Jones, J. Lehmann, R. Stern, R. Lu, C.H. Siantar, Human in vivo dose-response to controlled, low-dose low linear energy transfer ionizing radiation exposure, Clin. Cancer Res. (2006). doi:10.1158/1078-0432.CCR-05-2625.

[252] L. Liu, Y. Zhang, C.C. Wong, J. Zhang, Y. Dong, X. Li, W. Kang, F.K.L. Chan, J.J.Y. Sung, J. Yu, RNF6 promotes colorectal cancer by activating the Wnt/b-catenin pathway via ubiquitination of TLE3, Cancer Res. (2018). doi:10.1158/0008-5472.CAN-17-2683.

[253] L. Liu, S. Lee, J. Zhang, S.B. Peters, J. Hannah, Y. Zhang, Y. Yin, A. Koff, L. Ma, P. Zhou, CUL4A abrogation augments DNA damage response and protection against skin carcinogenesis., Mol. Cell. 34 (2009) 451–460. doi:10.1016/j.molcel.2009.04.020.

[254] B. Zhu, Y. Zheng, A.-D. Pham, S.S. Mandal, H. Erdjument-Bromage, P. Tempst, D. Reinberg, Monoubiquitination of Human Histone H2B: The Factors Involved and Their Roles in HOX Gene Regulation, Mol. Cell. 20 (2005) 601–611. doi:https://doi.org/10.1016/j.molcel.2005.09.025.

[255] Y. Shiloh, E. Shema, L. Moyal, M. Oren, RNF20-RNF40: A ubiquitin-driven link between gene expression and the DNA damage response., FEBS Lett. 585 (2011) 2795–2802. doi:10.1016/j.febslet.2011.07.034.

[256] E. Shema, J. Kim, R.G. Roeder, M. Oren, RNF20 Inhibits TFIIS-Facilitated

Transcriptional Elongation to Suppress Pro-oncogenic Gene Expression, Mol. Cell. (2011). doi:10.1016/j.molcel.2011.03.011.

[257] T. Prenzel, Y. Begus-Nahrmann, F. Kramer, M. Hennion, C. Hsu, T. Gorsler, C. Hintermair, D. Eick, E. Kremmer, M. Simons, T. Beissbarth, S.A. Johnsen, Estrogen-dependent gene transcription in human breast cancer cells relies upon proteasome-dependent monoubiquitination of histone H2B, Cancer Res. (2011). doi:10.1158/0008-5472.CAN-11-1896.

[258] Y. Kee, T.T. Huang, Role of Deubiquitinating Enzymes in DNA Repair, Mol. Cell. Biol. (2016). doi:10.1128/mcb.00847-15.

[259] D. Zhang, K. Zaugg, T.W. Mak, S.J. Elledge, A Role for the Deubiquitinating Enzyme USP28 in Control of the DNA-Damage Response, Cell. (2006). doi:10.1016/j.cell.2006.06.039.

[260] S. V. Khoronenkova, I.I. Dianova, N. Ternette, B.M. Kessler, J.L. Parsons, G.L.D. Dianov, ATM-Dependent Downregulation of USP7/HAUSP by PPM1G Activates p53 Response to DNA Damage, Mol. Cell. (2012). doi:10.1016/j.molcel.2012.01.021.

[261] B. Zhao, C. Schlesiger, M.G. Masucci, K. Lindsten, The ubiquitin specific protease 4 (USP4) is a new player in the Wnt signalling pathway, J. Cell. Mol. Med. (2009). doi:10.1111/j.1582-4934.2008.00682.x.

[262] L. Quick, R. Young, I.C. Henrich, X. Wang, Y.W. Asmann, A.M. Oliveira, M.M. Chou, Jak1-STAT3 signals are essential effectors of the USP6/TRE17 oncogene in tumorigenesis, Cancer Res. (2016). doi:10.1158/0008-5472.CAN-15-2391.

[263] J. Cai, M.K. Culley, Y. Zhao, J. Zhao, The role of ubiquitination and deubiquitination in the regulation of cell junctions, Protein Cell. (2018).

doi:10.1007/s13238-017-0486-3.

[264] X.Y. Zhang, M. Varthi, S.M. Sykes, C. Phillips, C. Warzecha, W. Zhu, A. Wyce, A.W. Thorne, S.L. Berger, S.B. McMahon, The Putative Cancer Stem Cell Marker USP22 Is a Subunit of the Human SAGA Complex Required for Activated Transcription and Cell-Cycle Progression, Mol. Cell. (2008). doi:10.1016/j.molcel.2007.12.015.

[265] Z. Zhang, A. Jones, H.Y. Joo, D. Zhou, Y. Cao, S. Chen, H. Erdjument-Bromage, M. Renfrow, H. He, P. Tempst, T.M. Townes, K.E. Giles, L. Ma, H. Wang, USP49 deubiquitinates histone H2B and regulates cotranscriptional pre-mRNA splicing, Genes Dev. (2013). doi:10.1101/gad.211037.112.

[266] A.K. Hock, A.M. Vigneron, K.H. Vousden, Ubiquitin-specific peptidase 42 (USP42) functions to deubiquitylate histones and regulate transcriptional activity, J. Biol. Chem. (2014). doi:10.1074/jbc.M114.589267.

[267] D. Trachootham, W. Lu, M.A. Ogasawara, N.R. Del Valle, P. Huang, Redox regulation of cell survival, Antioxidants Redox Signal. (2008). doi:10.1089/ars.2007.1957.

[268] P. Dent, A. Yacoub, J. Contessa, R. Caron, G. Amorino, K. Valerie, M.P. Hagan, S. Grant, R. Schmidt-ullrich, P. Hagan, R. Caron, P. Dent, A. Yacoub, Stress and Radiation-Induced Activation of Multiple Intracellular Signaling Pathways ', 159 (2013) 283–300.

[269] P. De Lanerolle, Nuclear actin and myosins at a glance, J. Cell Sci. (2012). doi:10.1242/jcs.099754.

[270] A. Turtoi, R.N. Sharan, A. Srivastava, F.H.A. Schneeweiss, Proteomic and genomic modulations induced by γ-irradiation of human blood lymphocytes, Int. J. Radiat. Biol. (2010). doi:10.3109/09553002.2010.486016.

[271] A.K. Cheema, R.S. Varghese, O. Timofeeva, L. Zhang, A. Kirilyuk, F. Zandkarimi, P. Kaur, H.W. Ressom, M. Jung, A. Dritschilo, Functional Proteomics Analysis to Study ATM Dependent Signaling in Response to Ionizing Radiation, Radiat. Res. (2013). doi:10.1667/rr3198.1.

[272] M.S. Poruchynsky, E. Komlodi-Pasztor, S. Trostel, J. Wilkerson, M. Regairaz, Y. Pommierb, X. Zhang, T.K. Maity, R. Robey, M. Burotto, D. Sackettc, U. Guha, A.T. Fojo, Microtubule-targeting agents augment the toxicity of DNA-damaging agents by disrupting intracellular trafficking of DNA repair proteins, Proc. Natl. Acad. Sci. U. S. A. (2015). doi:10.1073/pnas.1416418112.

[273] K. Burridge, M. Chrzanowska-Wodnicka, FOCAL ADHESIONS, CONTRACTILITY, AND SIGNALING, Annu. Rev. Cell Dev. Biol. (1996). doi:10.1146/annurev.cellbio.12.1.463.

[274] J. Heino, J. Kapyla, Cellular Receptors of Extracellular Matrix Molecules, Curr. Pharm. Des. (2009). doi:10.2174/138161209787846720.

[275] C.M. Fife, J.A. McCarroll, M. Kavallaris, Movers and shakers: Cell cytoskeleton in cancer metastasis, Br. J. Pharmacol. (2014). doi:10.1111/bph.12704.

[276] C.Y. Wu, M.W. Lin, D.C. Wu, Y.B. Huang, H.T. Huang, C.L. Chen, The role of phosphoinositide-regulated actin reorganization in chemotaxis and cell migration, Br. J. Pharmacol. (2014). doi:10.1111/bph.12777.

[277] K. Valerie, A. Yacoub, M.P. Hagan, D.T. Curiel, P.B. Fisher, S. Grant, P. Dent, Radiation-induced cell signaling: Inside-out and outside-in, Mol. Cancer Ther. (2007). doi:10.1158/1535-7163.MCT-06-0596.

[278] A.L. Hein, M.M. Ouellete, Y. Yan, Radiation-induced signaling pathways that promote cancer cell survival (Review), Int. J. Oncol. (2014).

doi:10.3892/ijo.2014.2614.

[279] C.-C. Huang, J.-L. You, M.-Y. Wu, K.-S. Hsu, Rap1-induced p38 Mitogen-activated Protein Kinase Activation Facilitates AMPA Receptor Trafficking via the GDI·Rab5 Complex, J. Biol. Chem. 279 (2004) 12286–12292. doi:10.1074/JBC.M312868200.

[280] D.X. Zhang, D.D. Gutterman, Mitochondrial reactive oxygen species-mediated signaling in endothelial cells., Am. J. Physiol. Heart Circ. Physiol. 292 (2007) H2023-31. doi:10.1152/ajpheart.01283.2006.

[281] Y.J. Choi, S.Y. Kim, J.M. Oh, Y.S. Juhnn, Stimulatory heterotrimeric G protein augments gamma ray-induced apoptosis by up-regulation of Bak expression via CREB and AP-1 in H1299 human lung cancer cells, Exp. Mol. Med. (2009). doi:10.3858/emm.2009.41.8.065.

[282] E.A. Cho, E.J. Kim, S.J. Kwak, Y.S. Juhnn, CAMP signaling inhibits radiation-induced ATM phosphorylation leading to the augmentation of apoptosis in human lung cancer cells, Mol. Cancer. (2014). doi:10.1186/1476-4598-13-36.

[283] T.R. Tuttle, M.L. Mierzwa, S.I. Wells, S.R. Fox, N. Ben-Jonathan, The cyclic GMP/protein kinase G pathway as a therapeutic target in head and neck squamous cell carcinoma., Cancer Lett. 370 (2016) 279–285. doi:10.1016/j.canlet.2015.10.024.

[284] H. Kalyanaraman, G. Schwaerzer, G. Ramdani, F. Castillo, B.T. Scott, W. Dillmann, R.L. Sah, D.E. Casteel, R.B. Pilz, Protein Kinase G Activation Reverses Oxidative Stress and Restores Osteoblast Function and Bone Formation in Male Mice With Type 1 Diabetes, Diabetes. 67 (2018) 607–623. doi:10.2337/db17-0965.

[285] A.R. Kidd, J.L. Snider, T.D. Martin, S.F. Graboski, C.J. Der, A.D. Cox, Ras-Related Small GTPases RalA and RalB Regulate Cellular Survival After Ionizing Radiation, Int. J. Radiat. Oncol. 78 (2010) 205–212. doi:https://doi.org/10.1016/j.ijrobp.2010.03.023.

[286] A.L. Marat, V. Haucke, Phosphatidylinositol 3-phosphates-at the interface between cell signalling and membrane traffic., EMBO J. 35 (2016) 561–579. doi:10.15252/embj.201593564.

[287] W. Wang, J. Lv, L. Wang, X. Wang, L. Ye, The impact of heterogeneity in phosphoinositide 3-kinase pathway in human cancer and possible therapeutic treatments., Semin. Cell Dev. Biol. 64 (2017) 116–124. doi:10.1016/j.semcdb.2016.08.024.

[288] G.K. Grewal, S. Kukal, N. Kanojia, L. Saso, S. Kukreti, R. Kukreti, Effect of oxidative stress on ABC transporters: Contribution to epilepsy pharmacoresistance, Molecules. (2017). doi:10.3390/molecules22030365.

[289] G.L. Semenza, Hypoxia-inducible factors in physiology and medicine., Cell. 148 (2012) 399–408. doi:10.1016/j.cell.2012.01.021.

[290] M. Koshiji, Y. Kageyama, E.A. Pete, I. Horikawa, J.C. Barrett, L.E. Huang, HIF-1alpha induces cell cycle arrest by functionally counteracting Myc., EMBO J. 23 (2004) 1949–1956. doi:10.1038/sj.emboj.7600196.

[291] E. Metzen, J. Zhou, W. Jelkmann, J. Fandrey, B. Brüne, Nitric oxide impairs normoxic degradation of HIF-1α by inhibition of prolyl hydroxylases, Mol. Biol. Cell. (2003). doi:10.1091/mbc.E02-12-0791.

[292] R.S. BelAiba, T. Djordjevic, S. Bonello, D. Flügel, J. Hess, T. Kietzmann, A. Görlach, Redox-sensitive regulation of the HIF pathway under non-hypoxic conditions in pulmonary artery smooth muscle cells, Biol. Chem. (2004).

doi:10.1515/BC.2004.019.

[293] S. Chen, N. Sang, Hypoxia-Inducible Factor-1: A Critical Player in the Survival Strategy of Stressed Cells, J. Cell. Biochem. 117 (2016) 267–278. doi:10.1002/jcb.25283.

[294] H. Huang, D.J. Tindall, Dynamic FoxO transcription factors, J. Cell Sci. (2007). doi:10.1242/jcs.001222.

[295] S. Osuka, O. Sampetrean, T. Shimizu, I. Saga, N. Onishi, E. Sugihara, J. Okubo, S. Fujita, S. Takano, A. Matsumura, H. Saya, IGF1 receptor signaling regulates adaptive radioprotection in glioma stem cells, Stem Cells. (2013). doi:10.1002/stem.1328.

[296] Z. Baharoglu, D. Mazel, SOS, the formidable strategy of bacteria against aggressions., FEMS Microbiol. Rev. 38 (2014) 1126–1145. doi:10.1111/1574-6976.12077.

[297] A. Wahba, S.L. Lehman, P.J. Tofilon, Radiation-induced translational control of gene expression, Transl. (Austin, Tex.). 5 (2017) e1265703. doi:10.1080/21690731.2016.1265703.

[298] K. Mazan-Mamczarz, P.R. Hagner, Y. Zhang, B. Dai, E. Lehrmann, K.G. Becker, J.D. Keene, M. Gorospe, Z. Liu, R.B. Gartenhaus, ATM regulates a DNA damage response posttranscriptional RNA operon in lymphocytes., Blood. 117 (2011) 2441–2450. doi:10.1182/blood-2010-09-310987.

[299] L.-C. Wei, Y.-X. Ding, Y.-H. Liu, L. Duan, Y. Bai, M. Shi, L.-W. Chen, Low-dose radiation stimulates Wnt/beta-catenin signaling, neural stem cell proliferation and neurogenesis of the mouse hippocampus in vitro and in vivo., Curr. Alzheimer Res. 9 (2012) 278–289. doi:10.2174/156720512800107627.

[300] Y. Zhao, L. Tao, J. Yi, H. Song, L. Chen, The Role of Canonical Wnt

Signaling in Regulating Radioresistance, Cell. Physiol. Biochem. 48 (2018) 419–432. doi:10.1159/000491774.

[301] G.B. Carballo, J.R. Honorato, G.P.F. de Lopes, T.C.L. de S.E. Spohr, A highlight on Sonic hedgehog pathway, Cell Commun. Signal. 16 (2018) 11. doi:10.1186/s12964-018-0220-7.

[302] Z.-Z. Hu, H. Huang, A. Cheema, M. Jung, A. Dritschilo, C.H. Wu, Integrated Bioinformatics for Radiation-Induced Pathway Analysis from Proteomics and Microarray Data., J. Proteomics Bioinform. 1 (2008) 47–60. doi:10.4172/jpb.1000009.

[303] M. Levitus, H. Joenje, J.P. De Winter, The Fanconi anemia pathway of genomic maintenance, Cell. Oncol. (2006).

[304] G.-L. Moldovan, A.D. D'Andrea, How the Fanconi Anemia Pathway Guards the Genome, Annu. Rev. Genet. (2009). doi:10.1146/annurev-genet-102108-134222.

[305] R. Ceccaldi, P. Sarangi, A.D. D'Andrea, The Fanconi anaemia pathway: New players and new functions, Nat. Rev. Mol. Cell Biol. (2016). doi:10.1038/nrm.2016.48.

[306] R. Che, J. Zhang, M. Nepal, B. Han, P. Fei, Multifaceted Fanconi Anemia Signaling, Trends Genet. (2018). doi:10.1016/j.tig.2017.11.006.

[307] A. Datta, R.M. Brosh, Holding all the cards—how fanconi anemia proteins deal with replication stress and preserve genomic stability, Genes (Basel). (2019). doi:10.3390/genes10020170.

ANNEXURES

Annexure I: List of biological processes enriched in 100 mGy irradiated cells.

Term	Count	Genes	Benjamini-Hochberg p-value
GO:0006355~regulation of transcription, DNA-templated	242	Q5JVG2, Q9NQW5, Q9H7Z6, Q8N4W9, P49795, Q8N587, Q9GZX5, Q15072, Q5VIY5, P57740, Q9C0F0, Q96SR6, Q08AN1, Q5PRF9, Q8N823, Q99676, Q8N1G0, Q6MZP7, O95780, Q8NB50, Q5THR3, Q6PK81, Q92794, Q969W8, Q15596, Q86UP8, Q9BY31, Q96RE9, Q86V15, P37023, Q86WP2, Q7Z3V5, Q9UHJ3, O75084, Q5M9Q1, Q3MIS6, P10073, Q9ULJ3, Q2M3W8, P35711, Q14839, Q8TAQ5, Q13330, A8MW92, Q9NQV7, Q5VV52, Q96T23, Q9BXP5, Q86XU0, Q8IYI8, Q8TF39, O75582, Q96AQ7, O43345, Q9HBT8, Q06730, Q96K83, Q06732, Q04724, Q86Z02, P42166, Q9UEG4, P49750, P58317, Q14584, Q9UBK2, Q5VTR2, O95218, Q7Z340, Q9H0M5, Q76KX8, Q8IYU2, Q8IUD2, P24928, Q4G112, P15498, Q8NHY6, Q8WV37, Q9BYN7, Q5JPB2, Q8N7M2, P57071, Q9UL36, Q96NJ6, Q6PG37, Q9UQB3, O43361, P27797, Q15935, Q9UJN7, Q86W11, Q33E94, O15047, Q02386, Q08AG5, Q8WYB5, Q0VGE8, Q460N5, Q6ZN08, Q8IYF1, Q05481, Q8NEK5, P21506, O14771, O14770, Q6ZS27, Q9P0L1, P17098, Q5TYW1, P51814, Q6ZN19, Q9Y620, P51531, Q9ULV5, P51532, O14709, Q9H7S9, Q8N883, E9PAV3, Q9UJL9, Q6PD62, P06213, Q7L945, Q9BXX3, Q9UKL3, Q8N782, Q99829, Q8IYB9, Q8NCK3, Q8N9K5, A8MQ14, Q9ULU4, Q8TDD1, Q6Q0C0, Q96NI8, Q9UPS6, Q0D2J5, Q8TA94, Q96SK3, Q2KHR2, O15015, P42704, Q6ZN55, Q15910, P56270, Q9NR11, P0CG24, Q96ME7, Q8IVP9, O14647, Q9H7R0, Q15678, Q96MU6, Q9UMX1, Q9H5Q4, P62508, Q9H422, O00470, P16415, O00167, Q8WY36, Q9HCZ1, P49116, Q14966, Q9HB58, Q96N58, O15535, Q92995, Q15788, Q96NG8, Q92499, Q32MZ4, Q13029, Q8N8Z8, Q5JVS0, Q96JL9, Q16513, P08047, Q9NUA8, Q7Z7L9, P52741, O60658, Q12873, Q5HYK9, P17813, P52746, Q5T7W0, Q9Y2H8, B7Z6K7, Q7LBC6, Q14241, P18615, Q6GYQ0, Q9H582, Q03938, Q9BZ95, Q86XN6, Q8NF99, Q8TDY2, Q9UPW6, Q9BX82, Q96ST3, Q92830, Q8NA42, Q9Y2G9, Q8TAF7, P00519, P17029, Q96MR9, O95159, Q7Z401, Q8N9F8, Q8TDI0, Q9UNY4, Q13398, P17035, Q9HCL3, Q9P2J8, Q9UGU0, Q9HAH1, Q6ZNG0, Q96RS0, P17024, P17027, Q9NQZ8, Q9NSD4, P84550, Q86T29, O14978, P40879, Q8NDQ6, Q9UBE8, Q9HBZ2, Q6ZQV5, Q86Y25, Q9UJW7, Q86UE3, Q14005, Q86YE8, Q96SE7, Q6ZMV8, Q9P0U4	2.39E-07
GO:0006351~transcription, DNA-templated	295	P27540, Q8N1W2, Q5JVG2, Q8IWY8, Q9H7Z6, Q8N4W9, Q8N587, Q9Y4A8, Q9UGL1, Q9GZX5, Q5VIY5, Q92539, Q92922, Q9C0F0, Q96SR6, Q13772, Q08AN1, Q9H9Y6, Q5PRF9, Q96JB3, Q8N823, Q99676, Q8N1G0, Q9UQL6, Q6MZP7, O95780, Q71F56, Q8NB50, O00411, Q5THR3, P41229, P12755, Q6PK81, P26358, Q92794, Q969W8, Q15596, Q86UP8, Q9BY31, Q8NFD5, Q96RE9, Q15303, Q9UBW7, Q86V15, Q8NFU7, O15090, Q86WP2, Q12789, Q7Z3V5, Q9UHJ3, Q7Z4V5, Q5M9Q1, Q3MIS6, Q9ULH7, P10073, Q8TAQ2, Q9ULJ3, Q2M3W8, Q8TAQ5, Q14839, Q13330, Q6ZSB9, Q9NQV7, Q99549, Q8IYI8, Q86XU0, Q8TF39, Q96AQ7, Q6EKJ0, Q9Y2P7, Q8TBZ8, Q9HC52, O43345, P41182, Q9HBT8, Q06730, Q14192, Q96K83, Q06732, Q15424, Q04727, Q04724, Q86Z02, Q9UEG4, P49750, P58317, Q9NQB0, Q14584, Q7Z340, Q9H0M5, Q8IYU2, Q76KX8, Q9Y5B6, Q4G112, Q8NHY6, Q8WV37, O14497, Q9BYN7, Q8NB12, Q9P2R6, P57071, Q8N7M2, Q9UL36, Q96NJ6, Q6PG37, Q9UBN7, Q9UQB3, Q13948, O43361, Q15935, Q9UJN7,	9.86E-07

		Q86W11, O15047, Q08AG5, Q9Y4C1, Q8WYB5, Q0VGE8, Q460N5, O95602, Q6ZN08, Q8IYF1, O14771, P21506, Q05481, Q8NEK5, Q6ZS27, Q9P0L1, P17098, Q5TYW1, P51814, Q15047, Q6ZN19, Q9Y620, P51531, P25440, Q9ULV5, P54259, Q9UPN9, P28358, P51532, O14709, O43318, Q9H2S9, Q9H7S9, Q8N883, E9PAV3, Q9UJL9, Q6PD62, P38935, Q7L945, Q9UKL3, Q8N782, Q99829, Q8IYB9, Q8N9K5, Q8NCK3, P08572, A8MQ14, Q8TDD1, Q6Q0C0, Q96NI8, Q9UPS6, Q0D2J5, Q8N108, Q8TA94, Q96SK3, O15015, P42704, Q6ZN55, Q15910, Q9NR11, P0CG24, Q96ME7, Q8IVP9, Q9H7R0, O14647, Q8NHM5, Q15678, Q9NWH9, Q96MU6, O15409, P62508, P30876, P16415, O94972, Q00613, O00167, O94763, Q8WY36, Q9HCZ1, Q9GZS1, P49116, Q14966, Q9HB58, Q96N58, O15535, P19525, Q15788, Q96NG8, Q32MZ4, Q92499, Q13029, Q8N8Z8, Q5JVS0, Q96JL9, P48552, Q16512, O14529, Q16513, O43719, Q9NUA8, Q7Z7L9, P52741, Q12873, P54198, Q5HYK9, Q9NYF8, P52746, Q7LBC6, Q9Y2H8, Q5T7W0, Q14241, O14802, Q9P2K5, Q58F21, Q6ZMY3, Q9H582, Q86TU7, O03938, Q9BZ95, Q8NF99, Q86XN6, Q2M1K9, Q96SF7, Q8TDY2, Q9UPW6, Q9UKY1, Q9BX82, Q9H8H0, Q96ST3, Q86Y01, Q9Y2G9, Q8NA42, Q8TAF7, P17029, Q5PSV4, Q9Y6X8, Q96MR9, Q92576, Q7Z401, Q8N9F8, Q8TDI0, Q13398, P17035, Q9HCL3, Q9P2J8, Q9H0D2, Q9BTC0, O75925, Q9BUG6, A6NGD5, Q9UGU0, Q9HAH1, Q6P1N0, Q6ZNG0, Q96RS0, P17024, P17027, Q8TAW3, Q9NQZ8, Q9NSD4, P38398, P84550, Q9P1T7, Q63HK5, Q86T29, Q99592, O14978, O94929, Q8NDQ6, Q9UBE8, Q9HBZ2, Q12888, Q6ZQV5, Q9UJW7, Q5T5J6, Q86Y25, Q6IE81, Q86UE3, Q14005, Q86YE8, P0CG00, Q96SE7, Q6ZMV8, Q9P0U4	
GO:0043547~positive regulation of GTPase activity	103	Q15283, O60890, Q6P4F7, P49815, P49795, P49796, P11274, Q92538, O75140, P20936, P05556, Q6ZUT9, Q0VAM2, Q9ULL1, Q9Y5W8, Q9NXL2, Q5VWQ8, Q13459, Q15910, Q9P2F8, Q9H7D0, Q9GZM8, P01133, Q92608, Q92888, Q9C0H5, Q96PE2, Q9Y4G8, Q9NP61, Q15303, P35609, Q14644, Q13017, Q17R89, O14827, Q9BZ29, Q3KRB8, A6NI28, Q9BTW9, Q9Y3M8, P22607, Q9H2M9, A8MVX0, Q8IZD9, P07196, Q9NZM3, Q68D51, Q6DN90, Q9NVN3, Q8N1I0, Q8TER5, Q02297, O15169, Q12774, P55160, Q96HP0, P35568, Q8TCU6, O14559, Q8TDY4, P01023, Q9BYX2, Q5TH69, O94887, P15882, P22455, Q96PV0, Q9Y4F1, O94988, Q86YV0, O43147, Q7Z401, P41595, Q6XZF7, P15498, Q14C86, Q68EM7, Q96DR7, A2RUS2, Q6ZNW5, Q5TG30, Q7Z628, Q8WXG6, O76039, Q15057, A1L390, Q8IWW6, Q6ZV73, Q8WU20, Q5VZ89, P0DJJ0, Q9Y6D5, Q5JSL3, Q92854, O75044, Q92556, P10721, Q96Q42, Q5JU85, A1IGU5, Q14185, Q12979, Q6IQ26	1.54E-04
GO:0007156~homophilic cell adhesion via plasma membrane adhesion molecules	40	Q9NPG4, Q96QU1, Q9UN75, Q9Y5I4, A6H8M9, Q9Y5I3, Q9UN74, Q9Y5I2, Q9UN73, Q9Y5I1, Q9UN72, O15031, Q9Y5I0, O95206, Q9Y5G7, Q9HC56, Q9HBT6, Q8TAB3, Q8TD84, Q9Y5G0, Q9H158, P28827, Q9HCK4, Q58EX2, P05556, Q9Y6N7, Q9Y5H7, Q9Y5H6, O14917, Q9Y5H5, O60245, Q9ULL4, Q9Y5H9, Q9Y5H8, Q9Y5F1, Q9HBB8, Q9P2E7, Q86SJ2, Q6ZTQ4, O60469	5.84E-04
GO:0035023~regulation of Rho protein signal transduction	25	O94887, Q92888, Q96PE2, Q7Z628, Q12774, A8MVX0, O15013, Q9Y4F1, Q9NZM3, Q9ULL1, A1L390, Q96Q42, Q9NXL2, Q6XZF7, P11274, Q6ZV73, Q13459, Q13009, A1IGU5, Q8TCU6, P15498, Q12979, O14827, Q8TER5, Q96DR7	0.002386
GO:0030049~muscle filament sliding	16	Q08043, P07951, P60660, P13533, P12883, P35609, P13535, P09493, Q9UKX2, P06753, P08670, P68032, P67936, P68133, P11055, Q9Y623	0.002966
GO:0007155~cell adhesion	82	O60500, P20908, O00533, P17813, Q9Y5I4, Q9UN74, Q9Y5I3, Q9C0A0, Q9UN73, Q9Y5I2, Q9Y5I1, Q9UN72, O15357, P26012, P18564, Q9H158, Q99062, O43312, P78357, Q9HCK4, Q13753, O94887, Q9P232, O75325, Q9Y6N7, Q9UGN4,	0.003322

		O00622, O14917, Q86W92, Q14714, P35580, Q9Y5F1, P24821, Q99965, Q9P2E7, Q14993, O00192, P35443, Q15262, P35442, O60279, Q9BWV1, P18206, P0C091, Q9UQB3, P32942, Q14162, P48960, P35609, Q13017, P10586, P56945, P14770, P42684, Q2UY09, Q8TD84, P07942, P11047, P07996, Q9BZ76, Q9UHC6, Q13332, P16284, Q9Y5H7, P16144, Q9Y5H6, Q92854, Q14511, A6NMZ7, Q16363, O75970, Q9Y5H9, Q9Y5H8, Q9UKX5, O15394, Q9HBB8, P12109, P38570, Q92752, Q08629, O60469, Q13683	
GO:0019228~neuronal action potential	13	Q9NZV8, Q7Z406, Q14524, Q9P0X4, Q7RTX7, Q9UQD0, Q15858, Q99250, P35498, P35499, Q9Y5Y9, Q9UI33, Q9NY46	0.007578
GO:0086010~membrane depolarization during action potential	13	Q14524, Q15858, Q9NY46, Q9UI33, Q9Y5Y9, O60840, Q9P0X4, Q9UQD0, Q7RTX7, Q04917, Q99250, P35498, P35499	0.007578
GO:0030048~actin filament-based movement	10	Q9Y4I1, Q9UM54, P35580, Q13459, Q12965, Q7Z406, P68032, P11055, P35579, Q9Y623	0.009133
GO:0007160~cell-matrix adhesion	25	P02671, P02679, P25940, P18206, P05556, P02675, Q5H8C1, Q9BX67, P16144, O75334, Q6UWN5, Q9UKX5, Q92574, Q8TER0, Q13444, P26012, Q13009, P18564, P56199, Q9UQP3, P58397, A6NGW2, Q13136, Q7RTU9, Q13683	0.009641
GO:0006936~muscle contraction	27	P62736, P18206, P07951, P54296, P13533, P13535, Q14BN4, P35749, P35499, Q08043, P60660, Q9NZM1, P12883, Q14714, P12882, Q9UKX3, P09493, Q9UKX2, P06753, P56199, P32418, P67936, P68133, O75923, P63267, P23327, Q9Y623	0.020884
GO:0000042~protein targeting to Golgi	10	Q7Z3J3, A6NKT7, O14715, Q6VY07, Q99666, Q8IWJ2, P0DJD0, P0DJD1, Q15643, Q96CV9	0.03541
GO:0030036~actin cytoskeleton organization	30	Q92608, O15259, P09341, Q96PE2, O60610, O60890, Q12774, P41182, Q13643, P07737, Q6ZV73, P11274, Q86XJ1, P42684, Q76I76, Q702N8, O43312, Q9UNF0, Q9ULL8, O94929, Q01518, Q8WYL5, P00519, Q6DN90, Q9NSV4, Q92556, Q5JU85, Q9Y2I1, Q56UN5, Q12979	0.038297
GO:0050775~positive regulation of dendrite morphogenesis	9	Q14999, O76039, O75147, Q9NZN1, Q9UJX6, P23468, Q13948, O14529, Q6IMN6	0.054257
GO:0090630~activation of GTPase activity	21	Q8NDY3, Q0IIM8, Q96N67, O60447, O15013, O95759, Q9Y2I9, Q8TEA7, Q9UPU7, Q92574, O43147, Q6GYQ0, O43166, Q13009, Q5VT97, Q6ZT07, Q6ZW31, Q9GZM8, Q2NKQ1, Q5R372, Q9BYX2	0.058467
GO:0060078~regulation of postsynaptic membrane potential	10	Q14524, Q7RTX7, Q9UQD0, Q15858, Q99250, P35498, P35499, Q9Y5Y9, Q9UI33, Q9NY46	0.068519
GO:0031032~actomyosin structure organization	11	Q9HCS5, P35580, Q7Z406, Q9Y2J2, Q9C0D0, Q5VT25, Q92614, P68032, Q96QT4, Q9HCM4, P35579	0.076898
GO:0007010~cytoskeleton organization	33	Q8TDZ2, Q9NYB9, O60610, Q5HYK7, O95425, P60709, Q9Y2H9, P16157, Q9UKE5, Q9UBW7, Q9BXF3, O75147, Q6ZV73, O15195, O94851, P78357, O60437, O94929, Q7RTP6, Q12934, Q6ZMZ3, Q9NZQ3, Q14511, Q6RI45, Q6P0Q8, Q9H2C0, O95789, P09493, Q71RC2, Q14185, O75400, Q9ULQ0, Q8WWQ0	0.095669
GO:0016601~Rac protein	9	Q92556, Q9NYB9, Q96Q42, O94887, Q13009, Q9Y2I1, Q7L576, Q9Y2A7, Q8IYU2	0.099525

signal transduction			
GO:0051056~regulation of small GTPase mediated signal transduction	29	Q9C0H5, Q5TG30, Q96PE2, O60890, Q6P4F7, Q7Z628, P49815, Q13017, Q8IWW6, Q6GYQ0, P11274, Q5VT97, Q6ZW31, Q17R89, O14559, O14827, P01023, Q3KRB8, P15882, Q9Y3M8, O94988, O75044, O43166, Q13459, Q13009, P15498, Q9P2F8, Q12979, Q68EM7	0.101556

Annexure II: List of biological processes enriched in non-primed cells.

Term	Count	Genes	Benjamini-Hochberg p-value
GO:0007156~homophilic cell adhesion via plasma membrane adhesion molecules	47	Q96TA0, Q9Y5E9, P32926, Q96QU1, Q9Y5I4, Q9UN75, Q9Y5I3, Q9Y5E8, Q9Y5G6, Q9UN73, Q9Y5I1, Q9UN72, O15031, Q9Y5G8, Q9Y5I0, Q9UN71, O95206, Q9UN70, Q9Y5G7, P12830, Q8TD84, P33151, Q9Y5G0, Q9Y5G2, P28827, P22223, Q9BZA8, Q58EX2, Q86SJ6, Q9Y6N7, Q9Y5F9, Q9Y5H7, O14917, Q9Y5H5, Q9Y5H4, Q9ULL4, Q7Z5N4, Q9Y5H9, O94985, Q9Y5H8, Q9P2J2, P55290, P42338, Q9Y5H0, Q9Y5H1, Q9UPX0, O60469	9.49E-07
GO:0030705~cytoskeleton-dependent intracellular transport	12	Q9NQT8, P33176, Q15058, B7ZC32, Q96L93, Q9ULI4, Q9HD67, Q9H1H9, O60333, Q2KJY2, Q12840, O60282	8.50E-04
GO:0035556~intracellular signal transduction	77	Q8N1W1, Q96J92, P12931, Q15811, Q5VT25, Q9Y2H9, Q7Z3F1, Q01970, P10398, Q02153, Q08828, Q63HR2, Q9P107, Q8WXH5, P11274, O14511, Q8TCU6, Q92828, P16885, P53355, O95622, Q8NI35, O75912, Q9Y6J8, P51828, Q6DT37, Q9UPW8, Q9Y3S1, Q8N4C8, Q68CZ2, Q9Y6R4, O94806, P16591, O60285, Q9NY57, Q8WV28, O14795, P20594, Q6P0Q8, Q13459, Q8WXI4, Q8IVT5, Q9Y5S2, Q8IU80, Q86XP1, P10911, P49768, Q9NQ66, Q9Y4G8, O95819, P42680, Q9NRM7, Q9Y4G2, P16066, Q9NRH2, Q96PN6, O95644, P43405, Q9UKA4, O14578, Q02846, Q92619, Q9P0L2, Q8N3E9, P51812, Q9HC29, Q13972, Q16760, P10721, O15211, Q9Y2I7, Q8IVF5, Q7KZI7, Q8TDM6, O75582, Q9BYP7, Q8NEN9	0.001138
GO:0007018~microtubule-based movement	26	Q86VH2, Q9ULI4, Q2TAC6, Q12756, O75037, Q86UP2, P33176, Q15058, Q2VIQ3, Q8TEQ0, O14576, Q9NQT8, O95239, Q12840, O60282, Q96Q89, B7ZC32, Q96L93, Q9H1H9, Q8N4N8, O60333, O95782, Q2KJY2, Q7Z4S6, O14782, Q9P2E2	0.00125
GO:0007155~cell adhesion	83	P49746, P08648, Q96NU0, P20908, O00533, Q9Y5I4, Q9Y5I3, Q9C0A0, Q9Y5E8, Q9UN73, Q9Y5I1, Q9UN72, Q9UN71, Q9UN70, Q14324, P55196, P18084, P26012, O43184, P33151, Q02246, Q9UMF0, P25090, P22223, P78357, Q9Y286, P78539, Q9P232, Q15517, P43121, Q9Y6N7, P16591, O14917, O60285, Q96RT1, P78536, O94985, P35580, P24821, P55290, A4D0S4, Q99965, P20701, Q14993, O00192, Q9UKB5, O60279, P18206, P0C091, O75077, Q96QZ7, Q8NCG5, Q15124, P10586, P17301, Q8TD84, P11047, P07996, Q9BZ76, Q29322, Q9UHC6, Q9BX66, Q13332, Q9Y5H7, P16144, Q14210, A6NMZ7, Q96RL6, P55268, O75970, Q9Y5H9, Q9Y5H8, Q9UKX5, Q4KMG0, O15394, P23515, P38570, O60462, P16671, O60469, P23229, Q9P266, Q14246	0.003234

GO:0006468~protein phosphorylation	82	Q96J92, Q13237, Q9NYY8, Q14289, Q32MK0, Q5VT25, Q9Y2H9, Q96RG2, P32298, Q96PY6, P27986, P53350, Q8IWU2, P11274, Q8IZX4, Q96QP1, P53667, P53355, Q9P2K8, Q9P278, Q38SD2, O95163, Q9NRS6, Q8IWQ3, Q6DT37, Q9Y3S1, Q8NCB2, Q8N4C8, Q9BX84, O94806, Q13464, Q9Y2K2, P16591, O60285, Q76MJ5, Q05823, O94804, P20594, P19447, Q6P0Q8, O43283, Q8TD19, Q96L96, Q96C45, Q9Y5S2, Q13557, Q99570, P07332, Q13882, O14920, P21675, Q96L34, Q8TEA7, O60566, Q09013, O95819, P42680, Q9NRM7, P16066, Q9NRH2, Q8TF05, P43405, Q8WXR4, O14578, Q02846, Q6ZS72, Q9P0L2, Q13233, P51812, Q9H2X6, Q6ZMQ8, Q14149, Q9NZJ5, O95382, Q9Y2U5, P42336, O75116, Q7KZI7, O75582, Q9BYP7, Q86TB3, P46019	0.003865
GO:0007160~cell-matrix adhesion	26	P49746, P18206, O43556, Q5H8C1, O75334, P18084, P26012, P17301, A6NGW2, Q7RTU9, Q99102, P25940, O75443, P14543, P02675, Q9BX66, P16144, Q92574, Q9UKX5, Q6UWN5, Q13009, O95274, Q9UQP3, P56199, P20701, P23229	0.004487
GO:0030198~extracellular matrix organization	41	Q8IU80, P08648, P05997, P20908, P01375, P53420, Q8IZC6, P26012, P18084, P12830, P17301, Q9UMF0, P28300, P11047, P07996, Q14118, P25940, O95980, P14543, P02675, P08572, Q86TH1, P16144, P23142, P55268, Q9UKX5, Q76M96, Q04656, P24821, P35968, P38570, P56199, Q96HE7, Q9NQ38, P20701, Q86YB8, P25067, Q14993, P12107, P23229, P59510	0.02996
GO:0048010~vascular endothelial growth factor receptor signaling pathway	21	P49767, P12931, Q14289, Q13464, P60709, Q9UQB8, Q8IZP0, Q96F07, P17948, O14786, P27986, P07900, P35968, O60462, P42338, P42336, Q7L576, O75116, P63261, P35916, Q13873	0.031413
GO:0046777~protein autophosphorylation	37	P07332, Q13882, P12931, Q14289, P21675, Q15303, Q96RG2, Q8IWU2, P11274, Q9H792, P27708, Q9P2K8, P53355, P43405, P35916, P06213, P29322, P36888, Q9Y3S1, Q8N4C8, Q9H2G2, P16591, P17948, P00519, P34947, O94804, P10721, P08069, P35968, O43283, Q6PHR2, Q9NZJ5, P14616, Q7KZI7, P00533, Q9BYP7, Q13557	0.03585
GO:0006936~muscle contraction	26	P62736, P36383, Q07001, P18206, P13533, Q14324, P13535, P18084, Q14BN4, Q04844, P14649, P35749, P35499, Q9BX66, P60660, Q9NZM1, P12883, P12882, Q9UKX3, Q9UKX2, P56199, Q13884, P68133, O75923, P63267, Q9Y623	0.058885
GO:0001843~neural tube closure	21	Q9NPG1, Q9HBG6, Q92830, Q8TF72, P49815, O15031, Q96QB1, Q96Q89, Q9UG01, Q13635, P11586, Q93074, O95487, Q9P2K1, Q92574, P07737, O15550, O75128, Q96B86, Q15468, O14497	0.062386
GO:0043547~positive regulation of GTPase activity	90	Q8N1W1, P46940, Q8TEU7, Q8WZ64, P32019, Q8NF50, Q15811, P49815, P18433, Q96PX9, O60292, P55196, P49796, Q9P107, P11274, O14511, Q8TCU6, O15399, Q8TE68, Q8TDY4, Q15389, Q5TH69, Q8NE09, Q96PV0, Q96QB1, O94988, P11277, Q9P2F6, Q5VWQ8, Q7Z401, Q13459, Q15910, Q9P2N2, Q9P2F8, P56159, Q9H7D0, P01133, Q07890, P98174, Q14957, Q13557, Q92608, A2RUS2, Q96PE2, P10911, Q4ADV7, Q9NQ66, Q9UPP2, Q8WXG6, Q9H3Q1, Q9Y4G8, O14924, O76081, Q15303, Q8WWN8, Q14644, Q8TF40, Q9UJF2, Q17R89, Q7Z6I6, Q9BZ29, Q92619, A6NI28, Q76NI1, Q9H2M9, Q13972, Q96P48, Q5JSL3, Q9Y6D6, Q96P47, Q8IZD9, Q99490, Q9NZM3, A7KAX9, Q9Y4H2, P10721, Q96Q42, O15211, A1IGU5, Q8IVF5, Q5JU85, Q8N1I0, Q5T5U3, Q6IQ26, P21860, Q13224, Q86Z14, P00533, Q8N6T3, P23229	0.063289
GO:0007010~cytoskeleton organization	34	O95425, O00291, P60709, P16157, Q9Y2H9, Q8WWN8, Q9UBW7, O60292, O75147, Q5T5Y3, O14639, P13646, O15195, O94851, Q9BUF5, P78357, O60437, Q9P0L2, Q7RTP6, Q5VZL5, P19012, Q8WX93, O14939, P11277, Q6RI45, Q6P0Q8, Q8IVF7, Q14202, Q9P286, Q16880, P98174, Q8WWQ0, Q9Y5S2, Q8NEN9	0.073747
GO:0007229~integrin-mediated signaling pathway	24	P08648, P12931, O75077, P78325, Q14289, P16144, Q9UHI8, P23142, Q96RT1, P35579, P42680, Q9UKX5, O95866, P18084, P26012, O15072, O43184, P38570, P17301, Q99965, P56199, P20701, P43405, P23229	0.0911

Annexure III: List of biological processes enriched in primed cells.

Term	Count	Genes	Benjamini-Hochberg p-value
GO:0007156~homophilic cell adhesion via plasma membrane adhesion molecules	53	Q8IZU9, Q9Y5E6, Q9Y5E5, Q9Y5I3, Q9UN74, Q9Y5I2, Q9UN73, Q9UN72, O15031, Q9Y5I1, Q9Y5E7, Q9UN71, Q9UN70, Q9HC56, Q9Y5E4, P12830, Q9H159, Q9H158, Q02413, Q9UN66, Q9NRJ7, P28827, Q9BZA7, P22223, Q9BZA8, Q9Y6N7, Q9Y5F9, Q9Y5F6, P55286, Q9ULL4, Q7Z5N4, P55289, Q9Y5F0, Q9P2J2, Q9P2E7, Q9HCL0, Q08554, Q8N6Y1, Q8TD84, Q9UJ99, P07949, Q58EX2, Q86SJ6, Q9Y5H7, Q9Y5H5, Q9Y5H9, Q9Y5H8, Q9Y5H2, Q9BYE9, P42338, Q9Y5H1, Q96JP9, O75309	1.75E-07
GO:0007155~cell adhesion	104	Q9Y5E6, Q92729, Q9UN74, Q9Y5E5, Q9UN73, O60711, Q9Y5E7, Q9UN72, Q9UN71, Q9UN70, P55196, O14514, Q14896, Q9BXX0, P18564, Q9Y223, P22223, P43121, Q69YQ0, P16591, O00219, O60285, P55286, P78536, P54764, Q9P2E7, P54760, Q14993, P98172, O60486, Q15262, O60279, P18206, P0C091, Q96QZ7, P35609, Q13443, Q13017, Q14CZ8, Q9UHC6, Q13332, Q9Y5H7, P02452, P32004, P16144, O14936, P14923, P05067, A6NMZ7, Q96RL6, P55268, O75970, Q9Y5H9, Q9Y5H8, Q9UKX5, Q4KMG0, P49023, Q9HCB6, O75309, P40200, P49747, P20908, Q96NU0, Q00872, Q9Y5I3, Q9Y5I2, Q9Y5I1, Q9H158, Q99062, P78357, O94887, Q9Y6N7, P05106, P35580, P24821, Q13308, A4D0S4, Q92839, P20701, Q9HCL0, Q9BZL6, P39060, Q9Y6C2, P48960, P50895, P56945, Q8NFZ3, Q8TD84, P11047, P29320, Q14393, P07996, Q9BZ76, P29322, Q07092, P16284, Q92854, Q14511, Q16363, O43854, O15394, Q92859, P52799, P23229	1.07E-05
GO:0043547~positive regulation of GTPase activity	116	Q8N1W1, P24386, Q8NF50, Q9Y2L1, Q9NZL6, Q96PX9, O60292, P55196, P11274, O14511, O15399, Q92538, O75140, Q6P3S1, Q7LDG7, Q99569, Q96QB1, Q07889, P11277, Q9Y2K9, Q5VWQ8, Q13459, Q9UJM3, P14784, Q9P2F8, P26951, O14641, P01133, Q9H7D0, Q07890, Q8IW93, Q92608, O95248, Q9P227, Q96PE2, Q9NQ66, Q9UPP2, A6NIR3, O76081, P35609, Q13017, Q8TF40, Q13905, O60674, Q9H6A0, P07949, Q9BZ29, Q92619, Q9NYI0, O94827, A6NI28, Q9ULH1, Q15276, Q8TB24, Q9H2M9, Q96P48, Q6R6M4, Q8IZD9, Q92502, Q9Y4H2, Q96P50, Q86X27, O15211, Q6ZSZ5, Q8N1I0, P09471, P42331, P00533, O75689, Q8TEU7, Q8WZ64, Q5VW22, Q15811, P55160, Q12879, Q8TDY4, Q8NDX1, Q5TH69, O94887, A5PLK6, O75064, Q92834, Q9Y4F1, Q7Z401, Q6XZF7, Q9UEF7, Q2M1Z3, Q96QF0, A2RUS2, Q4ADV7, Q9HCE6, Q5T5C0, Q9UJF2, Q6ZRI8, O00429, Q9NRY4, Q7Z6I6, Q7Z6B7, Q5VZ89, Q9HCU5, Q9Y6D5, Q5JSL3, Q9Y6D6, Q8TDF6, Q92854, A7KAX9, P10721, Q53QZ3, Q96Q42, P47736, Q5JU85, O43295, Q5T5U3, Q14185, Q6IQ26, P23229	2.74E-04
GO:0016579~protein deubiquitination	32	C9JPN9, Q9UPT9, C9J2P7, Q70EK8, D6R901, Q96RU2, P35125, Q0WX57, D6RBQ6, Q8TBZ3, Q9P275, D6R9N7, D6RA61, D6RCP7, Q13107, Q6R6M4, P54578, D6RJB6, P51784, Q93009, Q9H9J4, O94966, Q70CQ1, A6NCW7, Q9NVE5, Q9P2H5, C9JLJ4, Q8NFA0, Q7RTZ2, A6NCW0, C9JVI0, A8MUK1	0.001318
GO:0030049~muscle filament sliding	17	Q08043, P07951, Q00872, P13533, P12883, P35609, P13535, Q14896, P09493, Q9UKX2, P06753, P68032, P67936, P68133, P11055, P45379, Q9Y623	0.006382
GO:0015074~DNA integration	10	Q9H5L6, P63135, P63136, Q9UQG0, P63133, Q6R2W3, Q9QC07, P10266, Q9P2P1, Q13129, Q9BXR3, Q9WJR5	0.026429

GO term	Count	Proteins	P-value
GO:0007416~synapse assembly	21	Q9UPX8, Q9UQ16, Q9HDB5, Q8IZU9, Q9NZU0, Q9Y5E6, Q9Y5E5, Q9Y5E7, Q9Y4F1, Q9Y5E4, Q7Z5N4, Q9Y5F0, Q9H5Y7, Q8NFZ4, P12830, Q8NFZ3, Q9Y4C0, Q9BYB0, P51674, P58401, Q9P2S2, Q9NRJ7, Q58EX2	0.028079
GO:0000042~protein targeting to Golgi	11	Q7Z3J3, A6NKT7, O14715, Q8TD16, Q6VY07, Q99666, Q8IWJ2, P0DJD0, P0DJD1, Q15643, Q96CV9	0.029804
GO:0035556~intracellular signal transduction	80	Q8N1W1, Q96J92, Q9UEW8, O60503, O60307, Q15811, Q5VT25, Q9Y2H9, Q63HR2, Q5KSL6, P11274, O14511, P25092, Q9NRJ4, P16885, O75140, P56975, Q8NI35, P51828, Q9UPW8, Q6DT37, Q8TB45, Q9Y3S1, Q68CZ2, Q9Y6R4, P16591, O60285, Q9NNX6, Q9BRC7, Q9UGJ0, Q96BR1, O14795, Q6P0Q8, Q15418, Q6XZF7, P14314, Q13459, Q9BZL6, Q9UKI8, O14641, P52824, O95747, Q9HBL0, Q86UX6, Q9Y5S2, O14544, P56715, Q9NQ66, Q15349, Q5TCQ9, P23743, Q9NRM7, P16066, Q9Y243, O60674, Q9NSY0, P31751, P43405, Q9UKA4, Q9Y575, O14578, Q92619, P51812, Q9HC29, P51813, Q9Y6D5, Q05655, P40145, Q16760, P10721, Q04759, Q9Y2I7, O15211, Q8IWV1, Q9H093, Q8TDM6, Q9H2X3, P31749, Q8NEN9, Q05513	0.02983
GO:0006511~ubiquitin-dependent protein catabolic process	44	C9JPN9, Q9UPT9, C9J2P7, Q9Y297, D6R901, O75150, Q9Y252, Q96RU2, Q9Y5A7, Q9UJX2, Q6ZT12, P35125, Q0WX57, D6RBQ6, Q9P275, P63279, D6R9N7, Q96J02, D6RA61, D6RCP7, Q05086, Q13107, Q5VTR2, Q6R6M4, P54578, P51784, D6RJB6, Q9H9J4, Q93009, Q13309, Q9NZJ0, Q13620, O94966, Q70CQ1, Q9NVE5, Q96K76, Q9P2H5, C9JLJ4, Q8NFA0, Q7RTZ2, A6NCW0, C9JVI0, O95155, A8MUK1	0.030897
GO:0007018~microtubule-based movement	24	Q9NQT8, Q86VH2, O95235, O95239, Q12756, O75037, Q92845, P63010, Q86UP2, Q2M1P5, Q02241, Q9NS87, O15066, Q96L93, O43896, Q2VIQ3, Q8TEQ0, Q9H1H9, Q5T7B8, O60333, Q8N4N8, Q96FN5, Q2KJY2, Q7Z4S6	0.055227
GO:0006338~chromatin remodeling	25	Q9ULG1, O75478, Q8NFD5, P51532, O00267, Q58F21, Q86U86, P56524, Q92922, Q9H981, Q86SE8, Q8TAQ2, Q9Y2K1, O60264, Q9NRL2, P03372, P35659, Q96T23, Q7KZ85, Q9UQL6, Q9UER7, P28370, O14497, O14646, Q9P2R6	0.058472
GO:0070588~calcium ion transmembrane transport	31	Q9UBN4, Q01814, Q8IZF0, Q9UPR5, Q9NY47, Q12879, Q7Z3S7, Q7Z4N2, P51674, Q9P0X4, Q9HBA0, P48995, Q96QT4, Q14393, Q8IVV2, O94759, Q9GZU1, Q13698, Q13563, P23634, Q9BX84, Q01668, Q8IZK6, P20020, Q16720, Q7Z443, O60840, Q9HCF6, Q6IQ26, Q08289, Q9Y5S1	0.059241
GO:0006351~transcription, DNA-templated	301	Q9ULG1, Q4FZB7, Q5T0B9, O95125, P42771, O60711, Q9UL58, Q8N184, Q8N4W9, Q9UHL9, P11142, Q9UGL1, Q9GZX5, Q06455, Q92539, Q92922, Q9C0F0, Q96SR6, Q01538, Q9H9Y6, Q9NQX1, O75362, O00213, P39880, Q9Y2K7, Q9UL68, Q8N823, Q99676, Q9Y5W3, Q9UQL6, Q5MCW4, Q96FC9, O60315, Q71F56, P55201, Q9Y4B6, Q8NB50, Q5THR3, P41229, Q8NDW4, P26358, Q15973, Q92794, Q8NFD5, Q96RE9, Q9UBW7, Q86V15, Q8NFU7, Q8N8C0, O15090, Q5T619, Q12789, A0AVK6, Q9NTW7, P26367, Q8TAQ2, Q9ULJ3, Q14839, Q9BQW3, Q9BR84, Q9NQV8, Q96QS3, Q8IYI8, Q86XU0, Q8TF39, O43593, P81133, Q8TF32, Q9Y2P7, O75155, Q8NAP8, Q8TBZ8, O75151, Q9HC52, Q96NL3, Q9HBT8, Q8IZL8, Q3B8N5, Q9HBT7, Q06730, Q9Y4E5, Q96K83, Q8N8L2, Q06732, Q04726, Q15424, Q04727, C9JSJ3, P49750, Q96QT6, Q14584, Q10571, Q6ZN06, Q6AHZ1, Q96NM4, Q9H0M5, Q8IYU2, Q9Y5B6, Q15022, P41162, O14497, Q6ZNA1, Q9P2R6, P57071, Q8N7M2, Q8NAP3, Q15937, O95402, Q9UBN7, O95201, Q15935, P68400, O15047, Q08AG5, Q4LE39, Q8WYB5, Q96LI6, Q460N5, Q6ZN08, B1APH4, Q9NRY4, Q9Y5R5, Q8N196, Q9P0L1, Q9HCU5, P51814, Q7Z3I7, P86452, O15391, Q9Y620, Q8N7K0, Q6U7Q0, Q12906, Q14995, Q9H9C1, P54259, Q9UPN9, O60290, P51532, Q9Y6Q9, O14709, Q6PD62, Q9BUJ2, Q9UJ78, P36508, P0CG31, P51826, Q9HCX3, Q99829, P06401, Q6W2J9, O75820, P08572, Q2M218, Q9BXG8, Q96BN2, Q8N108, Q8TA94, Q96GN5, O15015, Q9NRL2, O14503, P42704, Q96ME7,	0.069144

| | | P28370, Q8IX12, P61964, Q9H7R0, O14647, O14646, Q8NHM5, Q15678, Q9UPT9, Q03112, Q9NWH9, Q8WW38, Q96MU6, O15409, Q8IZC7, Q9UPP1, Q9UIF8, P10588, Q5H9I0, Q7L3S4, Q53TQ3, Q86U86, O75123, P56524, Q2VWA4, Q96KM6, P08151, Q86WZ6, Q9GZS3, Q9UIG0, Q6P9G9, Q14966, Q6N043, Q96N58, O15535, Q16665, O60260, C9JN71, Q96RL1, P51504, Q15788, Q32MZ4, Q9UN79, Q7KZ85, Q13029, O14628, Q96JL9, Q7Z5L9, A6NHJ4, Q13129, Q16512, O14529, Q9UER7, Q68EA5, O43719, Q9NUA8, Q7Z7L9, Q13127, Q6ZN30, Q8TBE0, Q13045, Q86YW9, Q12873, Q5SVQ8, Q5HYK9, Q12872, Q12772, P52746, Q7LBC6, Q12778, Q8TF63, Q86UU0, O14802, Q58F21, Q9H582, Q9Y6X2, Q9Y2X9, Q9BZ95, Q2M1K9, Q9H981, P17040, Q8TDY2, Q96ST2, A6NJL1, Q9BX82, Q6EMB2, P17028, Q9Y2G9, Q8NA42, Q8TF50, Q9Y6X8, P17032, Q92576, Q7Z401, P17031, Q9NYW8, Q8TDI0, P17035, Q9P2J8, Q9H0D2, P17030, Q9BTC0, Q9BUG6, Q96T88, Q9UGU0, Q8N988, Q9NYD6, Q6P1N0, Q6ZNG1, Q96RS0, Q9NPC7, P17017, P17025, Q8TAW3, Q96I27, P38398, Q96F45, Q92945, Q96T92, Q63HK3, P22736, Q86T29, Q96T76, O94929, Q12888, Q6ZQV5, Q86UE3, Q14005, Q03923, Q8IYN0, Q8NI08, P03372, O60765, P57682, P17010, Q6ZT77, Q9P0U4 | |
| GO:0031032~actomyosin structure organization | 12 | Q9HCS5, P35580, Q7Z406, Q5VT25, P68032, Q96QT4, P11171, Q9HCM4, Q9H329, Q9UPQ0, P35579, Q9Y5S2 | 0.082327 |

Annexure IV: List of KEGG pathways enriched in 100 mGy irradiated cells.

Term	Count	Genes	Benjamini-Hochberg p-value
hsa04512:ECM-receptor interaction	28	P35443, Q13753, P35442, P25940, P05997, P05556, P20908, P08572, P16144, A6NMZ7, Q16363, P02462, Q9UKX5, P26012, P24821, P14770, P12109, P18564, P56199, P02458, Q9UQP3, Q92752, P07942, P11047, P13942, P12107, P07996, Q13683	3.50E-06
hsa05414:Dilated cardiomyopathy	26	O60503, Q8IZS8, P07951, P60709, Q08828, Q08462, P26012, P18564, P68032, P51828, P05556, Q02641, Q01668, Q8NFM4, P16144, P40145, Q9UKX5, O60840, P02545, P09493, P56199, P06753, P10600, P63261, P67936, Q13683	1.53E-05
hsa04510:Focal adhesion	44	P35443, P35442, P05997, P18206, O60610, P20908, P60709, P35609, P02462, Q13017, P12814, P26012, P56945, P18564, P02458, P07942, P35916, P11047, P13942, O43707, P07996, Q13753, P25940, Q08043, P05556, P08572, P16144, A6NMZ7, Q16363, Q9UKX5, P08069, P24821, P12109, P56199, P15498, Q9UQP3, P42336, Q14185, Q92752, P98170, P63261, P01133, P12107, Q13683	3.62E-05
hsa05410:Hypertrophic cardiomyopathy (HCM)	21	Q8IZS8, P05556, P07951, Q02641, Q01668, P60709, P16144, Q9UGJ0, Q9UKX5, O60840, P26012, P09493, P02545, P18564, P06753, P56199, P68032, P63261, P10600, P67936, Q13683	0.001689
hsa04530:Tight junction	22	A7E2Y1, Q08043, Q9BX67, O95049, Q9Y2K3, P60709, O75970, P35609, P35579, P13535, P12882, P12814, P35580, Q9UKX3, Q9UKX2, Q7Z406, P63261, Q8NI35, O43707, P11055, P35749, Q9Y623	0.002278

hsa04810:Regulation of actin cytoskeleton	39	O95996, Q9NYB9, Q92888, P18206, O60610, Q9Y6U3, P55160, P60709, Q96F07, P35609, P12814, P26012, P07737, P56945, P18564, Q7L576, Q76I76, O43707, Q08043, Q86VI3, P05556, P22607, Q8WYL5, P22455, P16144, Q9UKX5, Q9NSV4, Q13009, Q9Y2I7, P38570, P56199, P15498, P42336, Q14185, P63261, P14616, Q9Y2A7, P01133, Q13683	0.0027
hsa04520:Adherens junction	18	O94887, Q08043, P18206, Q9UBE8, Q12913, Q8WWI1, P23467, P60709, P35609, P12814, O43318, P08069, P10586, P63261, P28827, P06213, O43707, Q9NQB0	0.009502
hsa05146:Amoebiasis	22	Q13753, P25940, P05997, Q08043, P18206, P20908, P08572, P35228, Q16363, P35609, Q08828, P02462, P12814, P02458, P42336, P10600, P07942, P11047, P13942, P12107, O43707, P29992	0.02629
hsa05412:Arrhythmogenic right ventricular cardiomyopathy (ARVC)	16	Q8IZS8, P05556, Q02641, Q01668, P60709, P16144, Q9UKX5, O60840, P26012, P02545, P18564, P56199, P63261, Q99959, Q13683, Q9NQB0	0.035136
hsa04974:Protein digestion and absorption	19	P25940, P05997, P08473, P20908, P08572, Q9BYF1, P15085, A6NMZ7, P20849, P02462, P46059, Q14055, P12109, P02458, P32418, P13942, P12107, P57103, Q05707	0.033051
hsa04114:Oocyte meiosis	21	Q9UJX3, P51828, Q8NE35, Q9UJX6, O60503, Q9Y297, P24864, Q9H2G2, Q8NFM4, Q08462, Q08828, P40145, P08069, Q15418, P62258, Q14674, Q13616, Q9UJ98, Q04917, Q9UQE7, P63104	0.080434
hsa04151:PI3K-Akt signaling pathway	49	P20908, P49815, P35568, P02462, P26012, P18564, P02458, P13942, Q99062, P06213, Q13753, P05556, O60346, P08572, P24864, P22455, Q92574, P08069, P24821, P56199, P62258, Q9UQP3, P01133, P35443, P35442, P05997, O14920, P38398, P07942, P35916, P11047, P07996, P63104, P25940, P22607, P16144, A6NMZ7, Q16363, Q9Y264, P10721, Q9UKX5, P12109, P42336, Q92752, Q04917, Q16512, P12107, Q16513, Q13683	0.08143
hsa05217:Basal cell carcinoma	13	O60353, Q99835, Q14332, O95996, Q9Y6F9, Q96QV1, P10071, O15169, O75084, Q9UP38, Q9UMX1, O14905, Q9NQB0	0.076463
hsa00230:Purine metabolism	29	O60658, O60503, P49915, Q5TCS8, Q08462, Q08828, P05423, P30876, O14802, Q96PN6, P25092, Q8TCS8, P28340, O14638, O95602, P51160, Q9H9Y6, Q9GZS1, P51828, P47989, P09884, Q8NFM4, P56282, P24928, P20594, P22413, P40145, Q13370, O15067	0.07507
hsa04976:Bile secretion	15	P51828, O60503, P01130, Q8NFM4, Q9NPD5, Q08462, Q08828, P40145, Q9H222, P13569, Q9BY07, O15439, P46721, O15438, O95342	0.07796
hsa00562:Inositol phosphate metabolism	15	O15327, Q8N3E9, P19174, Q8NCE2, Q9NYA4, O15357, Q5T9C9, Q9Y217, Q92835, Q9Y2I7, O00443, P42356, Q96DU7, O00750, P42336	0.094584

Annexure V: List of KEGG pathways enriched in non-primed cells.

Term	Count	Genes	Benjamini-Hochberg p-value
hsa04510:Focal adhesion	50	P08648, P49746, P12931, P20908, Q32MK0, P60709, P53420, P26012, P18084, P27986, P13942, O43707, P08572, Q13464,	2.76E-06

		P17948, P08069, P24821, P35968, A4D0S4, P56199, Q9UQP3, Q9P286, Q07890, P01133, P49767, P05997, P18206, P08581, Q8IZC6, P12814, P17301, P14210, P35916, P11047, P07996, P25940, Q8WYR1, Q13972, P16144, A6NMZ7, P55268, O14974, Q9UKX5, P42338, P42336, O75116, P63261, P12107, P23229, P00533	
hsa04512:ECM-receptor interaction	27	P49746, P05997, P08648, P20908, P53420, Q8IZC6, P18084, P26012, P17301, Q7L1I2, P13942, P11047, P07996, Q14118, P25940, P08572, P16144, A6NMZ7, P55268, Q9UKX5, P24821, A4D0S4, Q9UQP3, P56199, P16671, P12107, P23229	4.15E-05
hsa04810:Regulation of actin cytoskeleton	45	P46940, O95996, P08648, P18206, P12931, Q32MK0, P60709, Q9UQB8, Q96F07, P10398, P12814, P07737, P26012, P18084, P27986, P17301, P53667, Q7L576, O43707, Q86VI3, Q8WYR1, Q13464, P16144, P19634, O14974, P30411, Q9UKX5, Q9NSV4, Q13009, Q9Y2I7, P06396, P38570, P56199, P42338, P20701, P42336, Q9P286, O75116, P63261, P14616, P01133, Q07890, P23229, P00533, P98174	2.34E-04
hsa04015:Rap1 signaling pathway	43	Q8TEU7, P49767, P12931, Q96QZ7, P08581, Q9NQ66, P60709, P21462, Q01970, Q9Y4G8, Q8WWN8, Q08828, O60292, P55196, P07737, P27986, P12830, P14210, O95622, P35916, P06213, P07996, Q86UL8, Q15389, P51828, Q8WYR1, O94806, P17948, P10721, P08069, P35968, Q13009, O43166, Q8N1I0, P42338, P20701, P47900, P42336, Q9P2F8, P63261, P01133, Q13224, P00533	0.001008
hsa04611:Platelet activation	30	P05997, Q3MJ16, P20908, P12931, Q13237, Q9NQ66, Q32MK0, P60709, Q01970, Q02153, Q8IZC6, Q08828, P27986, P17301, P16885, P43405, O95622, P13942, P51828, P25940, Q8WYR1, P02675, Q13464, O14974, P42338, P47900, P42336, P63261, O75116, P12107	0.00219
hsa04530:Tight junction	23	A7E2Y1, P12931, Q96QZ7, Q9Y2K3, P60709, O75970, P35579, P13535, P12882, P12814, P55196, P35580, Q8N7P3, Q9UKX3, Q96B33, Q9UKX2, Q7Z406, P63261, Q8NI35, O43707, P11055, P35749, Q9Y623	0.002123
hsa04520:Adherens junction	20	P46940, Q9HCS4, P18206, P12931, Q9BX66, Q12913, Q8WWI1, P08581, P60709, Q9UQB8, P12814, P55196, P08069, P10586, P12830, P63261, P28827, O43707, P06213, P00533	0.002591
hsa05414:Dilated cardiomyopathy	22	P51828, P08648, P54289, Q01668, P60709, P01375, P16144, Q9NY47, Q08828, Q9UKX5, O60840, P18084, P26012, P17301, P56199, O00305, P68032, P63261, O95622, P23229, Q14118, P45379	0.002822
hsa04024:cAMP signaling pathway	39	Q14432, Q8WWN8, Q08828, P55196, P13569, P16066, P27986, Q96PN6, P41587, P50993, O15399, O95644, O95622, Q13733, P08151, P05023, P30939, P51828, P10071, Q8WYR1, Q01668, Q13464, P19634, P19838, P20020, P25101, O14939, O14974, Q13635, P42261, O60840, Q13009, P42338, P42336, P23945, O75116, Q13224, Q14957, Q13557	0.00291
hsa04919:Thyroid hormone signaling pathway	26	P12931, Q86YW9, Q9NQ66, P60709, P49815, Q01970, Q9NYB5, Q93074, Q9UHV7, P27986, P50993, P16885, P05023, Q13733, Q8WYR1, Q96ST3, Q8N3E9, Q92830, P19634, O60244, Q92831, P42338, P42336, Q99466, P63261, Q71F56	0.005675
hsa04921:Oxytocin signaling pathway	31	Q3MJ16, P12931, Q9NQ66, Q32MK0, P60709, Q01970, Q02153, Q9NY47, Q08828, P16066, O00305, O95644, O95622, P14649, O94759, P51828, P54289, P60660, P48454, Q01668, Q13464, O14974, P20594, P28907, O60840, P13639, P63261, O75116, Q14934, P00533, Q13557	0.006058
hsa05410:Hypertrophic cardiomyopathy (HCM)	20	P08648, P54289, Q01668, P01375, P60709, P16144, Q9NY47, Q9UKX5, O60840, P18084, P26012, P17301, P56199, O00305, P68032, P63261, P23229, Q14118, P12821, P45379	0.005849
hsa04360:Axon guidance	27	P07332, P08581, O15031, O14786, P49796, O95025, O14639, P53667, P51805, P29323, P29322, P54756, P43146, Q9Y6N7, P48454, Q13464, P00519, Q9ULL4, Q9UIW2, O75051, Q8NFY4, Q9P286, O75116, Q14934, O75093, O75094, Q9UF33	0.008959

hsa05205:Proteoglycans in cancer	37	P46940, P08648, P12931, Q9NPG1, P08581, P60709, P16157, P01375, P10398, Q15303, P18084, P27986, P17301, P14210, P16885, O00755, P07996, Q9H461, Q9Y6F9, P56703, Q8WYR1, Q13464, P19634, O14974, Q13635, P08069, P35968, Q13009, P42338, P42336, P63261, O75116, Q53EL6, P21860, Q07890, P00533, Q13557	0.010394
hsa04973:Carbohydrate digestion and absorption	13	P09848, P27986, Q8TE23, O43451, P50993, Q8WYR1, P42338, P42336, Q01668, Q13733, P14410, P05023, Q2TB90	0.013959
hsa05146:Amoebiasis	23	P25940, P05997, P18206, P20908, Q8WYR1, P08572, Q9NQ66, P01375, Q01970, P53420, P19838, P55268, Q8IZC6, Q08828, P12814, P27986, A4D0S4, P42338, P42336, P11047, P13942, P12107, O43707	0.016227
hsa05412:Arrhythmogenic right ventricular cardiomyopathy (ARVC)	17	Q9HCS4, P08648, P54289, Q01668, P60709, P16144, Q9NY47, Q9UKX5, O60840, P26012, P18084, P17301, P56199, O00305, P63261, P23229, Q14118	0.015636
hsa04070:Phosphatidylinositol signaling system	21	O15327, Q86XP1, P32019, Q8WYR1, Q8N3E9, Q9NQ66, Q01970, Q16760, P27986, Q9Y2I7, O00443, P42356, O43314, P42338, P16885, O00750, P42336, Q13615, O75747, Q6PFW1, O75912	0.02977
hsa04972:Pancreatic secretion	20	P40879, P51828, Q9NQ66, P54315, P04920, P47872, P19634, Q01970, P20020, P16233, Q08828, P28907, P13569, P39877, P50993, P55011, O95622, Q13733, P05023, Q96IY4	0.035621
hsa04022:cGMP-PKG signaling pathway	29	Q13237, Q14432, Q9NQ66, Q32MK0, Q01970, Q02153, Q08828, P16066, P50993, O95644, O95622, P0DMS8, P06213, Q13733, P05023, P51828, P48454, Q01668, Q13464, P20020, P25101, O14974, P30411, P20594, Q9Y4H2, O60840, O75116, Q14934, P78347	0.036644
hsa04976:Bile secretion	16	P51828, P04920, P47872, P19634, P04035, Q9NPD5, Q08828, P13569, P50993, P08183, Q9BY07, O95622, P46721, O95342, Q13733, P05023	0.04767
hsa02010:ABC transporters	12	P13569, O15440, Q8N139, P33527, P08183, Q96J65, O95342, Q8IUA7, Q8WWZ4, O94911, Q8WWZ7, Q99758	0.04928
hsa04151:PI3K-Akt signaling pathway	52	P08648, P49746, O96020, P20908, P49815, P53420, P26012, P18084, P27986, P13942, P06213, Q6ZVD8, Q15389, O60346, P08572, P17948, Q92574, P08069, P24821, P35968, A4D0S4, P56199, Q9UQP3, P01133, Q07890, Q16537, P49767, P05997, P08581, O14920, Q8IZC6, P07900, P17301, P38398, P14210, P43405, P35916, P11047, P07996, P25940, Q8WYR1, P16144, A6NMZ7, P19838, P55268, Q9UKX5, P10721, P42338, P42336, P12107, P23229, P00533	0.051725
hsa04713:Circadian entrainment	19	P51828, Q13237, Q9NQ66, Q01668, Q01970, Q02153, Q08828, O15534, P42261, Q96PN6, O15055, O15399, P29475, Q9P0X4, O95622, Q13224, O75582, Q14957, Q13557	0.081141
hsa04270:Vascular smooth muscle contraction	22	P62736, P51828, Q3MJ16, P60660, Q9NQ66, Q32MK0, Q13464, Q01668, Q01970, P10398, Q02153, P25101, O14974, Q08828, P20594, O60840, P16066, P39877, O75116, O95622, P63267, P14649	0.080134
hsa04930:Type II diabetes mellitus	12	Q9Y4H2, P27986, P14672, Q8WXH5, Q8WYR1, P42338, O14920, P42336, Q01668, P01375, P06213, Q2TB90	0.082795
hsa04014:Ras signaling pathway	36	P49767, Q3MJ16, Q9UHD2, Q96KP1, O14920, P08581, Q14644, P55196, P27986, P14210, P16885, Q9UJF2, P35916, P06213, Q15389, Q8WYR1, Q13972, P17948, Q96PV0, P19838, P00519, O14939, P10721, P08069, P35968, P39877, Q13009, O15211, P42338, P42336, Q9P286, Q07890, Q8IVT5, P01133, Q13224, P00533	0.08252
hsa04724:Glutamatergic	21	P51828, Q3MJ16, Q9UPX8, Q9NQ66, O14490, P48454, Q01668, Q01970, P43003, O14939, Q08828, P42261, Q16478,	0.107938

		O15399, Q13003, O95622, Q9Y566, Q14416, Q13224, Q14957, Q99624	
synapse			
hsa00562:Inositol phosphate metabolism	15	O15327, P32019, Q8N3E9, Q9NQ66, Q01970, Q9Y2I7, O00443, P42356, P42338, P16885, Q4KWH8, O00750, P42336, Q13615, O75747	0.108907

Annexure VI: List of KEGG pathways enriched in primed cells.

Term	Count	Genes	Benjamini-Hochberg p-value
hsa04510:Focal adhesion	56	P49747, P20908, P60709, P48736, P29400, P18564, P02458, P13942, O43707, P08572, Q13464, P17948, P05106, Q07889, P08123, P08069, P24821, P35968, A4D0S4, Q9UQP3, P01133, Q07890, P18206, P08581, Q13489, Q8IZC6, P35609, Q13017, P12814, Q9Y243, Q13905, P56945, O00329, P14210, P31751, P35916, P11047, Q9NRY4, P07996, P25940, Q08043, P02452, P16144, A6NMZ7, Q16363, P55268, Q9UKX5, P49023, P42338, Q14185, O75116, P63261, P12107, P23229, P00533, P31749	4.42E-07
hsa04530:Tight junction	32	A7E2Y1, P62714, Q96QZ7, P51153, O95049, P60709, Q9UDY2, P35609, P13535, Q8TEW0, Q9P2M7, P12814, P55196, O15551, Q8N3R9, Q8NI35, O43707, P35749, Q08043, Q9Y2K3, O75970, P35579, P12882, P35580, Q9UKX3, Q9UKX2, Q7Z406, P67775, P63261, P11055, Q9Y623, Q05513	5.95E-07
hsa04360:Axon guidance	35	P08581, Q9BPU6, O15031, O94813, Q16555, O14639, P51805, P29320, P29323, P29322, Q7Z6B7, P54756, O94929, Q9H3T3, P43146, Q9Y6N7, P32004, Q13464, Q92854, Q9ULL4, P54764, O75051, O43295, Q9P283, P54760, Q8NFY4, O15041, P52799, O75116, O75093, O75094, Q14563, P98172, Q9UF33, O60486	1.91E-04
hsa04024:cAMP signaling pathway	45	Q01814, O60503, Q14432, Q8TEY5, P48736, P42262, Q12879, P55196, P16066, Q9Y243, O00329, P41587, O15399, P31751, P54710, P08172, P08151, P30939, P43220, P51828, Q13698, P10071, P23634, P48546, Q01668, Q13464, Q14028, P30559, Q08499, P19634, P19838, P20020, Q13635, Q16720, Q05469, O43306, P40145, P42261, O60840, O75899, Q13370, P42338, P23945, O75116, P31749	8.52E-04
hsa04015:Rap1 signaling pathway	47	Q8TEU7, O60503, Q96QZ7, P08581, Q9NQ66, P60709, P48736, Q5TCQ9, Q12879, Q8TEW0, O60292, P55196, Q9Y243, P07737, Q13905, P56945, P12830, O00329, P14210, P31751, P35916, Q7LDG7, P06213, Q86UL8, P07996, P51828, O94887, P17948, P05106, O43306, P40145, P10721, P08069, P35968, P47736, Q8N1I0, P42338, P09471, P20701, Q9P2F8, P63261, Q9BZL6, P01133, P21554, P00533, P31749, Q05513	0.001015729
hsa04512:ECM-receptor interaction	25	P25940, P49747, P20908, P08572, P02452, P16144, A6NMZ7, P55268, Q16363, P29400, P05106, P08123, Q8IZC6, Q9UKX5, Q7L0J3, P24821, P18564, A4D0S4, P02458, Q9UQP3, P11047, P13942, P12107, P23229, P07996	0.001761667
hsa05414:Dilated cardiomyopathy	24	P51828, O60503, Q13698, P07951, Q01668, P60709, P16144, Q9NY47, P05106, Q7Z3S7, O43306, Q9UKX5, P40145, O60840, Q14896, P09493, P18564, P06753, P68032, P63261, P67936, P23229, Q08289, P45379	0.002475711

hsa04261:Adrenergic signaling in cardiomyocytes	33	Q01814, O60503, P62714, Q14524, P07951, Q9NQ66, Q8TEY5, P13533, Q9NY47, Q7Z3S7, Q9Y243, P31751, P54710, P68032, P51828, Q13698, P23634, Q01668, P19634, P20020, P12883, Q16720, P40145, O43306, O60840, Q8IWT1, P09493, P06753, P67775, P67936, P31749, P45379, Q08289	0.002891576
hsa04151:PI3K-Akt signaling pathway	65	P49747, P62714, P20908, Q8TEY5, O00206, P48736, P29400, P18564, P02458, P08172, P13942, Q99062, P06213, P13807, P24394, P08572, O60346, P17948, P05106, Q07889, Q96BR1, P08123, Q92574, P08069, P24821, P35968, A4D0S4, Q9UQP3, P14784, P67775, P26951, P01133, Q07890, P08581, Q8IZC6, O15111, Q9Y243, P07900, O00329, O60674, P14625, P38398, P14210, P31751, P43405, P35916, P11047, P22736, P07996, P63104, P25940, P02452, P16144, A6NMZ7, P19838, Q16363, P55268, P10721, Q9UKX5, P42338, Q16512, P12107, P23229, P00533, P31749	0.003149105
hsa04915:Estrogen signaling pathway	26	P34931, O60503, Q8TEY5, Q9NQ66, P48736, Q9Y243, P07900, P11142, O00329, P14625, P31751, P51828, P54652, Q05655, Q07889, P0DMV9, P40145, O43306, O75899, P03372, P42338, P09471, P0DMV8, Q07890, Q13255, P00533, P31749	0.003576668
hsa05146:Amoebiasis	26	P18206, P20908, Q9NQ66, P48736, O00206, P35228, P29400, P35609, Q8IZC6, P12814, O00329, P02458, P13942, P11047, O43707, P25940, Q08043, P08572, P02452, P19838, P55268, Q16363, P08123, A4D0S4, P42338, P12107	0.008612292
hsa04611:Platelet activation	30	O60503, P20908, Q9NQ66, P60709, P48736, Q8IZC6, Q9Y243, O00329, P02458, P16885, P43405, P31751, P13942, Q9NRY4, Q7LDG7, P02671, P25940, P51828, P02452, Q13464, P05106, P08123, O43306, P40145, P42338, P63261, O75116, P12107, P31749, Q05513	0.009142616
hsa04520:Adherens junction	20	O94887, Q08043, P18206, Q8WWI1, P23467, P08581, P60709, P68400, P35609, Q8TEW0, P55196, P12814, P08069, P12830, P37173, P63261, P28827, O43707, P06213, P00533	0.009230569
hsa05410:Hypertrophic cardiomyopathy (HCM)	21	Q13698, P07951, Q01668, P60709, P16144, Q9NY47, P05106, Q9UGJ0, Q7Z3S7, Q9UKX5, O60840, Q14896, P09493, P18564, P06753, P68032, P63261, P67936, P23229, Q08289, P45379	0.009454011
hsa04919:Thyroid hormone signaling pathway	27	Q86YW9, Q9NQ66, P60709, P48736, Q12778, Q93074, Q9Y6Q9, Q9Y243, O00329, P16885, P31751, P54710, P12644, Q9Y2X0, Q16665, P19634, Q9BRC7, P05106, Q15788, Q8TF71, P03372, P42338, Q99466, P63261, Q71F56, P31749, Q15648	0.011549941
hsa04973:Carbohydrate digestion and absorption	14	P09848, Q01668, P48736, P19367, Q2TB90, Q9Y243, O00329, O43451, P42338, P52789, P31751, P54710, P14410, P31749	0.011895561
hsa04914:Progesterone-mediated oocyte maturation	22	P06401, P51828, O60503, Q9H1A4, P51812, Q15349, P48736, Q9UJX2, O43306, P40145, Q8WWL7, P08069, Q15418, Q9Y243, P53350, P07900, O00329, Q13370, P42338, P31751, P30260, P31749	0.013487545
hsa05100:Bacterial invasion of epithelial cells	20	P18206, Q9UQ16, P22681, Q13191, P08581, P60709, P48736, Q9Y5K6, Q96JJ3, Q96BJ8, P56945, P12830, O00329, Q8IYM1, P49023, P42338, Q14185, P63261, Q00610, P53675	0.019650958
hsa05222:Small cell lung cancer	21	Q13077, P08572, Q13489, P48736, P19838, P35228, P55268, Q16363, P29400, O00463, O15111, Q9Y243, O14727, Q13309, O00329, A4D0S4, P42338, P31751, P11047, P23229, P31749	0.022166684
hsa05200:Pathways in cancer	66	O60503, Q9NPG1, P48736, P42771, Q12778, P29400, P12830, P11274, Q06455, P16885, Q99062, Q7LDG7, P51828, Q9Y6F9, P08572, Q13191, Q13464, Q07889, P08069, Q13309, P37173, A4D0S4, P06753, O14641, P01133, Q07890, O95996, Q03112, P22681, P08581, Q9NQ66, Q13489, P35228, O00463, P20585, O15111, Q9Y243, P07900, O00329, P14625, P14210, P31751, P11047, P12644, P08151, P07949, O94827, Q13077, P10071, P10070, P43146, Q16665, Q8TDF6,	0.027718226

		P14923, P19838, Q16363, P55268, Q13635, O43306, P40145, P10721, P42338, O75116, P23229, P00533, P31749	
hsa04923:Regulation of lipolysis in adipocytes	15	P51828, O60503, P48736, Q05469, O43306, Q9Y4H2, P40145, P16066, Q9Y243, O00329, Q13370, P42338, P31751, P06213, P31749	0.053746184
hsa04022:cGMP-PKG signaling pathway	31	Q01814, O60503, Q14432, Q9NQ66, Q8TEY5, Q9UPR5, Q9UHL9, P16066, Q9Y243, P31751, P54710, P06213, A8MYU2, P18089, P51828, Q13698, P23634, Q01668, Q13464, Q14028, P20020, O76074, Q9Y6F6, Q16720, Q9Y4H2, P40145, O43306, O60840, Q13370, O75116, P31749	0.057383557
hsa03013:RNA transport	33	Q9H361, O14744, Q5VU65, Q14974, B5ME19, P0DJD0, P0DJD1, Q96F07, Q96RS0, Q9H074, O43432, Q7Z3J3, A6NKT7, Q92621, Q8TEM1, Q99666, A8CG34, Q8TEQ6, P63279, Q4VXU2, Q8WUM0, Q99567, Q04637, Q14152, P52948, P11940, O14715, Q9UKV3, Q9UKX7, O60841, Q8NI27, Q99613, Q9Y6A5	0.057579333
hsa04974:Protein digestion and absorption	20	P25940, P20908, P08572, P39060, P02452, A6NMZ7, Q9UPR5, Q8NFW1, Q9UMD9, P29400, P08123, Q8IZC6, Q8TF71, O43895, P02458, P54710, P13942, P12107, Q16820, Q07837	0.062008006
hsa04724:Glutamatergic synapse	24	Q16099, P51828, Q9UPX8, O60503, O00341, Q9NQ66, Q01668, P43003, P42262, Q12879, O43306, Q16478, P40145, P42261, O15399, P41594, Q9BYB0, P09471, Q9P2U8, P48995, Q13255, Q9P2U7, O00222, Q99624	0.063187322
hsa04066:HIF-1 signaling pathway	21	P04406, P02787, Q16665, O00206, P48736, P17948, P19838, P35228, P19367, Q2TB90, P08069, Q9Y243, O00329, P42338, P16885, P52789, P31751, P01133, P06213, P00533, P31749	0.070306853
hsa04930:Type II diabetes mellitus	13	Q9Y4H2, P14672, O00329, P42338, P52789, Q01668, Q09428, P48736, Q05655, P06213, P19367, Q2TB90, Q05513	0.076529626
hsa04120:Ubiquitin mediated proteolysis	27	Q16531, Q9C0C9, Q9H1A4, P22681, Q9Y297, Q13489, Q9Y385, Q14669, Q9UJX2, O00308, P38398, Q9Y6X2, P30260, Q15386, P63279, Q96J02, Q9UKB1, Q9H0M0, Q05086, Q13233, Q13191, O60260, P46934, Q13309, Q13620, O95155, Q13049	0.077885074
hsa04260:Cardiac muscle contraction	17	Q13698, P08574, P07951, Q01668, P13533, P19634, Q9NY47, P12883, Q7Z3S7, O60840, P09493, P06753, P54710, P68032, P67936, P45379, Q08289	0.099507904
hsa04068:FoxO signaling pathway	26	P48736, P04040, Q12778, O15111, Q8WWL7, Q9Y243, P53350, O00329, P31751, P06213, Q07889, Q9UGJ0, Q96BR1, Q93009, Q9Y4H2, P08069, Q13309, P14672, P37173, Q9Y5W3, P42338, Q07890, P01133, Q13255, P00533, P31749	0.102118289
hsa04810:Regulation of actin cytoskeleton	37	O95996, P18206, P55160, P60709, P48736, Q96F07, P35609, P12814, P07737, P56945, O00329, P18564, P08172, Q9NRY4, O43707, Q08043, Q13464, P16144, P19634, P05106, Q07889, Q9UKX5, Q9Y2I7, P06396, P42338, P49023, P20701, Q14185, P63261, P14616, Q9Y2A7, O75116, P01133, Q07890, P23229, P00533, Q13576	0.102657025
hsa04931:Insulin resistance	22	O15294, P51812, Q8TEY5, Q15349, P48736, Q05655, P19838, Q9Y2P5, Q12778, Q9UGJ0, Q9Y4H2, Q9Y243, Q15418, P14672, Q04759, O00329, P42338, P31751, P06213, P13807, P31749, Q05513	0.103431422